

UNIVERSITY OF BIRMINGHAM

THE DIRECT AND INDIRECT EFFECTS OF ATTENUATED *SALMONELLA* TYPHIMURIUM ON INTESTINAL TUMOUR EPITHELIUM

By

GILLIAN MAY MACKIE

A thesis submitted to the University of Birmingham for the degree of

DOCTOR OF PHILOSOPHY

Institute of Immunology & Immunotherapy

College of Medical and Dental Sciences

University of Birmingham

October 2023

UNIVERSITY OF
BIRMINGHAM

University of Birmingham Research Archive

e-theses repository

This unpublished thesis/dissertation is copyright of the author and/or third parties. The intellectual property rights of the author or third parties in respect of this work are as defined by The Copyright Designs and Patents Act 1988 or as modified by any successor legislation.

Any use made of information contained in this thesis/dissertation must be in accordance with that legislation and must be properly acknowledged. Further distribution or reproduction in any format is prohibited without the permission of the copyright holder.

ABSTRACT

Attenuated *Salmonella enterica* serovar typhimurium (*S*Tm) home to and colonise tumours, where it can induce tumour regression. In this thesis I aimed to identify how *S*Tm invade tumour cells and to what extent intracellular invasion is necessary for anti-tumour response. Bulk and single-cell RNA-sequencing were utilised to reveal differences between invasive versus extracellular-restricted *Salmonella*. $Apc^{Min/+}$ mice were treated with *Salmonella* that are invasion-sufficient or extracellular-restricted, then innate immune infiltrate and polyp burden were assessed. I used *in vitro* models to show that *S*Tm preferentially invades proliferating cells in patient and murine tumour organoids. Invasion of tumour cells was dependent on *Salmonella* binding host cell cholesterol via SipB expression. Previous studies have shown that cell-surface cholesterol is maximal during mitosis, thus I show mechanistic insight into why proliferating cells are preferentially targeted. $STm^{\Delta aroA}$ induce similar transcriptional changes in both mouse and human tumour organoids *in vitro* when restricted to the extracellular space or permitted to invade. I generated and validated a strain of *S*Tm which cannot invade intracellularly, $STm^{\Delta aroA\Delta sipB}$, but I show with oral gavage of $Apc^{Min/+}$ mice that this mutant can colonise the polyp environment *in vivo*. This extracellular survival resulted in similar innate cell recruitment but led to superior clearance of polyps, which warrants further investigation. In summary, *S*Tm specifically infects proliferating tumour cells via binding of cell surface cholesterol, which has implications for utilisation of bacteria as intracellular drug delivery systems. Intracellular invasion appears to be dispensable for the therapeutic effect, as we see reduction of polyps with $STm^{\Delta aroA\Delta sipB}$; this double mutant may then represent a superior and safer bacterial cancer therapy agent.

ACKNOWLEDGEMENTS

The work in this thesis was funded by Cancer Research UK.

Firstly, I need to thank Kendle for taking a chance on me in 2019, it has been so much fun to do this work with you and I cannot wait to see you build the lab up in Glasgow. Remember, we are all just bacterial girls living in a bacterial world! Amanda, thank you so much for having me for a summer in your lab – I learnt so much and it was huge for the project.

Ally, you are the most patient and knowledgeable post-doc anyone could ever ask for during their PhD, thank you for all your advice. Lisa, I have loved going through this whole process with you and I will always remember what we were supposed to be eating in 2020 and what we missed out on! The Maslab poop-scoopers and production-line ladies made some of the longest days deliriously fun.

FLABbies – it really does take a village to raise a PhD student and it has been completely invaluable to have such a supportive group of incredible scientists in which to work. I know I don't speak only for myself when I say the fellows have built something great.

To "The Work Lot" the consistency of 12pm lunchers and post-work pints with pals have been a much-needed source of silliness in the last few years, and I am SO glad those booths were soundproof.

Mum, Dad, Jen and Gail your support through this, at times insane, choice of mine has meant so much - you all thought it was doable when I was hitting my head against the wall.

Lastly, Tom it has been a real privilege to drag each other through yet another degree. I know wholeheartedly I could not have done this as well without you to bounce ideas off, help me count my cells and lend a hand to frube an intestine or two. Your turn next!

CONTENTS

ABSTRACT ..... **i**

ACKNOWLEDGEMENTS ..... **ii**

CONTENTS ..... **iii**

LIST OF FIGURES ..... **vi**

LIST OF TABLES ..... **ix**

LIST OF ABBREVIATIONS ..... **x**

PUBLICATIONS CONTRIBUTED TO DURING THESIS ..... **xiii**

CHAPTER 1 – INTRODUCTION **1**

1.1 Colorectal cancer **1**

1.2 Current treatments for CRC **6**

1.3 Modelling CRC in research **9**

1.4 Bacterial cancer therapy **12**

1.5 *Salmonella* typhimurium **16**

1.5.1 *Salmonella* typhimurium infection of intestinal epithelial cells **20**

1.6 Attenuated *Salmonella* typhimurium as an agent in BCT **26**

1.6.1 Review of Mackie et al., 2021 - 'Bacterial cancer therapy in autochthonous colorectal cancer affects tumour growth and metabolic landscape' **29**

1.7 Enhancing bacterial cancer therapy **32**

1.8 The immune response in bacterial cancer therapy **37**

1.9 Project aims **40**

CHAPTER 2 - MATERIALS AND METHODS **41**

2.1 Bacterial strains **41**

2.2 Immunohistochemistry **41**

2.3 Organoid culture and maintenance **42**

2.4 Infection of tumour organoids with attenuated *S*Tm strains **44**

2.5 Recovery of colony forming units from organoids **45**

2.6 RNA isolation, cDNA preparation and qPCR **45**

2.7 Stem-forming assay **47**

2.8 CellTrace Blue staining of patient-derived organoids and flow cytometry **47**

2.9 Mitomycin C pre-treatment of patient-derived organoids 49
2.10 Methyl-β-cyclodextrin pre-treatment of patient-derived organoids 49
2.10.1 Imaging of cholesterol after MβCD treatment of organoids 50
2.11 Single-cell RNA sequencing 50
2.11.1 Single-cell RNA sequencing analysis 51
2.12 Bulk RNA-sequencing 56
2.13 Amplification of Kan^{R} cassette from *S*Tm$^{\Delta sipB}$ 59
2.14 Generation of double-gene knockout *Salmonella* typhimurium 59
2.15 Animals 64
2.16 Recovery of colony forming units from tissue 64
2.17 *Ex vivo* gentamicin protection assay 65
2.18 Cell viability of organoids 65
2.19 Long term treatment protocol 66
2.20 Enzymatic digestion of polyp tissue for flow cytometry 66
2.21 Statistical analysis 70
CHAPTER 3 - STM$^{\Delta AROA}$ PREFERENTIALLY INVADE PROLIFERATING CELLS IN PATIENT-DERIVED ORGANOIDS 71
3.1 Introduction 71
3.2 Results 75
3.2.1 *S*Tm$^{\Delta aroA}$ restores epithelial identity of colon tumour epithelium *in vivo* 75
3.2.2 *S*Tm$^{\Delta aroA}$ infects human and mouse colon tumour organoids *in vitro* 77
3.2.3 *S*Tm$^{\Delta aroA}$ reduces stem-cell associated transcripts in some, but not all, PDOs 79
3.2.4 *S*Tm$^{\Delta aroA}$ infection *in vitro* reduces growth capacity in colorectal tumour organoids 81
3.2.5 *S*Tm$^{\Delta aroA}$ can be identified in the cells that were proliferating at the time of infection 84
3.2.6 Tumour cell proliferation is necessary for optimal intracellular infection of PDOs 88
3.2.7 *Salmonella*-host cell cholesterol interaction is necessary for invasion *in vitro* 90
3.3 Discussion 94
CHAPTER 4- EXTRACELLULAR AND INTRACELLULAR *S*Tm$^{\Delta aroA}$ ALTER THE TRANCRIPTIONAL LANDSCAPE OF TUMOUR ORGANOIDS 102
4.1 Introduction 102

4.2 Results 108

4.2.1 Preparation of samples and processing of data for single-cell RNA sequencing 108

4.2.3 Response A and response B PDO lines express different genes after *S*Tm$^{\Delta aroA}$ treatment 114

4.2.4 Extracellular-restricted *S*Tm$^{\Delta aroA}$ induces similar transcriptional changes in tumour organoids compared to intracellular-permitted *S*Tm$^{\Delta aroA}$ 117

4.2.5 Chemokines upregulated by PDOs following *S*Tm$^{\Delta aroA}$ treatment are expressed primarily by Paneth cells 127

4.3 Discussion 129

CHAPTER 5 - INTRACELLULAR INVASION OF TUMOUR CELLS BY ATTENUATED *SALMONELLA* TYPHIMURIUM IS DISPENSABLE FOR ANTI-TUMOUR EFFECT 137

5.1 Introduction 137

5.2 Results 143

5.2.1 Validation of deletion of *sipB* from *S*Tm$^{\Delta aroA}$ via λ-red recombination 143

5.2.2 STm$^{\Delta aroA\Delta sipB}$ cannot invade intracellularly but can survive in polyps *in vivo* 145

5.2.3 A small proportion of *S*Tm$^{\Delta aroA}$ intracellularly invades tumour cells *in vivo,* but *S*Tm$^{\Delta aroA\Delta sipB}$ survives in polyps *in vivo* exclusively extracellularly 147

5.2.4 *S*Tm$^{\Delta aroA\Delta sipB}$ stunts tumour growth *in vitro* and reduces tumour burden and load *in vivo* 149

5.2.5 *S*Tm$^{\Delta aroA}$ and *S*Tm$^{\Delta aroA\Delta sipB}$ significantly increase eosinophil recruitment to polyps *in vivo* 152

5.3 Discussion 156

CHAPTER 6 – FINAL DISCUSSION 163

BIBLIOGRAPHY 172

APPENDIX 1: SINGLE-CELL RNA-SEQUENCING SCRIPTS 189

APPENDIX 2: BULK RNA SEQUENCING SCRIPTS 199

LIST OF FIGURES

Figure 1.5.1	The structure of *Salmonella* typhimurium cell wall	18
Figure 1.5.2	Schematic of *Salmonella* typhimurium pathogenesis in the gut	24
Figure 1.5.3	The structure of the type-3 secretion system of *Salmonella* typhimurium	25
Figure 2.11.1	Quality assessment and filtering of single-cell RNA sequencing raw data	53
Figure 2.11.2	Jack Straw plot identifies 40 significant principal components	54
Figure 2.11.3	Cell type and cluster identification from single-cell RNA sequencing of PDOs	55
Figure 2.12.1	Experimental set up and analysis pipeline for bulk RNA sequencing	58
Figure 2.14.1	Position in SL1344 genome of primers used for generation and validation of *S*Tm$^{\Delta aroA\Delta sipB}$	63
Figure 2.20.1	Gating strategy for investigating innate immune infiltrate into polyps	69
Figure 3.2.1	*S*Tm$^{\Delta aroA}$ restores epithelial identity of colon tumour epithelium *in vivo*	76
Figure 3.2.2	*S*Tm$^{\Delta aroA}$ infects human and mouse tumour organoids *in vitro*	78
Figure 3.2.3	*S*Tm$^{\Delta aroA}$ reduces stem-cell associated transcripts in some, but not all, PDOs	80
Figure 3.2.4	*S*Tm$^{\Delta aroA}$ treatment reduces growth capacity of mouse and human colorectal tumour organoids *in vivo*	83
Figure 3.2.5	CellTrace Blue cannot stain organoids embedded in Matrigel	86
Figure 3.2.6	CellTrace Blue staining shows relative enrichment of *S*Tm$^{\Delta aroA}$ in proliferating cells at point of infection in PDOs	87

Figure 3.2.7	Optimal *S*Tm$^{\Delta aroA}$ infection requires actively proliferating cells in PDOs	89
Figure 3.2.8	Optimal invasion of tumour organoids by *S*Tm$^{\Delta aroA}$ is dependent on intact type-3 secretion system	90
Figure 3.2.9	Methyl-β-Cyclodextrin treatment of organoids reduces cell surface cholesterol	92
Figure 3.2.10	Methyl-β-Cyclodextrin treatment reduces bacterial burden in tumour organoids	93
Figure 4.1.1	Workflow for sequencing methods used	105
Figure 4.2.1	Cell populations in PDOs	112
Figure 4.2.2	There is a relative enrichment of response-specific clusters in response A PDOs and Paneth cells in response B PDOs following *S*Tm$^{\Delta aroA}$ treatment	113
Figure 4.2.3	*S*Tm$^{\Delta aroA}$ induces different transcriptional changes in different PDOs	115
Figure 4.2.4	*LCN2* expression is upregulated across PDOs following *S*Tm$^{\Delta aroA}$ treatment	116
Figure 4.2.5	PCA plots of the tumour-derived organoid samples in the bulk RNA-sequencing run	119
Figure 4.2.6	*S*Tm$^{\Delta aroA}$ induces a chemokine signature in mouse and human colon tumour organoids when intracellular or extracellular-restricted	120
Figure 4.2.7	Overlapping and unique DEGs in mouse tumour organoids after treatment with intra- or extracellular STm$^{\Delta aroA}$	122
Figure 4.2.8	Overlapping and unique DEGs in human tumour organoids after treatment with intra- or extracellular *S*Tm$^{\Delta aroA}$	123
Figure 4.2.9	Pathway analysis shows *S*Tm$^{\Delta aroA}$ induces changes to genes involved in cell junctions and innate signalling whether intracellular or extracellular-restricted in *Apc*$^{Min/+}$ tumour organoids	125

Figure 4.2.10 Pathway analysis shows *S*Tm$^{\Delta aroA}$ induces changes to genes involved in cell-cycle, innate signalling and pathogen detection whether intracellular or extracellular-restricted in PDO 389 126

Figure 4.2.11 Chemokine expression is upregulated in secretory and progenitor cells in PDOs after *S*Tm$^{\Delta aroA}$ treatment 128

Figure 5.2.1 Validation of deletion of *sipB* from *S*Tm$^{\Delta aroA}$ via λ-red recombination 144

Figure 5.2.2 *S*Tm$^{\Delta aroA\Delta sipB}$ cannot invade intracellularly *in vitro* but can survive in polyps *in vivo* 146

Figure 5.2.3 A small proportion of *S*Tm$^{\Delta aroA}$ intracellularly invades tumour cells *in vivo*, but *S*Tm$^{\Delta aroA\Delta sipB}$ survives in polyps *in vivo* exclusively extracellularly 148

Figure 5.2.4 *S*Tm$^{\Delta aroA\Delta sipB}$ stunts tumour growth *in vitro* and reduces tumour burden and load *in vivo* 151

Figure 5.2.5 Representative flow plots showing cell populations in *Apc*$^{Min/+}$ polyps 154

Figure 5.2.6 *S*Tm$^{\Delta aroA}$ and *S*Tm$^{\Delta aroA\Delta sipB}$ significantly increase eosinophil recruitment to polyps *in vivo* 155

LIST OF TABLES

Table 1	Components of media used during the maintenance of mouse colon tumour organoids	44
Table 2	Reagents which are combined with Ultra-Pure H_2O and RNA to a total volume of 20µl per sample for conversion to cDNA	46
Table 3	Gene-specific primer sequences for stem-related genes investigated using qPCR in chapter 3	46
Table 4	RNA concentrations (ng/µl) of samples for bulk RNA sequencing as measured using a nanodrop. Samples sent in 30µl volume	57
Table 5	Primers used for the amplification of Kanamycin resistance cassette, generation of mutant by lambda-red system and validation of deletion of *sipB*	62
Table 6	Antibody details for flow cytometry to define innate cell infiltration into polyps *in vivo*	68
Table 7	Patient derived organoid primary tumour information	81

LIST OF ABBREVIATIONS

µg	Microgram
µL	Microlitre
µm	Micrometre
µM	Micromolar
5-FC	5-fluorocytosine
5-FU	5-fluorouracil
Amp^R	Ampicillin resistance
AOM	Azoxymethane
APC	Adenomatous polyposis Coli
BCG	Bacillus Calmette-Guerin
BCT	Bacterial cancer therapy
BMP	Bone Morphogenetic Protein
CAC	Colitis-associated cancer
CAR-T cells	Chimeric antigen receptor T-cells
CD	Cytosine deaminase
CFU	Colony forming units
CIN	Chromosomal instability
CLR	C-type lectin receptors
CMS	Consensus Molecular Subtypes
CTB	CellTrace Blue
CTLA-4	Cytotoxic T-lymphocyte-associated protein 4
CRC	Colorectal cancer
DAMP	Damage-associated molecular patterns
DEG	Differentially expressed gene
DSS	Dextran Sulfate Sodium
E. coli	*Escherichia coli*
EET	Eosinophil extracellular traps
EGF	Epidermal growth factor
EGFR	Epidermal growth factor receptor
FACS	Fluorescence-associated cell sorting
FAP	Familial Adenomatous Polyposis
FBS	Fetal bovine serum
F. nucleatum	*Fusobacterium nucleatum* subsp. nucleatum
FOV	Field of view
g	Gram
GC-MS	Gas chromatography-mass spectrometry

GFP	Green fluorescent protein
HI-FBS	Heat-inactivated FBS
ICI	Immune checkpoint inhibitor
IEC	Intestinal epithelial cell
IFN-γ	Interferon-gamma
Kan^R	Kanamycin resistance cassette
kB	Kilobase
LPS	Lipopolysaccharide
MβCD	Methyl-β-cyclodextrin
mg	Milligram
MHC	Major histocompatibility complex
mL	Millilitre
mm	Millimetre
mM	Millimolar
MMC	Mitomycin C
MMR	Mismatch repair
MSI	Microsatellite instability
MSS	Microsatellite stable
MTT	(3-(4,5-dimethylthiazol-2-yl)-2,5-diphenyltetrazolium bromide
NF-κB	Nuclear factor kappa-light-chain-enhancer of activated B cells
ng	Nanogram
NLR	Nucleotide-binding oligomerization domain-leucin rich repeats-containing receptors
nm	Nanometre
nM	Nanomolar
NT	Non-treated
OD_{600}	Optical density at 600 nanometre wavelength
PAMP	Pathogen-associated molecular patterns
PBS	Phosphate buffered saline
PCA	Principal component analysis
PC	Principal component
PD-1	Programmed cell death protein 1
PD-L1/2	Programmed cell death ligand 1/2
PDO	Patient-derived organoids
PRR	Pattern recognitions receptors
RLR	Retinoic acid-inducible gene 1-like receptors
SCV	*Salmonella*-containing vacuole
SEM	Standard error of the mean
Sip	*Salmonella* invasion proteins

SPI	*Salmonella* pathogenicity island
***S*Tm**	*Salmonella enterica* serovar typhimurium
T3SS	Type-3 secretion system
TCA	Tricarboxylic acid
TCR	T-cell receptor
TGF-β	Transforming growth factor-β
TLR	Toll-like receptor
TME	Tumour microenvironment
TNF-α	Tumour Necrosis Factor-α
TRAIL	TNF-related apoptosis-inducing ligand

PUBLICATIONS CONTRIBUTED TO DURING THESIS

Alastair Copland, **Gillian M. Mackie**, Lisa Scarfe, David A. J. Lecky, Nancy Gudgeon, Riahne McQuaid, Masahiro Ono, Manja Barthel, Wolf-Dietrich Hardt, Hiroshi Ohno, Sarah Dimeloe, David Bending, Kendle M. Maslowski. *Salmonella cancer therapy metabolically disrupts tumours at the collateral cost of T cell immunity.* 2023. Pre-print on bioRxiv. https://doi.org/10.1101/2023.01.12.523780

Daniel Fisch, Moritz M. Pfleiderer, Eleni Anastasakou, Fabian Wendt, Xiangyang Liu, Barbara Clough, Samuel Lara-Reyna, Vesela Encheva, Ambrosius P. Snijder, Kendle M Maslowski, **Gillian M Mackie**, Andrew D Beggs, Hironori Bando[1-], Masahiro Yamamoto, Avinash R. Shenoy, Jason Mercer, Bernd Wollscheid, Wojtek P. Galej, Eva-Maria Frickel. *PIM1 kinase protects against GBP1-induced self-damage during infection.* Science. 2023.

Thomas A. E. Elliot, Emma K. Jennings, David A. J. Lecky, Sophie Rouvray, **Gillian M. Mackie**, Lisa Scarfe, Lozan Sheriff, Masahiro Ono, Kendle M. Maslowski, David Bending. *Nur77-Tempo mice reveal T cell steady state antigen recognition.* Discovery Immunology. 2022. https://doi.org/10.1093/discim/kyac009.

Bishop EL, Gudgeon N, **Mackie GM**, Chauss D, Roberts J, Tennant DA, Maslowski KM, Afzali B, Hewison M and Dimeloe S. *1,25-dihydroxyvitamin D_3 suppresses $CD4^+$ T cell effector functionality by inhibition of glycolysis.* Immunology. 2022. https://doi.org/10.1111/imm.13472

Giuseppe Bombaci, Mayuresh Anant Sarangdhar, Nicola Andina, Aubry Tardivel, Eric Chi-Wang, **Gillian M. Mackie**, Matthew Pugh, Vedat Burak Ozan, Yara Banz, Thibaud Spinetti, Cedric Hirzel, Esther Youd, Joerg C Schefold, Graham Taylor, Amiq Gazdhar, Nicolas Bonadies, Anne Angelillo-Scherrer, Pascal Schneider, Kendle M Maslowski, Ramanjaneyulu Allam. *LRR-protein RNH1 dampens the inflammasome activation and is associated with COVID-19 severity.* Life Science Alliance. 2022. https://doi.org/10.26508/lsa.202101226.

Lisa Scarfe, **Gillian M. Mackie**, Kendle M. Maslowski. *Inflammasome-independent functions of NAIPs and NLRs in the intestinal epithelium.* Biochemical Society Transactions. 2021. https://doi.org/10.1042/BST20210365.

Gillian M. Mackie, Alastair Copland, Masumi Takahashi, Yumiko Nakanishi, Isabel Everard, Tamotsu Kato, Hirotsugu Oda, Takashi Kanaya, Hiroshi Ohno and Kendle M. Maslowski. *Bacterial cancer therapy in autochthonous colorectal cancer affects tumor growth and metabolic landscape.* JCI Insight. 2021. https://doi.org/10.1172/jci.insight.139900.

CHAPTER 1 – INTRODUCTION

Colorectal cancer (CRC) is the presence of a malignant outgrowth of cells within the epithelium of the colon or rectum and is a leading cause of death globally. The current treatment options are limited in their effectiveness for the vast majority of patients, meaning that novel therapies are in demand. In this chapter I will outline the current known literature regarding CRC as a disease, and how bacterial agents may represent a promising opportunity for treating patients.

1.1 Colorectal cancer

Colorectal cancer represents a huge social, economic, and healthcare burden as it is currently the third most common form of cancer worldwide and has the second highest rate of mortality of all cancers (World Health Organisation, 2023). Over 90% of colorectal carcinomas originate from the epithelial cells in the mucosa as adenocarcinomas, characterised by glandular formation (Fleming et al., 2012). Initial diagnosis is primarily done by colonoscopy, where the entire large intestine is imaged to look for malignant growths. Tissue that appears abnormal is then taken for biopsy and histological grading. The stage of the cancer at the point of diagnosis is still by far the most accurate prognostic factor (Kolligs, 2016; World Health Organisation, 2023). Two large cohorts in the United States of America were followed over 22 years and identified that there was lower mortality from colorectal cancer in people that had multiple colonoscopies, compared to those who had not (Nishihara et al., 2013). These data suggest that population screening with regular colonoscopies could reduce the healthcare burden and mortality by diagnosing malignancies at earlier stages. Several long-term

randomized trials are currently underway to investigate this more thoroughly, however this would be a relatively inexpensive intervention if the outcomes are promising.

CRC is a largely heterogenous disease that arises from the accumulation of gene mutations. While there does appear to be a genetic component to spontaneous CRC development, only a small minority of cases are caused by hereditary syndromes, such as Familial Adenomatous Polyposis (FAP) and Lynch syndrome, which are inherited with high penetrance (Brosens et al., 2015). These cancer syndromes have been widely studied and modelled by researchers as the genetic basis is often very similar in sporadic cases. For example, almost all FAP cases are caused by a germline mutation in the tumour suppressor gene Adenomatous Polyposis Coli (*APC*) that results in the development of numerous polyps (Jasperson et al., 2010). The APC protein acts to negatively regulate canonical Wnt signalling both directly and via interactions with β-catenin. This negative regulation acts to inhibit proliferation and promote differentiation or apoptosis of epithelial cells (Hankey et al., 2018). In patients with non-inherited colorectal cancer, genetic alterations in *APC* occur in around 80% of cases, likely as an initiating event. Paradoxically, both loss of tumour suppressive function and gain of function mutations in this gene can result in colon carcinogenesis. The role of APC as a tumour suppressor via inhibition of the Wnt pathway is well-established, and more recently it has been shown that truncation of APC can result in oncogenic function such as promotion of cell survival via direct regulation of cell cycle-associated molecules such as Bcl2 (Zhang and Shay, 2017).

It is well established that aberrant Wnt signalling, often due to mutations in the *APC* gene leads to the development of intestinal tumours. The laboratory of Hans Clevers extensively

studied this pathway and identified using *in situ* hybridisation that the Wnt target gene *Lgr5* was specifically expressed in the crypts of mouse intestinal epithelium. Furthermore, they showed that *Lgr5* was expressed in the polyps of $Apc^{Min/+}$ mice, a genetic model of FAP (Barker et al., 2007). The identification of these proliferative cells that are enriched in adenomas led the group to hypothesise that these *Lgr5+* crypt base columnar cells are the cell of origin for CRC. To investigate this further, the group specifically deleted *Apc* in *Lgr5*-expressing stem cells in mice. This led to rapid adenoma formation, with the stem cells remaining in the crypt and continually proliferating. In contrast, when *Apc* was deleted in transit-amplifying cells there was formation of a small number of microadenomas, and these were almost all lost at the villus tip (Barker et al., 2009). This suggests that in non-stem cell types there may need to be a secondary genetic mutation to cause progression of disease and persistence of tumours. While it is clear that abnormal Wnt signalling within *Lgr5+* stem cells can lead to the development of CRC, it has since been shown that these are not the only cell of origin. Bone morphogenetic protein (BMP) in the intestine is expressed in an opposing gradient to Wnt, where Wnt is highest at the crypt and BMP is highest at the villus tip. One mechanism of regulating the expression of BMP is via localised expression of antagonists, such as Gremlin1, which prevent BMP signalling within the crypt and promote the stemness of these cells. Dysregulation of the Gremlin1 gene (*Grem1*) in the intestinal epithelium of mice led to a process of dedifferentiation in *Lgr5*-negative cells and induced to tumour formation in locations outside the crypt niche (Davis et al., 2015). This works demonstrates that there are varied cells of origin for CRC, as with many cancers, and that there are likely several synergistic molecular pathways involved in the development and progression of the disease.

CRC cases can be classified in various ways dependent on the mutation rate, immune activity, or the type of molecular changes that have occurred. Consensus Molecular Subtypes (CMS) combine these factors into 4 subtypes of CRC. CMS1 are hypermutated tumours with microsatellite instability (MSI) and resultant strong immune activation. CMS2 are epithelial in their phenotype and have increased Wnt and Myc signalling and chromosomal instability (CIN), representing nearly 40% of cases. CMS3 is a smaller subset of patients, whose tumours also have an epithelial phenotype but are characterised by dysregulated metabolism. CMS4 patients make up around a third of cases and have a mesenchymal phenotype with transforming growth factor β (TGF-β) pathway activation, invasion into stroma and evidence of angiogenesis. There is a small group of patients that have mixed features, either representative of a phenotype present in transition between subtypes or heterogeneity within tumours (Guinney et al., 2015). This classification system has been useful from a clinical point of view in predicting which patients will likely respond to new treatments, particularly new immunotherapies.

Furthermore, another classification system that has shown to be useful in terms of predicting patient outcomes and response to new therapies is whether the tumour cells are proficient in mismatch repair (MMR). Mismatch repair deficiency occurs in around 15% of CRC cases, and this deficiency is what results in the hypermutated MSI subtypes. MMR is the process by which errors in a cell's DNA replication are first detected, the cell cycle is arrested and either the fault is corrected, or the cell undergoes programmed cell death (Poynter et al., 2008). Therefore, cells which are incapable of MMR are more likely to encode mutations and be transformed into malignant cells. MMR deficiency was first associated with hereditary colon

cancer following the identification of germline mutations in components of the MMR system in families with Lynch Syndrome patients (Fishel et al., 1993; Fredrick S. Leach et al., 1993).

It has been repeatedly shown that a western diet, particularly the amount of dietary fibre intake, is highly related to prevalence of colorectal cancer. This, in addition to the fact that diseases such as colitis are also clear risk factors for the development of colorectal cancer, has led many researchers to hypothesise a role for the microbiome in the development and progression of the disease (Kim and Lee, 2022). The human intestinal microbiome is intricately involved in gut homeostasis in terms of control of pathogens and maintenance of host immunity. While there has been no "smoking gun" signature of a carcinogenic microbiome, it has been shown that both the diversity and richness of microbes is reduced in patients with CRC compared to healthy controls (Chen et al., 2012). One widely researched microbe is the gram-negative anaerobe *Fusobacterium nucleatum* subsp. nucleatum (*F. nucleatum*). This is an oral commensal that was observed to be enriched in human colorectal tumour samples compared to adjacent healthy tissue (Castellarin et al., 2012). *F. nucleatum* can adhere to and invade epithelial cells via expression of an adhesin, FadA which is expressed on the bacterium's surface. It was later shown that *F. nucleatum* stimulated proliferation of human CRC cell lines *in vitro*, in a FadA-dependent manner. Furthermore, this effect was specific to CRC cells, with no effect seen in the immortal human kidney cell line HEK293. Co-immunoprecipitation assays demonstrated that FadA could bind directly to E-cadherin on the surface of the CRC cells and promoted cell proliferation via activation of E-cadherin signalling (Rubinstein et al., 2013). These data suggest that there can be a causal role for microbes in CRC progression *in vitro*, however due to high variation between individuals and myriad

external influences it is difficult to determine to what extent dysbiosis is symptomatic of CRC compared to having a causative role in tumorigenesis.

1.2 Current treatments for CRC

Currently the standard of care for CRC patients is initial surgery to resect the primary tumour, with adjuvant chemo or radiotherapy depending on tumour location along the large intestine; however, this is not curative in patients with metastatic disease. Surgical intervention has around 90% 5-year survival rates for patients with mucosa-localised early disease. However, a quarter of patients initially present with metastatic disease, with this rising to approximately 40% one year after diagnosis (Vatandoust et al., 2015). The survival rate following surgery dramatically decreases once the disease is metastatic; chemotherapy is approved and moderately efficacious for regionally metastatic CRC, but in cases with distant metastases this is ineffectual (Siegel et al., 2020). Metastatic disease is unfortunately very common in CRC compared with other malignancies and there is some evidence that this occurs early in disease progression. The most common site for metastasis is the liver, likely due to the liver's venous blood supply draining from the colon. Recent work performed whole exome sequencing of primary and paired metastatic tumours of a cohort of CRC patients. They then utilised a bioinformatic framework to identify that in over three quarters of the patients tested there was an early seeding event of metastasis before the primary tumours were clinically detectable (Hu et al., 2019).

The enormous amount of literature which details various subtypes present in the population of CRC patients and their cancer's molecular basis, outcomes and immune phenotype has been instrumental in aiding research into new therapy options. Immunotherapy for CRC is a

large area of research, however current advances are largely beneficial only to the minority of patients with MSI-high cancers with MMR deficiency. Microsatellite instability results in the expansion or contraction of repeated microsatellite regions, a process that tends to result in frameshift mutations. This type of mutation is particularly likely to give rise to novel amino acid sequences, and therefore generate neoantigens which can then be targeted by immunotherapeutic approaches (Mlecnik et al., 2016). It has been demonstrated that characterisation of the immune infiltration of human colorectal cancers is more predictive of patient outcome than classical staging/classification. For example, it was shown that increased densities of CD3+ cells is correlated with outcome better than tumour invasion/differentiation and node invasion/mutational burden (TNM staging) (Galon et al., 2006). Therefore, ideal patient targets for immunotherapy are MSI-high patients, which are likely to express tumour-associated neoantigens, who have a high number of CD3+ cells. These tumours have immune infiltrate, it is just not being appropriately activated.

Immune checkpoint inhibitors (ICIs) are a huge area of research in the field of cancer treatment, and there has been success in using some ICIs in those previously described immune “hot” subtypes of CRC. ICIs prevent the interaction of checkpoint proteins and their adaptor proteins in immune cells, therefore boosting the adaptive immune response within the tumour microenvironment (Kumar et al., 2023). The co-inhibitory immune receptor programmed cell death protein 1 (PD-1) and its interacting proteins programmed cell death ligand 1/2 (PD-L1/PD-L2) are widely researched ICI targets. PD-1 and PD-L1/PD-L2 are often overexpressed in CRC, limiting the function of cytotoxic T-cells and negatively impacting patient survival. Therefore, inhibition of this pathway is an interesting therapeutic target in CRC patients with high levels of T-cell infiltration (Kitsou et al., 2020). A clinical trial using a

monoclonal antibody, Nivolumab, directed against PD-1 as a therapy for metastatic MSI-high patients has led to approval of its use for this specific subset of patients (Overman et al., 2017). Other clinical trials have been investigating combination checkpoint therapy, for example treatment using both Nivolumab and Ipilimumab, an antibody directed against another inhibitory receptor expressed by T-cells, Cytotoxic T-lymphocyte associated protein 4 (CTLA-4). The same group demonstrated this approach led to generally improved patient outcomes. This trial also looked at this combination therapy in patients with microsatellite stable (MSS) tumours, but no benefit was observed. This further demonstrates that the majority of CRC patients will likely not be strong candidates for classical immunotherapy (Overman et al., 2018). While microsatellite-stability and MMR status is useful in terms of predicting whether a patient will respond to ICIs, it is not an absolute determinant. A low level of clinical response has been observed in some MMR-proficient patients treated with checkpoint blockade. Early-stage colorectal cancer patients were treated with neoadjuvant combination immunotherapy of Ipilimumab and Nivolumab, and infiltration of CD8+ T-cells and slight reduction of tumour size was observed but this was much less effective than in the MMR-deficient cohort (Chalabi et al., 2020). Identification of further biomarkers such as the immunoscore of a patient's tumour are essential for understanding the mechanisms that dictate patient response to immunotherapy (Huyghe et al., 2019).

Monoclonal antibodies targeting non-immune related molecules are also being trialled in various cancers, including CRC, and this aims to overcome the MSI/MSS issues of immunotherapy. For example, use of monoclonal antibodies targeting Epidermal Growth Factor Receptor (EGFR) have shown good clinical benefit in patients with metastatic colorectal cancer, dependent on the patient's *KRAS* and *BRAF* mutation status (Lièvre et al., 2006).

Briefly, the mechanism of action of the EGFR-targeted antibody Cetuximab is that it competitively binds to EGFR, inhibiting the phosphorylation of EGFR and the downstream effects, such as activation of the mTOR and MAPK pathways. Panitumumab is a humanised monoclonal antibody against EGFR which has similar pharmacological effects to Cetuximab, however it is more commonly used in combination with other chemotherapies (Li et al., 2020). Mutations resulting in genetically altered components of the EGFR signalling pathway reduce the effectiveness of these therapies as the antibody can no longer competitively bind and inactivate signalling. Patients harbouring mutations in genes that confer resistance to this treatment represent upwards of 60% of CRC cases. This again is an example of novel therapies being successful in only a minority of CRC patients, due to a high level of inter-patient heterogeneity. Therefore, in order to develop effective new therapies and target them to specific individuals, it is imperative that researchers generate effective ways to model CRC which recapitulate treatment resistance factors such as tumour microenvironment and patient heterogeneity.

1.3 Modelling CRC in research

Representative disease models are an essential part of research, from understanding of disease progression to trialling therapies. As discussed above, human CRC is diverse in the genetic mutations, disease presentation and responsiveness to treatment and thus there are myriad ways that researchers model disease both *in vivo* and *in vitro*.

Adherent colorectal cancer derived cell lines provided the field with much of the fundamental molecular and genetic understanding we rely on today; however, they fail to fully recapitulate the complexity of human cancer. The identification and purification of intestinal stem cells directly led to the generation of complex organoid cultures (Barker et al., 2007; Sato et al.,

2009). Organoids are 3D recapitulations of the organs they are derived from that consist of heterogenous cell populations arranged in the physiological architecture of that tissue – for example crypts and villi occur in small intestinal organoids. It is worth distinguishing organoids from the simpler, earlier spheroid cultures which are 3D monocultures that lack the cell-type heterogeneity of organoids (Porter et al., 2020). Further work identified the optimal culture conditions that allowed for the long-term culture of intestinal tumour organoids, this allowed for more robust interrogation of specific tumours over subsequent passages rather than repeated need for fresh tissue to isolate new organoid structures (Sato et al., 2011). For colorectal cancer modelling, groups have generated organoids from various mouse models of colon and small intestinal tumours, as well as generating human patient-derived tumour organoids. These represent an opportunity to trial therapies *in vitro* on a library of patient organoids that more accurately depict the diversity of human cancers (Van De Wetering et al., 2015).

Organoids may begin to close the gap between observations made in heavily passaged cell lines and analysis of *ex vivo* tissue samples, but they still do not entirely portray the complexity of the tumour microenvironment. *In vivo* animal models of colorectal cancer have the benefit of being less static and can encompass the full complement of immune cells and surrounding supporting cells. The most rudimentary examples of *in vivo* models for colorectal tumours are heterotopic transplant of cell lines. This involves the injection of established cancer cell lines subcutaneously, often in the flank, of mice and allow a tumour to develop. This has the advantages of being time efficient, easy to manipulate and administer, and can be assessed visually throughout development. While there has been some accurate prediction of clinical response to therapies using such models there are significant limitations. Engraftments are

usually derived from historical, highly passaged cell lines which are largely homogenous and do not represent the heterogeneity of human colorectal cancer or the tumour microenvironment. An improvement over this is patient-derived xenograft models, which involve the transplantation of patient tumour tissue subcutaneously into the flank of immunodeficient mice. This technique was shown to retain the range of genetic alterations that are present in human CRC (Katsiampoura et al., 2018), however it is only feasible in immunocompromised mice and therefore cannot entirely recapitulate the tumour microenvironment. This has obvious limitations in trialling the use of therapies aimed at stimulating an immune response to the tumour.

In addition to transplant models, advances in genetic engineering in the last century have allowed for modelling of specific genetic mutations which have been identified to trigger CRC development in patients. An example of this is the $Apc^{Min/+}$ mouse which is a strong model of human FAP. This model was first generated in 1990 via the potent mutagen ethylitrosourea inducing a non-sense mutation in the *Apc* gene which resulted in a truncation of the APC protein (Moser et al., 1990). It was observed that this mutation caused formation of multiple intestinal adenomas, which are prone to loss of heterozygosity in *Apc*. Mutations in *APC* are thought to be driver mutations in a majority of human CRC cases, and therefore this model is useful not only for research into FAP but also sporadic tumour development and treatment. *In vivo* models such as this more accurately represent the whole tumour biology, as the tumours arise in the correct anatomical region along with immune infiltration and genetic components. However, this model is restricted in that it only depicts *APC* mutation, not the secondary mutations in genes such as *KRAS* and *TP53.* Mice with multiple mutations have been generated to reflect more faithfully the stepwise acquisition of mutations in human cancer,

however the number of mutations possible in a mouse is limited due to it causing severely reduced lifespan (Bürtin et al., 2020).

Carcinogen-induced models of CRC are frequently used to induce different mutations, broadening the genetic landscape of the tumours that can be researched. One such method is the combination of the carcinogen azoxymethane (AOM) with the inflammatory chemical dextran sulfate sodium (DSS) to generate a colitis-associated cancer (CAC) model. The DSS acts to directly impair the colonic epithelium, causing a model of inflammatory bowel disease. As well as inducing variable mutations in some CRC associated genes such as *KRAS* and *β-catenin*, the added inflammation is representative of sporadic human CRC as colitis is often a co-morbidity in patients (Baker et al., 2019). Furthermore, there is also a role for chronic gut inflammation in actively promoting tumourigenesis (Eaden et al., 2001; Terzić et al., 2010). Colitis has been shown to cause increased IL-6 signalling and thus STAT3 activation, driving increased proliferation in the gut (Grivennikov et al., 2009).

1.4 Bacterial cancer therapy

Bacterial cancer therapy (BCT) dates back to the late 19th century, where a physician named William Coley observed spontaneous regression of tumours in some cancer patients who contracted bacterial infections. He took this observation further and developed "Coley's toxin", a mixture of bacteria and bacterial lysates, and injected this directly into tumours and again saw cases where the tumours regressed (W.B. Coley, 1912). This was later refined to a safer mixture of heat-killed bacteria which were successfully used to treat a variety of cancers (McCarthy, 2006; Hoption Cann et al., 2003). Despite having resolved the issue of symptomatic infection by using inactivated bacteria there was still a degree of scepticism around use of BCT. The development of chemo- and radiotherapy led to this field stalling until recent years.

Interest is now growing again due to advances in microbiology and genetics allowing for more sophisticated bacterial agents to be developed (McCarthy, 2006).

Currently the only approved use of BCT clinically is the Bacillus Calmette-Guerin (BCG) vaccine for superficial bladder cancer. This has been used as a routine treatment for around 40 years, despite its mechanism of action not being fully understood. There are several gaps in the knowledge about the process by which the bacteria, the vaccine strain of *Mycobacterium bovis*, exert anti-tumour effects but the ability to stimulate the immune system is reasonably well documented. It was initially reported in 1990 that physical attachment of the bacteria to the urothelial cells in the wall of the bladder was essential for starting the anti-tumour effect (Kavoussi et al., 1990). It was later elucidated that BCG antigen 85 complex is the fibronectin binding protein of the bacteria and posited as one of the targets of the T-cell response (Zlotta et al., 1997). After attachment, the bacteria are internalised, digested and the fragments are captured by antigen presenting cells. This in turn causes a recruitment of immune cells to the bladder and a type 1 cytokine immune response (Han et al., 2020). It has been shown that neutrophil recruitment is one of the first key events in successful therapy; within the first few hours after treatment there is a large number of white blood cells present in the urine of patients, and the vast majority of these are neutrophils (Simons et al., 2008). These neutrophils have been shown to be recruited by release of IL-8 directly from the urothelial cells following BCG treatment and are the major source of TNF-related apoptosis-inducing ligand (TRAIL). The release of TRAIL acts to induce apoptosis and is thought to be instrumental in the initial response to BCG vaccine in bladder cancer cells (Ludwig et al., 2004). At present it is still debated whether the anti-tumour response is targeted or the consequence of a general local increase of immune activation. However, there is evidence that this is a tumour-

specific immune response which is dependent on T-cells. One group demonstrated that antibody depletion of CD4+ or CD8+ T-cells abolished the anti-tumour effect of BCG vaccine in a murine model of bladder cancer. They then demonstrated that this clearance of tumours was dependent on tumour-specific not BCG-specific T-cell responses. Mice which were cured of bladder cancer by BCG vaccine were completely resistant to rechallenge with the same line of bladder cancer cells, but not resistant to implantation with B16F10 melanoma cells. Furthermore, they demonstrated that transfer of T-cells from mice cured of bladder cancer with BCG vaccine into naïve tumour bearing mice were able to clear these tumours also, and this was not the case for T-cells transferred from non-tumour bearing mice treated with BCG (Antonelli et al., 2020). These data suggest there is a tumour-specific response that can confer immune memory to subsequent tumours.

The anatomical properties of the bladder make it an optimal organ for the use of BCT, via intravesical administration, and treatment usually follows surgical resection of the tumour. BCG is directly administered to the bladder via a catheter, held there to maximise interaction of the bacteria with the cancer cells before excretion. The hollow structure with the urethra means that the bacteria is well restricted physically, limiting systemic spread and infection (Fuge et al., 2015). Lessons learned from BCG vaccine mediated therapy may be used to optimise BCT for other solid tumours. Importantly, intravesical delivery of BCG acts to maximise contact between bacteria and tumour cells, reminiscent of the early intratumoral delivery of Coley's toxin. We hypothesise that use of oral delivery of bacteria such as *Salmonella enterica* serovar typhimurium (*S*Tm), which naturally infects via the intestinal epithelium ideally match the target of CRC.

It has been shown repeatedly that various strains of bacteria, including *Escherichia coli* (*E. coli*) and *Salmonella* typhimurium can selectively home to and colonise tumour tissue when delivered systemically in mouse models of cancer. Despite advanced methods of imaging bacteria *in vivo*, there is still debate about the processes by which this selectivity occurs. Obligate anaerobes (such as *Clostridium* and *Bifidobacterium*) cannot survive in oxygenated tissue, and thus they are primed to colonise the deep, hypoxic regions of tumours (Forbes, 2010). The more commonly researched facultative anaerobes can survive in normal tissue, and yet still preferentially colonise tumour tissues – it is thought this occurs through several combined mechanisms. In experimental models, BCT agents are often delivered systemically via intravenous injection, and it is thought that there is a somewhat passive accumulation of bacteria in the tumours due to increased vascularisation in solid tumours - with leaky vessels that allow increased extravasation into the tissue that does not occur so readily in normal tissue. Imaging of light-emitting strains of attenuated *S*Tm, *E. coli* and *V. cholerae* following injection into mice with various tumours demonstrated that there was colonisation of tumours, but also of wound sites – suggesting that damaged vessels indeed allow colonisation of tissues (Yu et al., 2004). There is also conflicting evidence that bacteria use chemotactic gradients to detect and migrate towards tumours *in vivo*. It was demonstrated *in vitro* using wild-type *Salmonella* that there was accumulation around the edges of tumour cylindroids before invasion, but this study lacked the control of cylindroids derived from normal cells and thus the bacteria may be attracted the mammalian cells non-specifically (Kasinskas and Forbes, 2006). A later study utilised a range of mutant strains of *Salmonella* and *E. coli* and demonstrated that deletion of genes involved in chemotaxis or motility did not significantly impair colonisation of 4T1 mammary tumours *in vivo*. However, they observed reduced

colonisation of these tumours when macrophage populations were depleted in the mouse, suggesting that dissemination via phagocytes is involved following intravenous bacterial delivery (Stritzker et al., 2010). It is likely that *in vivo* there are a range of influences on the bacteria that facilitate this preferential invasion of tumour tissue, and that the type of bacteria, what attenuations it has, and route of delivery impact the process by which this colonisation occurs.

1.5 *Salmonella* typhimurium

Salmonella are flagellated, gram-negative bacteria which are facultative anaerobes belonging to the *Enterobacteriaceae* family. Within the *Salmonella* genus is the species *Salmonella enterica* which can cause infection in warm-blooded animals, including humans. *Salmonella enterica* is further divided into over 2000 serovars, which can largely be classified as typhoidal or non-typhoidal (Gal-Mor et al., 2014). *Salmonella enterica* serovar typhimurium is a non-typhoidal serovar which is known to cause gastroenteritis in humans and typhoid-like illness in mice (Fàbrega and Vila, 2013; Chaudhuri et al., 2018).

As previously stated, *Salmonella enterica* are gram-negative bacteria which are characterised by the structure of their cell wall **(Figure 1.5.1)**. This is composed of inner and outer membranes and a peptidoglycan layer. These complex layers are specialised to enable the bacterium to selectively uptake essential nutrients and release metabolic waste while physically protecting the cell against the highly varied environments it encounters throughout its life cycle. The inner membrane is composed of a phospholipid bilayer. Unlike eukaryotic cells, bacteria lack intracellular organelles and instead the inner membrane is the site of many of the functions we associate with membraned organelles. These functions include energy

production, lipid biosynthesis and protein transport (Silhavy et al., 2010). Between the inner and outer membranes is an aqueous space termed the periplasm, which is a matrix-like compartment that is rich in proteins (Silhavy et al., 2010; Liu et al., 2016a). Finally, there is the outer membrane which is composed of an inner leaflet of phospholipids and an outer leaflet of glycolipids. Some of the proteins in the outer membrane include porins that act to diffuse small molecules across the outer membrane layer. The outer membrane acts as a protective barrier for the bacterium and has an underlying peptidoglycan layer that gives *Salmonella* its rod-like shape and rigidity (Silhavy et al., 2010). One major component of the outer membrane is lipopolysaccharide (LPS). LPS acts not only as a structural component of the *Salmonella* outer layer, but also as a virulence factor that modulates the host immune response during infection (Bertani and Ruiz, 2018). LPS is composed of lipid A, an oligosaccharide core and repeated units of O-antigen. Lipid A is a glucosamine disaccharide that anchors LPS within the outer membrane and provides a permeability barrier to protect the bacterium against molecules such as antibiotics (Kong et al., 2012). O-antigen is the outermost part of LPS, and has thus evolved highly diverse structures to evade immune detection (Bertani and Ruiz, 2018).

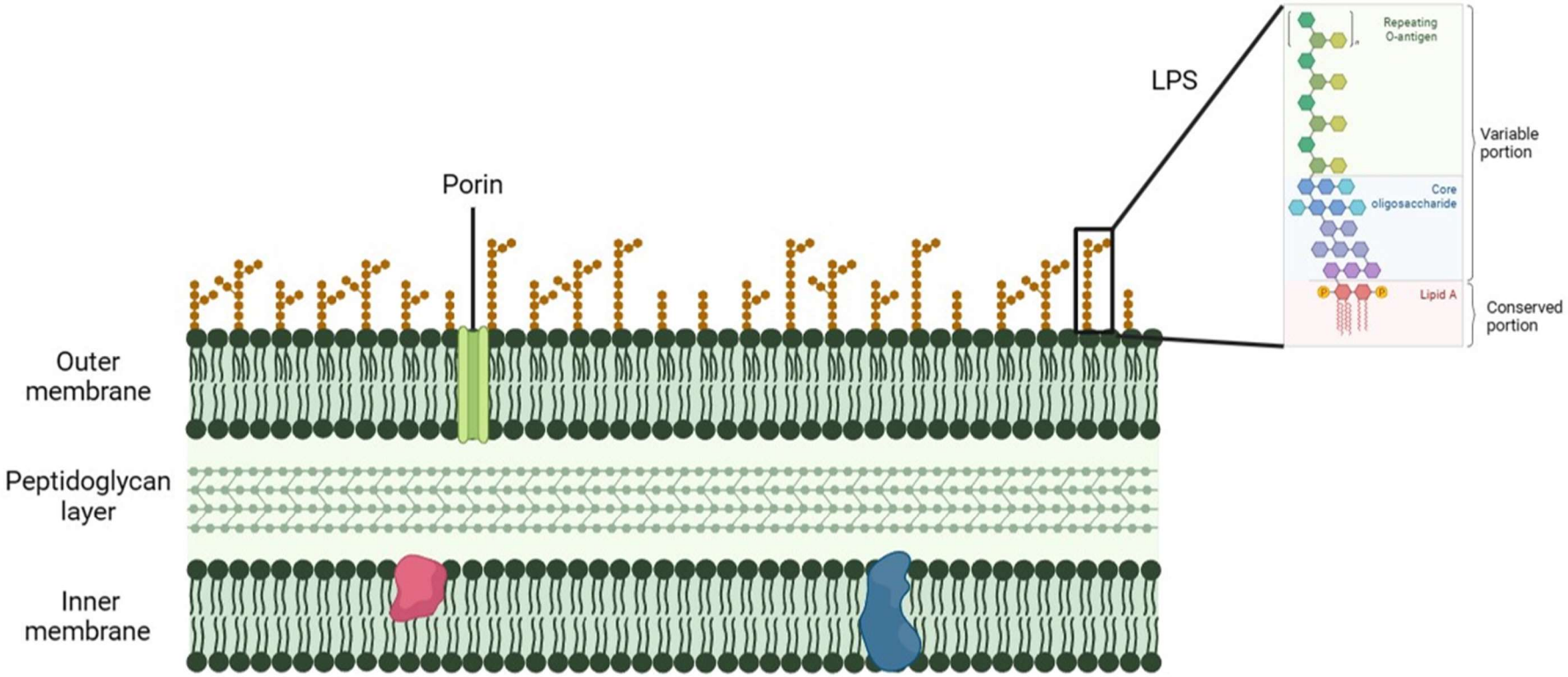


Figure 1.5.1: The structure of Salmonella typhimurium cell wall.

Depiction of the gram-negative cell wall of Salmonella. The inner membrane is a phospholipid bilayer, separated from the outer membrane by a protein-dense peptidoglycan layer. The outer membrane is an asymmetrical membrane, with a phospholipid inner leaflet and an outer leaflet containing glycolipids, including LPS. The structure of LPS is highlighted on the right. Figure was created on Biorender.com using templates and adapted from (Liu et al., 2016a; Bertani and Ruiz, 2018).

*S*Tm are ingested, and then must overcome competition with resident microbiota, the mucus layer that protects the epithelium, presence of antimicrobial peptides and recruitment of immune cells in order to successfully colonise the gut. *Salmonella* have evolved several mechanisms by which they are adapted to overcome colonisation resistance conferred by host microbiota. Firstly, it was shown that avirulent strains of *S*Tm were outcompeted by host microbiota in mice unless there was co-infection with wild-type strain, or the mice had inflammation of the gut before infection. This work suggested that there is a role for the induction of inflammation in the ability of *Salmonella* to colonise a host (Stecher et al., 2007). It was later shown that *S*Tm, along with other pathogens such as *Campylobacter jejuni,* were able to utilise tetrathionate as an electron acceptor in a way that commensal species could not. Tetrathionate is a product of reactive oxygen species in sites of inflammation that is used by these bacteria to gain a growth advantage in anaerobic conditions (Winter et al., 2010; Liu et al., 2013). The evolution of the enzyme to utilise tetrathionate, which is lacking in commensal bacteria, is one way that the selection pressures of the inflamed gut are used to the advantage of some pathogens such as *Salmonella* typhimurium.

There are a few separate routes of intracellular infection for *Salmonella* typhimurium which are governed by different uptake methods **(Figure 1.5.2 A)**. Firstly, in the small intestine microfold cells take up and transport *S*Tm across the epithelial barrier via transcytosis. The steady state role of microfold cells is to sample antigens from the gut lumen and transport these across to waiting lymphocytes (Nicoletti, 2000). However, it has been shown that *Salmonella* can have a cytotoxic effect on microfold cells and breach of the barrier in this manner can lead to bacterial spread and systemic infection (Jones et al., 1994). A second route of infection is phagocytosis of the bacteria by macrophages and dendritic cells. Once engulfed,

Salmonella upregulates the *Salmonella* pathogenicity island 2 (SPI-2) encoded type-3 secretion system (T3SS). The intracellular bacteria reside and replicate in a *Salmonella*-containing vacuole (SCV) which is maintained by virulence factors encoded in the SPI-2 T3SS. This is a specialised compartment which aids intracellular *Salmonella* in avoiding killing by the phagocytes (Haraga et al., 2008; Broz et al., 2012).

1.5.1 Salmonella typhimurium infection of intestinal epithelial cells

Salmonella typhimurium can also directly invade intestinal epithelial cells (IECs) via their apical membrane utilising SPI-1 encoded T3SS, which is activated upon contact with the host cell and aids both adherence to and invasion of these cells. Interestingly, this T3SS is essential only for invasion occurring via the intestinal epithelium **(Figure 1.5.2 B)**. It was shown that bacteria deficient for components of the SPI-1 T3SS (*invA/B/C)* were attenuated only when mice were treated orally, with no difference to colonisation or virulence when mice were treated systemically with these mutants (Galan and Curtiss III, 1989). The SPI-1 T3SS is also called the needle and rod complex due to its structure; this T3SS is composed of rings of proteins within the two membranes of the bacterium around an inner rod (PrgJ), with a hollow needle that projects out and contacts the host cell. At this point of contact, there is a family of proteins termed the translocon, which facilitate and regulate secretion of effectors into the host cell (Lou et al., 2019; dos Santos et al., 2019) **(Figure 1.5.3)**. In addition to its role in epithelial cell invasion, the SPI-1 T3SS has also been shown to suppress the early production of proinflammatory cytokines and in concert with SPI-2 T3SS to downregulate MHC-II expression in porcine macrophages (Pavlova et al., 2011; Parys et al., 2012).

Injection of bacterial effector proteins into mammalian epithelial cells acts to modulate host function to promote uptake and survival of the bacterium. Bacterial effectors influence a variety of processes and are activated at specific times during invasion (Galán, 2021). A key role of various bacterial effectors, such as SipA/SipC/SptP and Sop family members, is the ability to remodel the cytoskeleton of host cells. This process acts to promote internalisation by targeting the actin cytoskeleton (SipA/SipC/SopE) and induce membrane ruffling which leads to macropinocytosis. These effectors are then also involved in the generation of the SCV in non-phagocytic cells (Que et al., 2013; Lou et al., 2019). In addition, some effectors act to promote survival of the bacteria by inhibiting cell death and activation of innate immune pathways within the host cells. For example, SopB has been shown to induce phosphorylation, and thus activation, of Akt in infected HeLa cells (Steele-Mortimer et al., 2000). Activated Akt acts to promote survival via inhibition of apoptosis pathways, therefore maintaining a viable cell for the *Salmonella* to replicate in. In addition, AvrA is another SPI-1 effector protein which acts to maintain epithelial cell survival by limiting inflammation. *Salmonella* deficient for AvrA have increased dissemination in mice and increased cytokine release, leading to faster mortality (Lu et al., 2010). In summary, *Salmonella* typhimurium has a highly regulated process by which it intimately regulates IEC signalling to promote its own survival within the intracellular niche.

As described, the invasion machinery of *Salmonella* typhimurium is highly evolved to allow colonisation of the host, but the gut epithelial cells are also specialised to enable detection of pathogens and restrict the spread of infection. Intestinal epithelial cells express transmembrane and intracellular pattern recognition receptors (PRRs) which act to detect bacterial proteins and alarm signals from neighbouring infected/dying cells – pathogen-

(PAMPS) and damage- associated molecular patterns (DAMPS) respectively. There are 4 main families of PRRs, which are: Toll-like receptors (TLRs), nucleotide-binding oligomerization domain-leucin rich repeats-containing receptors (NLRs), retinoic acid-inducible gene 1-like receptors (RLRs) and C-type lectin receptors (CLRs) (Walsh et al., 2013). PAMPs are ligands for specific PRRs, and these include bacterial RNA or effector proteins in the cytoplasm of host cells or structural bacterial components such as flagellin and LPS in the bacterial outer membrane. Activation of PRRs in IECs results in inflammasome formation and activation. The inflammasome is a multi-protein complex which is composed of the PRR, adaptor proteins and inflammatory caspases, activation of which leads to restriction of infection via cell death (Amarante-Mendes et al., 2018; Ménard et al., 2022). Canonical inflammasome (NAIP/NLRC4 in IECs) signalling can induce caspase-dependent cleavage of pro-IL-1β, pro-IL-18 and Gasdermin D, the latter of which forms a pore that facilitates cytokine release (Rauch et al., 2017; Fattinger et al., 2021). By and large, the type of cell death induced by canonical inflammasome signalling is dependent on which caspases are activated. Activation of caspase-1 classically results in lytic, inflammatory cell death such as pyroptosis, whereas recruitment and activation of caspases-3/-7/-8 induces apoptotic cell death (Fattinger et al., 2021b). There is evidence of crosstalk and overlap between these caspase-induced pathways in macrophages and it has been posited that this is also the case in IECs (Christgen et al., 2020). Non-canonical inflammasome activation occurs when cytosolic LPS is detected directly by caspase-11 in mice and their human orthologues capase-4/5, this again results in Gasdermin D cleavage and pore formation leading to pyroptosis (Knodler et al., 2014). All these complex signalling pathways act to limit the spread of *S*Tm by inducing inflammation and cell death,

which leads to expulsion of infected cells into the gut lumen (Sellin et al., 2014; Rauch et al., 2017).

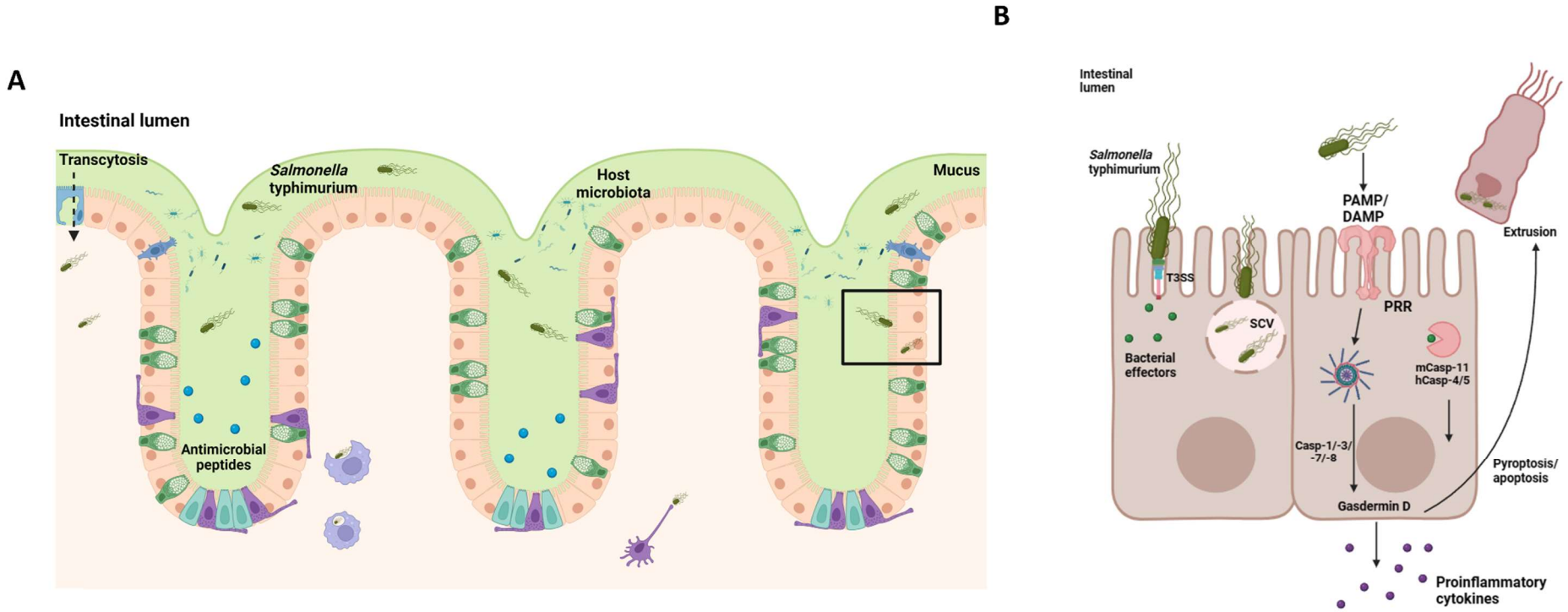


Figure 1.5.2: Schematic of Salmonella typhimurium pathogenesis in the gut
(A) *Overview of the intestinal compartment during infection by Salmonella typhimurium. Cells highlighted in the box are shown in* ***(B)*** *Details of infection of specifically intestinal epithelial cells by STm. Effects directed by the bacteria (left) and detected by the epithelial cell (right). Figure was created on Biorender.com and adapted from (Broz et al., 2012; Fattinger et al., 2021b; Galán, 2021).*

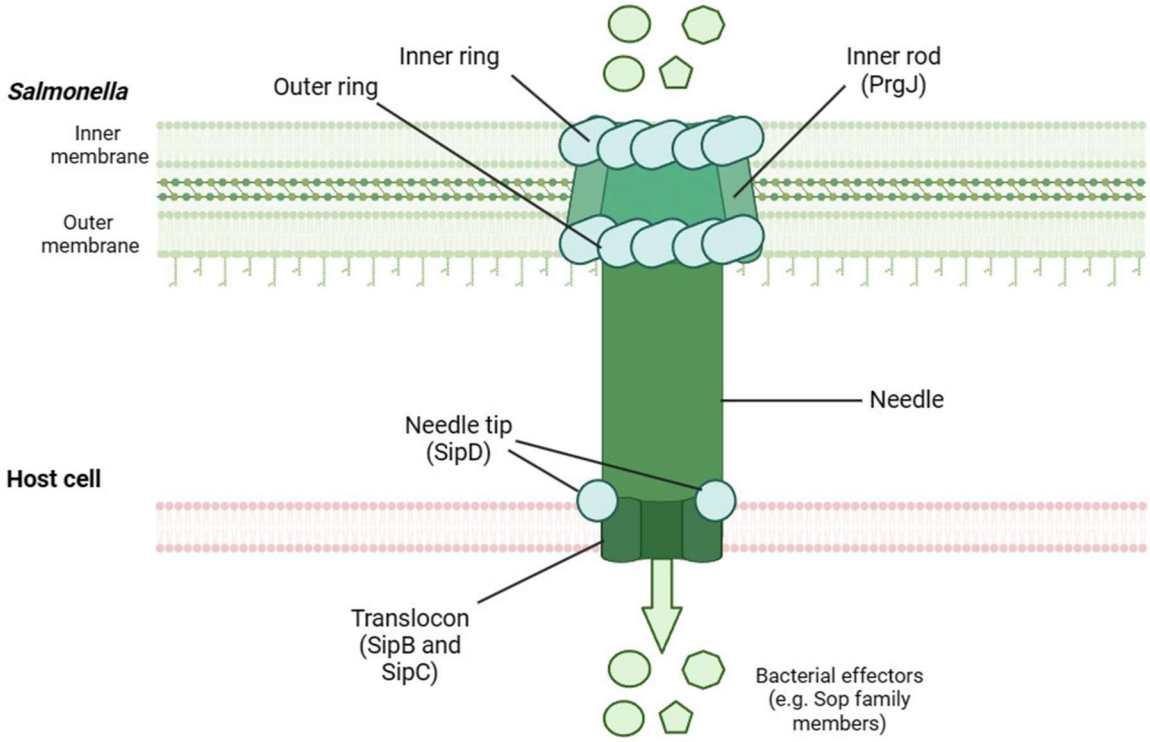


Figure 1.5.3: The structure of the type-3 secretion system of Salmonella typhimurium.
Depiction of the 'needle and rod' type-3 secretion system complex encoded by the Salmonella pathogenicity island 1 that facilitates invasion of intestinal epithelial cells. Rings of adaptor proteins form in the two membranes of the Salmonella cell wall around the inner rod, from which the hollow needle projects to contact the host cell. At the point of contact, Sip family proteins form the translocon that regulates delivery of bacterial virulence factors, such as Sop family proteins, into host cells. Figure was created on Biorender.com and adapted from (Lou et al., 2019).

1.6 Attenuated *Salmonella* typhimurium as an agent in BCT

Salmonella typhimurium is one of the most widely researched bacteria for the purpose of BCT, one of the reasons for this being that several effective and safe vaccine strains have been developed that are subsequently being investigated as vaccine carriers and as BCT agents. The trade-off that must be negotiated in generating bacteria to use in BCT is that they must be invasive and pathogenic enough to stimulate a response in the tumour, but not so immunostimulatory that they are cleared before an effect is seen or cause symptoms of infection in patients. *S*Tm is an interesting candidate for a BCT agent as it has been shown to be tumour-targeting *in vivo* (Pawelek et al., 1997); the exact mechanism of this selectivity is still unclear. It is possible that the bacteria favour the tumour microenvironment (TME) as it is enriched for various metabolites and that local immune suppression in the TME prevents clearance. *S*Tm are also facultative anaerobes, allowing them to colonise both normoxic and hypoxic regions of the tumour. There is a benefit to *S*Tm being an intracellular pathogen – several studies have modified strains to deliver anti-cancer therapeutics, such as encoding short hairpin RNAs to directly silence genes once the bacteria invade tumour cells or to deliver prodrugs which are activated in hypoxic conditions in the tumour core (Zheng and Min, 2016).

One commonly researched attenuated strain of *S*Tm, named VNP20009, was generated by chromosomal deletion of two genes, *purI* and *msbB*. Deletion of these genes caused the bacteria to be auxotrophic for adenine and have reduced LPS toxicity respectively. These mutations were shown to be genetically stable and did not confer any antibiotic resistance. (Clairmont et al., 2000). In mice transplanted with either murine and human tumours, injections of VNP20009 showed selective colonisation of tumour over normal tissue and inhibited tumour growth (Luo et al., 1999). The success in murine cancer models lead to a

phase I clinical trial utilising intravenous administration of VNP20009 in a dose-escalation study in 24 metastatic melanoma patients and 1 renal cell carcinoma patient. Only two patients had detectable colony forming units (CFU) within tumours, these were those with highest dose of VNP20009, and no patients exhibited cancer regression (Toso et al., 2002). A second group aimed to improve burden by delivering VNP200009 over a longer period, but still intravenously, and again saw only 1 colony in 1 patient's tumour biopsy (Heimann and Rosenberg, 2003). It is likely the bacteria were cleared from the blood before they colonised tumours as the human complement system is more robust than that of mice – trials in rats may be more appropriate if intravenous administration is to be used (Bergman et al., 2000). It was also later identified that VNP20009 had defective chemotaxis as a result of a point mutation in the gene *cheY,* which may also have led to poor colonisation in the 2002 clinical trial (Broadway et al., 2015). These results suggest that over-attenuation in the case of this vaccine strain, while providing high degree of safety in humans, acts to also limit the therapeutic benefit.

Another attenuated strain of *Salmonella* typhimurium which has been widely researched is A1-R, which is auxotrophic for both Leucine and Arginine. This strain had direct cytotoxic effects on PC-3, a prostate cancer cell line, *in vitro*; A1-R invaded these cells and replicated in the cytoplasm where it induced nuclear fragmentation and cell death. The group then investigated the *in vivo* effect of A1-R and demonstrated specific colonisation of xenografted tumour tissue compared to adjacent normal tissue, and reduced tumour growth when delivered intravenously in mice. They also enhanced the effect of A1-R by delivering it intratumorally, where mice were completely cleared of the transplanted prostate cancer cells (Zhao et al., 2005). Furthermore, imaging of A1-R within the tumours showed it localised to

non-necrotic areas, which had previously been posited as a limitation of the therapy. Intratumoral delivery is an effective system for ensuring colonisation of tumours, but it has limited utility in many solid tumours due to lack of access.

Deletion of the shikimate pathway gene *aroA* is another common attenuation of *S*Tm, resulting in the bacteria being auxotrophic for aromatic amino acids. This has been shown to be a stable mutation that is non-virulent and confers strong vaccine properties to subsequent challenges from virulent strains (Hoiseth and Stocker, 1981). In addition to vaccine properties, *S*Tm$^{\Delta aroA}$ is a particularly interesting candidate for BCT as aromatic amino acids are not freely occurring in normal tissue but often highly concentrated at tumour sites, conferring selectivity of the bugs to colonise tumours over normal tissue (Deng et al., 2012). One group thoroughly screened *S*Tm$^{\Delta aroA}$ and identified that, similarly to VNP20009, deletion of *aroA* was associated with additional alterations in the expression of apparently unrelated genes, modulating its virulence. Metabolic screening in several mutant strains of *Salmonella* typhimurium demonstrated that deletion of specifically *aroA* had global effects on the metabolism of the bacteria. These effects included reduced incorporation of fatty acids and altered rates of synthesis for some amino acids compared to wild-type *Salmonella*. In addition, this group used transcriptome analysis of *S*Tm$^{\Delta aroA}$ and demonstrated differential expression of several genes, some not directly associated with metabolism. These genes included differential expression of flagellin-associated genes and virulence factors, including upregulation of *ansB* in *S*Tm$^{\Delta aroA}$ compared to an attenuated strain lacking *aroA* deletion. Finally, it was demonstrated that systemic delivery of *S*Tm$^{\Delta aroA}$ led to increased induction of Tumour Necrosis Factor-α (TNF-α) and Interferon-β (IFN-β) in mice, which was posited to be a result of altered expression of genes encoding virulence factors (Felgner et al., 2016). In summary, this group confirm that

deletion of *aroA* metabolically attenuates *Salmonella* typhimurium, but also has global transcriptional effects that appear to enhance the anti-tumour capacity of the bacteria without inducing symptoms of bacterial infection.

1.6.1 Review of Mackie et al., 2021 - 'Bacterial cancer therapy in autochthonous colorectal cancer affects tumour growth and metabolic landscape'

Previous published work in Kendle Maslowski's research group aimed to identify whether *S*Tm$^{\Delta aroA}$ could be an effective treatment for intestinal cancers in mice, and to what extent tumour-derived organoids could model the therapy *in vitro* (Mackie et al., 2021). BCG vaccine efficacy in bladder cancer has been shown to rely on direct contact of the bacterial agent with the urothelium (Kavoussi et al., 1990; Zlotta et al., 1997); therefore, the group utilised oral gavage of *S*Tm$^{\Delta aroA}$ as this is the natural route of infection, which it was posited would enable maximal contact of the bacteria with the tumour epithelium. Firstly, two autochthonous models of colorectal cancer, *Apc*$^{Min/+}$ and AOM/DSS CAC-tumour bearing mice, were utilised. Repeated oral gavage with *S*Tm$^{\Delta aroA}$ caused a reduction in the number and size of small intestinal polyps and colonic tumours in comparison to phosphate-buffered saline (PBS) treated littermates in both models. This delivery route also resulted in preferential colonisation of the tumour tissue over surrounding normal tissue, with little to no dissemination to other organs.

Normal and tumour tissue from *S*Tm$^{\Delta aroA}$ or PBS treated CAC-tumour-bearing mice was dissected out after 4 weekly gavages, RNA was isolated and then bulk RNA-sequencing was performed on the samples. Colonisation of the tumour tissue resulted in an altered transcriptional landscape of the tumours compared with normal tissue. Pathway analysis

revealed that *S*Tm$^{\Delta aroA}$ treated tumours were enriched for genes associated with regulation of mesenchymal cell proliferation and mesenchymal-epithelial cell signalling, and a reduction in genes associated with epithelial-to-mesenchymal transition. These data suggest that there is a restoration of epithelial cell phenotype rather than the disease-associated mesenchymal phenotype. Furthermore, there was a reduction in terms associated with cell cycle progression, DNA repair and DNA damage response, all of which suggest there is a reduction in the level of proliferation within the tumour following infection.

It is well documented that *Salmonella* can utilise host-derived metabolites such as ethanolamine, succinate, and lactate to confer a growth advantage during inflammation, and that this occurs in the context of at least ethanolamine use in solid tumours (Thiennimitr et al., 2011; Silva-Valenzuela et al., 2016; Spiga et al., 2017; Gillis et al., 2018). Therefore, it was hypothesised that the specific colonisation of the tumour by *S*Tm$^{\Delta aroA}$ would alter the tumour metabolome. To measure this, tumour and normal tissue were dissected out from PBS or *S*Tm$^{\Delta aroA}$ treated CAC-tumour-bearing mice 24 hours after the first gavage or after 6 weekly gavages. The tissue was then processed and analysed for polar metabolites using gas chromatography-mass spectrometry (GC-MS). Pathway analysis showed a significant effect of *S*Tm$^{\Delta aroA}$ treatment on metabolites involved in glycine, serine, and threonine metabolism; arginine and proline metabolism; and the citric acid cycle at both time points compared to PBS controls. Within these pathways oncometabolites, metabolic intermediates and vital tumour fuel sources such as glucose and glutamate were reduced after treatment, presumably via competition by the bacteria on the tumour for nutrients. Importantly, there was an immediate (within 24 hours of gavage) effect on the tumour metabolome that then persisted throughout the treatment course. These initial decreases therefore are occurring before there is a

detectable reduction in tumour burden or size, and so cannot be a result of less tumour tissue. The metabolic effects are then sustained throughout the treatment, it is at present not known whether the alterations in tumour metabolome are driving the anti-tumour response or a read-out of the colonisation of the tumour by the bacteria.

As discussed previously, there is a hypothesised role of the microbiome in the development and progression of CRC and a known dysbiosis induced in intestinal infection models. Thus, impact of oral gavage of *S*Tm$^{\Delta aroA}$ on the microbiota in CAC-bearing mice was assessed. 16s RNA-sequencing was performed on the colonic content of AOM-DSS treated mice after 6 weeks of treatment with PBS or *S*Tm$^{\Delta aroA}$. There was no significant difference in the overall evenness of microbial species at the time point measured and no difference in the richness, as measured by the number of observed operational taxonomic units. This is in contrast to the known impact of infection with wild-type *S*Tm, possibly a result of the localised colonisation of the tumour tissue. Furthermore, efficacy of *S*Tm$^{\Delta aroA}$ treatment in tumour bearing germ-free mice was investigated. The role of the microbiota in the efficacy of BCT is of particular importance in the context of CRC, as it is well established that patients have altered microbial composition in the gut and are also treated with antibiotics during conventional therapies which will induce further dysbiosis. Germ-free mice were hyper-susceptible to both DSS treatment and subsequent *S*Tm$^{\Delta aroA}$ gavage and for this reason the n numbers are very low for each group. With this caveat, there was striking clearance of tumours in mice treated with *S*Tm$^{\Delta aroA}$ compared to PBS treated controls. However, these mice also had wider dissemination of the bacteria to peripheral organs. This confirms the role of the microbiome in maintaining barrier integrity and may have implications for safety of BCT as an adjuvant

therapy; oral gavage in patients will likely need to be in the absence of any antibiotic treatment.

To assess the potential of organoids to model the mechanism of bacterial cancer therapy, tumour organoids were generated from both CRC mouse models and treated *in vitro* with *S*Tm$^{\Delta aroA}$. Bulk RNA-sequencing was again used to evaluate whether *in vitro* infection could recapitulate the transcriptional findings. Indeed, in both *Apc*$^{Min/+}$ and CAC-derived tumour organoids, similar genes were altered after treatment. Finally, the GC-MS screen was repeated on the PBS or *S*Tm$^{\Delta aroA}$ treated tumour organoids and similar reductions in the metabolites were observed *in vitro*. Organoid models therefore faithfully recapitulated both the *in vivo* transcriptional and metabolic observations. These data suggest that the therapy has an effect, at least in part, directly on the tumour epithelium as there were no immune or supporting cells in culture. The data in this paper demonstrate promising efficacy of *S*Tm$^{\Delta aroA}$ for treating intestinal tumours in mice, and that organoids are an effective model for this therapy. This is evidence which should be interrogated in human tumour models, including patient-derived organoids.

1.7 Enhancing bacterial cancer therapy

The direct cytotoxic effect of bacteria in bacterial cancer therapy is often debated, particularly with heavily attenuated strains such as VNP20009, and so their usefulness in combination with other therapies has also been researched. The combination of BCT with chemotherapy has been investigated in an attempt to facilitate the reduction of therapeutic dose and thus reduce side effects in patients. One group utilised *S*Tm$^{\Delta aroA}$ with a further mutation in *asd* (making it also auxotrophic for diaminopimelic acid) in an autochthonous mouse model of breast cancer,

BALB-neuT, where mice develop mammary tumours spontaneously over time. Mice were treated with PBS, high dose doxorubicin, reduced dose doxorubicin, attenuated *S*Tm alone, or *S*Tm plus reduced doxorubicin. Mice had the best reduction in tumour growth following high doxorubicin treatment, followed by reduced dose plus bacteria. In addition, mice tolerated the reduced dose of doxorubicin much better than high dose, with or without bacterial treatment as measured by lower precent weight loss in low dose mice (Saltzman et al., 2018). This suggests that the combination of BCT and traditional chemotherapies can be beneficial in tumour reduction, while also lowering the required dose for therapeutic benefit.

Furthermore, many groups have been investigating the possibility of engineering the bacterial agents to deliver gene therapies to tumours *in vivo,* for example with cargos targeted to induce expression of pro-apoptotic genes or pro-inflammatory cytokines (Baban et al., 2010). One such group demonstrated the ability of *S*Tm$^{\Delta aroA}$ to deliver shRNA targeting *Bcl2* expression in melanoma cells *in vitro*. They demonstrated significantly reduced mRNA and protein expression of Bcl-2 and concurrent increased apoptosis in B16F10 cells after treatment. They then demonstrated improved clearance of B16F10 in C57BL/6 mice compared to *S*Tm$^{\Delta aroA}$ alone or *S*Tm$^{\Delta aroA}$ containing scrambled shRNA following oral gavage (Yang et al., 2008). The limitation of such gene therapy delivery systems is that they rely on intracellular invasion of tumour cells and then lysis of the bacteria to induce their effects, and as such the low level of colonisation seen in patients compared to mice has again limited the translation of such work. One example of the translation of this therapy is a clinical trial in 2003 using VNP20009 engineered to express *E. coli* cytosine deaminase (CD), an enzyme which converts 5-fluorocytosine (5-FC) into 5-fluorouracil (5-FU) – a commonly used chemotherapy agent. 3 patients with advanced, therapy-resistant cancers were given one dose of

intratumoral VNP20009 expressing CD every 28 days (6 cycles), followed by 5-FC three times daily for 10 days on days 4-14. Two patients had persistent colonisation of the tumours that induced specific conversion of 5-FC to 5-FU in the tumour compared to the blood. The treatment was well tolerated but the results were not significant in the small number of patients tested and so the trial was discontinued (Nemunaitis et al., 2003). The intratumoral delivery of VNP20009 likely improved bacterial burden in the tumours, but there was still one out of three patients in which there was no detectable colonisation.

As previously discussed, gastrointestinal tumours frequently metastasise to the liver, and this form of CRC is difficult to treat. Wild-type *Salmonella* is known to disseminate from the intestine to both the spleen and liver in mice, and thus some groups have focussed on the use of *Salmonella*-mediated BCT for treatment of hepatic metastases (Dunlap et al., 1991). One group utilised the avirulent $_{\chi}$4550 strain of *S*Tm which was modified to intratumorally deliver recombinant IL-2 ($_{\chi}$4550 pIL-2) to treat a murine model of MC-38 hepatic metastases. Mice were treated with a single oral gavage of either $_{\chi}$4550 or $_{\chi}$4550 pIL-2, or no gavage as a control. There was persistent colonisation of both the liver and the spleen by both strains of $_{\chi}$4550, although the group could not demonstrate detectable levels of IL-2 in the tumour homogenates. There was significant reduction in the number of metastases only with $_{\chi}$4550 pIL-2, so the group concluded that there must have been production of biologically active IL-2 (Saltzman et al., 1996). This group went on to use antibody depletion of immune cell subsets to demonstrate in the same model that reduction of murine liver metastases by $_{\chi}$4550 pIL-2 is dependent on NK cells and CD8+ T cells (Daniel Saltzman et al., 1996). A recent phase-I clinical trial attempted to translate these promising pre-clinical findings into human disease. 22 patients with gastrointestinal tumours with solid liver metastases were enrolled into the

study, of these patients 14 completed the trial with the remaining succumbing to the cancer progression in the course of the trial. The trial again used a single dose of oral gavage of χ4550 pIL-2, with dose escalation across treatment groups. All patients tolerated the treatment with no adverse effects, including those with the highest dose. Based on the previous work, peripheral blood lymphocytes were measured before and 5 weeks post gavage and the group identified significant increases in NK and NK T cells, but no difference in CD8+ T cells at this time point. Unfortunately, there was no partial or full response in any of the patients (Gniadek et al., 2020). *Salmonella* typhimurium infection is known to vary between mice and humans (Galán, 2021); causing systemic disease in mice and mostly being restricted to gastroenteritis in humans and thus without measuring bacterial burden of the liver metastases it is impossible to know whether χ4550 pIL-2 colonised the tumours in patients and produced immunologically active IL-2 *in situ*. However, this study does show that oral gavage of engineered bacteria is well tolerated in patients.

Other groups in the field of BCT have been researching the potential to use the bacteria as a vector for generally cytotoxic compounds, thus targeting the tumour environment rather than limiting the therapy by dependency on invasion of tumour cells. One group engineered an attenuated strain of *Salmonella* typhimurium, deficient in guanosine 5'-diphosphate-3'-diphosphate synthesis (ΔppGpp), to express a cytotoxic protein (ClyA) under the P_{BAD} arabinose-inducible operon. This strain also contained a luciferase reporter, which allowed real-time imaging of the bacteria in the mice following intravenous administration into mice bearing sub-cutaneous CT26 colorectal cancer tumours. This allowed the group to selectively administer L-arabinose to activate expression of ClyA only when the bacteria had been cleared from peripheral organs and selectively colonised the tumour to prevent widespread toxicity.

The group demonstrated significantly improved tumour clearance in mice where ClyA expression was induced compared to *S*Tm$^{\Delta ppGpp}$ alone. Indeed, they also induced lung metastases in these mice and repeated treatment with the bacteria, showing colonisation and clearance of these distant tumours as well (Nguyen et al., 2010). This work shows proof of concept for the potential to enhance BCT with inducible cytotoxic compounds. Another study demonstrated that combining ClyA-expressing *S*Tm$^{\Delta ppGpp}$ with radiotherapy enhanced the reduction in the volume of flank-injected CT26 tumours in mice, although radiotherapy was associated with a reduction in bacterial counts (Liu et al., 2016b). The group did not normalise burden to tissue weight/size and therefore the reduced bacterial counts may be a result of reduced tumour volume. This suggests that there are viable options in enhancing the effect of both BCT and classical treatment options in patients by combining the two.

Recent advances in BCT have utilised the improving field of nanotechnologies to modify the bacteria to allow the delivery of therapies to tumour sites even more specifically (Liang et al., 2022; Yin et al., 2022). One group has utilised a strain of anaerobic magnetotactic bacteria found in freshwater and conjugated it with nanoparticles which can be optically activated. It was demonstrated that the bacteria could be manipulated in intricate directions using magnetic fields, *in vivo* this movement could be done at the microscale. They demonstrated that these bacteria could be directed to tumours and penetrate to the core of tumours in mouse models. The group then demonstrated that lasers directed at the tumour activated the coating of nanoparticles and induced hyperthermia, which ablated both tumours and the remaining bacteria (Xing et al., 2021). This is one example of a new aspect of bacterial engineering for cancer therapy that utilises intrinsic properties of different bacterial strains

and combines this with classical immunotherapies, chemotherapies and enhances the therapeutic benefit of each.

1.8 The immune response in bacterial cancer therapy

BCG vaccine mediated BCT is dependent on an intact immune system. However, this mechanism does not appear to wholly translate to *Salmonella*-mediated anti-tumour responses, as a dependence on innate but not adaptive immune cell populations and function has been revealed repeatedly in the literature. MyD88 is an adaptor molecule expressed primarily on myeloid cells which is involved in the transduction of detection of PAMPs and IL-1 cytokines by TLR-family members to upregulation of downstream effectors such as signalling via nuclear factor kappa-light-chain-enhancer of activated B cells (NF-κB) (Deguine and Barton, 2014). One group tested the relative necessity of various components of TLR signalling pathways in the efficacy of BCG vaccine treatment of bladder cancer by generating a series of knockout mouse lines. The only molecule which abrogated the effect of BCG vaccine when deleted on its own was MyD88, suggesting a redundancy in the direct sensors of BCG vaccine but a dependency on the downstream adaptor for the anti-tumour effect (de Queiroz et al., 2021).

The role for myeloid cells has also been confirmed for *Salmonella*-mediated cancer therapy. The attenuated strain *S*Tm$^{\Delta ppGpp}$ was induced to overexpress and secrete a payload of a different bacterial flagellin strain (FlaB) in the tumour microenvironment, a PAMP which is known to induce TLR5 signalling, resulting in inflammasome activation. FlaB was inserted into a vector containing the P_{BAD} promoter, meaning it is inducible upon L-arabinose treatment. The group demonstrated that TLR5 was not expressed at the surface of the cancer cell lines

used, only on macrophages. C57BL/6 mice were injected with subcutaneous MC38 colon cancer cell line, once this was established the mice were given intravenous *S*Tm$^{\Delta ppGpp}$ followed by intraperitoneal L-arabinose. Expression of FlaB in tumours enhanced the anti-tumour effect of *S*Tm$^{\Delta ppGpp}$. This effect was abolished in mice with MyD88-/- or TLR4-/- and significantly reduced in mice lacking TLR5. There was also reduced infiltration of monocytes and macrophages into TLR4-/- mice, and to a lesser extent TLR5-/- mice, following *S*Tm$^{\Delta ppGpp}$ treatment. A human colon cancer cell-line was also xenografted into nude mice and the therapeutic effect of FlaB-expressing *S*Tm$^{\Delta ppGpp}$ was recapitulated (Zheng et al., 2017). Furthermore, it was recently shown that *S*Tm$^{\Delta aroA}$ reduce tumour growth in mice in a monocyte-dependent manner. It was identified that there was significant influx of Ly6C+MHC-II+ monocytes following bacterial colonisation of the tumours and that they expressed a range of pro-inflammatory cytokines. Treatment of the mice with clodronate liposomes was shown to deplete this phagocytic cell population, and this resulted in *S*Tm$^{\Delta aroA}$ having no effect on tumour burden (Johnson et al., 2021). These data demonstrate a clear role for the innate immune system, particularly myeloid cell populations, in triggering therapeutic benefit of *Salmonella*-mediated BCT. In addition, we previously demonstrated that there was significant recapitulation of the *S*Tm$^{\Delta aroA}$-mediated effects on tumour growth, transcriptome, and metabolome *in vitro* (Mackie et al., 2021). This suggests that there is an intrinsic effect on the tumour cells themselves that is at least in part independent of classical immune cell recruitment and function.

As described above, there is a wealth of evidence that T-cells are dispensable for the therapeutic effect of *Salmonella*-mediated BCT – in fact, the therapeutic effects of many attenuated strains were screened in nude, athymic mice with xenografted tumours (Luo et al.,

2001; Zheng et al., 2017; Johnson et al., 2021). One of the important limitations of *Salmonella*-mediated BCT currently is that it has been shown that mice cleared of tumours do not have subsequent immunity when rechallenged. One group engineered an *aroA/aroD* mutant strain of *Salmonella* to express and secrete interferon-γ (IFN-γ) and this bacteria was able to completely cure 8 out of 10 mice of subcutaneous B16F10 melanoma tumours. These mice were then rechallenged with B16F10 cells and there was no protection against development of tumours, suggesting that there was no immune memory generated from this BCT therapy (Yoon et al., 2017). Recent work by our group has aimed to identify why there is this redundancy in the T-cell population and whether this can be overcome to increase the efficacy of *Salmonella*-mediated therapy. Using a mouse strain with a fluorescent reporter of T-cell receptor (TCR) activation in which AOM-DSS CAC was induced, we have shown that the tumour infiltrating T-cells in mice treated with *S*Tm$^{\Delta aroA}$ were indeed functionally defective. There was a range of defects, namely a decoupling in the production of IFN-γ from TCR activation, reduced range of cytokines produced and inhibition of T-cell memory induction after *S*Tm$^{\Delta aroA}$ treatment. These effects were demonstrated to be due to bacterial depletion of asparagine causing depletion of c-Myc in T-cells. Deletion of the asparaginase enzyme (ansB) in *S*Tm$^{\Delta aroA}$ fully restored T-cell function but this was at the cost of the intrinsic effect of *S*Tm$^{\Delta aroA}$ on the tumour epithelium (Copland et al., 2023). This work uncovers the mechanism by which *Salmonella* inhibit T-cells in the tumour microenvironment, as well as a bacterial strain to combat this and may aid the generation of immune memory, however the collateral cost likely reduces the early effectiveness of the therapy. It may be of interest to generate an inducible *ansB* mutant in which early clearance of the tumour is intrinsic and functional T-cells can be recruited later by induced deletion/suppression of the gene.

1.9 Project aims

In summary, bacterial cancer therapy using attenuated *Salmonella* represents a promising strategy for treating intestinal cancers. Two examples of the most successful uses of BCT are intravesical delivery of BCG for superficial bladder cancer and intratumoral injection of bacteria into solid tumours. We hypothesise that the success of these in part hinges on matching the bacterial agent to an appropriate route of delivery for the target tumour. Therefore, using oral gavage of *Salmonella* for tumours in the intestinal tract is a logical step, as this is a bacterial strain which naturally infects via the gastrointestinal tract. This project aimed to translate previous results utilising *S*Tm$^{\Delta aroA}$ in murine models of colorectal cancers into human patient-derived organoids. There is evidence that *S*Tm$^{\Delta aroA}$ has a direct effect on tumour cells as we have previously observed recapitulation of results seen in mouse models in tumour organoids. Further to this, we have observed that *S*Tm$^{\Delta aroA}$ treatment causes dynamic changes in gene regulation in mouse tumour models and hypothesise that this underpins intrinsic anti-tumour responses and may trigger immune-mediated responses. We aim to utilise sequencing techniques to understand the entire landscape of effects of *S*Tm$^{\Delta aroA}$ infection of tumours, both in mouse and human tumour organoids.

CHAPTER 2 - MATERIALS AND METHODS

2.1 Bacterial strains

Salmonella typhimurium deficient for *aroA* were used throughout, these are either strain SL3261 or UF20 (mCherry tagged, with Ampicillin resistance where specified). SL3261 was shared with us by Professor Adam Cunningham (Institute of Immunology & Immunotherapy, University of Birmingham). Deletion of *sipB* in strain SL3261 was used to generate *S*Tm$^{\Delta aroA \Delta sipB}$. *Salmonella* typhimurium strains with mutations in the genes encoding T3SS components *sipB/sipC/sipD* were on the 14028s background and shared with us by Dr Amanda Rossiter (Institute of Microbiology & Infection, University of Birmingham). These strains were originally generated as part of a mutant library and brought to the University of Birmingham by Dr Manuel Banzhaf who duplicated this library during work with Dr Athanasios Typas (Infection Biology and Microbial Ecosystems, European Molecular Biology Laboratory) (Porwollik et al., 2014).

2.2 Immunohistochemistry

Paraffin samples were generated from AOM-DSS experiments performed before I joined the lab (animal experiments by Dr Kendle Maslowski and slide preparation at the RIKEN Institute for Integrative Medical Science, Yokohama, Japan). Briefly, C57BL/6 mice were injected intraperitoneally with 10 mg/kg azoxymethane (Sigma Aldrich, cat# A5486). Mice were then given 3 rounds DSS treatment, where for 6 days drinking water was supplemented with 3% DSS (MP Biochemicals, cat# MFCD00081551), followed by 2 weeks recovery with normal drinking water. The mice were then given weekly oral gavage with either PBS or $5x10^9$ CFU

*S*Tm$^{\Delta aroA}$ for 6 weeks. Weight was monitored throughout to ensure mice tolerated the AOM-DSS and UF20 *S*Tm$^{\Delta aroA}$ treatment. Colons were then removed and rolled before overnight fixation in 4% paraformaldehyde (Sigma-Aldrich, cat# 158127) and embedding in paraffin. 5 µm sections were cut with a microtome and mounted onto slides.

I then dewaxed the slides and rehydrated through xylene and decreasing concentrations of ethanol. Antigen retrieval was done via boiling the slides for 15 minutes in 0.1 M, pH 6.0 citrate buffer (ThermoFisher, cat# 005000). Slides were incubated in 0.1% triton in PBS to permeabilise the sections. Non-specific antibody binding was blocked by incubation with 1% BSA/PBS supplemented with 5% normal donkey serum. Primary antibody incubation was performed overnight with goat anti-E-cadherin (R&D Systems, cat# AF748) and rabbit anti-ki67 antibody (Cell signalling technologies, cat# 12202). This was followed by 0.1% triton-PBS washes, secondary staining with donkey anti-goat IgG Alexa-Fluor 488 (Invitrogen, cat# A-11055) or goat anti-rabbit IgG Alexa-Fluor 568 (Invitrogen, cat# A11011) and counterstained with DAPI (Invitrogen, cat# D1306). Samples were imaged on a Zeiss Axio Slidescanner, and images processed using Zeiss ZEN Blue software.

Quantification of Ki-67 staining was performed by Dr Kendle Maslowski (Institute of Immunology & Immunotherapy, University of Birmingham). Briefly, 10 non-overlapping 200 µm fields of view (FOV) were selected randomly within 2-3 tumours per mouse. The Ki-67 positive cells within these FOV were counted and the average number of positive cells per 200 µm was calculated per mouse.

2.3 Organoid culture and maintenance

Prior to the start of this project, tumours were removed from the colons of *Apc*$^{Min/+}$ mice. From these, organoids were established using the published protocol (Sato et al., 2009; Mackie et

al., 2021). As previously described by our group, tumours were rinsed with cold PBS and incubated in 10 mL chelation buffer (5.6 mMol/L Na_2HPO_4**,** 8.0 mMol/L KH_2PO_4**,** 96.2 mMol/L NaCl, 1.6 mMol/L KCl, 43.4 mMol/L sucrose, 54.9 mMol/L D-sorbitol, 0.5 mMol/L DL-dithiothreitol) with 2 mM EDTA for 1 hour on ice. Vigorous shaking was used to remove most of the attached 'normal' tissue. The buffer was then removed, and tissue was washed with chelation buffer (no EDTA). The tissue was then further incubated in digestion buffer (DMEM with 2.5% fetal bovine serum (FBS), 1% penicillin/streptomycin, 400 U/mL collagenase D, 25 U/mL dispase) for 30 minutes at 37°C. Supernatant was filtered through a 70 µm filter and the remaining tissue washed with basic medium before filtering. The cells were centrifuged at 300 XG for 3 minutes and the pellets washed with basic medium, then resuspended in Matrigel (Corning 356231). Organoids were plated in a 24-well plate in 50 µL Matrigel per well, each fed with complete medium **(Table 1)**. Established organoids were switched to epidermal growth factor (EGF)-only tumour medium **(Table 1)**.

During maintenance, organoids were passaged once a week. To reduce retention of organoids all tubes and tips were pre-coated with FBS. Matrigel domes were dissolved using Cell Recovery Solution (Corning, cat# 354253) and transferred to a 15 mL Falcon tube. Tubes were centrifuged at 300 XG for 5 minutes at 4^{o}C. Excess medium was removed carefully and organoids were resuspended in 1 mL TrypLE (Gibco 12605036) and incubated for 5 minutes at 37^{o}C with regular shaking to break up organoids into single cell suspension. Cells were centrifuged (300 XG, 5minutes, 4^{o}C), cell pellet was resuspended in 50 µL Matrigel/well and this was seeded in a 24-well plate. Matrigel was set in the incubator for 5-10 minutes and then wells were fed with 500 µL tumour medium **(Table 1)**. Passage ratios of around 1:10 to 1:12 depending on density and organoid size.

Human patient-derived organoids (PDOs) were kindly shared with us already established, by Professor Andrew Beggs (Institute of Cancer & Genomic Sciences, University of Birmingham). They were maintained with a weekly passage in the same way as the mouse tumour organoids, however they were fed Human IntestiCult organoid growth medium (StemCell – cat# 06010).

Table 1: Components of media used during the establishment and maintenance of mouse colon tumour organoids, adapted from (Sato et al., 2011; Han et al., 2017)

Media	**Components and concentrations**	**Product details**
Basic medium	Advanced DMEM/F12 100 U/mL Penicillin/streptomycin 2 mM GlutaMAX-I 10 mM HEPES	Invitrogen (cat# 12634028) Invitrogen (cat# 15140122) Invitrogen (cat# 35050061) Invitrogen (cat# 15630080)
2x N2/B27/NA medium	Basic medium with: 1x N2 supplement 1x B27 supplement 1 mM N-Acetylcysteine	 Invitrogen (cat# 17502001) Invitrogen (cat# 17504001) Sigma Aldrich (cat# A9165)
Tumour medium	1:1 Basic medium + 2x N2/B27/NA medium 50 ng/mL mouse recombinant EGF	 Invitrogen (cat# PMG8043)
Complete medium	Tumour medium with: 100 ng/mL mouse recombinant Noggin 1x R-spondin conditioned medium 5 µM CHIR99021 (GSK3β inhibitor) 10 µM Y-27632 (ROCK inhibitor)	 Peprotech (cat# 250-38) Shared with us by Professor Calvin Kuo (University of Stanford) Bio-techne (cat# 4423) Bio-techne (cat# 1254)

2.4 Infection of tumour organoids with attenuated *S*Tm strains

Tumour organoids were infected at day 5 post-split to ensure robust organoid size and integrity. *In vitro* infection protocol was the same for all mutant strains of STm used in this thesis. A stab culture of the *S*Tm strain of interest was grown overnight in LB Broth (Sigma-Aldrich, cat#L3022) in a shaking incubator at 37°C, 200 RPM. A 1:20 sub-culture was then

grown from this in the same conditions, until it had reached an optical density at 600 nanometre (nm) wavelength (OD_{600}) of 0.7. Bacteria was diluted to $1x10^8$ CFU/5 µL in PBS, and 5 µL was spiked into the culture medium (or PBS control) and incubated at 37°C for 2 hours to allow for invasion of the Matrigel and organoids. After 2 hours medium was removed and Matrigel washed twice with PBS and medium replaced and 50 µg/mL gentamicin (Scientific Laboratory Supplies, cat# G1397) added to kill remaining extracellular bacteria. Organoids were then collected at specified time-points for downstream analysis.

2.5 Recovery of colony forming units from organoids

Following infection **(2.4)**, organoids were recovered from Matrigel by incubation with Cell Recovery Solution for 1 hour at 4°C. Wells were collected into separate microtubes and centrifuged at 10,000 XG for 5 minutes. Supernatant was removed from pellets and discarded. Cell pellets were resuspended in 0.3% 100 µL Triton-x-100 (Sigma-Aldrich, cat# 11332481001) with a needle to lyse cells and liberate intracellular bacteria. Cell lysates were spread on LB agar (Sigma-Aldrich, cat# L2897) plates, incubated for 24 hours at 37°C before colonies were counted.

CFU/well of tumour organoids were calculated using the following formula:

$$(Bacterial\ colonies\ x\ \left(\frac{total\ volume}{volume\ plated}\right))x\ dilution\ factor$$

2.6 RNA isolation, cDNA preparation and qPCR

To isolate RNA, buffer RLT and β-mercaptoethanol was added directly to the culture plate 24 hours post infection, after washing the Matrigel dome with PBS. This buffer completely dissolved the Matrigel and these were then processed for RNA isolation following

manufacturer's instructions (Macherey Nagel 740955.50). 500 ng of RNA was converted to cDNA **(Table 2)**, using a T100 PCR Thermal Cycler (Bio-Rad, cat# 1861096).

Quantitative real-time PCR was carried out using the QuantStudio™ Real-Time PCR System (ThermoFisher Scientific, cat# A28140) in MicroAmp™ Optical 384-well plate (Applied Biosystems 4309849). Reaction mixtures were composed of 12.5 ng cDNA, PowerUp SYBR green master mix (ThermoFisher Scientific, cat# A25743) and gene-specific primers **(Table 3)** at a concentration of 0.5 µM.

Table 2: Reagents which are combined with Ultra-Pure H_2O and RNA to a total volume of 20 µL per sample for conversion to cDNA

Reagent	Final concentration	Product details
M-MLV Reaction Buffer	1x	Promega (cat# M5313)
dNTP mix	200 µg/mL	Promega (cat# U1511)
Oligo $(dT)_{15}$ primer	25 µg/mL	Promega (cat# C1101)
M-MLV Reverse Transcriptase	200 units	Promega (cat# M1701)
RNasin Ribonuclease Inhibitor	20 units	Promega (cat# N2611)

Table 3: Gene-specific primer sequences for stem-related genes investigated using qPCR in chapter 3

Gene name	Forward Primer Sequence (5' to 3')	Reverse Primer Sequence (5' to 3')	Species
18s	GATCCATTGGAGGGCAAGTCT	CCAAGATCCAACTACGAGCTTTT	Human
SMOC2	CAGCCGAAATGTGACAACAC	GTTCTGAGAGCCTGCCTGAC	Human
LGR5	TCAGTCAGCTGCTCCCGAAT	CGTTTCCCGCAAGACGTAAC	Human

2.7 Stem-forming assay

Human and mouse organoids were infected as described above **(2.4)**. After 24 hours organoids were removed from Matrigel using Cell Recovery Solution and collected into FBS-coated 15 mL tubes, ensuring each well was kept separate. Organoids were digested as above **(2.3)**, with each well diluted 1:12. Two wells were seeded from each test well and maintained in culture. On day 5 the cells were lifted and digested to single cell suspension and live cell counts taken using only cells which had not taken up Trypan Blue (Gibco, cat# 15250061), and an average of the two wells calculated. Images of organoids were also taken on day 5 of growth using a Zeiss Axiovert microscope and processed using Zeiss ZEN Blue software.

Total live cells were calculated using the following equation:

$$Trypan\ Blue\ negative\ cells\ x\ Dilution\ in\ Trypan\ Blue$$

$$x\ Square\ factor\ of\ haemocytometer\ x\ Volume\ of\ sample$$

2.8 CellTrace Blue staining of patient-derived organoids and flow cytometry

PDOs were grown for 4 days post-split to allow organoid structures to form and grow to a sufficient size. Two wells of each condition were seeded and combined in processing to provide enough cells for flow cytometric analysis.

CellTrace Blue (CTB) was added directly to culture medium of Matrigel condition wells at a final concentration of 10 µM and incubated in the dark for 20 minutes at room temperature. Culture medium was then aspirated, and wells were washed twice for 5 minutes each with heat-inactivated FBS (HI-FBS) (Sigma-Aldrich, cat# 12105) to quench the dye. Organoids were then removed from Matrigel with Cell Recovery Solution as before and each condition was

combined into HI-FBS coated 15 mL falcon tubes and cells pelleted by centrifugation at 300 XG for 5 minutes at 4°C.

For the suspension condition, organoids were recovered with Cell Recovery Solution into HI-FBS coated 15 mL falcons of each condition. Cells were pelleted by centrifugation at 300 XG for 5 minutes at 4°C. Supernatant was aspirated off and cells were resuspended in PBS with 10 µM CTB per well and incubated in the dark for 20 minutes at room temperature, with occasional gentle agitation. Cells were then pelleted as before and washed twice for 5 minutes each with equal volumes HI-FBS per well to quench the dye. For CTB infection experiments organoids were then again pelleted and resuspended in Matrigel. 50 µL domes were then re-seeded and fed with Intesticult human media. Wells were then directly inoculated with mCherry *S*Tm$^{\Delta aroA}$ (UF20) **(2.4)**. Organoids were then processed for flow cytometry after 24 hours as described below.

Throughout the rest of the processing for flow cytometry cells were kept on ice and supplemented with 10 µM Y-27632 (Bio-techne, cat# 1254), an inhibitor of p160 rho-kinase, in order to improve viability. All tips were coated in HI-FBS to prevent retention of cells on plastics. All cell conditions were then resuspended in TrypLE Express Enzyme (Gibco, cat# 12605010) and incubated for 5 minutes at 37°C to start the dissociation to single-cell suspension. Cells were then also manually digested via pipetting through a p10 tip on a p1000 tip. Cells were then centrifuged as before, then resuspended in 250 µL ice-cold fluorescence-associated cell sorting (FACS) buffer (PBS, 5% FBS, 5 mM EDTA, 0.1% sodium azide) and transferred to a 96-well round bottom plate. Appropriate wells were then stained with viability dye (ThermoFisher Scientific, cat# 65-0865-14) and samples acquired on the BD LSR Fortessa™ X-20 using FACSDiva software.

Data was then analysed using FlowJo v10 software.

After analysis of the uptake of dye by organoids stained in suspension or in Matrigel, organoids were stained in suspension for all infection CellTrace Blue (CTB) experiments.

2.9 Mitomycin C pre-treatment of patient-derived organoids

Prior to infection, wells were incubated with 0.01 µM or 0.05 µM of mitomycin C (Scientific Laboratory Supplies, cat# M4287) or 3.33% DMSO (Sigma-Aldrich, cat# D8418) vehicle control for 24 hours at 37°C in 5% CO_2. Wells were then washed twice with PBS and re-fed with medium. Organoids were then infected as described above **(2.4)** and collected for colony forming unit measurement after 24 hours **(2.5)**.

2.10 Methyl-β-cyclodextrin pre-treatment of patient-derived organoids

The protocol used in this work was adapted from the previously published work demonstrating cholesterol depletion from the surface of mammalian cells, without affecting mammalian or bacterial cell viability (Hayward et al., 2005; Garner et al., 2002). Organoids were recovered from Matrigel with Cell Recovery Solution (Corning, cat# 354253) for 1 hour at 4°C, before being centrifuged at 300 XG for 5 minutes to pellet. The supernatant was discarded, and then organoids were resuspended in media containing vehicle control or 5-15 mM methyl-β-cyclodextrin (MβCD) (Scientific Laboratory Supplies, cat# C4555) and incubated for 1 hour at 37°C, before being twice washed with warm PBS. Organoids were then resuspended in Matrigel and re-fed with media before being infected as in section **2.4**. After 24 hours in media supplemented with 50 µg/mL gentamicin the organoids were recovered and processed for assessment of bacterial burden, as described in **2.5.**

2.10.1 Imaging of cholesterol after MβCD treatment of organoids

This protocol was carried out protected from light to prevent the degradation of filipin and throughout the cells are resuspended via flicking, not pipetting, to retain organoid structure. Filipin is an antibiotic which specifically binds to cholesterol and is naturally fluorescent in the UV wavelengths, making it a useful tool for the visualisation of cell surface cholesterol (Miller, 1984; Maxfield and Wüstner, 2012).

Organoids were removed from Matrigel as before and transferred to a round bottom 2 mL tube before treatment with 5 mM MβCD for 1 hour as above **(2.10)**. Organoids were centrifuged at 300 XG for 5 minutes to pellet and resuspended in 5 µg/µL filipin (Cayman Chemical, cat# 70440) in PBS for 15 minutes at room temperature. Cells were then pelleted and washed twice with PBS before being resuspended in 4% paraformaldehyde for 15 minutes at room temperature to fix cells. Following fixation organoids were centrifuged at 900 XG as they are more resilient, and this improves the number of organoids retained. Organoids were washed twice more with PBS and then resuspended in NucSpot650 (Biotium, cat# 40082) for 10 minutes at room temperature to stain nuclei. Organoids were then washed twice more with PBS before being resuspended in mounting medium (Vector laboratories, cat# H-1700) and transferred to conclave slides (Amscope, cat# BS-C6) and mounted with coverslips. Organoids were then imaged on the Zeiss LSM780 confocal microscope and images analysed with Zeiss ZEN Blue software.

2.11 Single-cell RNA sequencing

Patient-derived organoids were maintained as described previously and seeded as two 50µL Matrigel domes per well in 6-well plates 5 days before infection with $1x10^8$ CFU/5 µL *S*Tm$^{\Delta aroA}$

or PBS control as described in section **2.4**. After 24-hour infection, organoids were collected from the Matrigel into FBS-coated 15 mL tubes. Samples were topped up with ice cold PBS and centrifuged at 400 XG for 5 minutes, at 4°C. Supernatant was removed, pellets resuspended in TrypLE with 10µM Y-27632 (STEMCELL 72304) and incubated for 5 minutes at 37°C with intermittent vigorous shaking to achieve a single cell suspension. Ice cold basic medium with 10% FBS was added and samples centrifuged again at 400 XG for 5 minutes, 4°C. Pellet was then washed three times in ice cold PBS before a final resuspension in PBS for viability check and cell count.

Genomics Birmingham then used Chromium Next GEM Single Cell 3' Library and GelBead v3.1 kits to generate libraries of each sample. All samples had 65% - 95% viability, with between $2.35x10^5$ and $1.06x10^6$ cells used. All libraries were normalised to 4 nM and 5 µL of each library was pooled. Libraries were sequenced on the NextSeq 500 (Illumina) platform, using 150 cycle high v2.5 flowcells.

Patient lines 064, 389, 411 and 964 were used for the sequencing as they were determined to be a mix of patients that responded to *S*Tm$^{\Delta aroA}$ treatment *in vitro* by reducing stem transcripts and those which did not to attempt to identify what drives the differences.

2.11.1 Single-cell RNA sequencing analysis

Quality checking and filtering of dead cells/debris was performed in R 4.0.0 using the 'Seurat V4' workflow (Hao et al., 2020). Cells with fewer than 200 or more than 2500 genes were excluded as being likely dead or doublet cells, respectively. Mitochondrial read percentage was cut off at 15% to remove the cells that were likely dying and spilling mitochondrial

contents **(Figure 2.11.1 A)**. One sample (patient 389, *S*Tm treated) required further filtering by excluding cells with more than 1000 counts **(Figure 2.11.1 B)**.

Downstream processing included log normalizing all data prior to integrating all samples. A Jack Straw plot was run to identify the number of principle components for UMAP clustering analysis **(Figure 2.11.2)**. Cell cycle scoring was performed and only the differences between G2M and S phase was regressed out (Kowalczyk et al., 2015) **(Figure 2.11.3 A)**. The Seurat object was used in 'scCATCH' (Shao et al., 2020) which ran an unbiased approach to cluster identification, and these results were used in combination to assign cell type identities to each cluster **(Figure 2.11.3 B)**. Top genes for each cluster were also identified and common colonic cell type markers were used to identify putative cell types. Common colonic cell type markers were identified by cross-references our top genes with a database of cell type markers used in other 10x Chromium single-cell experiments using human colonic material (Franzén et al., 2019) **(Figure 2.11.3 C)**. Differentially expressed genes (DEGs) were calculated using the 'FindMarkers function' in Seurat, with >0.3 $\log_2$ fold change set as the threshold for differential expression.

All single-cell RNA sequencing R scripts are in appendix 1.

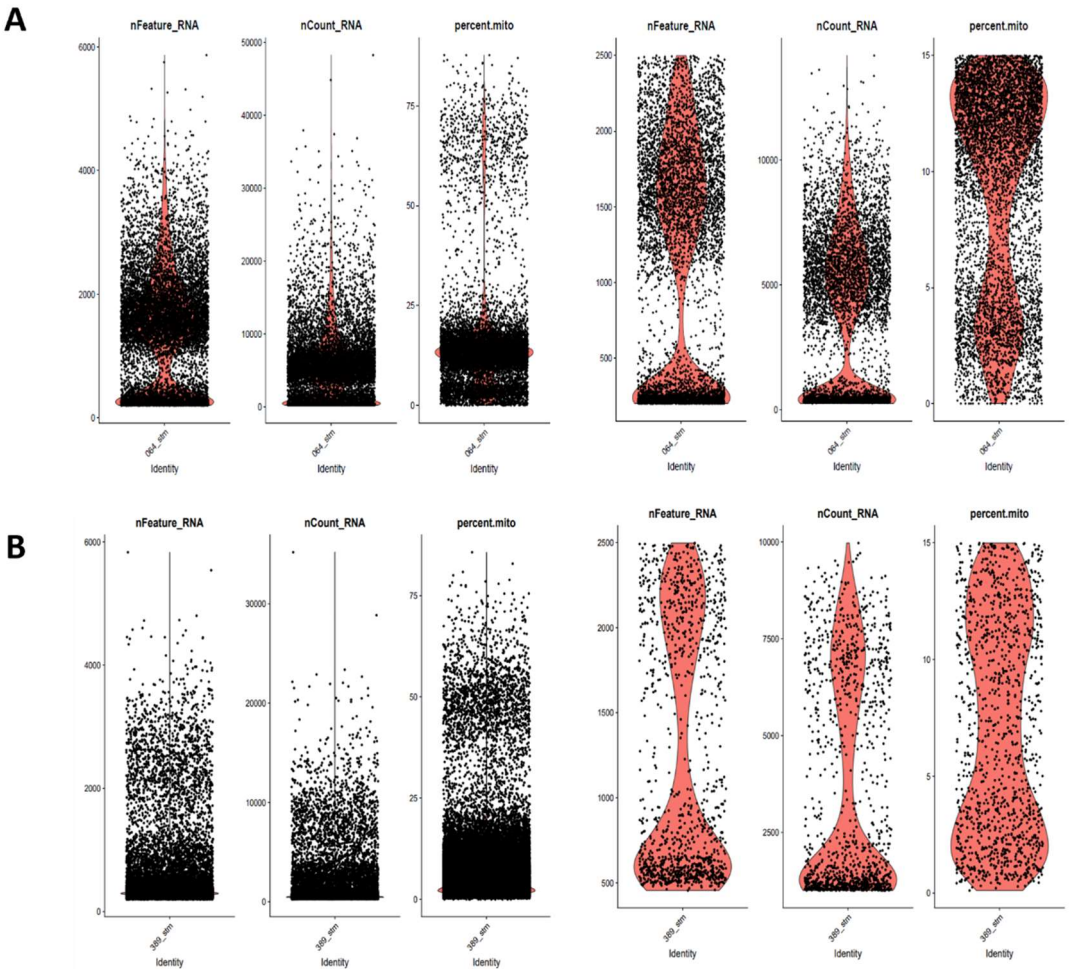


Figure 2.11.1: Quality assessment and filtering of single-cell RNA sequencing raw data
(A) *Representative plots of number of features/cell, number of counts/cell and percentage of mitochondrial genes/cell pre- (left) and post-filtering (right).* ***(B)*** *The same plots of sample 389_stm, which required an extra filter due to high number of low-quality cells.*

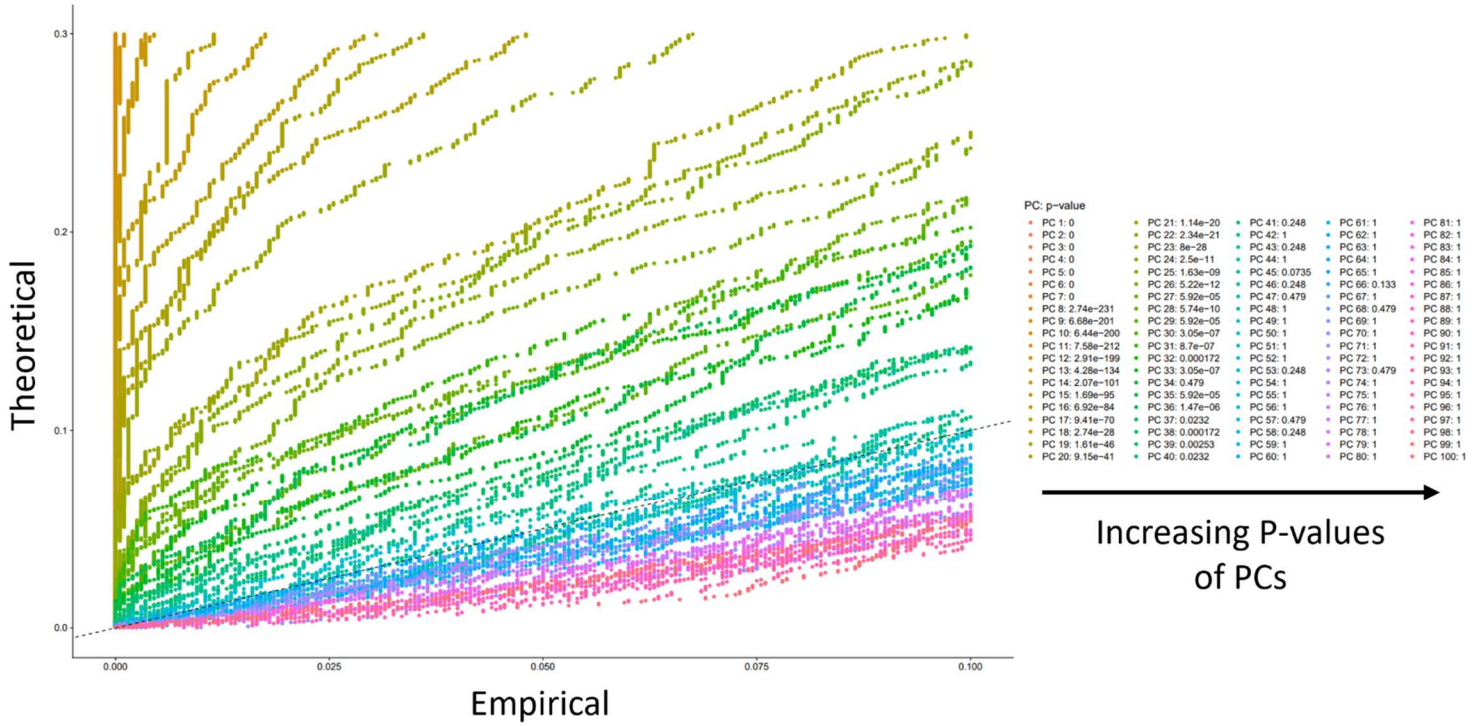


Figure 2.11.2: Jack Straw plot identifies 40 significant principal components
Jack Straw plot of integrated data set of principal components (PCs) 1-100. Dotted line indicates threshold for significant components. PCs 1-40 were used for clustering and further analysis.

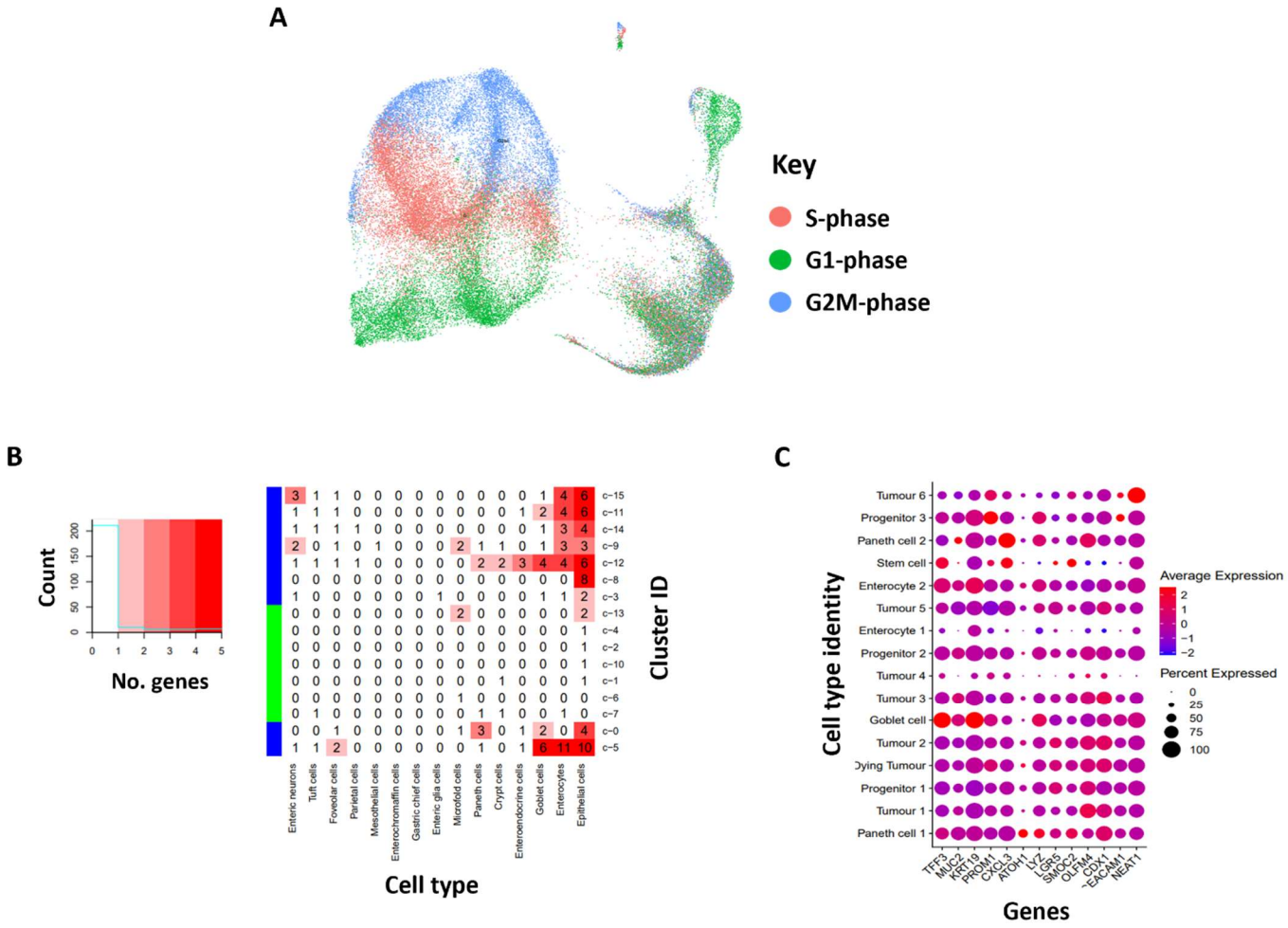


Figure 2.11.3: Cell type and cluster identification from single-cell RNA sequencing of PDOs

(A) UMAP clustering of integrated data coloured by cell cycle phase (red = S-phase, green = G1-phase, blue = G2M-phase). (B) Number of upregulated genes in each cluster that align with cell types from the Panglao databases associated with gut tissue. Clusters indicated in blue are identified as epithelial-like tumour cells whereas green clusters are classed as "Tumour" cell types. (C) Dot plot showing the average expression and percent of cells in each cluster expressing classical gut cell-type markers.

2.12 Bulk RNA-sequencing

One patient-derived organoid line (Patient #389) and *Apc*$^{Min/+}$ tumour derived organoids were seeded as 3 domes/well for each condition (NT, MβCD, *S*Tm$^{\Delta aroA}$ and MBCD + *S*Tm$^{\Delta aroA}$) in 6-well plates with 3 repeats of each condition. On day 4 of growth media was refreshed as follows: 13% DMSO in tumour media for NT well; 5 mM MβCD in tumour media for MβCD and MβCD + *S*Tm$^{\Delta aroA}$ wells and tumour media alone in *S*Tm$^{\Delta aroA}$ only wells. Plates were incubated for 1 hour at 37°C before wells were washed with PBS and re-fed with tumour media. *S*Tm$^{\Delta aroA}$ and MBCD + *S*Tm$^{\Delta aroA}$ wells were then infected as in section **2.4**, NT and MβCD wells were treated with PBS for the duration of infection. After 4 hours incubation wells were collected and processed for RNA isolation as in section **2.6**. RNA concentrations were measured using a nanodrop **(Table 4)** and sent to Lexogen GmBH for sequencing and quality checking. Aligned reads were sent to us for downstream processing. 'DESeq2' pipeline (Love et al., 2014) was used for analysis of bulk RNA-sequencing data **(Figure 2.12.1)**. Briefly, aligned count data were log normalised and filtered out genes with fewer than 10 reads total. Differentially expressed genes (DEGs) between conditions to be compared (*S*Tm$^{\Delta aroA}$ vs NT; *S*Tm$^{\Delta aroA}$ + MβCD vs *S*Tm$^{\Delta aroA}$; *S*Tm$^{\Delta aroA}$ + MβCD vs MβCD) were calculated with a threshold of >1.5 log2 fold change up or down. Log_2 fold change was then shrunk using 'apeglm' function to improve visualisation on volcano plots. 'PathfindR' (Ulgen et al., 2019) was used to perform pathway analysis on the defined DEGs.

All bulk RNA-sequencing R scripts are in appendix 2.

Table 4: RNA concentrations (ng/µL) of samples for bulk RNA-sequencing as measured using a nanodrop. Samples sent in 30 µL volume

Sample	Concentration (ng/µL)	Sample	Concentration (ng/µL)
389 NT1	22.2	CT NT1	244
389 NT2	17.9	CT NT2	214.1
389 NT3	10.5	CT NT3	267.1
389 MBCD1	124.5	CT MBCD1	110.8
389 MBCD2	63.9	CT MBCD2	82.3
389 MBCD3	95.4	CT MBCD3	120.2
389 STm1	163.8	CT STm1	206.3
389 STm2	223.6	CT STm2	164.2
389 STm3	10.8	CT STm3	192.7
389 STm+MBCD1	124.4	CT STm+MBCD1	111.1
389 STm+MBCD2	111.9	CT STm+MBCD2	124.6
389 STm+MBCD3	97.8	CT STm+MBCD3	90.5

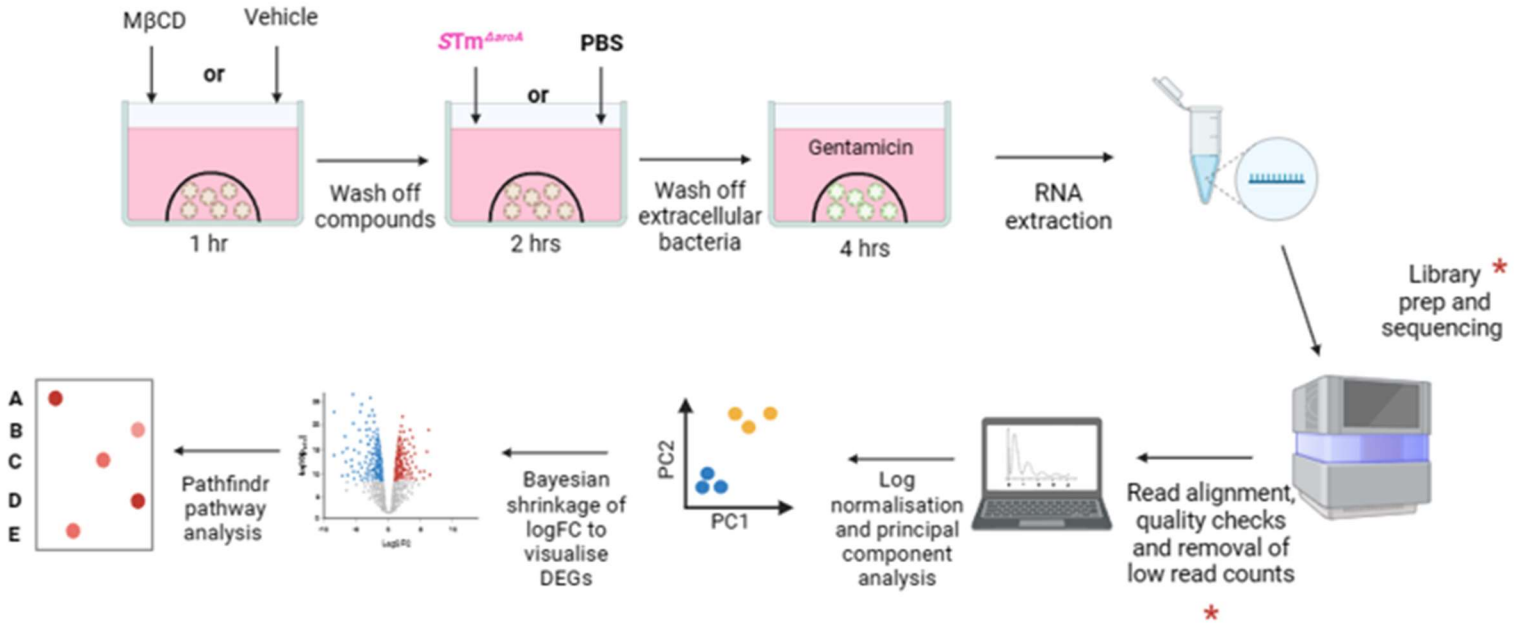


Figure 2.12.1: Experimental set up and analysis pipeline for bulk RNA sequencing

*PDO line 389 and Apc$^{Min/+}$ tumour organoids were treated with either vehicle control or MβCD for 1 hour, then compounds were washed off and organoids were then treated with either PBS or STm^{ΔaroA} to generate the conditions NT (vehicle + PBS), STm^{ΔaroA} (vehicle + STm^{ΔaroA}), MβCD (MβCD + PBS) or STm^{ΔaroA} + MβCD (MβCD + STm^{ΔaroA}). RNA was then isolated using a kit, and samples sent to Lexogen GmbH. RNA libraries were prepared and samples sequenced on an Illumina NextSeq 500. Samples were demultiplexed and reads were then aligned to human or mouse genome and low read counts removed. Aligned reads were analysed using the DESeq2 pipeline. Principal component analysis calculated the effect of each treatment on the gene expression in samples, before visualisation of differentially expressed genes and pathway analysis using pathfindr package. Steps with a * indicate processes undertaken by Lexogen GmbH.*

2.13 Amplification of Kan^R cassette from *S*Tm$^{\Delta sipB}$

*S*Tm$^{\Delta sipB}$ on the 14028s background was shared with us by Dr Amanda Rossiter (Institute of Microbiology & Infection, University of Birmingham). *S*Tm$^{\Delta sipB}$ was generated using pKD4 plasmid, which contains a Kanamycin resistance cassette (Kan^R) in place of the *sipB* sequence in the genome. pKD4 was received as a gift from Professor Barry L. Wanner (Addgene plasmid # 45605; http://n2t.net/addgene:45605; RRID:Addgene 45605) (Datsenko and Wanner, 2000).

A stab culture of *S*Tm$^{\Delta sipB}$ was grown overnight in LB Broth containing 50 µg/mL Kanamycin (Merck, cat# K4000) in a shaking incubator at 37°C, 200 RPM. Genomic DNA was then isolated from the suspension using the QIAamp DNA Mini Blood kit (Qiagen, cat#51104) as per manufacturer's instructions. The isolated DNA was then quantified using a Qubit and 250ng used in the PCR reaction with Phusion High-Fidelity DNA Polymerase (New England Bioscience, cat# M0530) as per manufacturer instructions. The primer sequences used to amplify the Kanamycin resistance cassette from *S*Tm$^{\Delta sipB}$, termed 'Kan^R' primers **(Table 5)**, were used at 0.5 µM.

PCR product was run on a 1% agarose gel (ThermoFisher, 16500500) with a 0.1-10 kilobase (kB) ladder (New England BioLabs, cat# N3200) and the band at ~1.6 kB was excised and DNA purified using QIAquick Gel Extraction kit (Qiagen, cat# 28706).

2.14 Generation of double-gene knockout *Salmonella* typhimurium

Deletion of *sipB* in *S*Tm$^{\Delta aroA}$ was achieved by following a widely used protocol (Datsenko and Wanner, 2000), described below. A stab culture of *S*Tm$^{\Delta aroA}$ was grown overnight in LB Broth in a shaking incubator at 37°C, 200 RPM. A sub-culture was then grown 1:50 in LB Broth at the

same conditions to an OD_{600} of 0.7. *S*Tm$^{\Delta aroA}$ was then pelleted at 3000 XG for 10 minutes, before being washed 2 times with ice-cold 10% glycerol for 20 minutes to make the cells electrocompetent. A stab culture of the λ-red recombinase containing plasmid pKD46 was grown overnight at 30°C, 200 RPM. Plasmid DNA was isolated by following instructions for the QIAprep Spin Miniprep kit (Qiagen, cat# 27104). The isolated plasmid DNA was electroporated into *S*Tm$^{\Delta aroA}$ using an electroporator (Eppendorf #4309000035) and 0.1-centimetre cuvettes (GeneFlow, cat# E6-0050) at 1.8 kilovolts. LB Broth was added immediately and *S*Tm$^{\Delta aroA}$-pKD46 was recovered at 30°C for 1.5 hours. Bacteria were then pelleted at 3000 XG, resuspended in 100 µL LB Broth and plated on LB Agar with 100 µg/mL Ampicillin (Sigma Aldrich, cat# PHR2838).

Amp^R (Ampicillin resistant) colonies of *S*Tm$^{\Delta aroA}$-pKD46 were selected and grown in LB Broth supplemented with 10 mM L-arabinose (Sigma Aldrich, cat# A3256) to induce λ-red, to an OD_{600} of 0.6. Bacteria were then pelleted at 3000 XG and washed twice with ice-cold 10% glycerol (Scientific Laboratory supplies, cat #CHE2072) to make the cells electrocompetent. PCR product of Kan^R-cassette was electroporated into cells as before, and bacteria recovered at 37°C for 1.5 hours to remove the pKD46 plasmid. *S*Tm$^{\Delta aroA\Delta sipB}$ were then selected for on LB Agar containing Kanamycin and resulting colonies grown overnight in LB broth and glycerol stocks made. Lastly, removal of the pKD46 plasmid was confirmed by lack of growth on Ampicillin containing agar.

To confirm that the Kanamycin resistance gene had been inserted into the correct location in the genome and resulted in loss of *sipB* expression, colonies were collected and lysed in 30 µL Ultrapure H_2O (Scientific Laboratory Supplies, TMS-011-A) at 90°C for 5 minutes. A colony of

*S*Tm$^{\Delta aroA}$ was also collected to use as a control. DNA from each colony was amplified in a 50 µL PCR reaction, with 4 µL of DNA and Go-Taq G2 DNA Polymerase (Promega, cat# M7841) as per manufacturer instructions. Primers used are listed **(Table 5),** and were all used at 0.5 µM – their location in the genome is shown below **(Figure 2.14.1)**. Three reactions were run for each colony – 'reaction one' using Screen_kan_fwd and Kan_int_rev; 'reaction two' using Kan_int_fwd and Screen_kan_rev; 'reaction three' using SipB_int_fwd and SipB_int_rev.

Table 5: Primers used for the amplification of Kanamycin resistance cassette, generation of mutant by lambda-red system and validation of deletion of sipB

Primer name	Primer Sequence (5' to 3')	Use
Kan^R_fwd	GAAAAGGAATAATTATGGTAAATGACGCAAG	Upstream primer for amplification of kanamycin resistance cassette
Kan^R_rev	TTGGCAGTTTTTATGGCGCGAC	Downstream primer for amplification of kanamycin cassette
Kan_int_fwd	CCTGCAAAGTAAACTGGATG	Anneals to the internal of the kanamycin cassette on top strand
Kan_int_rev	CATGCTCTTCGTGCAGATCA	Anneals to the internal of the kanamycin cassette on bottom strand
Screen_kan_fwd	CTCTGCGGGCAAAAGCGTTG	Anneals 50bp upstream of sipB
Screen_kan_rev	CTATTCTCAACAGAATGATTATTTAAATAA	Anneals 50bp downstream of sipB
SipB_int_fwd	GGGCAATTGACATTACTGCTTGGC	Anneals to the internal of the sipB gene on the top strand
SipB_int_rev	CGCACCAACAATGCTGCCGG	Anneals to the internal of the sipB gene on the bottom strand

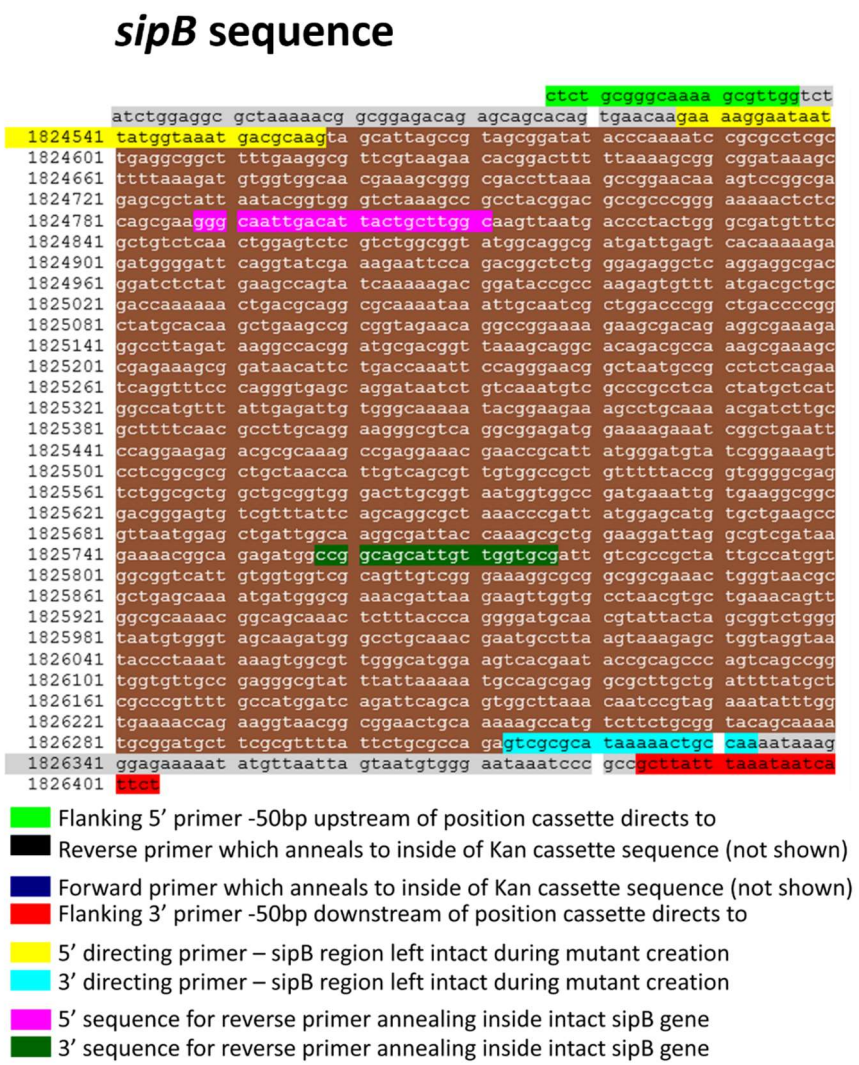


Figure 2.14.1: Position in SL1344 genome of primers used for generation and validation of STm$^{\Delta aroA\Delta sipB}$
Sequence of SL1344 (parent strain of SL3261 STm$^{\Delta aroA}$) sipB gene with highlighted regions showing primers designed for: directing the cassette to sipB for deletion using λ-red recombination (yellow and pale blue); confirming deletion of sipB by amplifying an internal portion of the gene which should be absent in the mutant (pink and dark green); confirming insertion of cassette in correct location by amplifying flanking region and internal cassette region (light green and black/dark blue and red). Kanamycin cassette primer sequences are shown in ***table 5****. Sequence taken from NCBI database submission* (Kröger et al., 2012).

2.15 Animals

Wild-type C57BL/6J female mice were bred with heterozygote *Apc*$^{Min/+}$ males, litters weaned at 4 weeks of age and genotype confirmed, all by staff at the Biomedical Services Unit. *Apc*$^{Min/+}$ mice were transferred to us on the procedural floor from 6 weeks of age and begun treatment protocols at minimum of 8 weeks. The exact age of mice used in specific experiments is detailed below. All mice were maintained under specific pathogen free conditions. *In vivo* mouse experiments were conducted with approval from the UK Research Animal Ethics Committee, under Procedure Project Licence number P06118734.

2.16 Recovery of colony forming units from tissue

Overnight cultures of UF20 *S*Tm$^{\Delta aroA}$-mCherry and SL3261 *S*Tm$^{\Delta aroA\Delta sipB}$ were grown in LB broth at 37°C, shaking at 200 RPM, before 1:20 subcultures were grown to an OD_{600} of ~0.7. Bacteria were centrifuged at 3000 XG for 10 minutes and resuspended to $5x10^9$CFU/100 µL PBS. 12-week-old *Apc*$^{Min/+}$ mice were gavaged with $5x10^9$ CFU of either *S*Tm$^{\Delta aroA}$ or *S*Tm$^{\Delta aroA\Delta sipB}$ and small intestines, liver, spleen and lungs dissected out 24 hours post infection. Tissues were weighed and transferred to round bottom tubes containing two 5 millimetre (mm) stainless steel beads (Qiagen, cat# 69989) and 0.1% triton-PBS. Tissues were then lysed using the TissueLyser II (Qiagen, cat# SM100250-1) for 3 minutes 300 RPM. Lysates were then diluted appropriately and plated on LB agar (with Ampicillin supplemented for *S*Tm$^{\Delta aroA}$ and Kanamycin supplemented for *S*Tm$^{\Delta aroA\Delta sipB}$). Colonies were grown at 37°C overnight and then counted.

CFU/g of tissue was calculated using the following calculation:

$$\frac{((Bacterial\ colonies\ x\ dilution\ factor)x\left(\frac{total\ volume}{volume\ plated}\right))}{tissue\ weight\ (g)}$$

2.17 *Ex vivo* gentamicin protection assay

Bacterial strains UF20 *S*Tm$^{\Delta aroA}$-mCherry and SL3261 *S*Tm$^{\Delta aroA\Delta sipB}$ were cultured as above **(2.16)** and resuspended in 5x10^{9}CFU/100µl PBS. 11–13-week-old *Apc*$^{Min/+}$ mice were gavaged with 5x10^9 CFU of either *S*Tm$^{\Delta aroA}$ or *S*Tm$^{\Delta aroA\Delta sipB}$ and mice culled 48 hours post infection. Small intestines were removed and washed before the polyps were dissected out. The gentamicin protection assay protocol was adapted from a previously published protocol (Avogadri et al., 2005). Briefly, polyps were weighed and split into two groups per bacterial condition. Polyps were mashed through a 70 µm cell strainer (Greiner, cat# 542070) into RPMI (ThermoFisher, cat#11875093) with or without 50 µg/mL gentamicin and incubated for 1 hour at 37°C. Cells were then pelleted at 500 XG for 5 minutes and transferred to round bottom tubes with two 5 mm stainless steel beads and 0.1% triton-PBS. Cells were then lysed using the TissueLyser II for 3 minutes 300 RPM. Lysates were then diluted appropriately and plated on LB agar (with Ampicillin supplemented for *S*Tm$^{\Delta aroA}$ and Kanamycin supplemented for *S*Tm$^{\Delta aroA\Delta sipB}$). Colonies were grown at room temperature for 3 days and then counted.

2.18 Cell viability of organoids

Confluent wells of *Apc*$^{Min/+}$ organoids were treated with PBS or 1x10^8 CFU/well of either *S*Tm$^{\Delta aroA}$ or *S*Tm$^{\Delta aroA\Delta sipB}$ (as in **2.4**). 24 hours post infection the Matrigel was dissolved with Cell Recovery Solution and organoids digested using TrypLE and manually digested as above **(2.3** and **2.7)**. Wells were diluted 1:12, with each original well resuspended in 50 µL Matrigel and seeded as 5 wells in a 96-well plate. Wells were grown for 5 days before cell viability measured. Wells of Matrigel only were also seeded for blank controls.

Cell viability was indirectly measured using a colorimetric plate-based assay. In this assay the rate of NADPH-dependent reduction of tetrazolium salt (3-(4,5-dimethylthiazol-2-yl)-2,5-diphenyltetrazolium bromide or MTT) to formazan crystals is proportional to the level of metabolically active (or viable) cells. Therefore, the higher the optical density, the higher the number of viable cells in culture. Equal volumes of tumour media and MTT solution (Invitrogen, M6494) was added to each well and plate was incubated for 45 minutes at 37°C to allow formazan crystal formation. 1.5x total volume of MTT solvent (4 mM HCl (Sigma-Aldrich, cat#320331), 0.1% triton x-100 in isopropanol (Fisher Chemical, cat# P/7507/17)) was added and pipetted to mix while shaking continuously until crystals dissolve. Optical density was then measured at 550 nm.

2.19 Long term treatment protocol

Bacterial strains UF20 *S*Tm$^{\Delta aroA}$-mCherry and SL3261 *S*Tm$^{\Delta aroA\Delta sipB}$ were cultured as above **(2.16)** and resuspended at 5x10^{9}CFU/100µl PBS. 8-week-old *Apc*$^{Min/+}$ mice were given PBS or 5x10^9 CFU of either *S*Tm$^{\Delta aroA}$ or *S*Tm$^{\Delta aroA\Delta sipB}$ by oral gavage once a week for 8 weeks. On week 9 the mice were culled, and small intestines removed. Polyp burden was counted, and all polyp volumes measured under the dissection microscope using a graticule with a 10x10 mm^2 grid for each mouse. Areas of hyperplasia were not measured in this experiment.

2.20 Enzymatic digestion of polyp tissue for flow cytometry

Apc$^{Min/+}$ mice of 12 weeks old were treated with PBS, 5x10^9 CFU *S*Tm$^{\Delta aroA}$ or *S*Tm$^{\Delta aroA\Delta sipB}$ and culled after 48 hours. Mesenteric lymph nodes and small intestines were removed, and polyps dissected out of small intestines. Polyps were manually minced and transferred to a 50 mL falcon in RPMI. Polyp fragments were centrifuged for 10 minutes at 500 XG and supernatant

aspirated off. Polyp fragments were resuspended in digestion buffer (DMEM containing 2.5% FBS, 1% penicillin-streptomycin, 0.1 mg/mL DNAse (Roche, cat# 10104159001) and 1 mg/mL Collagenase D (Roche, cat# 11088866001)). Polyps were incubated in the digestion buffer for 40 minutes at 37°C, shaking at 300 RPM. Digested polyp fragments and lymph nodes were transferred to and mashed through a 70 µm cell strainer, which was washed with ice cold PBS to maximise recovery. Cells were centrifuged at 300 XG for 10 minutes and supernatant aspirated off.

Cells were resuspended in FACS buffer (as above in section **2.8**) and transferred to a 96-well plate for staining. Cells were centrifuged at 300 XG for 5 minutes before being resuspended in Fc block (Biolegend, cat# 156604, clone S17011E) for 5 minutes on ice to reduce non-specific staining before adding the antibody cocktail to polyp cells. Antibody cocktail was made by diluting the antibodies listed **(Table 6)** in FACS buffer with 1x BD Horizon™ Brilliant Stain buffer (BD Biosciences, cat# 563794) to reduce binding of brilliant violet dyes to each other. Single stains for the antibodies were done on UltraComp eBeads (ThermoFisher, cat# 01-2222-41), apart from viability dye which was done on lymph node cells. Fluorescence minus one controls were also done on lymph node cells to aid gating. Cells were incubated with the relevant antibodies for 30 minutes on ice before being centrifuged as before and resuspended in FACS buffer and samples acquired using a BD LSR Fortessa™ X-20 and FACSDiva software. Data was then analysed using FlowJo v10 software. Gating strategy used to identify leukocytes is adapted from a published strategy for characterising myeloid cells in mouse gut tissue (Liu et al., 2020) **(Figure 2.20.1)**. For the gut-macrophage gating, the intermediate CD11c population was identified using the fluorescence minus PE and the single stain PE to distinguish between negative, intermediate and positive fluorescence in this channel **(Figure 2.20.1 B)**.

Table 6: Antibody details for flow cytometry to define innate cell infiltration into polyps in vivo

Marker	**Fluorophore**	**Clone**	**Manufacturer and catalogue number**
Viability Dye	eFluor780	/	Invitrogen, cat# 65-0865-14
CD3ε	FITC	145-2C11	BioLegend, cat# 100306
CD19	FITC	1D3/CD19	BioLegend, cat# 152403
CD45	BUV395	17A2	BD Biosciences, cat# 740268
Ly6G	BUV737	1A8	BD Biosciences, cat# 741813
CD11b	BV421	M1/70	BioLegend, cat# 101236
Siglec F	PerCP	S170072	BioLegend, cat# 155525
CD64	APC	S18017D	BioLegend, cat# 161005
CD11c	PE	N418	BioLegend, cat# 117308
Ly6C	Alexa-Fluor 700	HK1.4	BioLegend, cat# 128024
I-A/I-E (MHC-II)	Pe-Cy7	M5/114.15.2	BioLegend, cat# 107629

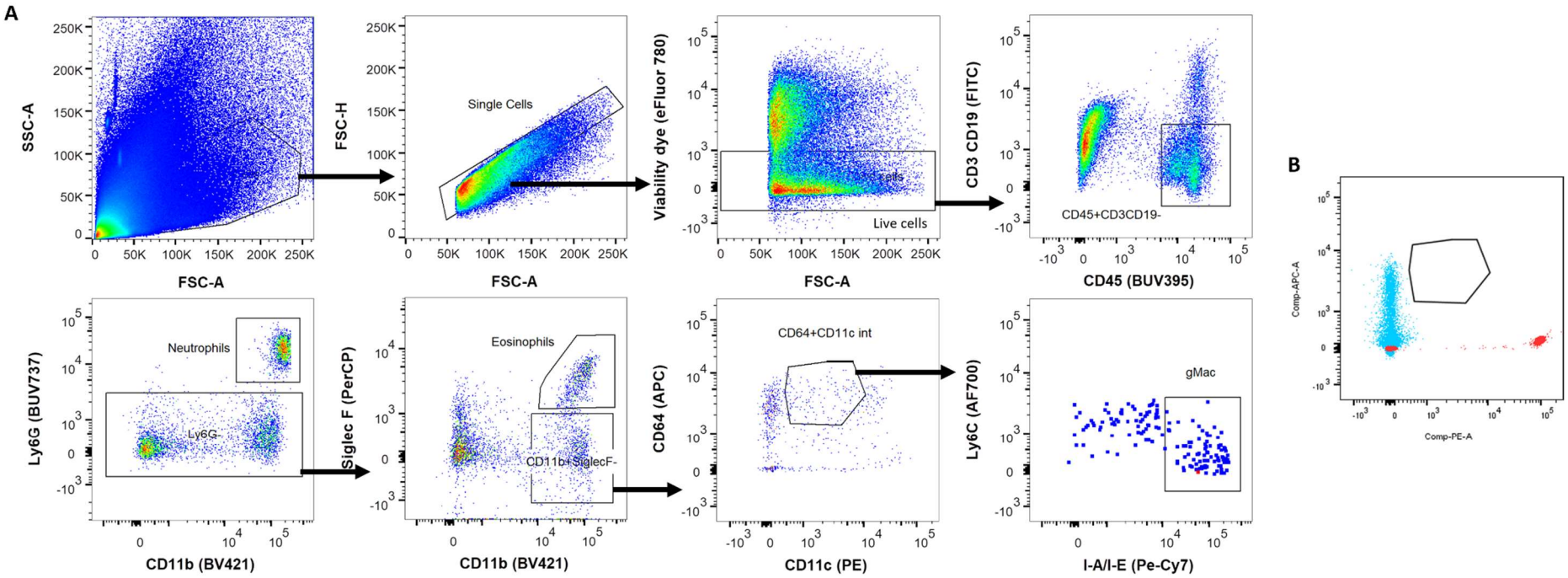


Figure 2.20.1: Gating strategy for investigating innate immune infiltrate into polyps

(A) *Representative gating strategy of innate immune cell populations in polyps of $Apc^{Min/+}$ mice. Cells were gated based on morphology and then live singlets gated. CD45+ CD3-CD19- cells were then gated on to remove adaptive cells and focus on leukocytes only. CD45+CD11b+Ly6G+ cells were gated on as neutrophils. CD45+Ly6G- CD11b+SiglecF+ cells were gated as eosinophils. CD45+Ly6G-Siglec F-CD11b+CD64+$CD11c^{int}$ Ly6C-MHCII+ cells were gated as gut macrophages. Example plots used are a PBS treated mouse.* ***(B)*** *Gating for CD11c intermediate population was set using the fluorescence minus one CD11c-PE control (blue) and CD11c-PE single positive (red) to distinguish between positive, negative, and intermediate fluorescence.*

2.21 Statistical analysis

Shapiro-Wilk normality testing was done on all data sets (as all experiments n=<50) to assess the distribution of data. If normality tests were passed, then parametric tests were done to measure the p-values. These were either paired or unpaired t-tests if there were two conditions, with Welch's correction for unpaired t-tests where standard deviations differ between the groups. For experiments with more than two conditions one-way (with Tukey's multiple comparison test) or two-way (with Dunnett's multiple comparison test) ANOVAs were used to calculate p-values. If normality tests were not passed then non-parametric tests were used to measure p-values. These were Mann-Whitney tests to compare the ranks of two conditions or Kruskal-Wallis test to compare more than two conditions. Tests used are indicated in the figure legends. All data analysis was done in GraphPad Prism 10.

CHAPTER 3 - STm$^{\Delta aroA}$ PREFERENTIALLY INVADE PROLIFERATING CELLS IN PATIENT-DERIVED ORGANOIDS

3.1 Introduction

In the previous work utilising attenuated *Salmonella* in intestinal cancer which was discussed in the introduction of this thesis, we also identified via pathway analysis of bulk RNA-sequencing data changes to cell cycle associated genes, implying alterations to the proliferation of tumour cells after infection (Mackie et al., 2021). Furthermore, we gave mCherry fluorescent *S*Tm$^{\Delta aroA}$ by oral gavage to *Lgr5*-green fluorescent protein (GFP) reporter mice and analysed the tumours by flow cytometry. We identified an enrichment of the bacteria within the GFP-positive Lgr5 stem cells, and this was recapitulated *in vitro* using organoids from these reporter mice (Mackie et al., 2021). This work suggested that *S*Tm$^{\Delta aroA}$ has a direct effect on tumour cells and the tumour microenvironment via specific invasion of stem cells in mice. In this chapter I aim to identify how stem cells are targeted by *S*Tm$^{\Delta aroA}$ and whether these anti-tumour effects can be translated into human models of colorectal cancer.

Salmonella typhimurium has two type 3 secretion systems which are encoded by SPI-1 and -2. T3SS components encoded by SPI-1 are essential for invasion of *S*Tm into host epithelial cells. Structural proteins form the needle and rod structures that bind STm to host cells, while chaperone proteins act to aid the transfer of effector proteins via the needle directly into the host cell cytoplasm. In *S*Tm, a key family of SPI-1 T3SS proteins are the *Salmonella* invasion proteins (Sip) A/B/C/D. SipA is an important co-factor which aids efficient entry of *S*Tm into host cells but is not essential in the invasion process (Zhou et al., 1999). SipB, C and D are

chaperone and effector proteins involved in formation of the needle apparatus and the subsequent secretion of effectors. SipD is located at the very tip of the needle and acts to promote and regulate the secretion of effectors into host cells. Once the bacteria contact a host cell the needle structure is formed and allows the transmembrane proteins SipB and SipC to form a channel through which effectors can be injected (Ghosh, 2004; Lou et al., 2019). Early work demonstrated that SPI-1 encoded T3SS components induced remodelling of host cell cholesterol, namely formation of cholesterol-rich foci at the point of contact by the bacteria (Garner et al., 2002). SPI-1 encoded SipB was then shown to directly bind host cell cholesterol, and this process was demonstrated to be essential for entry of bacterial effector proteins into mammalian cells (Hayward et al., 2005). SipC binds F-actin in host cells and induces remodelling of actin into bundles which acts to promote the internalisation of *Salmonella* (Myeni and Zhou, 2010). To investigate the mechanism by which there is preferential infection of stem cells in mouse tumour organoids I will be using *Salmonella* strains with mutations in these T3SS component genes and comparing their invasion into organoids.

Previous work to translate the promising effect of BCT in mouse models of cancers through to clinical trials and benefits for patients have largely been unsuccessful. By utilising organoids derived from mouse intestinal tumours we have identified that there is a direct effect of *S*Tm$^{\Delta aroA}$ infection on the tumour epithelium *in vitro* (Mackie et al., 2021). In this chapter I am aiming to bridge the gap between mouse models of colorectal cancer and human disease, by directly comparing the *in vitro* effects of attenuated *Salmonella* on *Apc*$^{Min/+}$ colon tumour organoids and organoids derived from biopsies of human colorectal cancer patients. Organoids are 3-D structures grown in a supportive matrix (in this case Matrigel) which are

composed of a heterogenous mix of cell types that more faithfully represents the tissue of origin compared to a 2-D monoculture. Some groups have taken this further and co-cultured organoids with immune cells to demonstrate the complex cell-cell interactions within the tumour microenvironment (Magré et al., 2023; Porter et al., 2020). It has been shown by transcriptomic profiling that cells within human tumour organoids retain the genetic mutations and even epigenetic signatures present in the primary tumour (Kraiczy et al., 2019). This represents a great tool to analyse individual patient responses to *S*Tm$^{\Delta aroA}$ and compare these to not only the response in mouse models, but also each other.

Our group use direct inoculation of the culture medium with *Salmonella* typhimurium to study invasion and colonisation of tumour organoids. *Salmonella* typhimurium is a pathogen which invades IECs via their apical membrane and so this system may not wholly represent the mechanics of *in vivo* invasion, as the apical membrane of normal organoids is in the centre. Some groups overcome this by use of microinjection of bacteria into the lumen of the organoids, which allows contact with and invasion through the apical membrane (Bartfeld and Clevers, 2015). While this is technically more physiological, it is currently low-throughput and can cause structural damage to the organoids if the injection is done improperly or too large a volume is used. Recent work has shown that this can be scaled up with custom robotics and was successfully validated in microbiota studies. These systems are at present very costly, and the size of the organoids was shown to be a limiting factor in the success of automated injection, with a larger luminal space being more desirable (Williamson et al., 2018) . Another method that has been established is the generation of “apical-out” organoids in which intestinal organoids are grown in a matrix and then transferred to growth in suspension which induces a flip in the polarity of the cells over time, while maintaining the barrier integrity (Co

et al., 2021). This group demonstrated that ileal organoids that were apical-out had a higher burden of *Salmonella* typhimurium compared to basolateral-out organoids, and this was in contrast to basal membrane-invading bacteria such as *Listeria monocytogenes* (Co et al., 2019). These data show that there are different invasion mechanics preferred by specific pathogens, rather than a generic improved infection of these flipped organoids. However, we think it is likely that in tumour organoids, and tumours *in vivo*, the architecture is disorganised in such a way that infection mechanics occur differently to that in normal tissue (Lechuga and Ivanov, 2017). In addition, we have shown that our *in vitro* infection model recapitulates the characteristics of *in vivo* infection in our model, therefore we continue to utilise direct inoculation.

Due to these previous findings by our laboratory and others, we hypothesised that there is specific infection of the actively proliferating cells by *S*Tm$^{\Delta aroA}$ - which in the context of cancer are the cells which drive tumour growth and development. In this chapter, the ability of *S*Tm$^{\Delta aroA}$ to target proliferating cells in patient-derived organoids was assessed. Firstly, to confirm that *S*Tm$^{\Delta aroA}$ induced a reduction in growth capacity, we performed stem-forming assays on the PDOs. Secondly, we aimed to identify whether active proliferation was necessary for infection. Lastly, we hypothesised that increased cholesterol on proliferating cells is driving preferential invasion in our PDOs, and so wanted to assess the extent to which cholesterol binding on the outside of cells drove invasion. This work will attempt to dissect which cells BCT is capable of targeting within the tumour and how this occurs. It will therefore be useful to inform more nuanced engineering of the therapy to manipulate the natural invasion mechanism of *S*Tm$^{\Delta aroA}$ in tumours.

3.2 Results

3.2.1 *S*Tm$^{\Delta aroA}$ restores epithelial identity of colon tumour epithelium *in vivo*

We previously identified that repeated gavage of mice with colonic tumours with *S*Tm$^{\Delta aroA}$ reduced tumour burden and load with a significant effect on the tumour metabolome compared to mice given PBS. We next wanted to assess whether this reduction in tumours was associated with a restoration of the epithelium structure. To measure this, mice with colonic tumours induced via AOM-DSS were gavaged once a week for 6 weeks with either PBS or *S*Tm$^{\Delta aroA}$ before colons were removed and processed for immunohistochemistry. Markers used were E-cadherin, which has reduced expression in colonic tumours compared to normal colon due to increased aberrant Wnt signalling (Zhao et al., 2022) and Ki-67, a proliferation marker which is upregulated in tumours compared to normal tissue (Liu et al., 2023). Imaging showed qualitatively more organised epithelial structure after *Salmonella* treatment compared to the PBS treated mice. This was associated with increased expression of E-cadherin in the colonic epithelium and fewer Ki-67 positive cells in mice treated with *S*Tm$^{\Delta aroA}$ compared to PBS **(Figure 3.2.1 A)**. The number of Ki-67 positive cells was quantified by Dr Kendle Maslowski and shows that repeated gavage with *S*Tm$^{\Delta aroA}$ significantly reduces the number of proliferating cells in tumours of mice with CAC **(Figure 3.2.1 B)**.

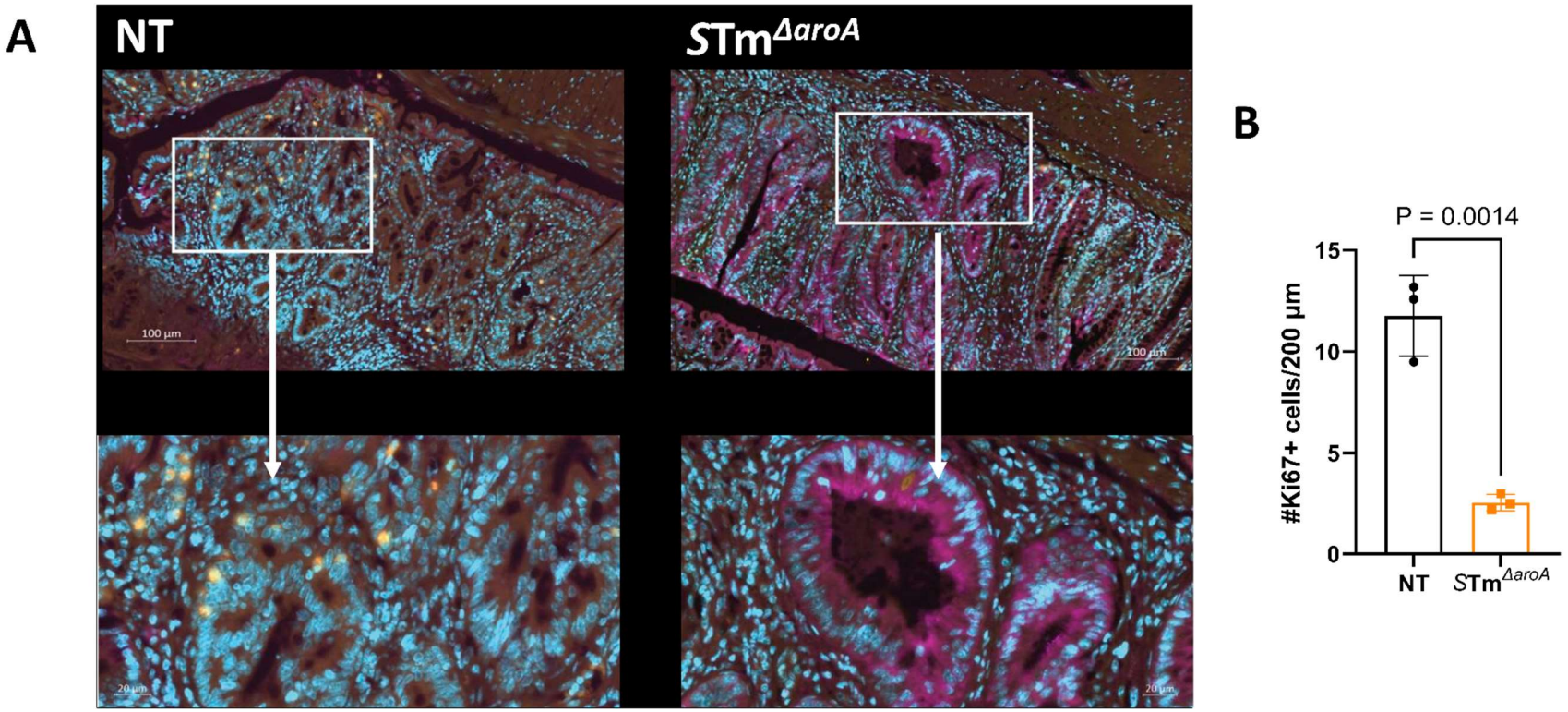


Figure 3.2.1: STm$^{\Delta aroA}$ restores epithelial identity of colon tumour epithelium in vivo

(A) *Representative image of colons which were removed from AOM-DSS treated mice after 6 weeks of PBS (left panels) or STm$^{\Delta aroA}$ (right panels) gavage, fixed and embedded in paraffin. 5µm sections were cut and stained for E-cadherin (purple), Ki-67 (yellow) and nuclei (blue). Scale bars in upper panels 100 µm. Lower images are digital magnification of boxed region in upper images. Scale bars 20 µm.* ***(B)*** *Ki-67 staining was quantified by Kendle Maslowski. This was done by counting the number of stained cells within a 200 µm FOV. Ten FOV were randomly selected for measurement, from 2–3 tumours per mouse. Data points represent the average number of positive cells per mouse. P-value was measured using a two-tailed unpaired t-test. Error bars represent the mean and the standard error of the mean (SEM). (n = 3 mice per treatment group).*

3.2.2 *S*Tm$^{\Delta aroA}$ infects human and mouse colon tumour organoids *in vitro*

Attenuated *Salmonella* can colonise mouse intestinal tumour organoids *in vivo*, as has been shown by our group previously (Mackie et al., 2021). Before we investigated the effects of *S*Tm$^{\Delta aroA}$ on the PDOs we wanted to confirm that there was invasion of the organoids with the bacteria. We inoculated the media of the PDO and *Apc*$^{Min/+}$ organoid wells with equal CFU, allowed the bacteria to adhere and invade over 2 hours before supplementing the media with gentamicin to prevent overgrowth of extracellular bacteria. After a further 24 hours in culture, we collected the wells, keeping patient lines separate, lysed the cells and plated on agar for enumeration **(Figure 3.2.2 A)**. *S*Tm$^{\Delta aroA}$ colonised all patient-derived organoids to similar levels, at an average of ~6.5 x 10^3 CFU/well, around 1.5 log fold lower burden than that in *Apc*$^{Min/+}$ colon tumour organoids **(Figure 3.2.2 B)**. It is worth noting that the bacterial burden is measured as CFU recovered from each well, and not CFU recovered per cell. Cell number per well was not quantified for each of the organoid lines although there was qualitatively similar cell density at seeding and point of infection.

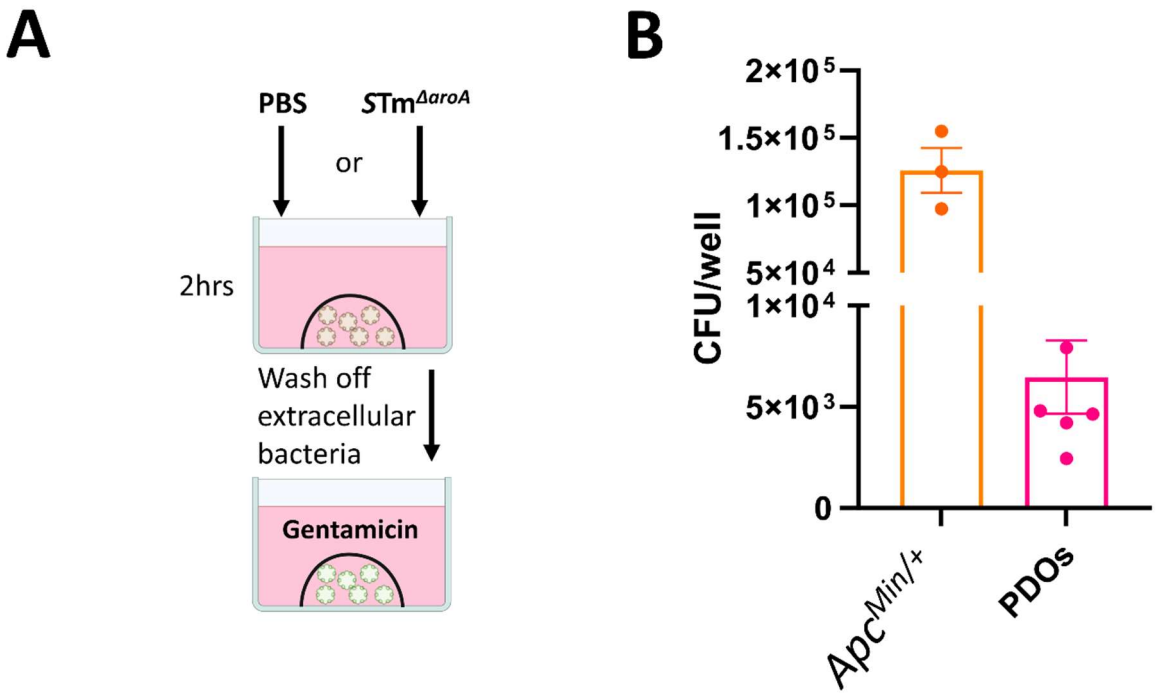


Figure 3.2.2: STm$^{\Delta aroA}$ infects human and mouse colon tumour organoids in vitro
(A) *Schematic of in vitro infection protocol for organoids used throughout, unless stated otherwise.* ***(B)*** *STm$^{\Delta aroA}$ CFU/well recovered 24 hours post inoculation from Apc$^{Min/+}$ colon tumour organoids and patient-derived organoids. Each data point represents the mean of 3 technical repeats. PDO data points represent individual patient lines, average of 3 technical repeats. (n=3 for Apc$^{Min/+}$ and n=5 individual PDO lines).*

3.2.3 *S*Tm$^{\Delta aroA}$ reduces stem-cell associated transcripts in some, but not all, PDOs

We identified a reduction in Ki-67 positive, proliferating cells, *in vivo* in the tumour epithelium of mice treated with *S*Tm$^{\Delta aroA}$ **(Figure 3.2.1)** and a reduction in the transcripts of stem-associated genes in infected tumours and tumour organoids of colorectal cancer mouse models (Mackie et al., 2021). We next wanted to investigate whether the *S*Tm$^{\Delta aroA}$ colonisation of PDOs resulted in a similar effect on the same stem-cell associated transcripts. PDOs were collected following PBS control or *S*Tm$^{\Delta aroA}$ inoculation as before, and qPCR was used to measure expression of stem-cell associated transcripts, *LGR5* and *SMOC2.* Transcript levels were measured as relative expression compared to the housekeeping gene 18s. PDO lines were initially plotted as paired points, each line PBS (NT) and *S*Tm$^{\Delta aroA}$ treated expression levels of the target transcripts **(Figure 3.2.3 A)**. Patients separated based on either no change in expression following infection or consistent, significant reduction of both stem markers and so were divided into two response groups based on this **(Figure 3.2.3 B** and **3.2.3C)** with p-values calculated using paired t-tests. These were termed “response A” for patients with no difference in stem transcript and “response B” for patients in which we see a reduction. We next wanted to identify if there were any correlations between the two response groups and the characteristics of the original tumours from which the PDO lines were generated **(Table 7)**. These details included patient sex, location of the tumour, cancer stage and TNM (Tumour/Node/Metastasis) staging, grade of the tumour, mutation status of key genes and whether the tumours were proficient in mismatch repair. The was no observable correlation in any of these characteristics and the *in vitro* response to *S*Tm$^{\Delta aroA}$, although the n number for this is low (3 patients in each response) and this may limit conclusions.

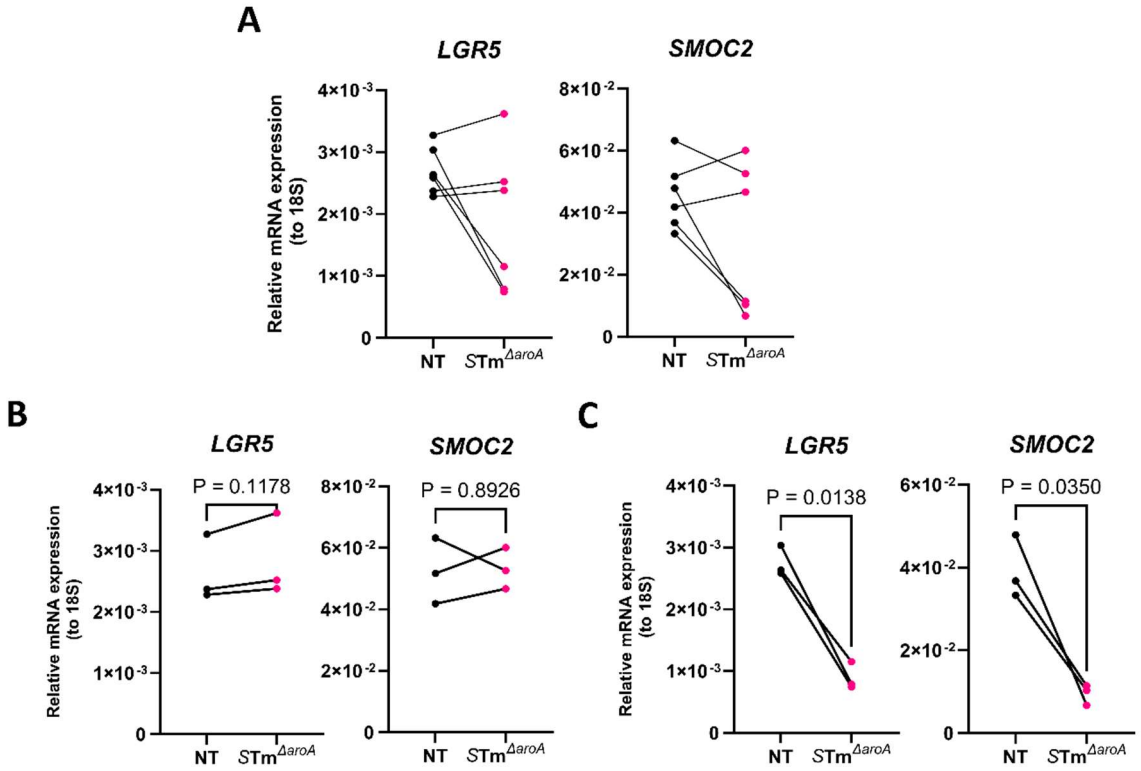


Figure 3.2.3: STm$^{\Delta aroA}$ reduces stem-cell associated transcripts in some, but not all, PDOs

qPCR for the indicated stem transcripts 24 hours post infection with STm$^{\Delta aroA}$. ***(A)*** *All patient lines tested, shown paired for the average expression of stem-cell marker genes with PBS (NT) or STm$^{\Delta aroA}$ treatment.* ***(B)*** *Subset of patient derived organoids in which STm$^{\Delta aroA}$ does not reduce transcript levels of LGR5 and SMOC2.* ***(C)*** *Subset of patient derived organoids in which STm$^{\Delta aroA}$ infection consistently and significantly reduces transcript levels of LGR5 and SMOC2. Each set of paired data points represents an individual patient line, average of 3 technical repeats. Normality was assess using Shapiro-Wilk test and p-values measured by student's t-test. (n = 6 individual patient lines).*

Table 7: Patient-derived organoid primary tumour information
Details of patients and their tumours from which the PDO lines used in this work were derived (table adapted from Oliver Pickles thesis, University of Birmingham). "n/a" indicates tumours were not tested for these mutations, "-" indicates tumours were tested and did not harbour mutations in these genes.

Organoid Line	**389**	**557**	**064**	**964**	**884**	**411**
Sex	M	F	M	M	M	F
Left/Right sided primary	R	R	L	R	L	R
Stage	III	II	III	I	IV	IV
T	4	3	2	2	3	3
N	2	0	1	0	2	2
M	0	0	0	0	1	1
Grade	Mod	Poor	Mod	Mod	Poor	Mod
RAS	-	KRAS	-	n/a	NRAS	-
BRAF	-	-	-	n/a	-	V600
MMR	MMRp	MMRd	MMRp	MMRp	MMRp	MMRp
***S*Tm$^{\Delta aroA}$ response**	"A"	"A"	"A"	"B"	"B"	"B"

3.2.4 *S*Tm$^{\Delta aroA}$ infection *in vitro* reduces growth capacity in colorectal tumour organoids

Following on from the observation of reduced stem cell-associated transcripts in mouse and some human tumour organoids, we next hypothesised that the reduction in tumour growth *in vivo* was due to a loss of stem cell capacity. To test this in both our *in vitro* models, we performed a stem-forming assay. Colon tumour-derived organoids from *Apc*$^{Min/+}$ mice and the 6 lines of PDOs were given either PBS as a control or infected with *S*Tm$^{\Delta aroA}$. The bacteria were allowed time to invade the organoids, before being washed off and gentamicin was added to the culture to prevent extracellular colony overgrowth. After 24 hours the organoids were digested to a single cell suspension, embedded into Matrigel at equal cell density between conditions, and grown for 5 days. At this point the cells were again digested, and live cells were counted **(**Schematic in **Figure 3.2.4 A)**.

The total live cell counts from these organoids at 24 hours post infection showed an early reduction in the capacity of organoids to re-grow. Qualitatively, wells seeded from infected cells had smaller, less dense organoids in the first week of growth in both mouse and human (**Figure 3.2.4 B** and **3.2.4 D**). There was also trend for fewer live cells in wells seeded from infected organoids, with this occurring in both mouse tumour organoids and human PDOs to similar extents (**Figure 3.2.4 C** and **3.2.4 E**). Importantly, the observed reduced growth capacity in PDOs was irrespective of whether the line reduced stem transcripts in earlier experiments.

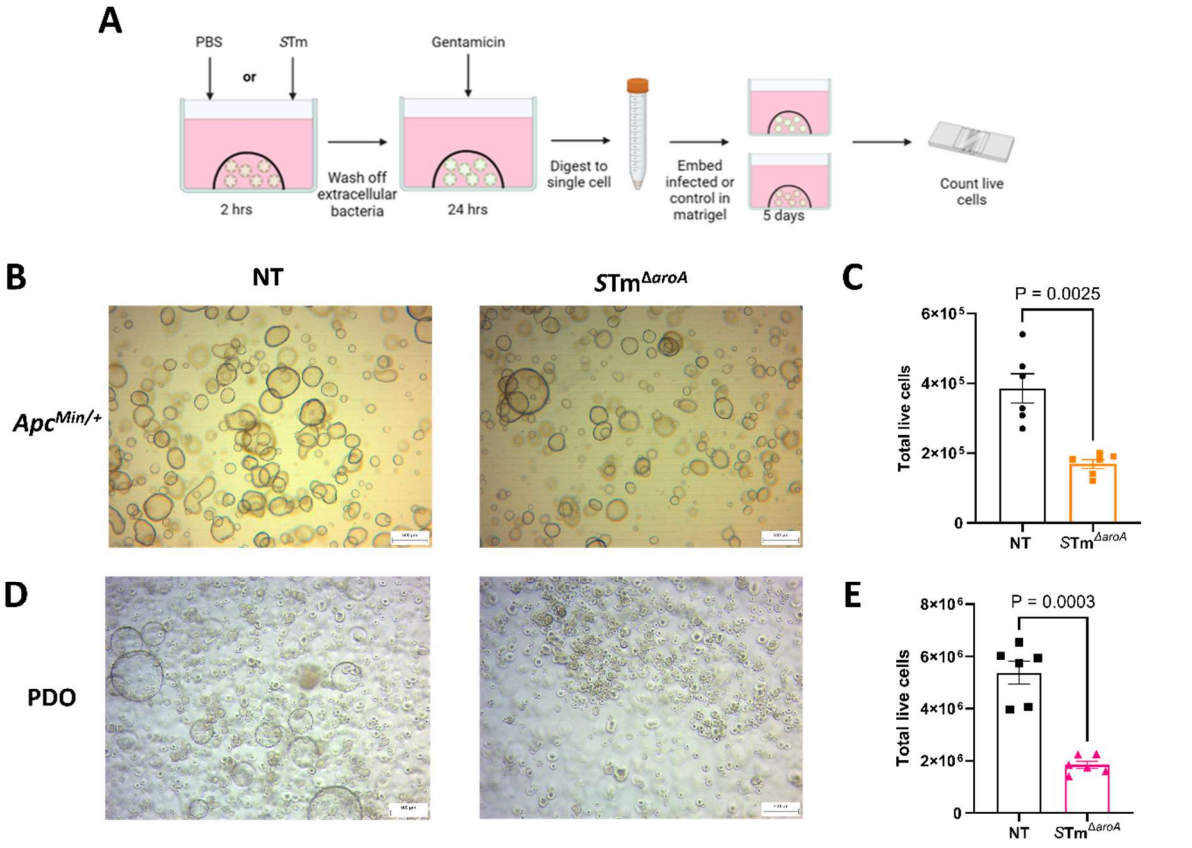


Figure 3.2.4: STm$^{\Delta aroA}$ treatment reduces growth capacity of mouse and human colorectal tumour organoids in vivo

(A) *Schematic of protocol for the stem-forming assay - 24 hours post-infection, organoids were collected and digested to single-cell suspension, keeping treatment conditions separate. Cells were re-seeded into Matrigel and cultured for 5 days.* ***(B*** *and* ***D)*** *Representative light micrographs were taken with a 4x objective on day 5 post infection of Apc$^{Min/+}$ tumour organoids* ***(B)*** *and PDO line 964* ***(D)****. Scale bars 500 µm.* ***(C*** *and* ***E)*** *Total live cell counts on day 5 of outgrowth from PBS treated (NT) or STm$^{\Delta aroA}$ treated Apc$^{Min/+}$ tumour organoids* ***(B)*** *and PDOs* ***(D)****. Data points for Apc$^{Min/+}$ organoids average cell counts of 2 wells deriving from individual infected wells, data points for PDOs represent average cell counts of 2 wells of an individual patient line. Error bars represent the mean and SEM. P-values were measured unpaired t-tests with Welch's correction. (n = 6 technical repeats for both Apc$^{Min/+}$ experiments and PDO experiments).*

3.2.5 *S*Tm$^{\Delta aroA}$ can be identified in the cells that were proliferating at the time of infection

We previously used *Lgr5*-GFP reporter mice (and colon tumour organoids derived from these) to show that *S*Tm$^{\Delta aroA}$ preferentially invades stem cells both *in vivo* and *in vitro* in mouse models of colorectal cancer (Mackie et al., 2021). To assess whether these findings translated to human PDOs, we sought to assess whether we could similarly see preferential invasion of stem or stem-like cells. Given that we could not use a lineage tracer as we had in murine experiments, and that there is a lack of good antibodies for human Lgr5, we used an indirect method. We stained organoids with CellTrace Blue (CTB) - a dye that is taken up equally by cells and diluted via cell division. As we infect our organoids via direct inoculation of the media while they are embedded in Matrigel, we first needed to confirm whether the dye could permeate the Matrigel and uniformly stain the organoids. To test this, we stained organoids either in suspension or in Matrigel and immediately processed for flow cytometry **(Figure 3.2.5)**. We noted that a majority of cells stained in suspension were able to take up the dye, even though organoid structure was maintained. However, organoids that were embedded in Matrigel were largely unable to take up the dye and this was at a rate not significantly detectable above unstained cells **(Figures 3.2.5 B** and **3.2.5 C)**. We therefore stained all subsequent experiments in suspension before embedding in Matrigel for *S*Tm$^{\Delta aroA}$ infection, using the protocol developed in this section **(Figure 3.2.5 D)**.

Following CTB labelling, organoids were infected with an mCherry-expressing strain of *S*Tm$^{\Delta aroA}$ for 24 hours before processing into single cell suspension for flow cytometry analysis. Cells were gated on live singlets and all CTB positive cells before gating mCherry positive or negative cells. In both infected and uninfected cells, we then gated on CTB high (cells which are proliferating at low levels or not at all) and CTB low (cells which are actively proliferating)

(Figure 3.2.6 A). We then calculated the ratio of cells in the CTB low to CTB high gates as a percentage of parent (mCherry positive or negative). *S*Tm$^{\Delta aroA}$-mCherry positive cells were on average 4x more likely to be in the CTB low fraction compared to *S*Tm$^{\Delta aroA}$-mCherry negative cells. We found that in 4 separate PDO lines there was a relative enrichment of *S*Tm$^{\Delta aroA}$-infected cells in the CTB low, highly proliferating cell fraction **(Figure 3.2.6 B)**. The PDOs used were an equal mix of response A and response B lines, and this had no impact on the level of enrichment of bacteria in dividing cells.

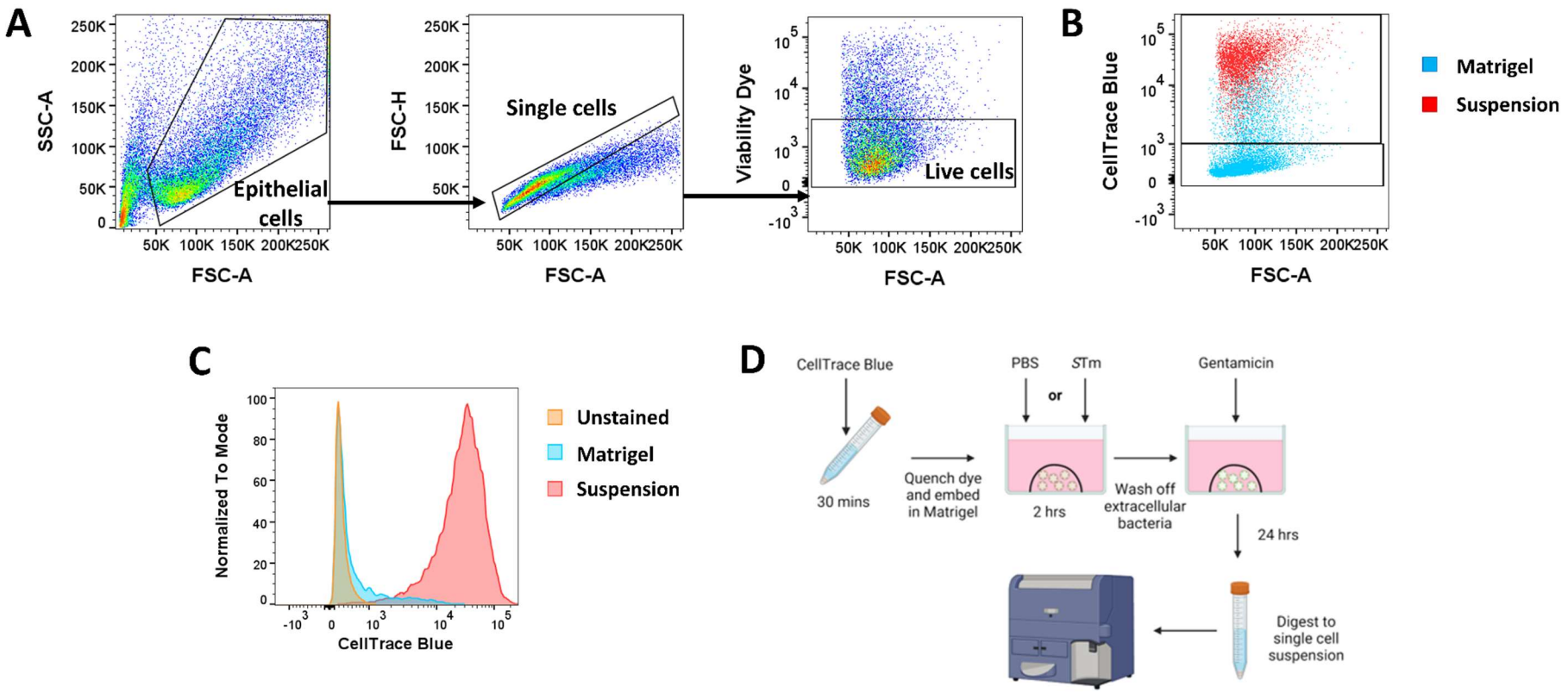


Figure 3.2.5: CellTrace Blue cannot stain organoids embedded in Matrigel
(A) *Cells were treated with CellTrace Blue (CTB) for 30 minutes before processing for flow cytometry. Gating strategy used; live singlets were gated on before percentage of CTB positive cells was assessed.* ***(B)*** *Dot plot of CTB staining in organoids stained while embedded in Matrigel (blue) and organoids stained in suspension (blue).* ***(C)*** *Histogram showing rate of CTB staining in Matrigel (blue) and suspension (red) compared to unstained cells (orange).* ***(D)*** *Schematic of suspension staining developed for CTB experiments.*

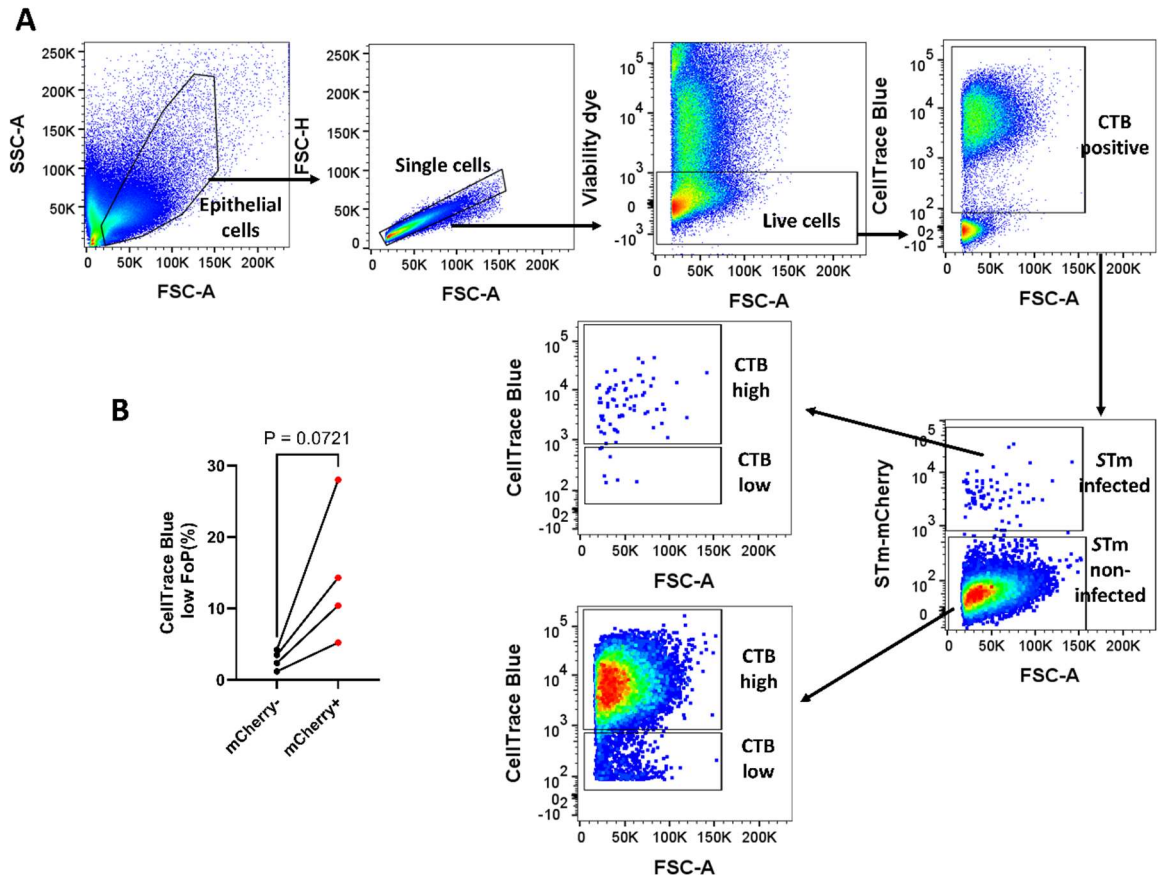


Figure 3.2.6: CellTrace Blue staining shows relative enrichment of STm$^{\Delta aroA}$ in proliferating cells at point of infection in patient-derived organoids

(A) *Example gating strategy (patient #389) of CTB panel. Live, singlet epithelial cells were gated on. CTB-negative cells were gated out to remove unstained cells. mCherry positive and negative cells (STm$^{\Delta aroA}$-infected and –uninfected) were gated and for each CTB high and low cells gated on, representing un-proliferating and proliferating cells respectively.* ***(B)*** *There is a relative enrichment of STm$^{\Delta aroA}$-mCherry positive cells in the highly proliferating, CTB-low fraction. Each paired data points represent 3 pooled wells of one individual patient. P-value was measured by paired t-test. (n = 4 technical repeats, 2 response A and 2 response B).*

3.2.6 Tumour cell proliferation is necessary for optimal intracellular infection of PDOs

The recapitulation of preferential intracellular invasion of proliferative cells and induction of impaired tumour cell growth following this invasion led us to question whether the presence of proliferating cells in the tumour is necessary for invasion. As previously discussed, it has been widely reported that bacteria, including attenuated strains exhibit specific colonisation of tumour tissue over surrounding normal tissue (Zu and Wang, 2014). Our previous observations of specific intracellular invasion of proliferative cells suggest this colonisation may be an active process seeking these dividing cells, which are increased in tumour tissue. To investigate this, we pre-treated PDOs with mitomycin C (MMC) to inhibit cell proliferation before infection. Treatment of tumour organoids with MMC induced a dose-dependent decrease in invasion of host cells by *S*Tm$^{\Delta aroA}$ **(Figure 3.2.7 B)**. As MMC is known to cause cytotoxicity, we measured cell viability. MMC was used at low concentrations (0.01 µM or 0.05 µM) for a short period, and we observed no significant reduction in the total live cell number **(Figure 3.2.7 C)**.

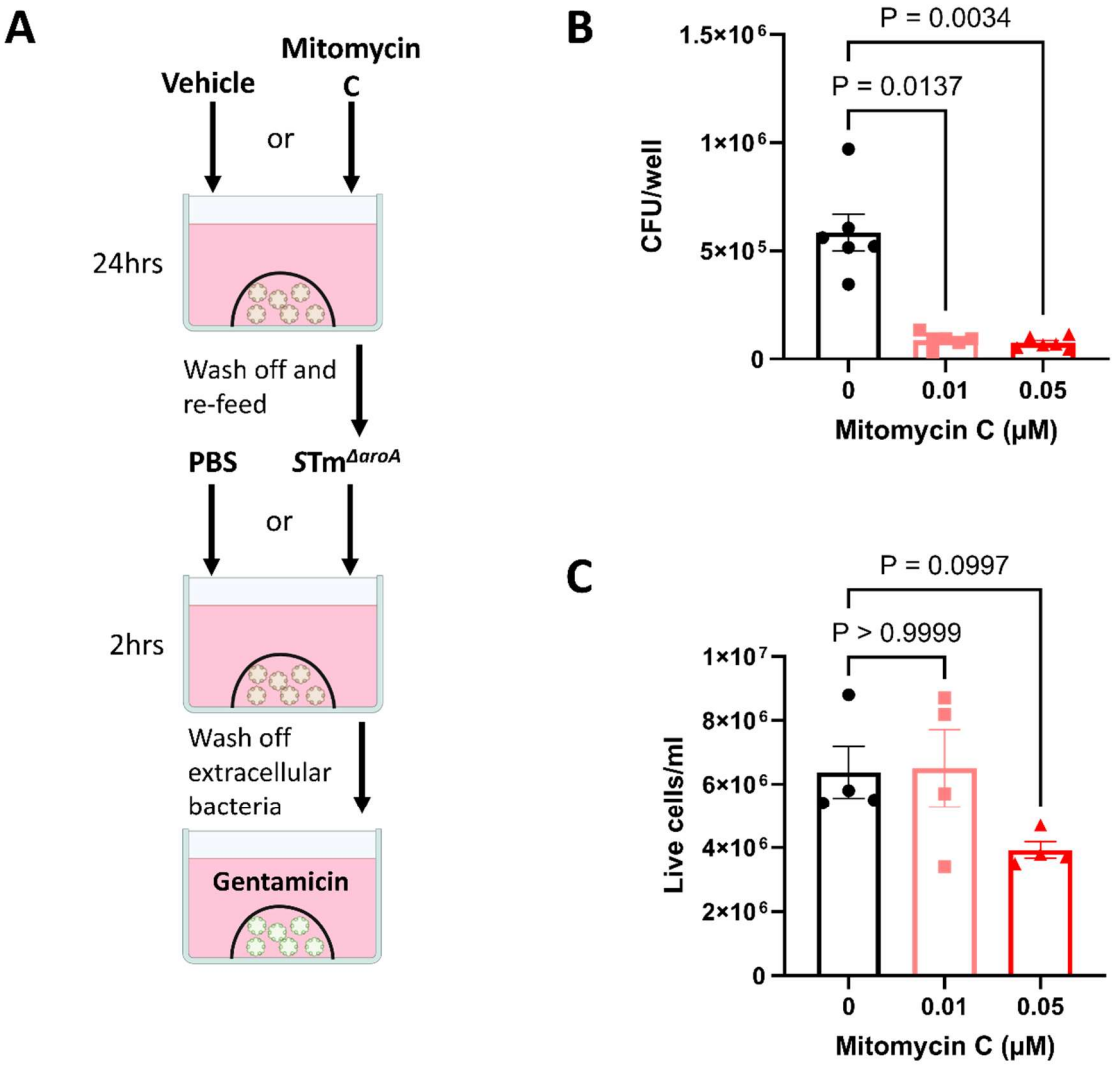


Figure 3.2.7: Optimal STm$^{\Delta aroA}$ infection requires actively proliferating cells in PDOs
(A) *Schematic showing treatment protocol of PDOs with mitomycin c before infection.* ***(B)*** *CFU recovered from organoids treated with increasing concentrations of mitomycin C.* ***(C)*** *Total live cell count was used to indicate cell viability after treatment with mitomycin C. Individual data points represent wells of either patient 411 or 389 (****(B)*** *n=6 technical repeats, 3 of each line;* ***(C)*** *n=4 technical repeats, 2 of each line). P-values were measured by Kruskal-Wallis tests.*

3.2.7 *Salmonella*-host cell cholesterol interaction is necessary for invasion *in vitro*

I further investigated whether *S*Tm invasion of *Apc*$^{Min/+}$ tumour organoids was dependent on the cholesterol-binding component of the T3SS, *sipB.* I compared the CFU recovered from organoids following *in vitro* inoculation with *S*Tm strains with Sip proteins genetically deleted, using *S*Tm$^{\Delta aroA}$ as a control. We found that there was a reduction in bacterial burden following deletion of all Sip proteins, however this was most significant with *sipB* deletion **(Figure 3.2.8)**. *Salmonella* with deleted *sipC* or *sipD* genes infected organoids at a rate of approximately 100-fold and 10-fold fewer colonies than *S*Tm$^{\Delta aroA}$, respectively. Unsurprisingly, these data suggest an intact T3SS apparatus is essential for maximal invasion of organoids. Strikingly, *sipB* deletion led to an almost complete inability to invade mouse tumour organoids. Colonies were recovered from only one experimental repeat, and this was at a dramatically reduced level of 4 CFU/well compared to an average of 8x10^3 CFU/well for *S*Tm$^{\Delta aroA}$.

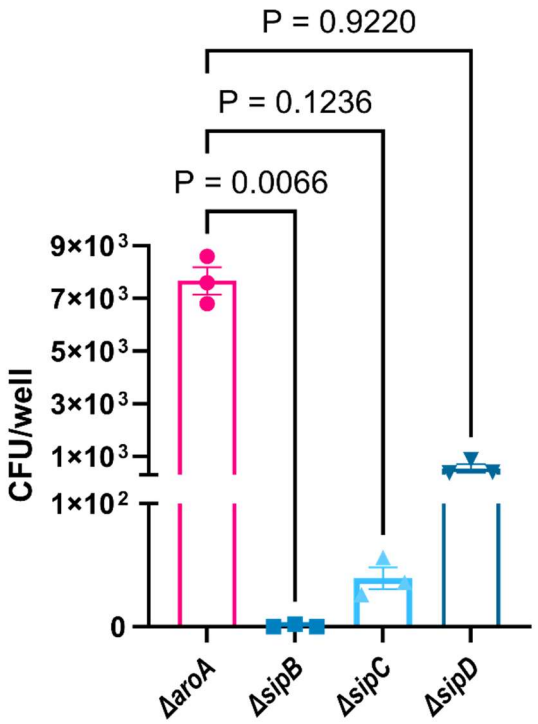


Figure 3.2.8: Optimal invasion of tumour organoids by STm$^{\Delta aroA}$ is dependent on an intact type-3 secretion system

Apc$^{Min/+}$ organoids were infected with either STm$^{\Delta aroA}$ or STm with mutations in the components of the infection machinery. Data points represent CFU of one well of organoids. Error bars represent the standard error of the mean. P-values measured by Kruskal-Wallis test. (n = 3 biological repeats).

To confirm that reduced bacterial burden in *S*Tm$^{\Delta sipB}$ was due to diminished binding of host cell cholesterol via SipB, we sought to recapitulate the effect by depleting host cholesterol at the cell membrane. Organoids were pre-incubated with methyl-β-cyclodextrin (MβCD), which is known to sequester cholesterol from the cell membrane for up to 2 hours, the duration of the interaction with extracellular bacteria. This was then removed and wells washed thoroughly to prevent an effect on the *S*Tm$^{\Delta aroA}$. Confocal imaging of *Apc*$^{Min/+}$ organoids with filipin shows that 5 mM MβCD is sufficient to deplete the cell surface cholesterol **(Figure 3.2.9 B)**. There was a striking reduction in bacterial CFU of around 100-fold after treatment with 5 mM MβCD, and at 10 or 15 mM *S*Tm$^{\Delta aroA}$ invasion is entirely blocked **(Figure 3.2.10 A)**. This was not associated with toxicity as there was no reduction in live cell number with treatment of 5 or 10 mM, but 15 mM did show some toxicity **(Figure 3.2.10 B)**. We therefore confirm a role for cholesterol in the invasion of tumour cells by *S*Tm. This is in agreement with Hayward at al. (2005) who demonstrated that *Salmonella* could not invade mammalian cells treated with MβCD (Hayward et al., 2005).

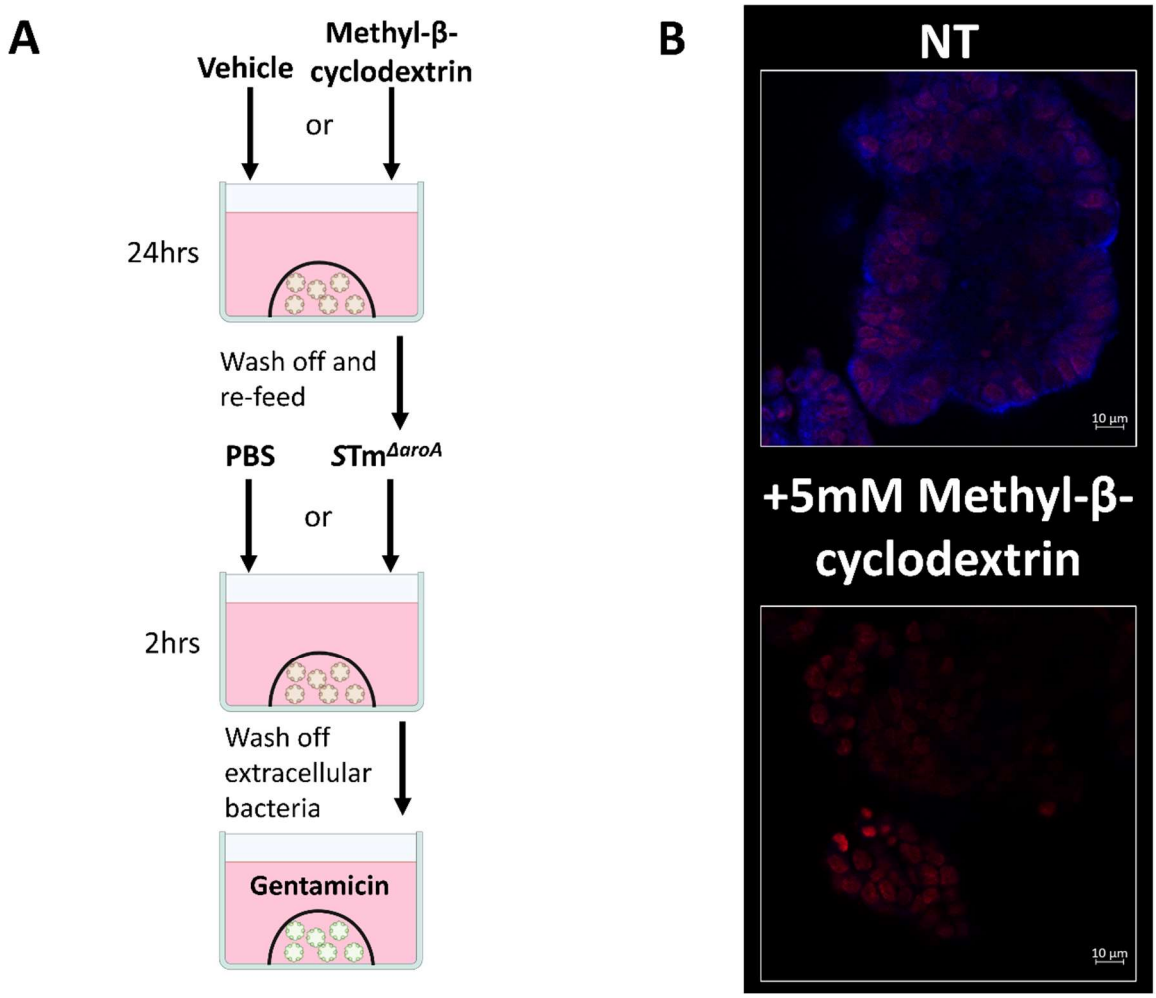


Figure 3.2.9: Methyl-β-cyclodextrin treatment of organoids reduces cell surface cholesterol
(A) *Schematic showing methyl-β-cyclodextrin (MβCD) pre-treatment of organoids and infection.* ***(B)*** *Representative image of cell surface cholesterol of one organoid stained using filipin (blue) and DAPI stains the nuclei (red) in* $Apc^{Min/+}$ *organoids after 1 hour treatment with 5mM MβCD. Images taken at 63x magnification; scale bars indicate 10 µm.*

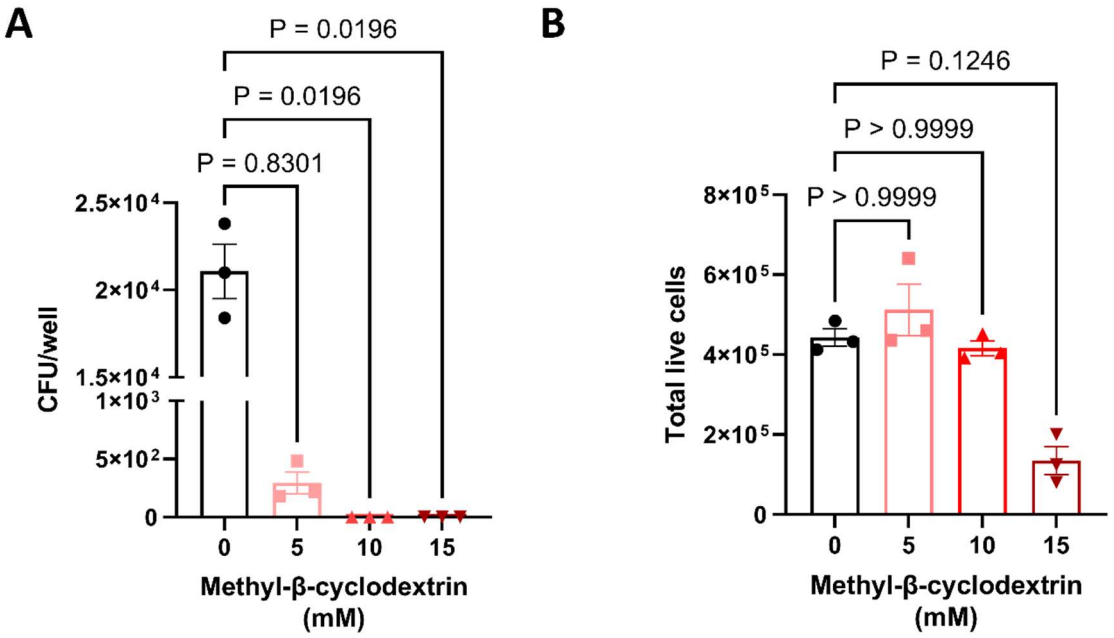


Figure 3.2.10: Methyl-β-cyclodextrin treatment reduces bacterial burden in tumour organoids
(A) *$Apc^{Min/+}$ organoids were treated with increasing concentrations of MβCD prior to infection with $STm^{\Delta aroA}$. Data points represent CFU recovered from one well of organoids. (n = 3 biological repeats)* ***(B)*** *Live cell count was used to measure cell viability after MβCD treatment. Data points represent one well of $Apc^{Min/+}$ tumour organoids. Error bars represent the mean and SEM. P-values were measured by Kruskal-Wallis tests. (n = 3 biological repeats).*

3.3 Discussion

Intestinal cancers are characterised by an epithelial-to-mesenchymal transition which is driven in part by aberrant Wnt signalling inducing loss of E-cadherin expression, leading to disorganised epithelial layers and increased proliferation of cancer stem cells (Peng et al., 2014). We utilised immunohistochemistry to investigate the effect of repeated oral gavage of *S*Tm$^{\Delta aroA}$ on the gut epithelium in a colitis-associated colon cancer mouse model **(Figure 3.2.1)**. These data demonstrate that BCT with *Salmonella* delivered by oral gavage in mice can significantly alter the structure of the tumour epithelium, while also altering protein expression to result in a reduction of some of the key characteristics of colorectal cancer.

We have now shown reduced Ki-67 protein expression in the tumour epithelium of treated mice and reduced expression of stem-cell associated genes in RNA-sequencing data and qPCR of colorectal tumour tissue in mice following *S*Tm$^{\Delta aroA}$ treatment (Mackie et al., 2021). To see if this translated to human disease, I utilised an *in vitro* infection model of several PDO lines. First, I assessed whether PDOs could be infected *in vitro* by *S*Tm$^{\Delta aroA}$ by utilising the same inoculation of the media we had previously used with mouse tumour organoids. We found PDOs could also be infected using this method, albeit at a lower level compared to mouse organoids **(Figure 3.2.2 B)**. However, while the mouse and human organoids grew at qualitatively similar densities, I did not account for differences in cell number or proliferation rates between organoid lines at the point of infection. The difference in burden between the species further highlights the need to interpret *Salmonella*-mediated BCT findings in mouse models with some caution and may add to the understanding of why the translation of findings in mice into humans has been as yet disappointing. qPCR of untreated and *S*Tm$^{\Delta aroA}$

infected PDO lines showed around half of the panel recapitulated the effects we had previously observed in mouse tumour organoids and half not **(Figure 3.2.3)**. These data suggested that the panel of PDO lines we investigated may model patient heterogeneity.

We then received the details of the primary tumours from which the PDO lines were established and investigated these in relation to the response to *S*Tm$^{\Delta aroA}$ *in vitro* **(Table 7)**. The bacterial load of the microbiome increases along the intestinal tract from the stomach to the rectum, and the composition of the microbiome also changes (Lkhagva et al., 2021). This is thought to be a result of decreasing pH and oxygen content along the intestine, meaning that the epithelial cells themselves are optimised to their location (Wlodarska et al., 2015). We therefore hypothesised that there may be a link between left or right sided tumours and response to BCT. However, we saw no correlations between the details of the patients or their tumours and response to *Salmonella*. The details we have regarding the tumours is limited, as is the number of patients per response and so it may be that we do not have enough data to draw meaningful comparisons here so further PDO lines should be generated and tested. It is of note that the stem cell markers were identified in RNA-sequencing of mouse intestinal tumours. There is evidence that although LGR5 is known to be increased in developing human colorectal tumours, later stage poorly differentiated cells have much lower levels (Martin et al., 2018). Therefore, these markers may not be appropriate readouts for human cancer response to infection, and so we progressed on to assessing the functional impact of the treatment on PDOs.

We show that in *in vitro* mouse and patient-derived organoid models of colorectal cancer there is a direct effect of *S*Tm$^{\Delta aroA}$ on the tumour epithelium itself. In wells seeded from the

single cell digest of infected organoids we observed stunted regrowth, shown quantitatively by cell counts and qualitatively in the size, shape and density of organoids after outgrowth **(Figure 3.2.4)**. These data suggest that the efficacy of BCT – at least in part – relies on tumour-intrinsic mechanisms. Interestingly, reduced live cells were observed in all patient-derived organoids, including the lines which did not have reduced levels of stem-cell marker transcripts after infection. This suggests there may be patient-specific effects that result in a convergence on a similar functional outcome, which may imply that there are different mechanisms of action in different tumours. It would be of clinical benefit to identify the characteristics of the tumours that induces the "mouse-like" response B compared to response A to use this as a predictor of response in patients.

To assess whether the bacteria also preferentially invaded proliferating cells in human organoids we utilised an indirect method by staining of PDOs with a proliferation dye that is absorbed by all cells and dilutes through subsequent cell division. The CellTrace Blue dye is quenched by FBS during the protocol, and we think it is likely that the protein content of the Matrigel acts to inhibit the dye in a similar way and therefore developed a protocol whereby we stained the organoids whole in suspension. We found that in four individual PDO lines, there was a relative enrichment of *S*Tm$^{\Delta aroA}$ in the CellTrace Blue low population, those cells which have been actively proliferating since the point of infection **(Figure 3.2.6 B)**. These data recapitulate the findings described above of *S*Tm$^{\Delta aroA}$ colonising Lgr5+ stem cells in the mouse intestinal tumour (Mackie et al., 2021) and occurred in all 4 PDO lines used, regardless of whether they were "response A" or "response B". The extent of the enrichment in the proliferating cells was not correlated with bacterial burden. It is worth noting that this was a relative enrichment, and thus there was a minor population of *S*Tm$^{\Delta aroA}$-positive cells in the

CellTrace Blue high fraction, suggesting that there is a preference but that infection can occur in non-proliferating cells. It is possible that these were recently divided or non-actively dividing stem cells.

Following on from this observation that *S*Tm$^{\Delta aroA}$ are enriched in the proliferating cells of tumours, we assessed whether proliferation was a requirement for host cell invasion. Mitomycin C acts to block proliferation by preventing DNA replication and has been historically used as a therapeutic in a range of cancers for this reason (Bradner, 2001). We treated two PDO lines with MMC or vehicle control for 24 hours before inoculation of the media with *S*Tm$^{\Delta aroA}$. This resulted in a significant reduction in bacterial burden in both patient lines **(Figure 3.2.7)**. This did not completely abolish intracellular invasion which aligns with the data from the CTB experiment above, again suggesting a passive preference of invading proliferating cells rather than active dependence on them. While the ability of MMC to inhibit cell division is well characterised it is worth highlighting that arrest of proliferation was not confirmed in this experimental set up, and this should be done in the future. One method of doing this would be to measure uptake of iododeoxyuridine into cells, which is incorporated into DNA of cells undergoing mitosis and can directly measure rates of proliferation in cells in culture.

Quiescent haematopoietic stem cells have been shown to be more resistant to infection by *Salmonella* typhimurium *in vitro* than partially differentiated, proliferating progenitor cells (Kolb-Mäurer et al., 2002). Another study demonstrated undifferentiated murine embryonic stem cells were highly susceptible to intracellular infection by *Salmonella* typhimurium in a SipB- and host cell cholesterol synthesis-dependent manner (Yu et al., 2009). Further, cell

membrane cholesterol is present at highest concentrations during cell division (Santos et al., 2013). It has also been shown previously that *Salmonella* uses its T3SS protein SipB to bind cholesterol at the cell surface of host cells to anchor and effectively invade (Hayward et al., 2005). We therefore hypothesised that in our models of colorectal cancer we see preferential invasion of the proliferative cells due to increased cholesterol on tumour stem cells leading to increased chance of SipB binding, which facilitates host cell invasion. To assess this, we compared the invasion capacity of *S*Tm after deletion of genes for the Sip family proteins B, C and D. We did not use SipA as it has been previously shown to be important for host cell actin remodelling, but not essential for intracellular invasion (Zhou et al., 1999). Unsurprisingly, we saw a reduction in bacterial burden following deletion of *sipB, C* or *D* as the invasion machinery had been disrupted. However, this reduction was most striking in *Salmonella* with deletion of *sipB* **(Figure 3.2.8)**. These data indicate that while an intact needle and rod are needed for maximal invasion of host cells in mouse tumour organoids, it is SipB which is essential for infection.

As SipB binds host cholesterol, I took the further step of using MβCD to deplete cholesterol in the cell membranes of our $Apc^{Min/+}$ tumour organoids before inoculation with $STm^{\Delta aroA}$ **(Figure 3.2.9 B)**. I observed a dose-dependent reduction in bacterial burden following cholesterol depletion at the cell surface of tumour organoids. It has been shown previously that there was no impact to cell viability of cell lines treated with MβCD at the concentrations used (Garner et al., 2002) and we confirm this in our organoids **(Figure 3.2.10)**. Thus, we conclude that the reduced bacterial burden is due to depletion of cholesterol preventing invasion into host cells. These data taken with the known literature and the striking reduction of invasion with SipB-deficient *Salmonella* suggests a mechanism by which proliferative cells in the tumour can be

directly targeted by *S*Tm$^{\Delta aroA}$ for intracellular infection. It would be of benefit to further interrogate the role of cholesterol by increasing the available cell surface cholesterol prior to infection. I hypothesise that *S*Tm$^{\Delta aroA}$ burden would be increased, but the *S*Tm$^{\Delta sipB}$ would remain unable to invade, if this is correct this would confirm the mechanism of interaction between *Salmonella* and host tumour cells.

One major avenue for BCT is engineering the bacteria to act as tumour-specific delivery systems for various payloads, whether it be to target the tumour microenvironment or intracellular delivery. We have shown that only a small proportion of cells are directly infected in PDOs, as seen in the representative flow plot of mCherry+ cells in the *S*Tm$^{\Delta aroA}$ treated condition **(Figure 3.2.6 A)**. We hypothesise that this is due to a small number of cells actively proliferating at the point of infection. It is possible that *in vivo* and in patients that there would be local re-infection events occurring that would allow for newly proliferating cells to be colonised that cannot occur in our *in vitro* models due to the presence of gentamicin post-infection. However, this is unlikely to occur at a high rate as it has been shown that bacterial burden of tumours reduces over time (Mackie et al., 2021). Therefore, these findings will be critical in considering the type of therapeutic to deliver into tumours. For example, studies which utilise BCT to deliver treatments more generally to the tumour microenvironment rather than treatments with intracellular targets are likely to show better efficacy. One group has recently used attenuated *Salmonella* typhimurium engineered to overexpress L-asparaginase selectively to sub-cutaneous tumours in mice to deplete the TME of asparagine, a key energy source for tumours (Kim et al., 2015). The effectiveness of this therapy was likely due its targeting of the tumour microenvironment rather than tumour cells themselves, as we have shown here that only a small number of tumour cells are directly infected *in vivo*. This

work may lead to more rationalised design of BCT as a delivery system for therapeutic payloads as it suggests that this approach could work if used to target specifically the proliferative cells, however this risks missing most cells. There are many malignant but dormant cells in tumours and so targeting the TME is likely to have the most significant anti-tumour effect.

Future work to evaluate the involvement of internalisation of bacteria and downstream intracellular effects in the mechanism of action of BCT is needed; it has recently been shown that *Salmonella* induces mixed cell death pathways within host cells but whether this is necessary to reduce tumour burden is unknown (Fattinger et al., 2021a). We previously showed that lytic cell death was not increased in *Apc*$^{Min/+}$ tumour organoids treated with *S*Tm$^{\Delta aroA}$ when measured with a lactate dehydrogenase assay (a marker of pyroptosis), but a slight increase in cleaved caspase-3 was observed (Mackie et al., 2021). It is possible that this represents specific apoptotic cell death in the directly infected cells, which I have now shown are the proliferative cells.

It remains to be shown whether direct invasion of tumour cells in this context is essential to reduce tumour burden. We hypothesise that *S*Tm$^{\Delta sipB}$, which we have shown is almost entirely incapable of invading tumour organoids, would be able to exert some anti-tumour effects. We hypothesise that the bacteria would establish extracellular, but intratumoural, colonies and induce metabolic competition on the tumour as we saw with *S*Tm$^{\Delta aroA}$ (Mackie at al., 2021). As discussed in chapter 1 there is currently only one approved use of BCT in patients, which is BCG vaccine for superficial bladder. While the mechanism of this therapy is not entirely known, it has been shown that direct contact and binding of the bacteria to the urothelial cells

is essential for the downstream anti-cancer effects (Kavoussi et al., 1990; Zlotta et al., 1997). This possibly suggests that a large portion of BCT efficacy indeed relies on intracellular bacteria or the induction of antimicrobial responses via extracellular-elicited signals mediated by adherence to host cells.

We conclude from the findings in this chapter that *S*Tm$^{\Delta aroA}$ preferentially binds to and invades proliferating cells, of which there is an enrichment in tumours, via increased interaction between *Salmonella* SipB and host cell surface cholesterol. This specific colonisation leads to reduced growth capacity of murine and human tumour organoids *in vitro*.

CHAPTER 4- EXTRACELLULAR AND INTRACELLULAR *S*Tm$^{\Delta aroA}$ ALTER THE TRANCRIPTIONAL LANDSCAPE OF TUMOUR ORGANOIDS

4.1 Introduction

We have shown that *S*Tm$^{\Delta aroA}$ only invade a small proportion of cells intracellularly, and yet there are transcriptional and functional effects on the tumour cells both *in vivo* and *in vitro*. I therefore wanted to assess if there was a distinction between the intracellular and extracellular effects of the bacteria on the tumour cells. I hypothesised that the direct infection of a few cells in the organoids would induce paracrine effects to propagate the alarm signals and remodel the environment in response. The extracellular bacteria may also be detected through either secreted factors or contact with the tumour cell surface and act to similarly propagate an antimicrobial response, although we hypothesise this will be to a lesser extent.

The gut epithelium is constantly sensing its local environment and relaying the information via cell-cell signalling to neighbouring epithelial and immune cells. One mechanism of this surveillance is the expression of PRRs expressed both on the cell surface and intracellularly in epithelial cells, allowing them to detect microbial products known as PAMPs and host-derived DAMPs (Tang et al., 2012). PRRs then act to amplify this detection via downstream signalling, often via assembly of inflammasome complexes. These are multi-protein complexes that ultimately result in inflammatory mediator release and activation of programmed cell death pathways (Tsuchiya, 2020). Co-ordinated extrusion of infected cells from the epithelium is further orchestrated by components of the inflammasome pathway, and this step is essential

for limiting pathogen burden in the gut (Sellin et al., 2014). This initial expulsion has been shown to occur at the same time as IL-18 and eicosanoid release to promote luminal flushing and recruitment of phagocytes to further limit spread of pathogens (Rauch et al., 2017). Detection of shedding by neighbouring cells is not completely understood but must occur to ensure that barrier integrity is maintained. One mechanism of detection by neighbouring cells is thought to be physical contractile events relaying the location of infected cells, importantly before their expulsion (Samperio Ventayol et al., 2021; Sadeghipour et al., 2018). It is thought that detection of this by adjoining cells allows packing of intestinal epithelial cells at the site of infection and upregulation of cell adhesion molecules, meaning cells are primed to form new tight junctions. Furthermore, it has been shown that cells infected with *Shigella, Listeria* or *Salmonella* propagate NF-κB induction to surrounding bystander, uninfected cells and this induces an inflammatory IL-8 response in all cells, regardless of infection status (Kasper et al., 2010). These data suggest that the small population of infected cells within the tumour organoids will likely be able to affect global inflammatory and structural signalling.

In this work I have utilised both single-cell RNA sequencing and bulk RNA-sequencing of tumour organoids to answer different questions about the effect of *S*Tm$^{\Delta aroA}$ on the tumour epithelium. In the early 1990s it was first described that cDNA could be amplified from single cells and gene expression analysed (Eberwine et al., 1992; Brady et al., 1990). This early work was limited in its dependence on techniques such microinjection of reagents into individual cells. Advances in experimental practice first allowed the whole transcriptome sequencing and analysis of a single mouse blastomere (Tang et al., 2009), and then microfluidic and computational improvements enabled high-throughput sequencing and analysis of single cells

in samples containing millions of cells from mixed lineages, as reviewed here in 2018 (Hwang et al., 2018).

The single-cell library in this work was generated and sequenced at Genomics Birmingham, using the workflow shown below **(Figure 4.1.1A)**. Briefly, after digesting samples to single cell suspensions and confirming cell viability was above the threshold, the cells are mixed with Gel beads at a flow rate that ensures one cell/bead. The Gel Beads contain barcoded oligonucleotides and reverse transcriptase, and once bound to a cell the pair are encapsulated in an oil droplet. Within this droplet the bead dissolves and the cell is lysed, releasing the RNA which is then reverse transcribed and barcoded with the unique sequence from the bead. The barcoded cDNA is then pooled, and adaptors attached to the cDNA for sequencing. The unique barcodes attached in the droplet allow transcripts to be mapped to the individual cell during analysis. Single-cell RNA-sequencing generates high resolution datasets and analysis generally focusses on identifying cell populations present in the samples based on gene expression profiles and differences between cell-types at steady state and with treatments (Li and Wang, 2021). Bulk RNA-sequencing uses a simpler workflow **(Figure 4.1.1 B)** in which total RNA is isolated from cells and undergoes reverse transcription to cDNA. This cDNA library is then fragmented and amplified, with adaptors added to the DNA fragments to allow sequencing initiation. Bulk RNA-sequencing data is lower resolution than single-cell but is a useful tool for analysing global changes to gene expression as it measures the average level of expression of specific genes in all the input cells.

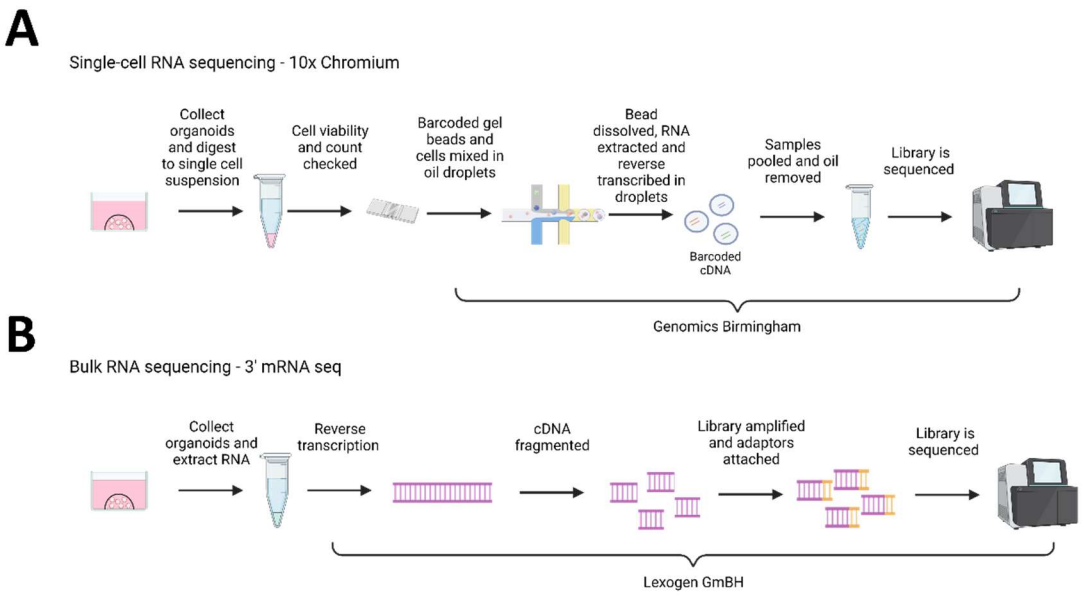


Figure 4.1.1: Workflow for sequencing methods used
Schematic detailing the workflows used for the sequencing methods used in chapter 4. Figure created using (Li and Wang, 2021) *and product literature from and 10x Genomics **(A)**, product literature from Lexogen GmBH **(B)** and Biorender.com*

I first employed single-cell RNA sequencing of human patient-derived organoids 24 hours after inoculation of the organoid media with PBS or *S*Tm$^{\Delta aroA}$ to investigate the effect of bacteria on cell-type composition of the organoids and global transcription. We have previously published work using mice with a fluorescent reporter for Lgr5+ stem cells that *S*Tm$^{\Delta aroA}$ was enriched in stem cells of polyps *in vivo* (Mackie et al., 2021). I then showed in chapter 3 that there is preferential invasion of cells which are dividing at the point of infection in PDOs **(Figure 3.2.6)**, and that actively proliferating cells are necessary for optimal invasion **(Figure 3.2.7)**. This was associated with a reduction in the growth capacity of organoids following infection **(Figure 3.2.4)**; thus, I hypothesised that there would be a proportionally larger impact on the stem cell population of PDOs following *S*Tm$^{\Delta aroA}$ treatment. Furthermore, preliminary work in the previous chapter identified 2 distinct responses to *S*Tm$^{\Delta aroA}$ in PDO lines **(Figure 3.2.3)**. To

investigate the transcriptional characteristics of these two responses, I used 2 “response A” PDO lines (patients 064 and 389) and 2 “response B” lines (patients 964 and 411) for the single-cell RNA-sequencing experiment. By using a mixture of response lines, I aimed to draw comparisons between non-treated and *Salmonella* treated samples of each patient line, and more generally what features are conserved within response types and what differs between them.

Single-cell RNA sequencing analysis includes the identification of distinct cell typers within a sample, therefore with this pipeline I aim to identify the cell-types present in individual PDO lines. There is evidence that the proportions of cell-types in the gut change following infection with *Salmonella* typhimurium, and therefore I will also investigate the changes, if any, that occur in the cell-type populations following *S*Tm$^{\Delta aroA}$ treatment. One group demonstrated that in mice infected with wild-type *S*Tm there is an enrichment in the number of Paneth cells in the small intestine, yet a decrease in lysozyme expression (Rodriguez et al., 2012). Paneth cells are a type of secretory cell which are present in the small intestine of healthy mice and humans and largely absent from the colon; however, colonic Paneth cells have long been shown to be increased in inflammatory diseases such as ulcerative colitis and cancers (Lewin, 1969). One study screened early-stage colonic tumours from 38 patients using immunohistochemistry and found the presence of Paneth cells (using the marker lysozyme) in around half the cohort. The presence of the Paneth cells was correlated with increased expression of Wnt signalling pathway components and poor patient prognosis (López-Arribillaga et al., 2021). Furthermore, aggressive colorectal tumours are characterised by a loss of epithelial identity of the tumour epithelium and an increase in more mesenchymal markers, a process termed epithelial-to-mesenchymal transition (Vu and Datta, 2017). I

showed in chapter 3 that we see a restoration of epithelial cell marker E-cadherin in the tumour epithelium of mice treated with *S*Tm$^{\Delta aroA}$ **(Figure 3.2.1)**, suggesting a fundamental change in the make-up of the epithelium. Therefore, I hypothesise that there will be global changes in expression of genes associated with healthy gut and more epithelial identity and associated reduction in mesenchymal markers.

Finally, in this chapter I have also performed bulk RNA-sequencing of both *Apc*$^{Min/+}$ colon tumour organoids and one patient-derived organoid line (patient 389) at 6 hours post infection either with or without pre-treatment with MβCD to prevent intracellular infection. In chapter 3 I demonstrated that MβCD effectively removed cell surface cholesterol in tumour organoids and acted to restrict *S*Tm$^{\Delta aroA}$ to the extracellular space. By using an earlier timepoint than in the single-cell RNA sequencing experiment, I aimed to include the directly infected cells. I hypothesised that this would enable comparison of organoids with some intracellular infection and those with only external contact with the bacteria for the initial 2 hours of culture. With this work I aimed to dissect the extent to which *S*Tm$^{\Delta aroA}$ can be detected by and influence tumour organoids when limited to the extracellular space. *Salmonella* typhimurium is regarded as primarily an intracellular pathogen; therefore, we hypothesise that *S*Tm$^{\Delta aroA}$ will have the largest impact on the transcriptome of the tumour organoids in the context of intracellular invasion.

4.2 Results

4.2.1 Preparation of samples and processing of data for single-cell RNA sequencing

We first wanted to investigate the cell-type composition of PDOs before and after treatment with *S*Tm$^{\Delta aroA}$, hypothesising that there would be reduced proliferative cells and a shift toward expression of more normal epithelial cell markers. 4 patient organoid lines were infected with *S*Tm$^{\Delta aroA}$ *in vitro,* bacteria were removed, and the media supplemented with gentamicin for 24 hours. Cells were harvested, digested to single-cell suspension, and taken for live cell counting and preliminary quality-checking. Cells were then processed for library preparation and sequencing using 10x Chromium system by Genomics Birmingham. All analysis was performed using R, with training and guidance from Csilla Varnai (Centre of Computational Biology, University of Birmingham) who was co-opted onto this project as a bioinformatics post-doctoral scientist.

Single-cell RNA sequencing reads were processed into a Seurat object and filtered using established cut-offs for number of features per cell and percentage of mitochondrial reads (Hao et al., 2020). This acts to remove cell debris, low viability cells and clumps of cells from the analysis. The initial quality checking and processing is described in chapter 2, but to recap briefly, seven of the eight samples returned appropriate distribution of cells and cell numbers (an average of ~6,500 cells/sample) post-filtering. However, one sample ('389_stm') had higher number of cells post-filtering than there had been entered into the experiment, suggesting that fragments and debris were being classed as viable cells. To account for this an extra filter was added to adjust for this sample, removing cells with abnormally high counts, this resulted in the sample being more consistent with the others **(Figure 2.11.1)**.

Cell cycle phase can impact the clustering of single-cell RNA sequencing data (Kowalczyk et al., 2015; Barron and Li, 2016). To assess the extent of this in our dataset, the cell cycle phases were scored for each cluster and coloured on the UMAP **(Figure 2.11.3 A)**. In the gut and in gut-derived organoids there are cell-type specific differences in cell cycle and so this was not normalised across the data and instead considered when assessing the identity of cells (i.e., proliferative stem cells vs differentiated cells). The online Panglao database was mined for all datasets using human intestine samples with 10x chromium sequencing (Franzén et al., 2019). All cell-type markers identified in these data sets were compared with the top upregulated genes for each cluster for this integrated data set. In combination with this, the scCATCH (Shao et al., 2020) pipeline was utilised as a further unbiased approach to match cluster markers with known cell markers. By using both these methods some, but not all, clusters were assigned identities- suggesting that some clusters were patient-specific **(Figure 2.11.3 B)**. Known classical markers were used to confirm the suggested cell types from the database comparisons. Markers used for this were *TFF3, MUC2* and *KRT19* (goblet cells); *PROM1* (progenitor cells); *CXCL3, ATOH1* and *LYZ* (Paneth cells); *LGR5, SMOC2* and *OLFM4* (stem cells), *CDX1* (enterocytes); *CEACAM1* and *NEAT1* (tumour cells) **(Figure 2.11.3 C)**. The combination of these methods led to cell-type identities being assigned.

4.2.2. *S*Tm$^{\Delta aroA}$ treatment has limited effects on cell-type composition of PDOs

We first aimed to identify whether *S*Tm$^{\Delta aroA}$ altered the composition of PDOs, either via targeted cell death of infected cells or inducing differentiation programmes in response to detection of bacteria. To assess this, we combined all PDO lines and plotted the identified cell type clusters on a UMAP, split by NT and *S*Tm$^{\Delta aroA}$ treated samples **(Figure 4.2.1)**. We hypothesised there would be a change in the stem and other proliferative cell clusters

(identified from cell cycle phase analysis as clusters toward the top clusters of the UMAP) **(Figure 2.11.3 A**). We observed no striking changes in the densities of clusters as shown on the UMAP. The only altered cluster following *S*Tm$^{\Delta aroA}$ treatment appeared to be Paneth cell 1 which was increased.

Cells from each sample were classified as RA (response A) or RB (response B) in the Seurat object. The total cell numbers of RA and RB samples was determined, and the proportion of different cell types making up these samples was calculated. Proportions of cell-types was calculated as a percentage of total RA or RB non-treated and *Salmonella* treated cells to account for differences in cell numbers per sample. Cell types that are separated into more than one cluster have been combined for clarity **(Figure 4.2.2)**.

Response A and response B lines have different proportions of cell-types before any treatment and these populations are affected differently after treatment. Response A lines are more secretory-cell dominant (Paneth and goblet cells) than response Bs in the steady state. The response B lines are made up more of proliferative cells such as progenitors, tumour and stem cells. Response A lines appear to slightly reduce the relative proportion of secretory cells following *S*Tm$^{\Delta aroA}$ treatment **(Figure 4.2.2 A)**. In contrast, treatment with *S*Tm$^{\Delta aroA}$ induced an expansion of Paneth cells and relative reduction in tumour cell proportion in response B compared to NT samples of these lines **(Figure 4.2.2 A)**.

Looking specifically at the tumour cell clusters highlights patient- and response-specific populations. Clusters termed tumour 1, 2, 3 and 6 originated from all samples in comparable proportions, however tumour 4 is only present in response B lines (almost entirely 964-derived) and tumour 5 is more prevalent in response A lines **(Figure 4.2.2 B)**. The proportion

of response B-specific tumour 4 cluster is reduced after treatment, whereas response A-specific cluster tumour 5 is increased. This shows a relative reduction in the tumour cells and relative expansion of differentiated (or “normal”) cells in the response B lines, whereas in response A lines there is a relative expansion in tumour cell clusters. Therefore, there appears to be a minor response-specific modulation of cell types in PDOs after infection.

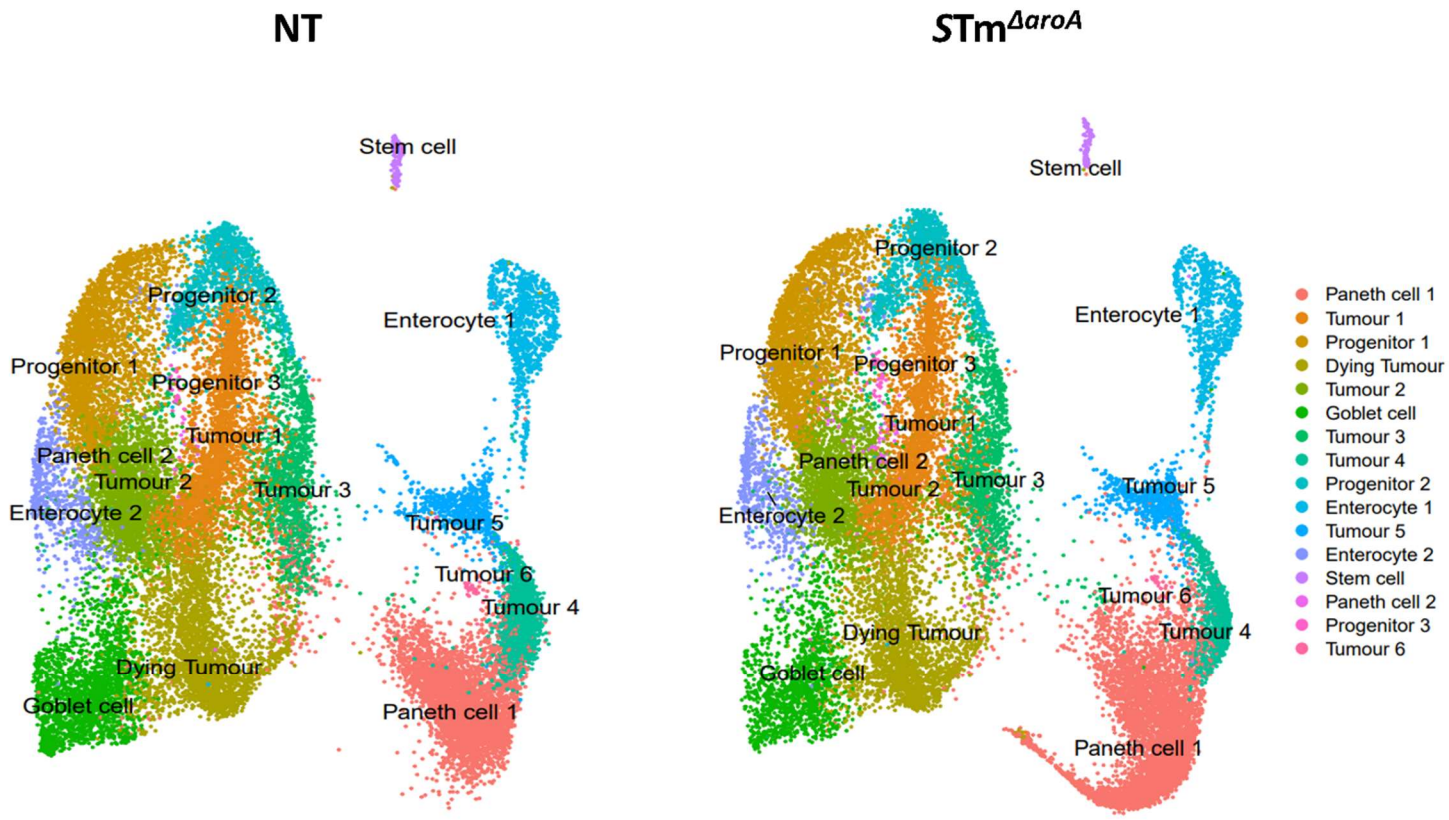


Figure 4.2.1: Cell type populations in PDOs
Combined UMAPs of all patients labelled with assigned cell-type identities show populations present in PBS treated (NT) (left) and STm$^{\Delta aroA}$ treated (right) PDOs.

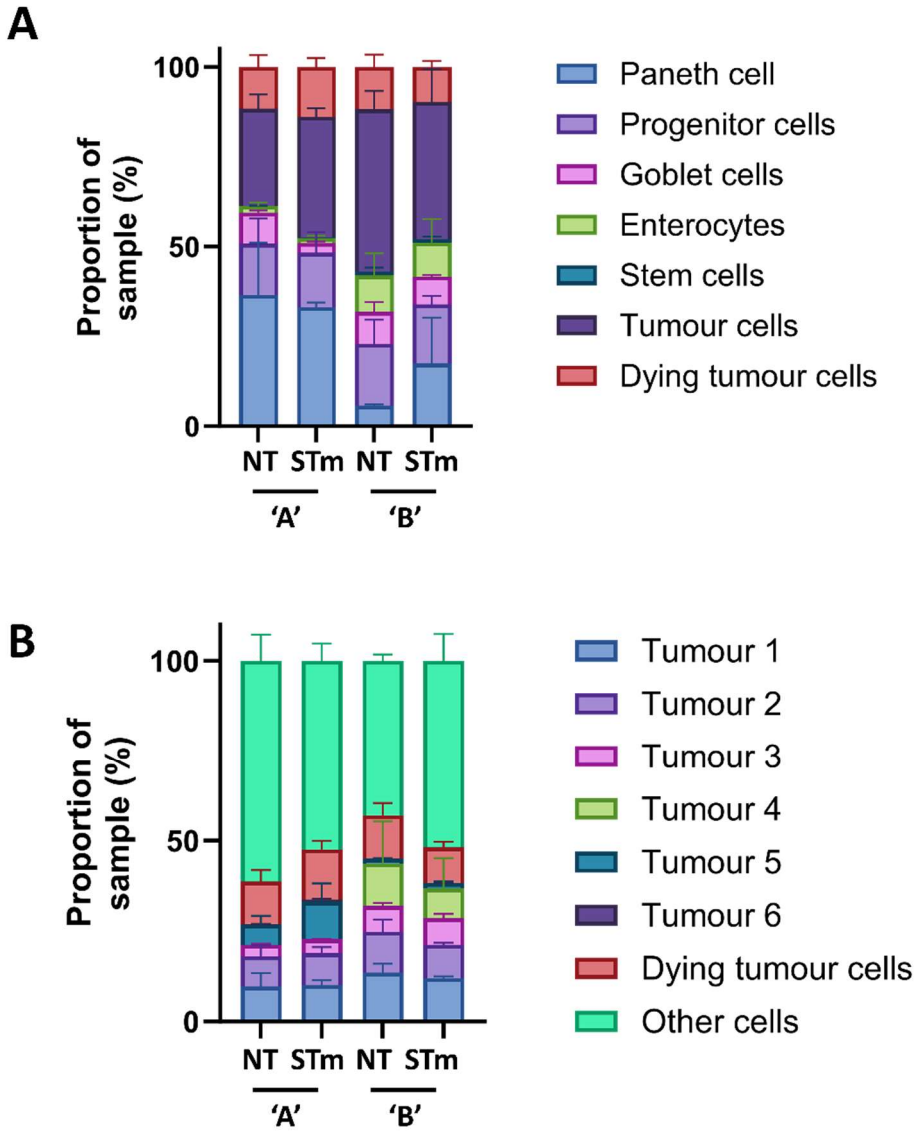


Figure 4.2.2: There is a relative enrichment of response-specific clusters in response A PDOs and Paneth cells in response B PDOs following STm$^{\Delta aroA}$ treatment

Cell numbers per cluster were calculated from the single-cell RNA sequencing data and used to calculate the proportion of each cell type in the original sample. Distinct epithelial cell types that are split into several clusters in the UMAP have been grouped. ***(A)*** *A stacked bar graph of the proportion of cell types as a percentage of the total samples in response 'A' and response 'B' PDOs in NT and STm$^{\Delta aroA}$ treated samples.* ***(B)*** *A stacked bar graph of the proportion of cells in each tumour cluster in response 'A' and response 'B' PDOs in NT and STm$^{\Delta aroA}$ treated samples. "Other cells" includes all other clusters. Error bars represent the standard error of the mean.*

4.2.3 Response A and response B PDO lines express different genes after *S*Tm$^{\Delta aroA}$ treatment

The up- and downregulated genes in *S*Tm-treated compared to non-treated samples show again differences between response A and response B lines **(Figure 4.2.3)**. Genes were considered differentially expressed if they were more than 0.3 $\log_2$ fold change up- or down-regulated. P-values were measured using Wilcoxon Rank Sum test and adjusted for false positives using Bonferroni correction. *S*Tm$^{\Delta aroA}$ treatment of response A lines induced upregulation of the two heat-shock protein genes *HSP90AA1* and *HSP90AB1*. HSP90 has been shown to lead to NF-κB signalling via IκK activation, the latter of which has been shown to lead to increased barrier permeability in the gut following LPS treatment (Broemer et al., 2004; Nighot et al., 2019). This may indicate detection of *S*Tm$^{\Delta aroA}$-derived LPS by these patient lines. There was also increased *HMGB1* expression, which has been demonstrated to have a protective role in the intestine against bacterial infection (Zhang et al., 2019). Response B lines appear to be upregulating classical inflammatory response pathway genes such as Major Histocompatibility Complex Class I (MHC-I) gene *HLA-B, IL32* and *TNFAIP2.* Furthermore, the downregulation of *SNHG25* in both response A and response B lines may be of therapeutic benefit, as recent work has shown this long non-coding RNA promotes progression of another epithelial cancer (Liu et al., 2021). The similarities and differences highlighted here imply both subsets of PDOs respond to *S*Tm$^{\Delta aroA}$ treatment at the transcriptional and population level, albeit possibly by separate mechanisms.

Samples of both response A and response B lines show significant upregulation of the gene encoding lipocalin-2, *LCN2,* in *S*Tm$^{\Delta aroA}$ conditions. Lipocalin-2 is known to be linked to innate immune response to bacterial infection and intestinal inflammation (Singh et al., 2016).

Expression of this marker of infection was upregulated in all cell types across the PDOs, suggesting it is globally upregulated after detection of bacteria, not only in infected cells **(Figure 4.2.4)**. Thus, invasion of a small number of cells is sufficient to induce global changes across the tumour organoids.

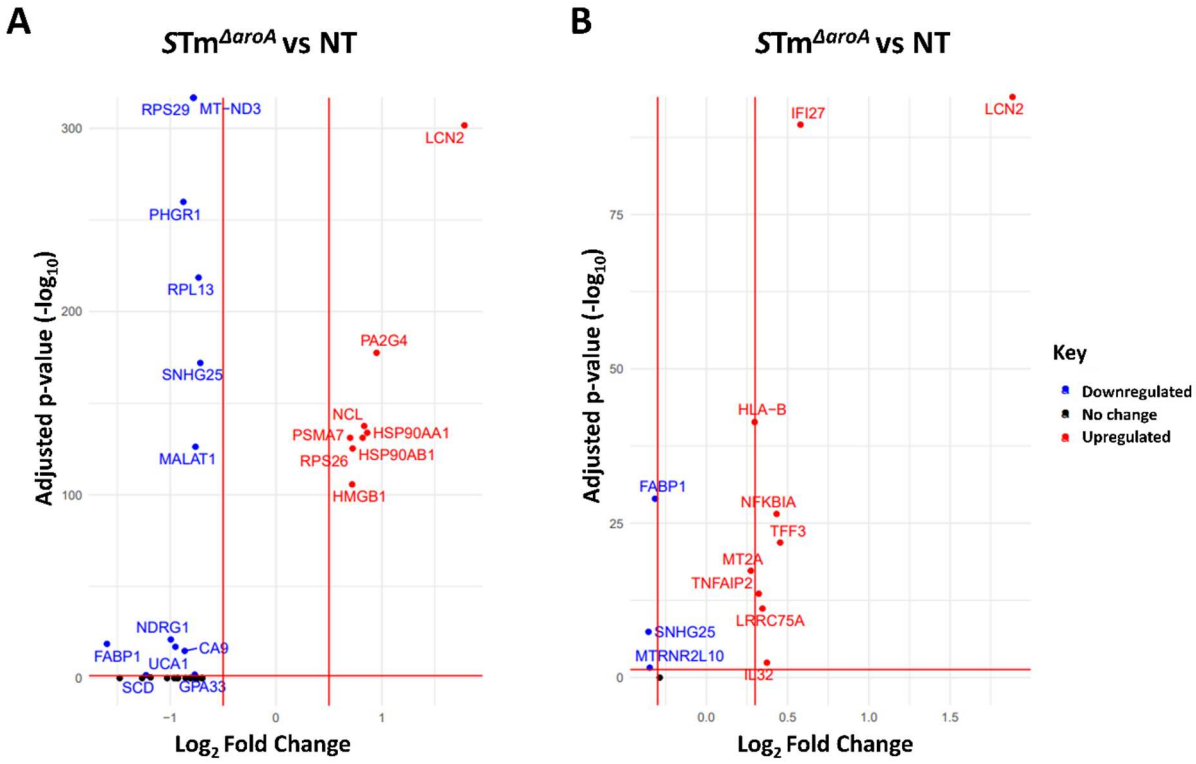


Figure 4.2.3: STm$^{\Delta aroA}$ induces different transcriptional changes in different PDOs
*Differentially expressed genes (DEGs) up-regulated (red) or down-regulated (blue) in STm$^{\Delta aroA}$ treated organoids compared to PBS-treated (NT) controls of the same patient were identified from the single cell RNA sequencing data as having log_2 fold change >0.3 up or down. Volcano plots of the DEGs conserved in response 'A' patients **(A)** and response 'B' patients **(B)**. P-value adjustment performed using Bonferroni correction method, based on total number of genes.*

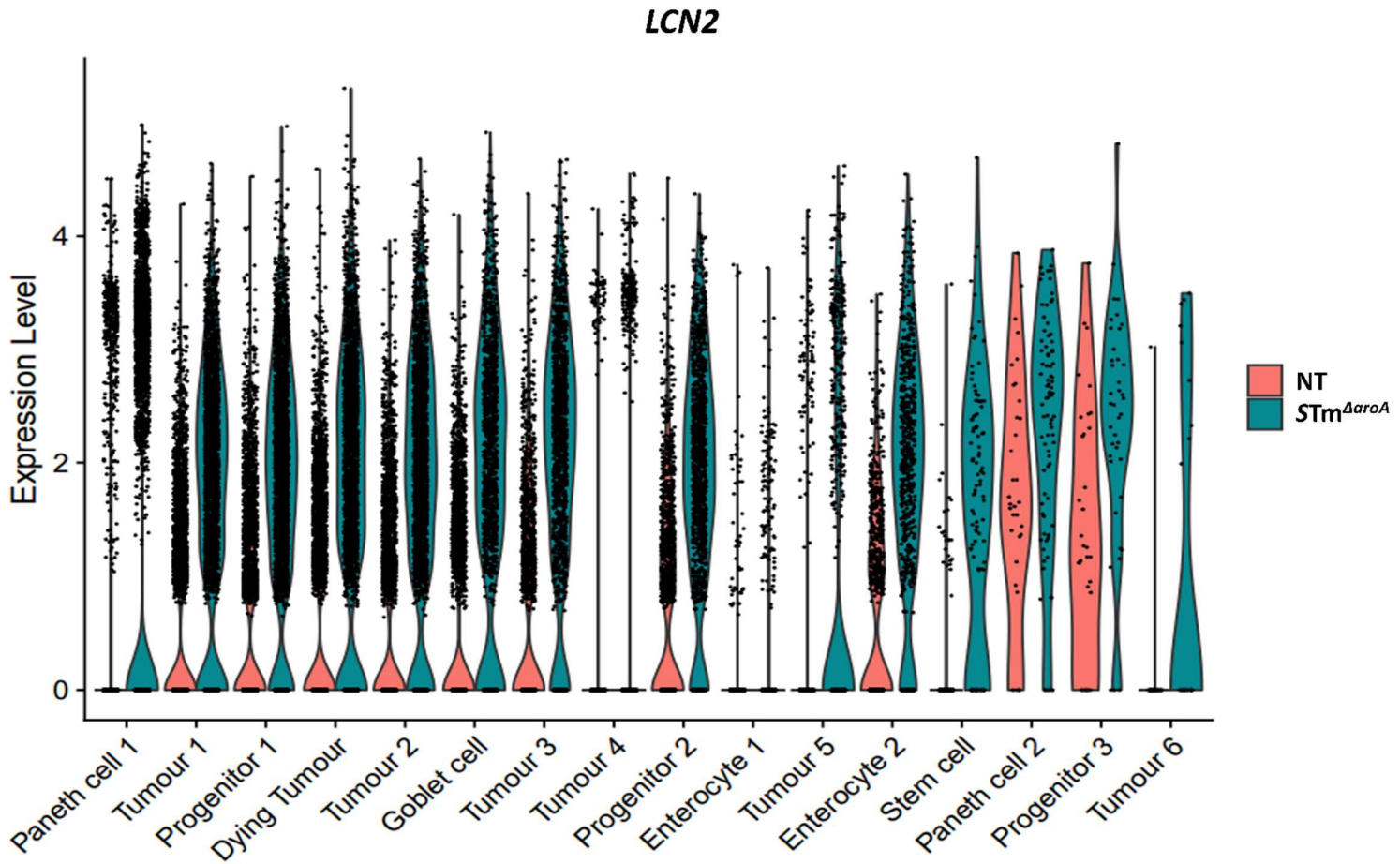


Figure 4.2.4: LCN2 expression is upregulated across PDOs following STm$^{\Delta aroA}$ treatment

Single-cell RNA-sequencing data of all PDOs split by treatment – PBS (NT) data in pink and STm$^{\Delta aroA}$ treated in blue. Violin plot representing the expression level of LCN2 in cell type clusters. Expression level represents log normalised values. Data points represent individual cells. (n=4 patients pooled).

4.2.4 Extracellular-restricted *S*Tm$^{\Delta aroA}$ induces similar transcriptional changes in tumour organoids compared to intracellular-permitted *S*Tm$^{\Delta aroA}$

We have previously shown that there is intracellular invasion of a small number of tumour cells by *S*Tm$^{\Delta aroA}$, both in PDOs *in vitro* **(Figure 3.2.6 A)** and mouse colonic tumours *in vivo,* where there are also large extracellular colonies of *Salmonella* (Mackie et al., 2021). I next wanted to investigate the relative effects of the intracellular and extracellular populations on the tumour epithelium. To model this *in vitro* I utilised the compound MβCD which sequesters cholesterol from the cell surface (Hayward et al., 2005), and which I previously showed inhibits intracellular invasion of organoids by *S*Tm$^{\Delta aroA}$ without compromising cell viability **(Figures 3.2.9 B** and **3.2.10)**. *Apc*$^{Min/+}$ colon tumour organoids and patient line 389 (response A PDO) were used to compare the effect on mouse and human, as I have previously identified response A to vary more from what we observe in mouse models. The conditions used were: Vehicle control (NT), *S*Tm$^{\Delta aroA}$ treated, MβCD-treated and MβCD pre-treatment followed by *S*Tm$^{\Delta aroA}$ treatment. MβCD treatment was 1 hour, then the bacteria were inoculated into the media and in contact with the organoids for 2 hours. Media was then removed and organoids re-fed with media supplemented with gentamicin to kill extracellular bacteria for a further 4 hours. Organoids were then collected, RNA isolated and measured and sent to Lexogen GmBH for 3' mRNA library prep and sequencing. Principal component analysis (PCA) was performed on the samples and plotted to visualise what conditions were driving separation of the samples **(Figure 4.2.5)**. With all the mouse or human samples combined, Principal component (PC) 1 represented 70% of the variance in the mouse samples and 55% of the variance in the human samples, this appeared to separate the samples based on MβCD treatment **(Figure 4.2.5 A** and **D)**. If we compare only non MβCD-treated or only MβCD-treated samples we see

that PC1 is now *S*Tm$^{\Delta aroA}$ treatment in both comparisons, in the mouse samples **(Figure 4.2.5 B** and **C)** and the human samples **(Figure 4.2.5 E** and **F)**. PC1 where the effect of MβCD is removed is slightly more heavily weighted in non MβCD-treated samples, contributing 51% of variance compared to 35% variance in mouse samples **(Figure 4.2.5 B** and **C)** and 93% of variance compared to 90% of variance in human samples **(Figure 4.2.5 E** and **F)**. As we were not interested in the effect of the MβCD itself, we removed the impact of this treatment in the downstream analysis of both mouse and human samples by comparing [*S*Tm$^{\Delta aroA}$ + MβCD vs MβCD] with [*S*Tm$^{\Delta aroA}$ vs NT].

Count data were log-normalised and low count genes filtered out to remove noise. DEGs were then identified as genes >1.5 $\log_2$ fold change up- or downregulated in one sample compared to sample of interest. P-values were calculated using the Wald test and adjusted with multiple-test correction performed using the Benjamini and Hochberg method, where genes are ranked by p-value and then ranked p-value is multiplied by the total number of genes/rank. To assess the effect of the intracellular-permitted bacteria on the tumour organoids I have visualised genes enriched in *S*Tm$^{\Delta aroA}$ treated organoids compared to the NT (vehicle control) sample for both mouse **(Figure 4.2.6 A)** and human **(Figure 4.2.6 C)**. As described above, this can then be compared to the effect of the extracellular-restricted bacteria by visualising the DEGs between *S*Tm$^{\Delta aroA}$ + MβCD and MβCD alone **(Figure 4.2.6 B** and **4.2.6 D)**. This acts to "balance the equation" and remove the effect of MβCD on the organoids, to interrogate purely the effect of external *S*Tm$^{\Delta aroA}$. We observe that there is an upregulation of several chemokines in both contexts and that this is a conserved signature between human and mouse tumour organoids. There is also upregulation of genes involved in regulation of TNF signalling in PDOs in both intra- and extra-cellular bacterial contexts.

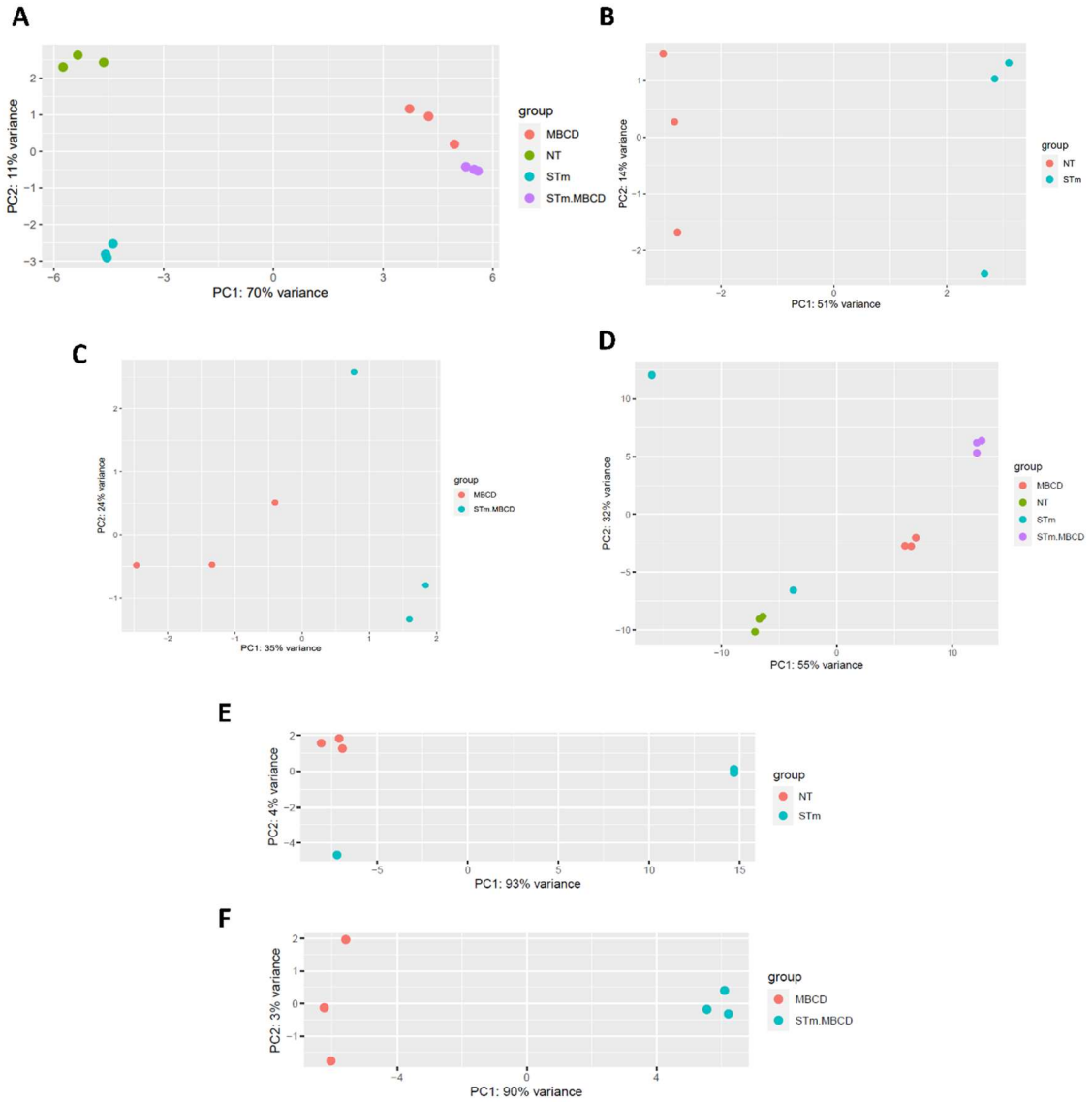


Figure 4.2.5: PCA plots of the tumour-derived organoid samples in the bulk RNA-sequencing run
Bulk RNA-sequencing was performed on Apc$^{Min/+}$ colon tumour organoids and one patient-derived tumour organoid line - on wells treated with PBS (NT), STm$^{\Delta aroA}$, MβCD and STm$^{\Delta aroA}$ + MβCD prior. PCA plots of all conditions, with mouse (A) and human (D) samples. PCA plots showing separation of NT and STm$^{\Delta aroA}$ samples, with mouse (B) and human (E) samples. PCA plots showing separation of MβCD and STm$^{\Delta aroA}$ + MβCD, with mouse (C) and human (F) samples.

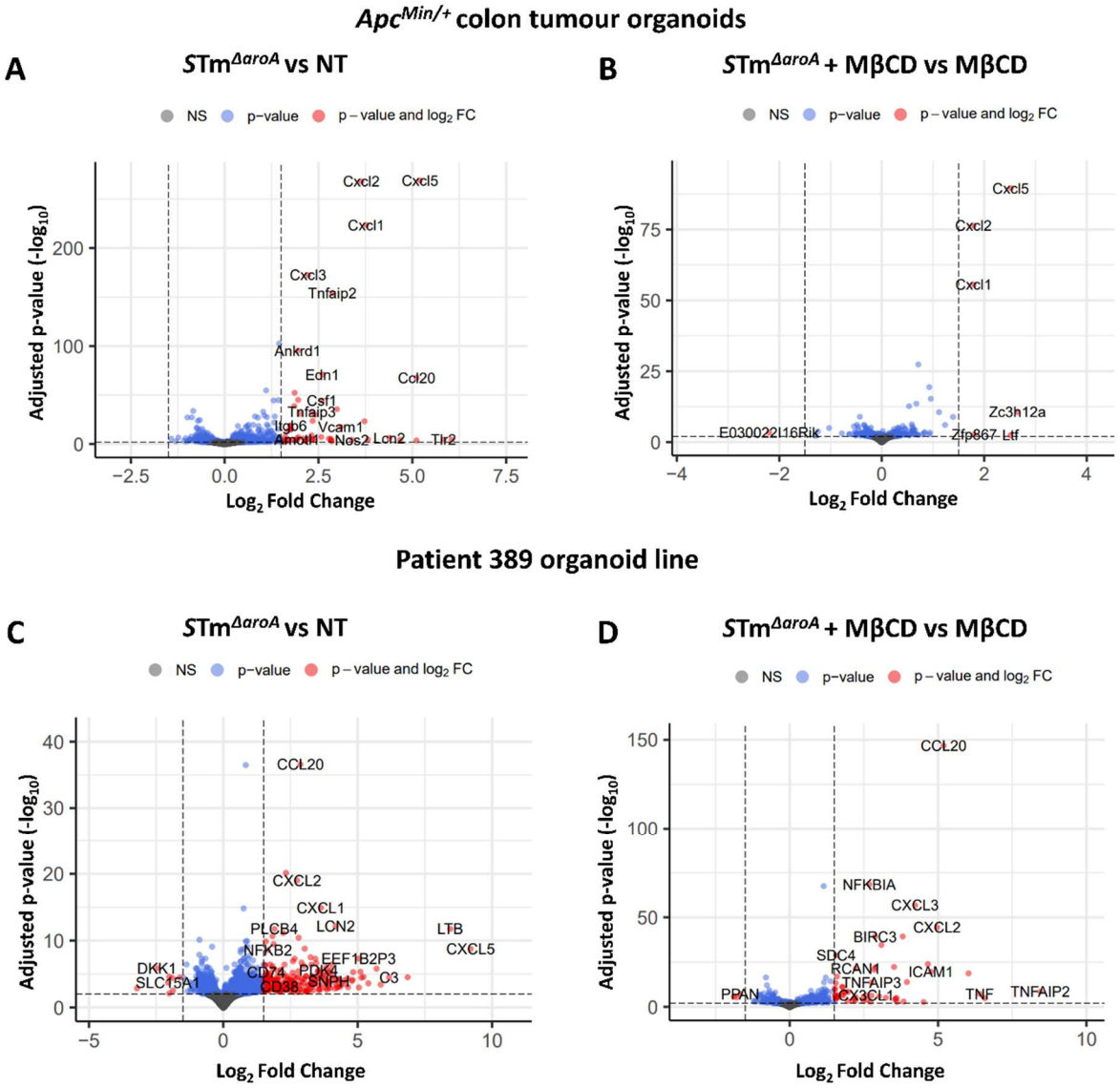
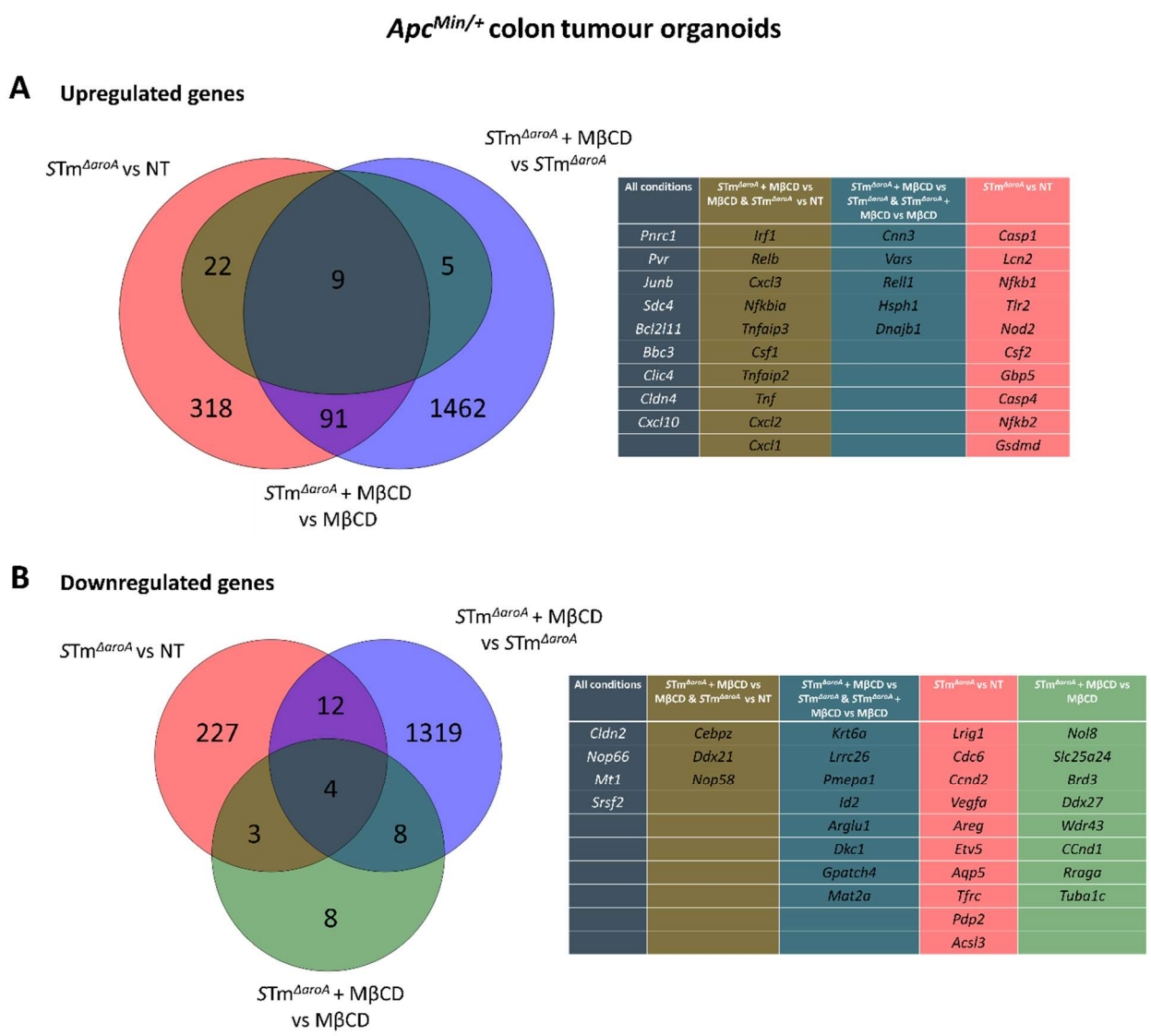


Figure 4.2.6: STm$^{\Delta aroA}$ induces a chemokine signature in mouse and human colon tumour organoids when intracellular or extracellular-restricted

*Bulk RNA-sequencing was performed on colon tumour organoids in wells treated with PBS (NT), STm$^{\Delta aroA}$, MβCD and STm$^{\Delta aroA}$ + MβCD prior. Volcano plot of the genes that are differentially expressed when STm$^{\Delta aroA}$ infection is compared to non-treated baseline in mouse **(A)** and human **(C)** tumour organoids. Volcano plot of the differentially expressed genes when comparing MβCD-induced extracellular restricted STm$^{\Delta aroA}$ and MβCD alone in mouse **(B)** and human **(D)** tumour organoids. Dotted lines represent cut off for differential expression, set at 1.5 log$_2$ fold change. P-values calculated by the Wald test and multiple-test correction is done using Benjamini and Hochberg method.*

To investigate further what effect we observe with the different populations of bacteria I used the DEGs over 1 log_2 fold change to calculate overlapping up- or down-regulated genes and plot these as Venn diagrams. MβCD treatment is again seen to have a large impact on the transcriptome of both mouse and human tumour organoids, as shown by the large number of unique DEGs both up- and down-regulated when comparing *S*Tm$^{\Delta aroA}$ + MβCD vs *S*Tm$^{\Delta aroA}$ **(Figures 4.2.7** and **4.2.8**, light blue section**)**. This, combined with the separation on the PCA plots shown before confirms that the effect should be ameliorated in the analysis by comparing [STmΔaroA vs NT] with [STmΔaroA + MβCD vs MβCD]. In both human and mouse tumour organoids we see that there a significant number of unique DEGs enriched in *S*Tm$^{\Delta aroA}$ compared to NT (pink section, **(Figures 4.2.7** and **4.2.8)**, suggesting that intracellular *Salmonella* exerts distinct transcriptional effects on tumour organoids. In the mouse tumour organoids, the upregulated unique genes are largely related to pathogen recognition (*Nod2, Tlr2*) and induction of cell death pathways via caspases and Gasdermin-D **(Figure 4.2.7 A)**. The effects we observed were similar in the human tumour organoid but with different genes effected; intracellular *S*Tm$^{\Delta aroA}$ caused reduced expression of cell-cycle associated genes (*FOSB, FOSL1, CCND3*) and increased expression of innate regulators of inflammation and barrier integrity **(Figure 4.2.8)**. In contrast to this, the extracellular-restricted condition in both human and mouse tumour organoids induces a very small number of unique DEGs, with some overlap with the intracellular-permitted bacteria **(Figures 4.2.7** and **4.2.8**, green and brown sections respectively**).**

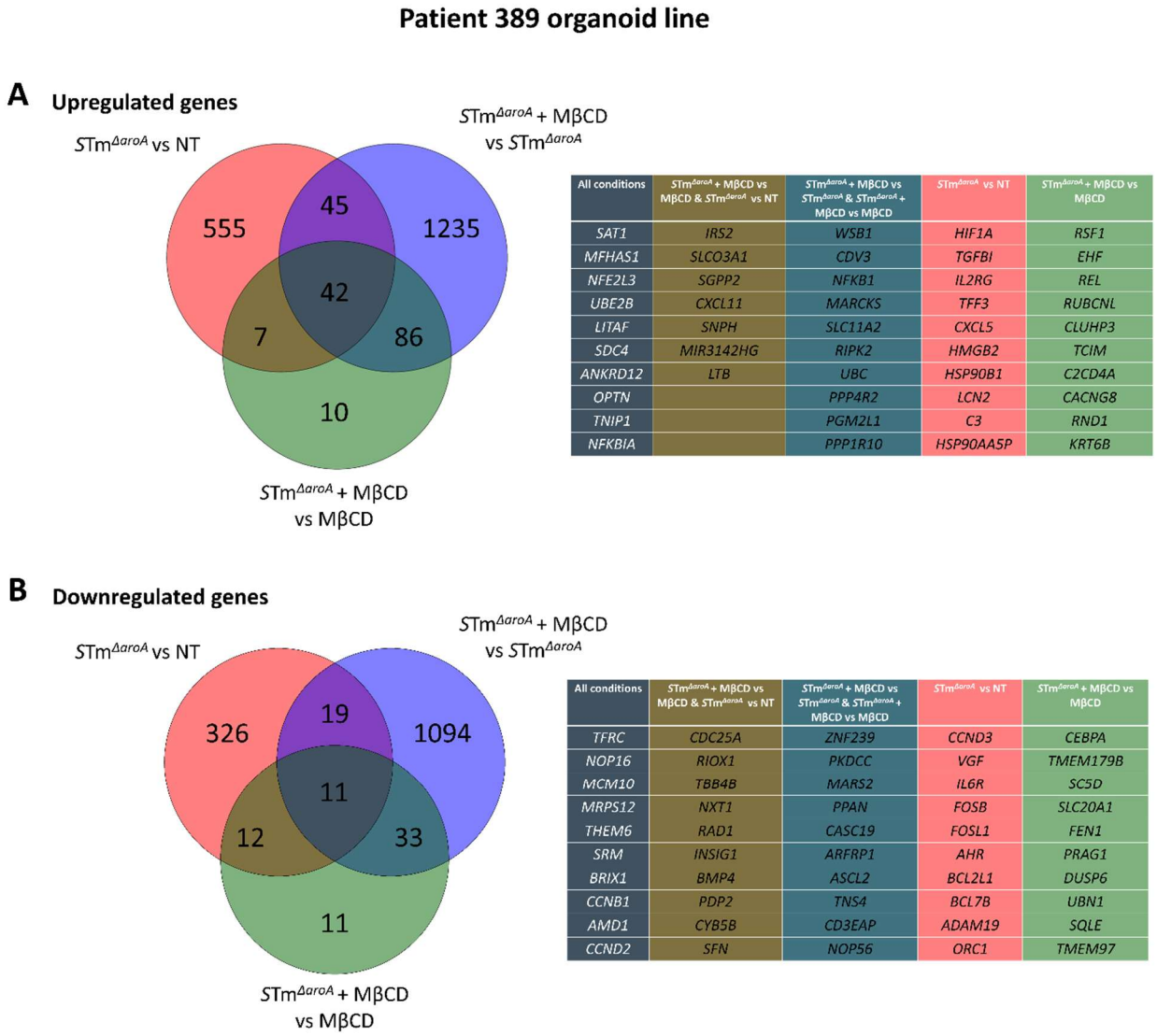


All conditions	STm^ΔaroA + MβCD vs MβCD & STm^ΔaroA vs NT	STm^ΔaroA + MβCD vs STm^ΔaroA & STm^ΔaroA + MβCD vs MβCD	STm^ΔaroA vs NT
Pnrc1	Irf1	Cnn3	Casp1
Pvr	Relb	Vars	Lcn2
Junb	Cxcl3	Rell1	Nfkb1
Sdc4	Nfkbia	Hsph1	Tlr2
Bcl2l11	Tnfaip3	Dnajb1	Nod2
Bbc3	Csf1		Csf2
Clic4	Tnfaip2		Gbp5
Cldn4	Tnf		Casp4
Cxcl10	Cxcl2		Nfkb2
	Cxcl1		Gsdmd

All conditions	STm^ΔaroA + MβCD vs MβCD & STm^ΔaroA vs NT	STm^ΔaroA + MβCD vs STm^ΔaroA & STm^ΔaroA + MβCD vs MβCD	STm^ΔaroA vs NT	STm^ΔaroA + MβCD vs MβCD
Cldn2	Cebpz	Krt6a	Lrig1	Nol8
Nop66	Ddx21	Lrrc26	Cdc6	Slc25a24
Mt1	Nop58	Pmepa1	Ccnd2	Brd3
Srsf2		Id2	Vegfa	Ddx27
		Arglu1	Areg	Wdr43
		Dkc1	Etv5	CCnd1
		Gpatch4	Aqp5	Rraga
		Mat2a	Tfrc	Tuba1c
			Pdp2	
			Acsl3	

Figure 4.2.7: Overlapping and unique DEGs in mouse tumour organoids after treatment with intra- or extracellular STm$^{\Delta aroA}$

*Bulk RNA-sequencing was performed on colon tumour derived organoids from Apc$^{Min/+}$ mice, with wells treated with PBS (NT), STm$^{\Delta aroA}$, MβCD and STm$^{\Delta aroA}$ + MβCD prior. Upregulated **(A)** and downregulated **(B)** differentially expressed genes were identified for each comparison of conditions and plotted as Venn diagrams to show the number of DEGs which overlap between comparisons. Genes of interest are annotated in the tables to the right of the corresponding Venn diagrams.*



All conditions	STm^ΔaroA + MβCD vs MβCD & STm^ΔaroA vs NT	STm^ΔaroA + MβCD vs STm^ΔaroA & STm^ΔaroA + MβCD vs MβCD	STm^ΔaroA vs NT	STm^ΔaroA + MβCD vs MβCD
SAT1	IRS2	WSB1	HIF1A	RSF1
MFHAS1	SLCO3A1	CDV3	TGFBI	EHF
NFE2L3	SGPP2	NFKB1	IL2RG	REL
UBE2B	CXCL11	MARCKS	TFF3	RUBCNL
LITAF	SNPH	SLC11A2	CXCL5	CLUHP3
SDC4	MIR3142HG	RIPK2	HMGB2	TCIM
ANKRD12	LTB	UBC	HSP90B1	C2CD4A
OPTN		PPP4R2	LCN2	CACNG8
TNIP1		PGM2L1	C3	RND1
NFKBIA		PPP1R10	HSP90AA5P	KRT6B

All conditions	STm^ΔaroA + MβCD vs MβCD & STm^ΔaroA vs NT	STm^ΔaroA + MβCD vs STm^ΔaroA & STm^ΔaroA + MβCD vs MβCD	STm^ΔaroA vs NT	STm^ΔaroA + MβCD vs MβCD
TFRC	CDC25A	ZNF239	CCND3	CEBPA
NOP16	RIOX1	PKDCC	VGF	TMEM179B
MCM10	TBB4B	MARS2	IL6R	SC5D
MRPS12	NXT1	PPAN	FOSB	SLC20A1
THEM6	RAD1	CASC19	FOSL1	FEN1
SRM	INSIG1	ARFRP1	AHR	PRAG1
BRIX1	BMP4	ASCL2	BCL2L1	DUSP6
CCNB1	PDP2	TNS4	BCL7B	UBN1
AMD1	CYB5B	CD3EAP	ADAM19	SQLE
CCND2	SFN	NOP56	ORC1	TMEM97

Figure 4.2.8: Overlapping and unique DEGs in human tumour organoids after treatment with intra- or extracellular STm$^{\Delta aroA}$

Bulk RNA-sequencing was performed on PDO line 389 on wells treated with PBS (NT), STm$^{\Delta aroA}$, MβCD and STm$^{\Delta aroA}$ + MβCD prior. Upregulated (A) and downregulated (B) differentially expressed genes were identified for each comparison of conditions and plotted as Venn diagrams to show the number of DEGs which overlap between comparisons. Genes of interest are annotated in the tables to the right of the corresponding Venn diagrams.

Pathway analysis of the DEGs expressed by tumour organoids in the context of intracellular-permitted or extracellular-restricted *S*Tm$^{\Delta aroA}$ again show significant overlaps and the top 10 most enriched pathways are shown. In *Apc*$^{Min/+}$ tumour organoids there is enrichment of genes associated with TNF signalling, NF-κB signalling and innate sensing pathways such as NOD-like receptors **(Figure 4.2.9)**. There is also enrichment of genes associated with necroptosis specifically in the context of intracellular invasion in the mouse organoids **(Figure 4.2.9 A)**. There are fewer conserved pathways between the 2 comparisons in patient 389, as shown by the lower number of overlapping DEGs **(Figure 4.2.8)**. We observed changes to genes associated with cell cycle and NF-κB, again in both contexts, as well as various viral pathways, which are likely a readout for pathogen recognition **(Figure 4.2.10)**. Necroptosis-related genes are upregulated in the patient line with extracellular-restricted bacteria, in contrast to mouse tumour organoids **(Figure 4.2.10 B)**.

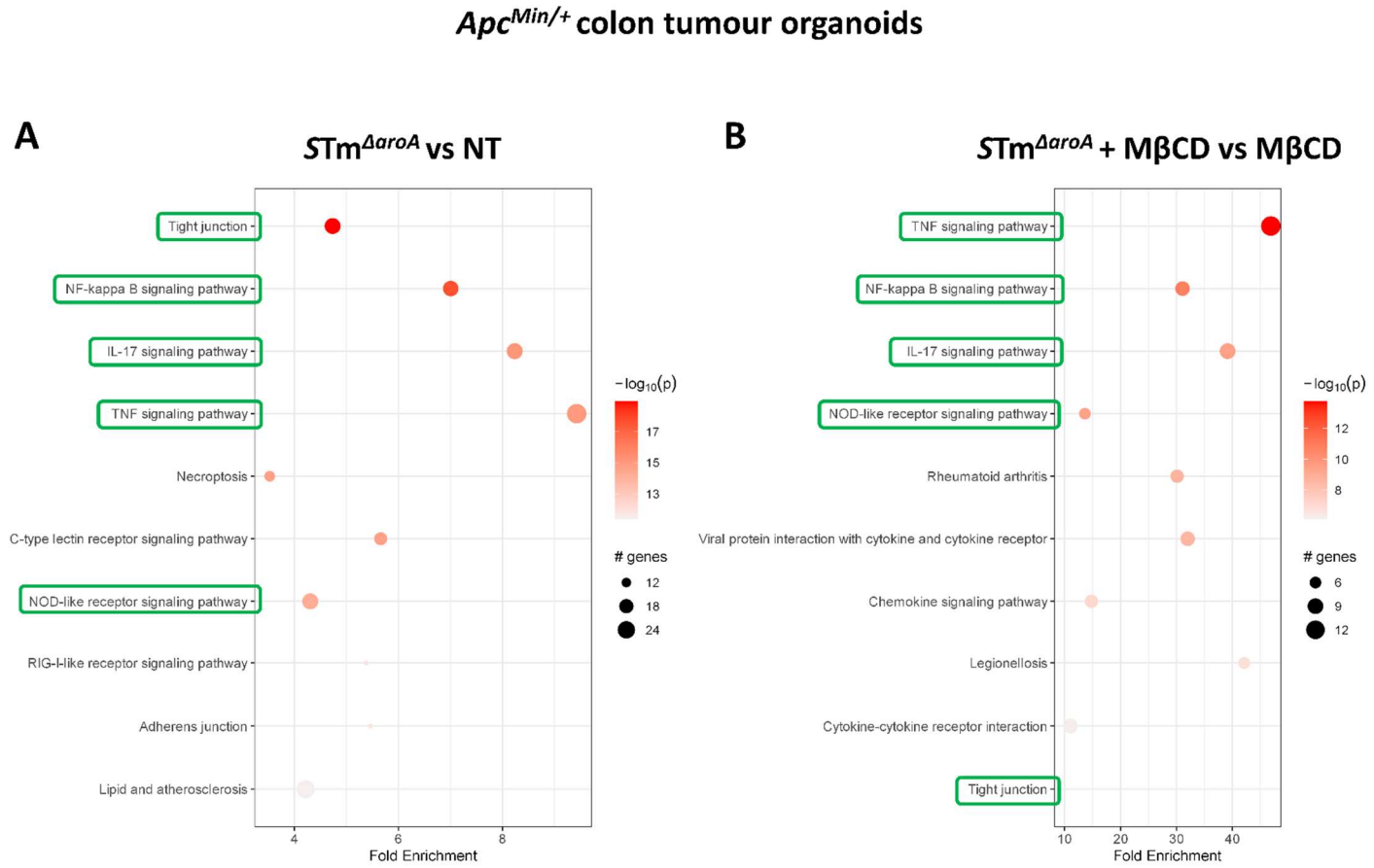


Figure 4.2.9: Pathway analysis shows STm$^{\Delta aroA}$ induces changes to genes involved in cell junctions and innate signalling whether intracellular or extracellular-restricted in Apc$^{Min/+}$ tumour organoids

Bulk RNA-sequencing was performed on Apc$^{Min/+}$ colon tumour organoids on wells treated with PBS (NT), STm$^{\Delta aroA}$, MβCD and STm$^{\Delta aroA}$ + MβCD prior and pathway analysis performed on differentially expressed genes. ***(A)*** *Pathways enriched in STm$^{\Delta aroA}$ treated wells compared to NT.* ***(B)*** *Pathways enriched MβCD-induced extracellular restricted STm$^{\Delta aroA}$ compared to MβCD alone. Green boxes indicate pathways enriched in both comparisons. Size of the data point correlates to number of related genes expressed and the darker red of the data point the lower the p-value. Top 10 enriched pathways are shown.*

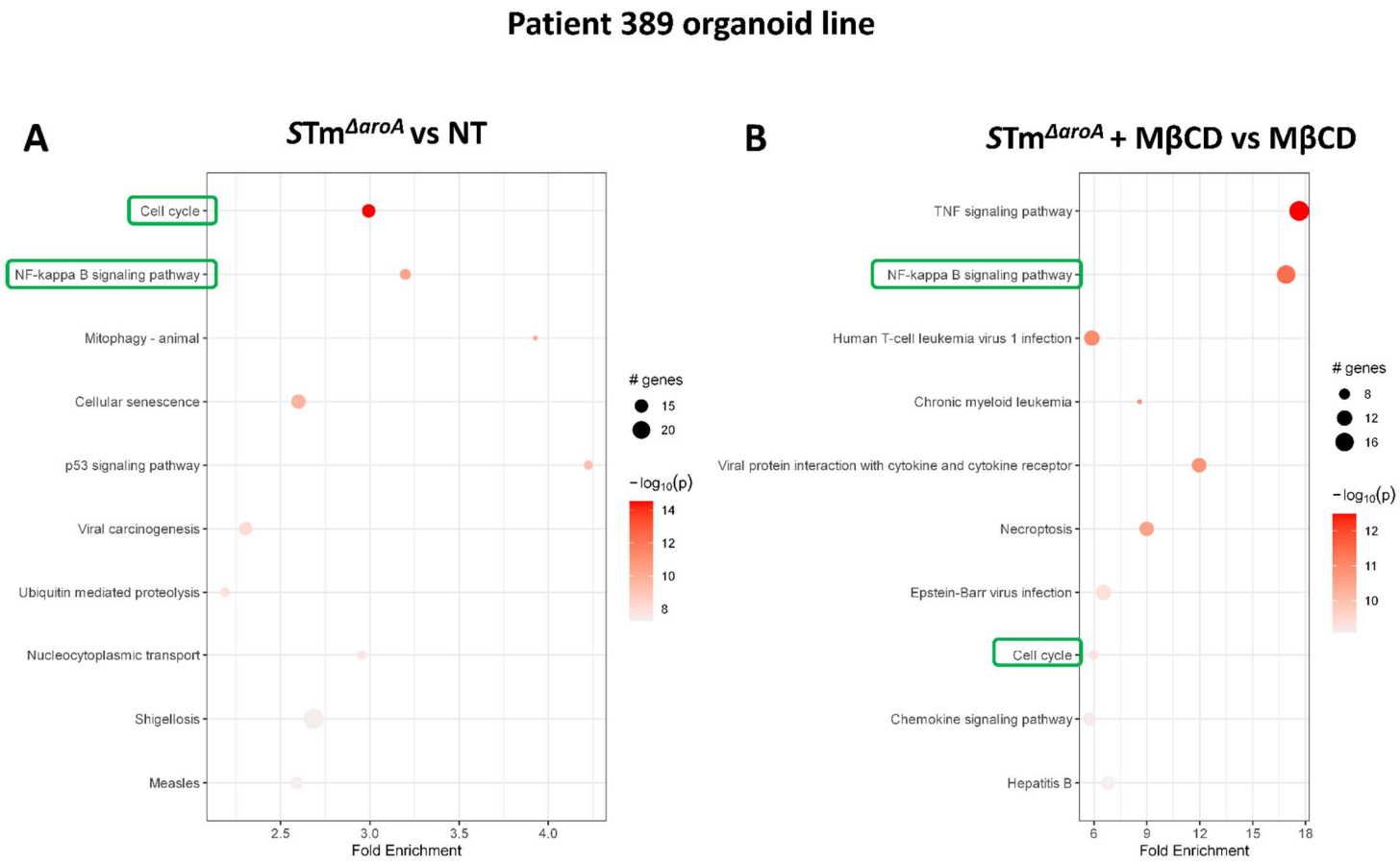


Figure 4.2.10: Pathway analysis shows STm$^{\Delta aroA}$ induces changes to genes involved in cell cycle, innate signalling, and pathogen detection whether intracellular or extracellular-restricted in PDO 389

Bulk RNA-sequencing was performed on PDO line 389 on wells treated with PBS (NT), STm$^{\Delta aroA}$, MβCD and STm$^{\Delta aroA}$ + MβCD prior. Pathway analysis performed on differentially expressed genes. ***(A)*** *Pathways enriched in STm$^{\Delta aroA}$ treated wells compared to NT.* ***(B)*** *Pathways enriched MβCD-induced extracellular restricted STm$^{\Delta aroA}$ compared to MβCD alone. Green boxes indicate pathways enriched in both comparisons. Size of the data point correlates to number of related genes expressed and the darker red of the data point the lower the p-value. Top 10 enriched pathways are shown.*

4.2.5 Chemokines upregulated by PDOs following *S*Tm$^{\Delta aroA}$ treatment are expressed primarily by Paneth cells

The key conserved genes upregulated in human and tumour organoids treated with intracellular-permitted or extracellular-restricted *Salmonella* were *CXCL1*, *CXCL2*, *CXCL3* and *CCL20.* We hypothesised that these chemokines may be driving the early therapeutic response in mice *in vivo*, and so we questioned which cells in particular are producing the chemokines, as this population may be of interest to target for increased anti-tumour effect. To assess which cells are producing these chemokines we re-analysed our single-cell dataset. Initially expression of these chemokines in cell types was interrogated in PDO lines individually, but there was no difference between patients (data not shown) and so the data are shown pooled. I used violin plots to visualise expression of these chemokines and split by identified clusters to investigate the cell-types expressing them.

All 4 chemokines are upregulated in *S*Tm$^{\Delta aroA}$ across the cohort of 4 patients **(Figure 4.2.11)**. Expression level is visualised as the $\log_2$ normalised value and in non-treated samples there is no expression of any chemokines in the vast majority of cells. The average expression of all 4 chemokines was increased most dramatically in Paneth cells (particularly Paneth cell 1 cluster) in response to *S*Tm$^{\Delta aroA}$ treatment, and *CCL20* expression is also increased in the other main secretory cell cluster- goblet cells. There was increased average expression of *CXCL3* in the stem cell cluster of *S*Tm$^{\Delta aroA}$ treated samples. *CXCL1, CXCL2* and *CCL20* also had increased expression in progenitor cell types. Therefore, I conclude that *S*Tm$^{\Delta aroA}$ induces expression of specific chemokines in progenitor and secretory cells (particularly Paneth cells) in PDOs.

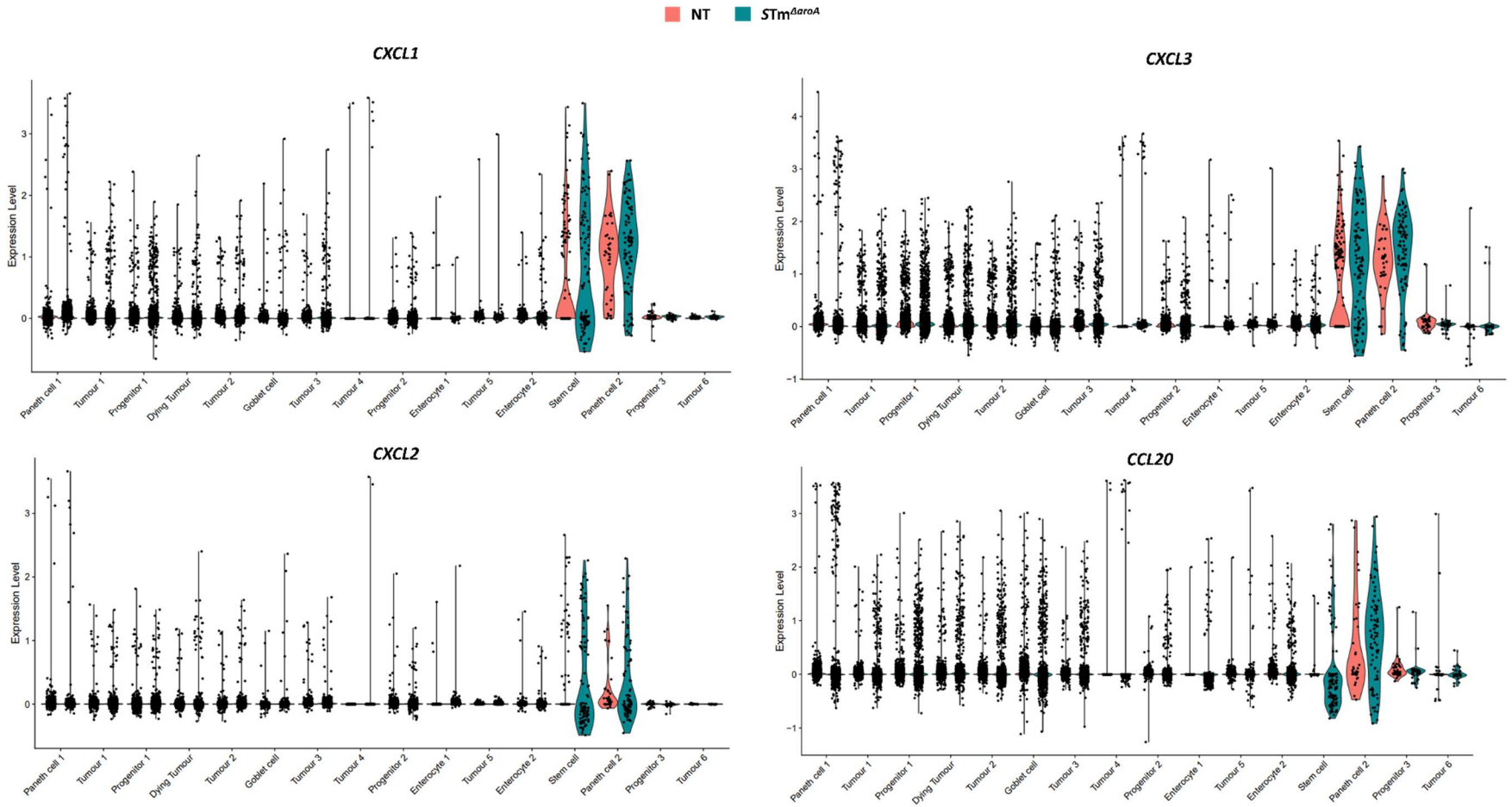


Figure 4.2.11: Chemokine expression is upregulated in secretory and progenitor cells in PDOs after STm$^{\Delta aroA}$ treatment

Single-cell RNA-sequencing data of all PDOs split by treatment – PBS (NT) data in pink and STm$^{\Delta aroA}$ treated in teal. Violin plot representing the expression of CXCL1, CXCL2, CXCL3 and CCL20 in cell type clusters. Expression level represents log_2 normalised values. Data points represent individual cells. (n=4 patients pooled).

4.3 Discussion

In vitro infection with *S*Tm$^{\Delta aroA}$ has a direct effect on the tumour epithelium, where infected mouse or human tumour organoid cultures have stunted regrowth capacity after infection compared to non-treated controls. In this chapter I aimed to characterise the global effect of bacteria on tumour organoids at the transcript level using sequencing techniques. Initially, the patient-derived organoids were split into two groups termed 'response Bs' and 'response As' based on whether stem-cell associated transcripts were reduced following treatment. We identified the two lines with the most consistent downregulation of these genes and two without and took these forward as the samples for single-cell RNA sequencing. The aim of this was to identify how the two groups differ before treatment at a cell population level, and how global transcriptional changes occur after treatment to determine whether there was a different mechanism of response between the groups. The low n number means that comparisons across the two responses are limited, however by using the most stringent p-value corrections on the single-cell RNA sequencing analysis I have limited the number of false positives and therefore highlighted differentially expressed genes should be both biologically and statistically significant.

The majority of identified tumour and gut cell populations were largely present in all samples, whereas clusters tumour-4 and -5 appear to correlate with response B and A phenotypes respectively. It is possible that these populations are driven by mutations developed later in the cancer's progression, as both these response-specific clusters are characterised by differential expression of cell cycle associated markers compared to other clusters. This suggests that these cells may be the proliferating cells in these PDO lines. We showed

previously that proliferating cells were more likely to be infected in PDOs **(Figure 3.2.6 B)** and so these may represent the cell population that is preferentially infected. It has previously been shown using single-cell RNA sequencing that colorectal tumours show distinct, varied cell types in patient tumours (Dai et al., 2019) and this shows that this heterogeneity is preserved in the organoid model, to the extent where patient-specific differences can be seen. The cellular heterogeneity of the samples is further shown by calculating the proportion of different cell types making up the samples from each patient **(Figure 4.2.2)**. Observation of cell-type heterogeneity in passaged PDO lines highlights the strengths of organoid models compared to immortal cell lines in more accurately depicting human disease.

Response A lines respond to *S*Tm$^{\Delta aroA}$ with a relative increase in the tumour populations compared to "normal" cell-types. It is unclear whether this is due to increased cell death in the differentiated cells compared to tumour cells and these were filtered out in the processing of the data. There appeared to be an increased proportion of dying tumour cells, a cluster which was annotated as such due to an enrichment of mitochondrial reads **(Figure 4.2.2 A)**, however when we looked at the tumour-specific clusters this was not increased **(Figure 4.2.2 B)**. Intriguingly, there is a relative increase in the tumour 5 cluster following *S*Tm$^{\Delta aroA}$ treatment, which is present in response A PDOs and almost entirely absent in response B PDOs **(Figure 4.2.2 B)**. In contrast, response B PDOs exhibit a relative expansion of the secretory Paneth cell populations following *S*Tm$^{\Delta aroA}$ treatment. As described above, an increase in Paneth cell number has been seen *in vivo* in mouse models of *Salmonella* typhimurium infection (Rodriguez et al., 2012) and has been suggested to be a key mediator in the first-line innate response to wild-type bacteria. In response B lines we also observed a relative contraction of the tumour cell clusters, with the patient-specific tumour 4 cluster appeared to

be reduced after treatment. The alterations in cell populations were subtle following *S*Tm$^{\Delta aroA}$ treatment, and likely do not represent part of the early mechanism of action. It is possible that at later time points there would be more striking shifts in cell populations, although this is a limitation of the *in vitro* model as the bacteria are depleted through lysis of infected cells into the gentamicin-containing media. This could be investigated by analysis of the cell populations present in polyps and normal tissue from treated and untreated mice at the start, mid- and end-point of the long-term treatment protocol. I hypothesise based on our observations of increases in E-cadherin and restoration of epithelial structure that there would be a gradual increase in differentiation cell-types and loss of the "tumour" clusters.

Response A PDO lines upregulate stress associated HSP90 genes and *HMGB1*, both possibly indicative of detection of PAMPs **(Figure 4.2.3 A)**. Secretion of *HMGB1* has been identified as a marker of caspase-independent necrosis in urothelial carcinoma cells following treatment with BCG vaccine, the only currently used example of BCT (See et al., 2009). This implies that there may be a similar mechanism of action in our response A lines, however it remains to be determined whether the HMGB1 is being released from PDO cells as it has different functions intracellularly and extracellularly. Extracellular HMGB1 is classified as a DAMP which induces inflammatory signalling such as IL-6 and TNF release (Chen et al., 2022). Nuclear HMGB1 has been shown to bind to DNA and also promotes binding of various regulatory complexes to DNA, where it is associated with a pro-proliferative role (Lotze and Tracey, 2005). Cytosolic HMGB1 has also been shown to limit *Salmonella* infection in colonocytes. Mice lacking expression of *Hmgb1* in intestinal epithelial cells had higher bacterial burden, and this was associated with impaired induction of autophagy (Zhang et al., 2019). Thus, a key next step in

delineating the differences in patients should be to assess whether HMGB1 is released from infected PDOs or its cellular location if it is retained.

Interestingly, the genes that are upregulated after *S*Tm$^{\Delta aroA}$ in the response B lines represent a canonical epithelial response to bacteria. I observed increased expression of pro-inflammatory mediators *TNFAIP2, HLA-B* and *IL32.* In addition to this, both *MT2A* and *NFKBIA* were upregulated **(Figure 4.2.3. B)**, genes whose products act to inhibit the NF-κB signalling pathway and limit apoptotic cell death (Pan et al., 2013). Mice that have a deficiency for *Nfkbia* specifically in intestinal epithelial cells have constitutively active NF-κB signalling which results in both pro-apoptotic and pro-proliferative signalling. This causes reduced barrier function and IBD-like inflammation, demonstrating the importance of regulated NF-κB signalling in the gut (Mikuda et al., 2020). It is possible that the response B lines are initially activating a more apoptosis-mediated cell death of directly infected cells via TNF signalling and this causes a resultant inhibition of NF-κB signalling to maintain integrity of the organoid tight junctions. It may be a useful future experiment to look at key gene expression at different time points to assess the progression of the response. An indirect inhibitor of NF-κB signalling, *Tnfaip3/TNFAIP3*, and *NFKBIA* were also upregulated in the mouse and patient 389 (response A) tumour organoids in the bulk RNA-sequencing analysis **(Figures 4.2.6** and **4.2.7)**. This is at the 6-hour timepoint, suggesting similar pathways are being activated across the human and mouse organoids that result in an early inhibition of NF-κB signalling.

In this chapter I also utilised bulk RNA-sequencing to assess the effect of *S*Tm$^{\Delta aroA}$ on *Apc*$^{Min/+}$ tumour organoids and PDOs when it was able to invade host cells, or when restricted to the extracellular space by pre-treatment of the organoids with MβCD. Extracellular *S*Tm$^{\Delta aroA}$ had

a striking effect on the transcriptome of both mouse and human tumour organoids, and it is worth noting that gentamicin was added to the culture after 2 hours, so the effects seen were induced after a short contact between host and bacteria. The key signature conserved between *S*Tm$^{\Delta aroA}$ and MβCD + *S*Tm$^{\Delta aroA}$ was an upregulation of chemokines in both human and mouse. In the mouse tumour organoids *Cxcl1, Cxcl2* and *Cxcl5* were upregulated after any contact with *S*Tm$^{\Delta aroA}$, and *Cxcl3* and *CCl20* were upregulated specifically with intracellular *S*Tm$^{\Delta aroA}$ **(Figure 4.2.6 A** and **B)**. *CXCL1, CXCL2, CXCL3, CXCL11* and *CCL20* were upregulated in both contexts in PDOs, additionally *CXCL5* was upregulated without MβCD treatment **(Figure 4.2.6 C** and **D)**. We hypothesise that *in vivo* production of these chemokines in the tumour sites will aid recruitment and activation of immune cells, primarily neutrophils, immature dendritic cells and macrophages. Investigation of this in our mouse models is explored in the next chapter. An important next experiment would be to confirm that the increase in transcripts of these genes is translated into increased production of these chemokines, measurement of the protein levels using ELISA should be done either on the supernatants of the organoids or on digested polyps following infection.

Here I demonstrate that intracellular invasion of *Salmonella* into epithelial cells is not necessary to induce upregulation of chemokines. In 2003, Bäumler and colleagues identified that these chemokines were expressed by the cells in the ileal crypts of bovine gut following inoculation with wild-type *Salmonella*, but not a T3SS-deficient strain. The location of these chemokine producing cells in the crypt led the group to posit that the chemokine producers were not the directly infected cells, as the crypt is a relatively protected area in the healthy small intestine, which is in agreement with our observations in this chapter (Zhang et al., 2003). They saw in mice that there was substantially lower induction of chemokine expression

compared to their bovine infection model, and this was not impacted by the deletion of T3SS genes. It is possible that in our context *S*Tm$^{\Delta aroA}$ are still able to bind host cells, but not invade and that this is sufficient to trigger detection and paracrine signalling that induces expression of chemokines. Having observed significant upregulation of chemokines following *S*Tm$^{\Delta aroA}$ treatment of tumour organoids, we next wanted to return to the single cell RNA sequencing dataset to identify which cells were responsible. We identified that increased expression of chemokines was primarily occurring in Paneth cells, and to a lesser extent stem and progenitor cell types **(Figure 4.2.11)**. This is again in agreement with the observations of Zhang et al., where with in situ hybridization they observed transcripts of these chemokines in the crypts and Peyer's patches of bovine intestine, which would be the location of these cell types (de Lau et al., 2012; Zhang et al., 2003). It is interesting that response A patients have relative enrichment of the Paneth cell population following infection, as these are the cell types upregulating expression of chemokines, which appear to be a key player in the mechanism of *S*Tm$^{\Delta aroA}$ in tumour organoids.

We next sought to identify the extent to which the extracellular bacteria induced transcriptional changes in the tumour organoids by comparing DEGs between the different conditions. We see that there is still a significant number of unique DEGs in the context of total infection (i.e., *S*Tm$^{\Delta aroA}$ only compared to non-treated) in both *Apc*$^{Min/+}$ tumour organoids and the PDO line. In the mouse tumour organoids, there is increased expression of inflammasome pathway-mediated pyroptosis associated genes, such as *Casp1* and *Gsdmd,* possibly linked to increased expression of NF-κB genes *Nfkb1* and *Nfkb2* **(Figure 4.2.7)**. This suggests that in our model programmed cell death of tumour cells requires intracellular invasion. In both mouse and human tumour organoids there is downregulation of a variety of

cell cycle associated genes after *S*Tm$^{\Delta aroA}$ infection, particularly enriched when there was intracellular invasion **(Figures 4.2.6** and **4.2.10)**. Therefore, it will be important to assess ability of extracellular bacteria to impact tumour cell growth *in vivo,* which will be explored in the next chapter.

One conserved DEG between all patients and mouse tumour organoids was upregulation of *LCN2/Lcn2,* the gene which encodes lipocalin-2. Lipocalin-2 is an antimicrobial protein which can be induced by IL-22 signalling in the context of *Salmonella* infection. It has been shown previously that in human colonic epithelial cells *in vitro* lipocalin-2 expression could be induced by IL-22 or IL-17, and not *Salmonella* alone (Raffatellu et al., 2009). In our model of both mouse and human tumour derived organoids we see lipocalin-2 gene expression is upregulated by *S*Tm$^{\Delta aroA}$ infection, across two different sequencing runs **(Figures 4.2.3, 4.2.6 A** and **4.2.6 C)**. There is no cellular source of IL-22 in the organoid cultures (sequencing data mined, data not shown) and therefore these data represent an unknown trigger of lipocalin-2 induction. Interestingly, induction of *LCN2/Lcn2* required intracellular invasion of cells, as it was a DEG uniquely enriched in *S*Tm$^{\Delta aroA}$ compared to NT in the bulk RNA-sequencing dataset **(Figures 4.2.7 A** and **4.2.8 A)**. Other unique DEGs after specifically intracellular infection may shed light on the mechanism of lipocalin-2 upregulation as there is also upregulation of PRR *Tlr2*. *Lcn2* has been shown to be upregulated in mouse neuronal cells following infection with the intracellular parasite *Toxoplasma gondii*, but not if the mice lack TLR2 (Umeda et al., 2017). In addition, stimulation of TLR2 in kidney epithelial cells induces upregulation of *Lcn2 in vitro,* further implicating this intracellular PRR in regulation of lipocalin-2 expression (Eller et al., 2013). Again, it is of importance to confirm that this specific increase in *Lcn2* after intracellular

infection translates to increased protein expression to interrogate whether this observation is relevant to the therapeutic mechanism.

Together, these data show that extracellular *Salmonella* can be detected by tumour cells and induce significant transcriptional changes to the tumour epithelium *in vitro* in both mouse and human contexts. We next aim to evaluate the extent to which, and mechanism by which, the population of extracellular bacteria can exert a functional anti-tumour response.

CHAPTER 5 - INTRACELLULAR INVASION OF TUMOUR CELLS BY ATTENUATED *SALMONELLA* TYPHIMURIUM IS DISPENSABLE FOR ANTI-TUMOUR EFFECT

5.1 Introduction

In the last chapter I compared the transcriptional effect of extracellular-restricted *S*Tm$^{\Delta aroA}$ to intracellular invasion. This showed that there is a similar global effect on tumour organoids that have internalised pathogen to those which have only interacted at the cell surface or through secreted factors. Of note, we have previously reported that only a small proportion of tumour cells harbour intracellular *S*Tm$^{\Delta aroA}$, while it is clear there are also large extracellular, intratumoral colonies *in vivo* (Mackie et al., 2021). The extent to which the few intracellularly infected cells drive the therapeutic response of *S*Tm$^{\Delta aroA}$ in intestinal cancers is as yet unknown and I aim to unpick this in this chapter.

Salmonella typhimurium is characterised as an intracellular pathogen that depends on invasion of gut epithelial cells and macrophages for survival, however it has also been shown previously that the survival of *S*Tm in solid tumours does not rely on intracellular invasion. One study in 2016 used *S*Tm with mutations in both *invA* and *ssaD,* genes which encode components of SPI-1 and -2 respectively and facilitate internalisation into host cells. They demonstrated that this strain was able to colonise 4T1 tumours *in vivo* to similar levels to wild-type *Salmonella* when delivered either intratumorally or intravenously (Silva-Valenzuela et al., 2016). Furthermore, Crull et al. utilised intravenous injection of attenuated *Salmonella* typhimurium (deletion of *hisG* and *aroA*) in BALB/c mice with subcutaneous CT26 tumours, a cell line derived from mouse colon carcinoma. They identified using an *ex vivo* gentamicin

protection assay that recovered CFUs were reduced by around 80% with gentamicin treatment, suggesting that the majority of bacteria were residing extracellularly in this context They further identified that the extracellular survival was dependent on expression of biofilm production-associated genes by the bacteria (Crull et al., 2011). *Salmonella* typhimurium has also been shown to persist in extracellular colonies in the tonsils of healthy pigs, suggesting this is not a tumour niche-specific trait. In this context the *Salmonella*'s ability to survive extracellularly was not dependent on biofilm production, this contradiction may be due to a comparison of wild-type and attenuated bacteria, site of infection or the host organism.

In chapter 4, the transcriptional signature observed in *S*Tm$^{\Delta aroA}$ treated organoids in both intracellular invasion and extracellular restricted contexts included upregulation of a variety of chemokines. The chemokines which were upregulated by the tumour organoids following interaction with both intracellular and extracellular-restricted bacteria were CXCL1, CXCL2 and CCL20 (the latter was only conserved in human PDOs with extracellular bacteria.) CXCL1 and CXCL2, along with CXCL3 and CXCL5, are both ligands for the receptor CXCR2. This receptor is expressed on most leukocytes but has been shown to be most functionally significant in neutrophils, monocytes, macrophages and mast cells (Olson and Ley, 2002).

CXCL1 has been shown to drive recruitment and activation of neutrophils to sites of infection and lead to killing of microbes (Sawant et al., 2016). Thus, in the context of these extracellular colonies of bacteria in the polyps inducing CXCL1 release, we are hypothesising that there will be an influx of neutrophils to the site, which then function as anti-microbial agents. Neutrophils have been demonstrated to be both pro- and anti-tumorigenic depending on contexts. One early study established a paradigm whereby the tumour microenvironment

acted to induce a phenotypic switch in anti-tumorigenic tumour-associated neutrophils (N1) whereby they become more pro-tumorigenic (N2), a process similar to that known in macrophages. This group further demonstrated that TGF-β induced the N2 phenotype in neutrophils and inhibition of TGF-β *in vivo* slowed tumour growth, with the infiltrating neutrophils retaining their N1 phenotype (Fridlender et al., 2009). The N1 phenotype is characterised by increased expression of immunogenic cytokines and chemokines, enhanced cancer cell killing and decreased arginase expression. On the contrary, N2 cells act in a tumour promoting way by producing angiogenic factors and suppressing the anti-tumour immune response of other cells (Wang et al., 2018).

Despite this conflicting literature, neutrophils have been repeatedly implicated in the therapeutic response during BCT. It has been shown in bladder cancer patients treated with BCG that there is early recruitment of granulocytes and among these a role has been shown for neutrophils in driving the anti-tumour effect. One group have identified that neutrophils in the urine of patients recently treated with BCG vaccine expressed high levels of TRAIL which is thought to be a key step in the mechanism of the therapy (Ludwig et al., 2004). Neutrophils playing a key role in the initiation of BCT is somewhat unsurprising as they have been demonstrated repeatedly to be the first-responders in bacterial infection. It is thought that the pro-tumorigenic effect of neutrophils is driven in part by an inhibition of T-cell responses in the TME. Intratumoral neutrophils in both mouse models and patients were shown to express high levels of arginase and induce production of reactive oxygen species, both processes which reduce cytotoxic T-cell function (Veglia et al., 2021). The fact that BCT does not rely on T-cell function may explain how neutrophils can be of therapeutic benefit in this context.

The bulk RNA-sequencing in chapter 4 also showed increased expression of CCL20 in organoids treated with *S*Tm$^{\Delta aroA}$. CCL20 acts as a chemoattractant via its receptor CCR6, which is expressed by macrophages, natural killer cells, various T-cell subsets, B-cells, dendritic cells and neutrophils (Schutyser et al., 2003). CCL20 has a wide range of functions due to the receptor being expressed by such a variety of immune cells and throughout different contexts. It has been shown that CCL20-driven recruitment of macrophages can actively promote tumorigenesis via secretion of pro-inflammatory mediators which stimulate cancer cell proliferation (Nandi et al., 2016). CCL20 expression routinely being implicated as a marker of poor prognosis in a variety of tumours makes manipulation of this pathway an interesting therapeutic target. One group injected CT26 subcutaneous tumours with adenovirus vectors expressing human *CCL20* and observed an influx of immature dendritic cells to the tumour site, and subsequent reduction in tumour growth rate (Fushimi et al., 2000). Furthermore, in addition to a complex role in cancer, CCL20 expression has shown to be involved in control of pathogens by a directly antimicrobial role. It was shown *in vivo* that parasitic load was reduced in mice after oral delivery of recombinant CCL20, and that this was not associated with increased recruitment of immune cells or production of cytokines (Guesdon et al., 2015). It has been posited that CCL20 can act in a similar way to the antimicrobial peptides β-defensins due to a similar structure and a strong positive charge, which confers anti-microbial properties (Hoover et al., 2002).

Eosinophils are classically known to respond to parasites and induce a type 2 immune response, however they have also been shown to respond to colonies of bacteria in tissues with extracellular traps (EETS) (Yousefi et al., 2008, 2012). This work demonstrated that eosinophils are not capable of acting as phagocytes but have antimicrobial function in the

extracellular space. We hypothesise that the extracellular bacteria present in polyps colonised by attenuated *Salmonella* will attract eosinophils. Again, this is an immune population which has an unclear role in the development and treatment of cancer. Presence of eosinophils has been correlated with a poor prognosis in some contexts, such as Hodgkin's lymphoma and cervical cancer. However, clinical scoring of high eosinophil numbers in colorectal tumours was associated with better survival and decreased risk of metastasis (Varricchi et al., 2018). Furthermore, in $Apc^{Min/+}$ mice with spontaneous intestinal polyps and AOM-DSS models of colitis associated cancer there is recruitment of eosinophils to the tumour sites over time. Induction of CAC in ΔdblGATA mice, which lack eosinophils, resulted in a 4-fold increase in mortality. A similar increase in mortality was seen in $Apc^{Min/+}$/ΔdblGATA mice, as well as an increase in polyp burden. The anti-tumorigenic role of eosinophils in these tumours appeared to be dependent on IL-5 within the tumour microenvironment and was independent of CD8+ T cells (Reichman et al., 2019). These data suggest an active protective role for eosinophils during intestinal tumour development in mice.

In this chapter I aimed to identify whether extracellular bacteria are sufficient to induce a therapeutic response *in vivo* to intestinal cancer. To assess this, I used lambda-red recombination to generate a double mutant strain of *Salmonella* typhimurium, which have deletions in both *aroA* and *sipB* and compared colonisation and polyp clearance to $\textit{S}\text{Tm}^{\Delta aroA}$. This double mutant strain cannot bind cell surface cholesterol and I have shown that this binding is essential for intracellular invasion of our tumour organoids *in vitro* in the previous chapter **(Figure 3.3.4)**. We hypothesise that there will be early recruitment of innate cells, particularly neutrophils, macrophages and eosinophils, into the polyps of *Salmonella* treated $Apc^{Min/+}$ mice. In this chapter I assess whether these cell populations are present in polyps, and

how they alter following colonisation, using flow cytometry. Despite the conflicting evidence for each of these immune cell populations for protection against cancer we believe that the therapeutic response will be initially antimicrobial, not specifically anti-tumour.

5.2 Results

5.2.1 Validation of deletion of *sipB* from *S*Tm$^{\Delta aroA}$ via λ-red recombination

I have shown in chapter 3 that *S*Tm$^{\Delta aroA}$ relies on binding to host cell cholesterol via the sipB protein to invade tumour organoids *in vitro*. Next, I wanted to explore the role of intracellular invasion for anti-tumour effect in bacterial cancer therapy and to do so generated a *S*Tm$^{\Delta aroA\Delta sipB}$ double mutant using λ-red recombination, as described initially in 2000 (Datsenko and Wanner, 2000)**.** Colony PCR and visualisation of PCR products on agarose gel was used to confirm deletion of *sipB* and insertion of the Kanamycin resistance (Kan^R) cassette in the correct genomic location. Primer pairs were designed to amplify the intact flanking region of *sipB* and an internal portion of the Kan^R cassette in both directions (primer sequences in **Table 5** and schematic of primers in the genome in **2.14.1**). Reaction one (**Figure 5.2.1 A)** and two **(Figure 5.2.1 B)** amplified products from the DNA of *S*Tm$^{\Delta aroA\Delta sipB}$ colony only, with molecular weights around the expected product size of 1 kB and 1.2 kB respectively. A final primer pair were designed from the internal portion of *sipB* that is expected to now be absent in *S*Tm$^{\Delta aroA\Delta sipB}$*.* Reaction three **(Figure 5.2.1 C)** amplified from *S*Tm$^{\Delta aroA}$ only with a molecular weight of ~0.95 kB, where the expected weight was 0.95 kB.

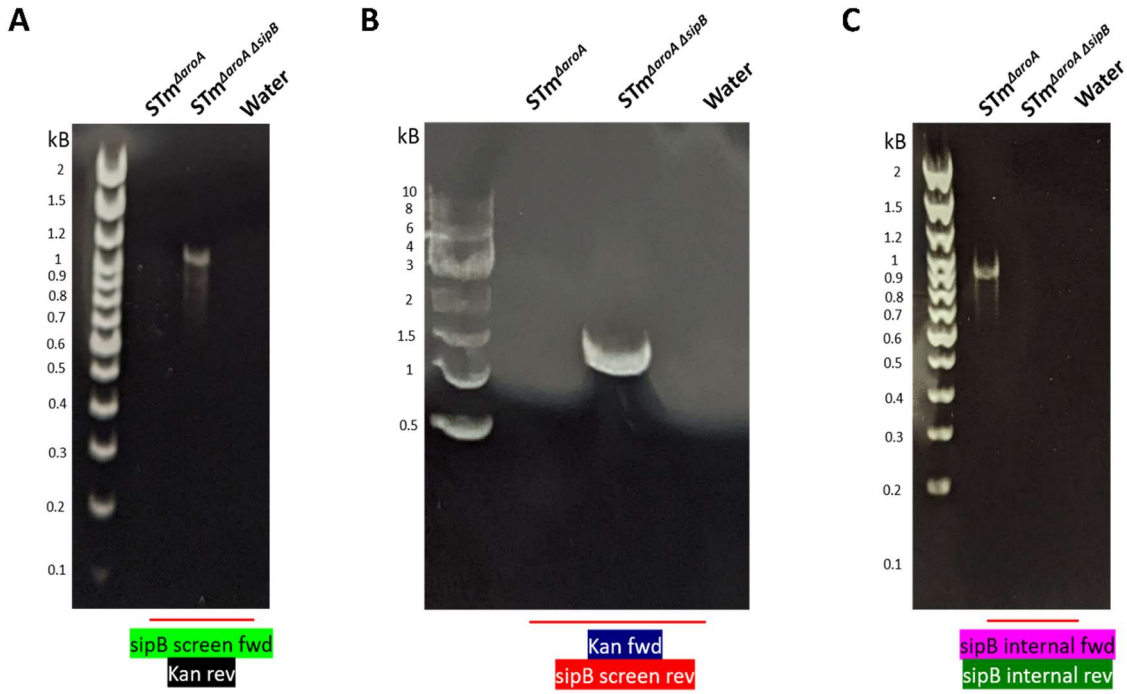


Figure 5.2.1: Validation of deletion of sipB from STm$^{\Delta aroA}$ via λ-red recombination
Primer combinations indicated were used to confirm sipB deletion, Kanamycin cassette insertion and correct placement. ***(A** and **B)** Primers annealing to the preserved flanking region of sipB and the inside of the Kanamycin cassette with expected product sizes of 1 kB **(A)** and 1.2 kB **(B)**. **(C)** Primers which anneal to an internal portion of sipB with an expected product size of 0.96 kB.*

5.2.2 STm$^{\Delta aroA\Delta sipB}$ cannot invade intracellularly but can survive in polyps *in vivo*

In chapter 3 I demonstrated that *sipB*-deficient *S*Tm could not invade organoids, however this was a different background strain of *S*Tm. To assess whether *S*Tm$^{\Delta aroA\Delta sipB}$ was also unable to invade intracellularly, the media of *Apc*$^{Min/+}$ tumour organoids was inoculated with *S*Tm$^{\Delta aroA}$ to show baseline level of invasion or *S*Tm$^{\Delta aroA\Delta sipB}$ and incubated for 2 hours. Wells were then washed, and media replaced with media containing gentamicin to kill extracellular bacteria. After 24 hours the organoids were collected, lysed, and plated on agar for overnight growth at 37°C. *S*Tm$^{\Delta aroA\Delta sipB}$ resulted in no bacterial colonies grown **(Figure 5.2.2 A)**, confirming that deletion of *sipB* in SL3261 prevents intracellular invasion of tumour organoids *in vitro.*

I next assessed whether this extracellular-restricted double mutant could survive in the tumour microenvironment. We have previously shown using scanning electron microscopy that a large majority of *S*Tm$^{\Delta aroA}$ is localised to extracellular, but intratumoural, colonies *in vivo* (Mackie et al., 2021). *Apc*$^{Min/+}$ mice of 12 weeks old were gavaged with equal CFU of either *S*Tm$^{\Delta aroA}$ or *S*Tm$^{\Delta aroA\Delta sipB}$. 24 hours post gavage normal small intestinal tissue had very low level of colonisation for both strains, with specific colonisation of polyps at around $2x10^4$ CFU/g for both bacterial strains **(Figure 5.2.2 B)**. Furthermore, there was no significant difference in the bacterial burden of the two strains. Tissue from liver, lung, spleen, and mesenteric lymph nodes was also taken from all mice. These were lysed in the same way as the intestinal tissue, plated neat on LB agar and grown overnight. No bacterial colonies were recovered from any peripheral tissues and thus data not shown.

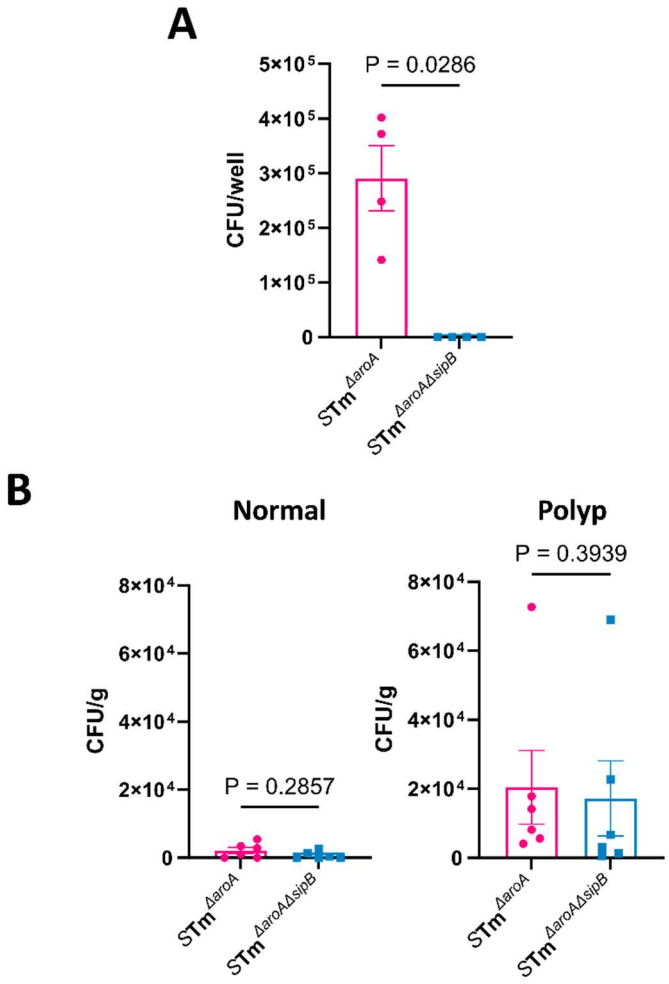


Figure 5.2.2: STm$^{\Delta aroA\Delta sipB}$ cannot invade intracellularly in vitro but can survive in polyps in vivo

(A) *Media of Apc$^{Min/+}$ organoids was infected with either STm$^{\Delta aroA}$ or STm$^{\Delta aroA\Delta sipB}$ for 2 hours before media was replaced with gentamicin supplemented in, and colony forming units grown to assess intracellular invasion of both strains. Data points represent CFU from 1 well of organoids, error bar shows standard error of the mean and p-value was measured using Mann-Whitney test. (n = 4 individual wells of organoids)* ***(B)*** *CFU of STm$^{\Delta aroA}$ and STm$^{\Delta aroA\Delta sipB}$ in polyp and adjacent normal tissue 24 hours after gavage of Apc$^{Min/+}$ mice. Data represents one experiment using a mixture of 12-week-old male and female mice with littermates across both treatment groups (n= 6 mice per treatment group). Error bar shows standard error of the mean and p-value was measured using Mann-Whitney test.*

5.2.3 A small proportion of *S*Tm$^{\Delta aroA}$ intracellularly invades tumour cells *in vivo,* but *S*Tm$^{\Delta aroA\Delta sipB}$ survives in polyps *in vivo* exclusively extracellularly

Building further on the observation that *S*Tm$^{\Delta aroA\Delta sipB}$ could not invade tumour cells *in vitro* but could survive in polyps *in vivo*, I wanted to validate the double mutant's inability to reside intracellularly in polyps *in vivo.* To do this I utilised an *ex vivo* gentamicin protection assay that has been published previously (Avogadri et al., 2005). Briefly, 11–13-week-old *Apc*$^{Min/+}$ mice were given oral gavage with equal CFUs of either *S*Tm$^{\Delta aroA}$ or *S*Tm$^{\Delta aroA\Delta sipB}$ before small intestines were removed 48 hours later. Tissues were cleaned and polyps dissected out using a stereo microscope. Polyps from each mouse were then split by weight and mashed through a cell strainer into media with or without gentamicin supplement. The cells were incubated in the media before CFUs were measured from each condition.

A low number of bacteria were protected from killing by gentamicin in *S*Tm$^{\Delta aroA}$ treated polyps (average of $1.9x10^3$ CFU/g) and far fewer protected in *S*Tm$^{\Delta aroA\Delta sipB}$ treated polyps (average of 80 CFU/g) **(Figure 5.2.3 B)**. This equates to a small proportion of *S*Tm$^{\Delta aroA}$, between 1.5 and 8% per mouse, compared to 0.2% in two mice and 0% in the remaining mice for *S*Tm$^{\Delta aroA\Delta sipB}$ **(Figure 5.2.3 C)**. These data clarify, using a different approach than previously, that *S*Tm$^{\Delta aroA}$ exists largely extracellularly within tumours or polyps, and demonstrates that loss of *sipB* ablates any intracellular invasion of tumours *in vivo*.

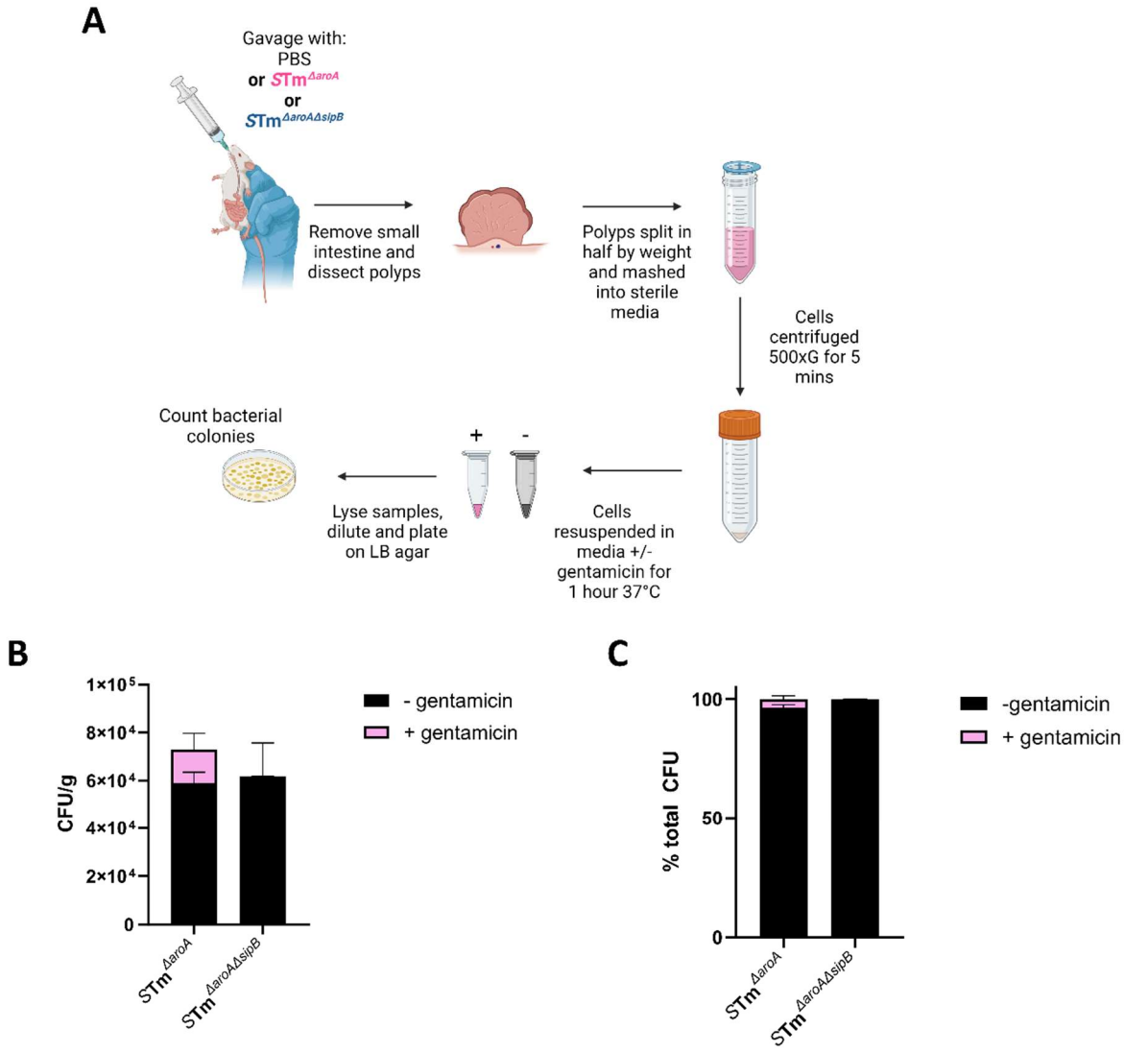


Figure 5.2.3: A small proportion of STm$^{\Delta aroA}$ intracellularly invades tumour cells in vivo, but STm$^{\Delta aroA\Delta sipB}$ survives in polyps in vivo exclusively extracellularly

(A) *Schematic of the gentamicin protection assay of polyps.* ***(B*** *and* ***C)*** *Apc$^{Min/+}$ mice were gavaged with STm$^{\Delta aroA}$ or STm$^{\Delta aroA\Delta sipB}$ and polyps dissected after 48 hours. Polyps were weighed and divided into media +/- gentamicin for 1 hour before cells were lysed and bacteria plated and enumerated after growth at room temperature for 3 days. Data represents one experiment with a mixture of males and females between 11 and 13 weeks old, age and sex matched between treatment groups (n=7 mice per treatment group).*

5.2.4 *S*Tm$^{\Delta aroA\Delta sipB}$ stunts tumour growth *in vitro* and reduces tumour burden and load *in vivo*

I next aimed to identify whether *S*Tm$^{\Delta aroA\Delta sipB}$ could still functionally impact tumour growth, both *in vitro* and *in vivo.* To measure this *in vitro,* the media of *Apc*$^{Min/+}$ colon tumour organoids was directly inoculated with PBS, *S*Tm$^{\Delta aroA}$ or *S*Tm$^{\Delta aroA\Delta sipB}$ and incubated for 2 hours before extracellular bacteria were washed away, and organoids were re-fed with media containing gentamicin. Organoids were incubated for a further 24 hours before Matrigel was dissolved and organoids digested to single cell suspensions. Cells of each condition were diluted equally, seeded into 96 well plates and grown to form organoids for 5 days. On day 5 an MTT assay was used to measure cell viability of the resulting wells. *S*Tm$^{\Delta aroA}$ significantly reduced cell viability, confirming our previous observations of stunted regrowth after *in vitro* infection. *S*Tm$^{\Delta aroA\Delta sipB}$ also induced a significant reduction in cell viability compared to PBS control wells, but to a lesser extent that *S*Tm$^{\Delta aroA}$, suggesting there was an intermediate level of effect on the organoids with *S*Tm$^{\Delta aroA\Delta sipB}$ **(Figure 5.2.4 A)**. The observation of an effect with *S*Tm$^{\Delta aroA\Delta sipB}$ *in vitro* was striking as we treat the culture with gentamicin-supplemented media after 2 hours. We have shown that this mutant cannot invade intracellularly **(Figure 5.2.2 A)** and so the effect must be triggered within those 2 hours of contact.

As described above, we have shown that extracellular bacteria are present in our *S*Tm$^{\Delta aroA}$ model and that the *S*Tm$^{\Delta aroA\Delta sipB}$ double mutant is capable of surviving in polyps for at least 24 hours. Our previous work showed that *S*Tm$^{\Delta aroA}$, which we know exists both intracellularly but also extracellularly in polyps, led to dramatic changes in the tumour metabolome. This competition for metabolites likely comes from the proliferation of intratumoral bacteria, and so with the tool of *S*Tm$^{\Delta aroA\Delta sipB}$ we wanted to unpick the intra- vs extracellular effects in BCT.

I hypothesised that part of the anti-tumour effect of *S*Tm$^{\Delta aroA}$ *in vivo* is driven by these extracellular bacteria and therefore *S*Tm$^{\Delta aroA\Delta sipB}$ would reduce polyp burden to some extent.

To assess this, 8-week-old *Apc*$^{Min/+}$ mice were divided into 3 treatment groups, PBS (NT), *S*Tm$^{\Delta aroA}$ and *S*Tm$^{\Delta aroA\Delta sipB}$ and given weekly gavages for 8 weeks before culling on the 9th week and removing small intestines. The polyps were counted and measured to assess polyp burden and load **(Figure 5.2.4 B)**. Firstly, these data confirmed that *S*Tm$^{\Delta aroA}$ significantly reduces polyp burden and load in *Apc*$^{Min/+}$ mice in this facility. Secondly, I showed that *S*Tm$^{\Delta aroA\Delta sipB}$ reduced polyp burden and load even more significantly than *S*Tm$^{\Delta aroA}$ **(Figure 5.2.4 C** and **D)**. PBS control mice of the same age had an average of 27 polyps per mouse, this was reduced to 9.75 polyps per mouse with repeated *S*Tm$^{\Delta aroA}$ treatment and 3.5 polyps per mouse after *S*Tm$^{\Delta aroA\Delta sipB}$ treatment. Polyp volume was varied in the PBS treated controls, with significantly more polyps above 5mm^2 than either of the treatment groups **(Figure 5.2.4 D)**. Therefore, oral gavage of extracellular-restricted *Salmonella* is not only sufficient but superior at clearing intestinal polyps in *Apc*$^{Min/+}$ mice.

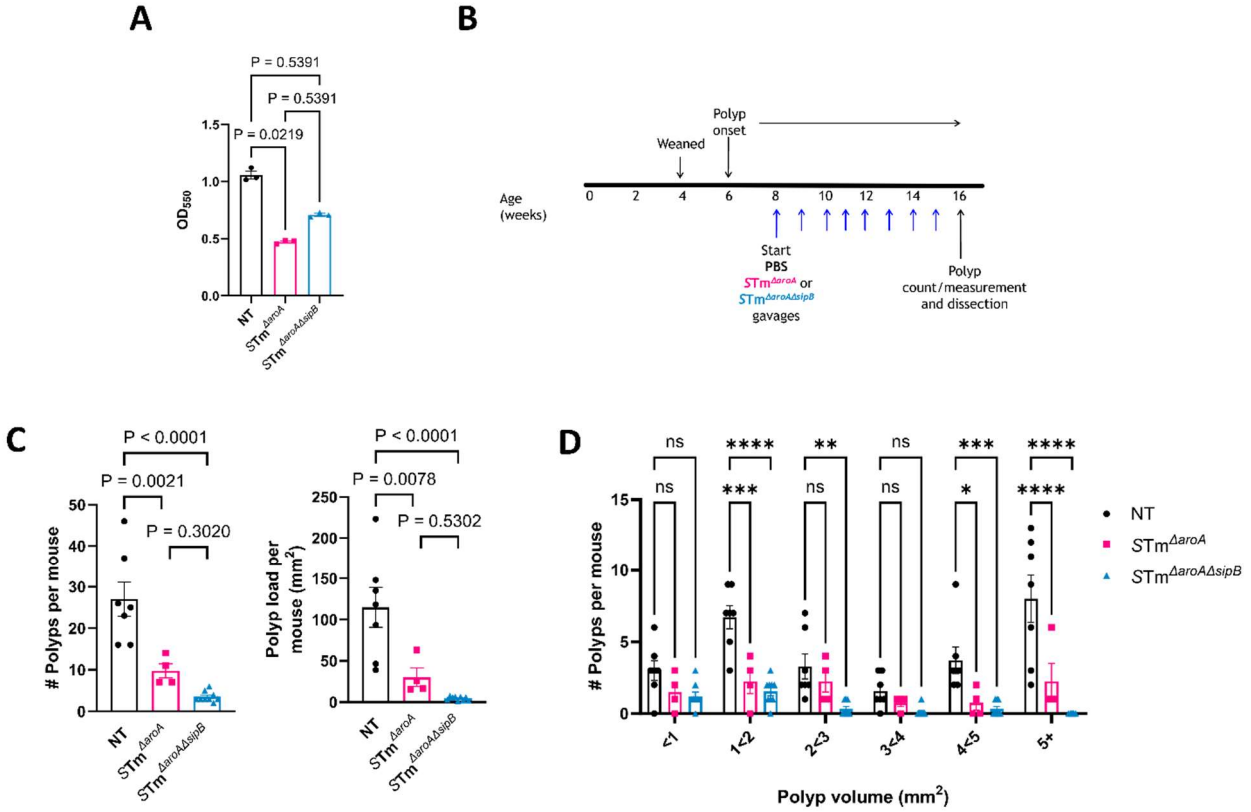


Figure 5.2.4: STm$^{\Delta aroA\Delta sipB}$ stunts tumour growth in vitro and reduces tumour burden and load in vivo

(A) *Cell viability of Apc$^{Min/+}$ organoids grown for 5 days from organoids treated with PBS (NT), STm$^{\Delta aroA}$ or STm$^{\Delta aroA\Delta sipB}$ as measured by MTT assay. Each data point represents average of 5 wells grown from one initial treatment well. Error bars represent the standard error of the mean. (n = 3 biological repeats).* ***(B)*** *Schematic of long-term treatment protocol for Apc$^{Min/+}$ mice. From 8 weeks of age, mice were given 8 weeks of weekly gavages of either PBS (NT), STm$^{\Delta aroA}$ or STm$^{\Delta aroA\Delta sipB}$. Polyps were counted and measured a week after the last gavage.* ***(C)*** *Polyp burden (number of polyps/mouse) and load (cumulative polyp volume per mouse, mm^2).* ***(D)*** *The burden and size of polyps per mouse in PBS (NT), STm$^{\Delta aroA}$ and STm$^{\Delta aroA\Delta sipB}$ treated mice. Data represents two combined experiments (n=7 PBS, n=4 STm$^{\Delta aroA}$, n=9 STm$^{\Delta aroA\Delta sipB}$). Error bars represent the standard error of the mean. P values were measured by one way ANOVA with Tukey's multiple comparisons* ***(A** and **C)*** *and two-way ANOVA with Dunnett's multiple comparisons, p-values: ns = >0.05, * = <0.05, ** = <0.01, *** = <0.001, **** = <0.0001* ***(D)***.

5.2.5 *S*Tm$^{\Delta aroA}$ and *S*Tm$^{\Delta aroA\Delta sipB}$ significantly increase eosinophil recruitment to polyps *in vivo*

In chapter 4, bulk RNA-sequencing data revealed that *S*Tm$^{\Delta aroA}$ induces a chemokine signature in colorectal tumour organoids, when intracellular-permitted or extracellular-restricted, which would suggest recruitment of both neutrophils and macrophages *in vivo*. We wanted to investigate recruitment of these cells early after colonisation, as well as eosinophil infiltration in response to the extracellular bacteria. To do this, 11–13-week-old littermates were divided into treatment groups and gavaged with PBS (NT) or equal CFUs of either *S*Tm$^{\Delta aroA}$ or *S*Tm$^{\Delta aroA\Delta sipB}$ before they were culled 48 hours later and small intestines removed. Polyps were enzymatically digested and stained for a panel of innate immune cell markers and analysed using flow cytometry. Cells were gated on based on morphology and then live singlets and specific leukocytes were gated based on the strategy in chapter 2 **(Figure 2.20.1)**. Representative plots of the specific cell types for each treatment condition are included here **(Figure 5.2.5)**.

Analysis of these data showed there was a very slight trend for increased non-lymphocytic leukocytes (CD45+CD3-CD19- cells) as a percentage of live cells in polyps from *S*Tm$^{\Delta aroA}$ treated mice compared to non-treated mice and *S*Tm$^{\Delta aroA\Delta sipB}$ **(Figure 5.2.6 A)**. There was a significant and consistent increase in the level of eosinophils (CD45+CD3-CD19-Ly6G-CD11b+Siglec F+) as a percent of total CD45+CD3-CD19- cells infiltrating polyps in mice treated with either bacterial strain compared to the non-treated controls. This infiltration did not vary between the bacterial strains **(Figure 5.2.6 B)**. Analysis of the neutrophils (CD45+CD3-CD19-Ly6G+CD11b+) showed a slight trend for increased proportion of the total CD45+CD3-CD19- cells in *S*Tm$^{\Delta aroA}$ and slightly increased again in *S*Tm$^{\Delta aroA\Delta sipB}$ compared to non-treated mice but

this was not significant and varied widely within treatment groups **(Figure 5.2.6 C)**. Gut macrophages were defined as has been previously published (Liu et al., 2020) (CD45+CD3-CD19-Ly6G-Siglec F-CD11b+CD64+CD11c^{int}Ly6C-MHCII+) and there was a trend for increased proportion of infiltrating gut macrophages in *S*Tm$^{\Delta aroA}$ treated mice but not *S*Tm$^{\Delta aroA\Delta sipB}$. Again, this was not significant and the proportions of macrophages within the polyps was low in all treatment groups (<3.5% of total CD45+CD3-CD19- cells) **(Figure 5.2.6 D)**. These data suggest that eosinophils are the first responder to attenuated *Salmonella* colonisation of intestinal polyps.

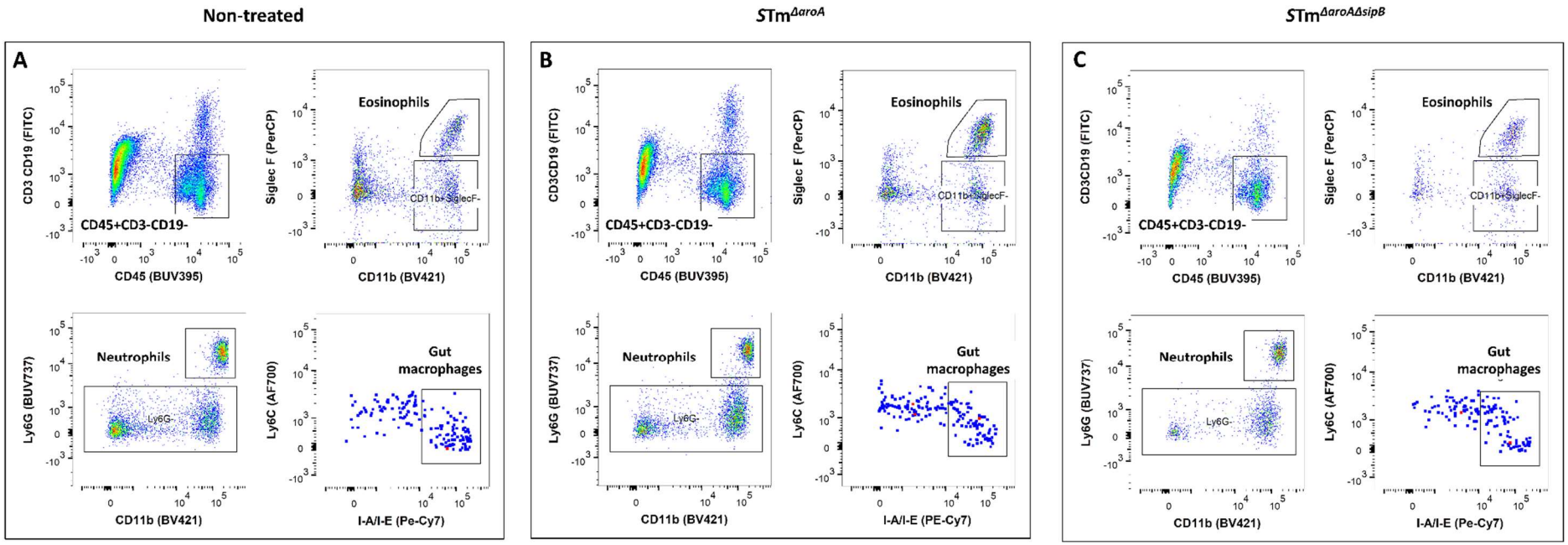


Figure 5.2.5: Representative flow plots showing cell populations in Apc$^{Min/+}$ polyps

*Representative plots of cell types in the polyps of non-treated **(A)**, STm$^{\Delta aroA}$ treated **(B)** and STm$^{\Delta aroA\Delta sipB}$ treated **(C)** 12-week-old Apc$^{Min/+}$ mice. Cells were gated on morphology and then live singlets gated on. CD45+ CD3-CD19- cells were termed non-lymphocytic leukocytes. Eosinophils were defined as CD45+CD3-CD19-Ly6G-CD11b+Siglec F+. Neutrophils were defined as CD45+CD3-CD19-Ly6G+CD11b+. Gut macrophages (gMacrophages) were defined as CD45+CD3-CD19-Ly6G-Siglec F-CD11b+CD64+CD11c^{int}Ly6C-MHCII+.*

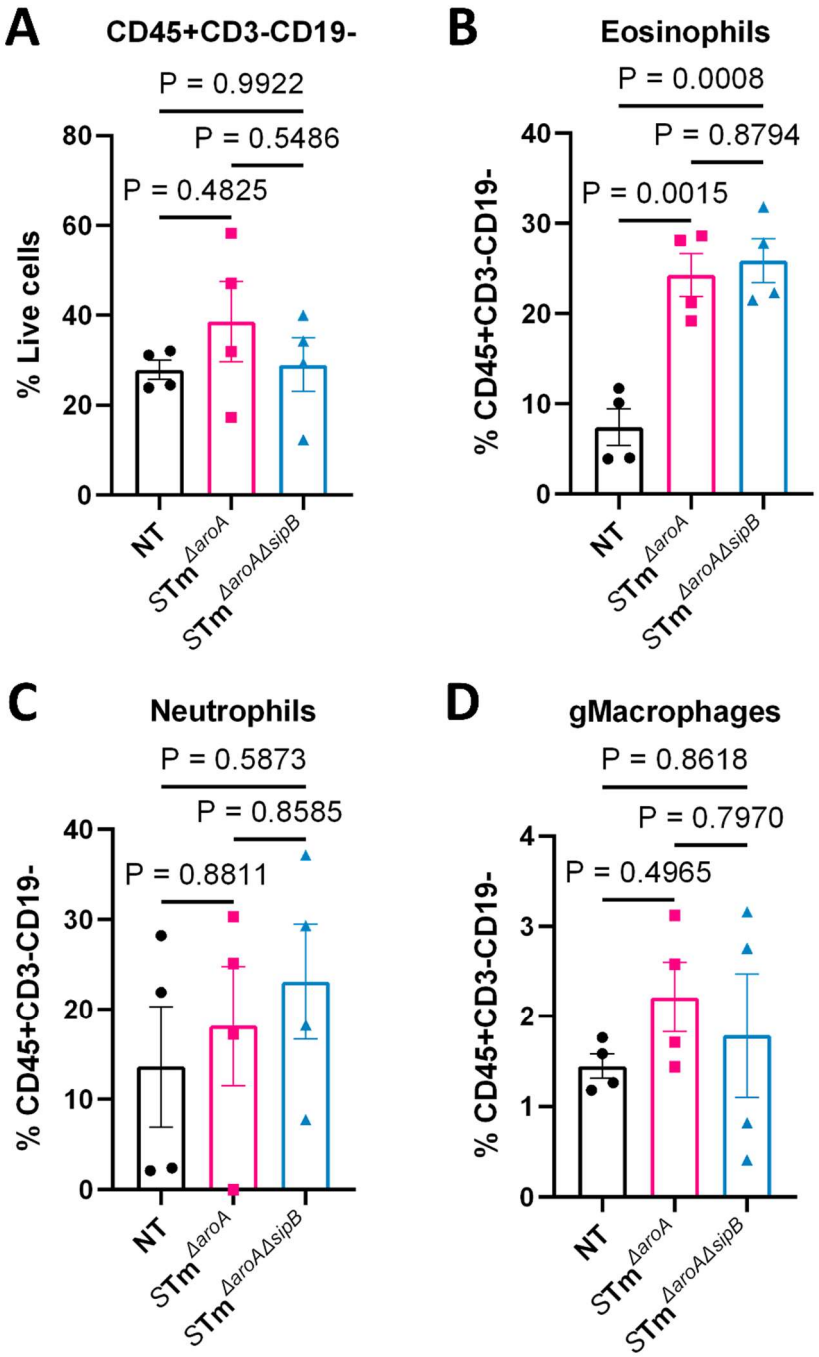


Figure 5.2.6: STm$^{\Delta aroA}$ and STm$^{\Delta aroA\Delta sipB}$ significantly increase eosinophil recruitment to polyps in vivo

*Innate cell infiltration was analysed in 12-week-old mice 48 hours post oral gavage with either PBS (NT), STm$^{\Delta aroA}$ or STm$^{\Delta aroA\Delta sipB}$. Cells were gated on morphology and then live singlets gated on. Non-lymphocytic leukocytes as defined as CD45+ CD3-CD19- cells were measured as a percentage of total live cells **(A)**. Eosinophils were defined as CD45+CD3-CD19-Ly6G-CD11b+Siglec F+ **(B)**. Neutrophils were defined as CD45+CD3-CD19-Ly6G+CD11b+ **(C)**. Gut macrophages (gMacrophages) were defined as CD45+CD3-CD19-Ly6G-Siglec F-CD11b+CD64+CD11c^{int}Ly6C-MHCII+. Data points represent combined polyps dissected from one mouse. Data represents 2 combined experiments, with age and sex matched mice. Littermates were divided amongst the treatment groups. (n= 4 per treatment group). Error bars represent SEM. P-values were measured by one-way ANOVA with Tukey's multiple comparisons.*

5.3 Discussion

Salmonella typhimurium are known as intracellular pathogens which invade host cells and proliferate in intracellular vacuoles. In chapter 3, I identified that sipB was an essential component of intracellular invasion in tumour organoids *in vitro.* However, using sequencing data I showed that chemically extracellular-restricted *S*Tm$^{\Delta aroA}$ could still induce substantial transcriptional changes in the tumour organoids. Therefore, I wanted to assess *in vivo* the extent to which intracellular bacteria drive the anti-tumour response of *S*Tm$^{\Delta aroA}$ in our models. I demonstrated in this chapter that while *S*Tm$^{\Delta aroA\Delta sipB}$ is unable to invade *in vitro*, it can colonise polyps to a comparable level to *S*Tm$^{\Delta aroA}$. Using a gentamicin-protection assay of infected polyps, I confirmed that this was not due to a recovery of intracellular infection *in vivo.* This validation of *S*Tm$^{\Delta aroA\Delta sipB}$ surviving in the extracellular space of polyps in *Apc*$^{Min/+}$ mice demonstrates its potential as a useful tool for investigating extracellular-restricted *Salmonella* typhimurium *in vivo.* Another group have previously shown that deletion of *sipB* led to reduced (but not abolished) invasion in HeLa cells without impacting the growth of *Salmonella* typhimurium (Chen et al., 2015). This difference may be due to a different background strain of *Salmonella* or adherent cells compared to tumour organoids. Interestingly, this paper showed that *S*Tm$^{\Delta sipB}$ had reduced adherence to the HeLa cells, suggesting that this would also be impaired in our double mutant. This remains to be shown in our model but would be an important future experiment to assess whether direct contact is necessary for the therapeutic effect.

A key mechanism used by bacteria to survive extracellularly in the host is production of a biofilm. It has been shown, as described earlier, that both wild-type and attenuated *S*Tm can

survive in tumours (Crull et al., 2011; Silva-Valenzuela et al., 2016) and lymphoid structures such as tonsils (Van Parys et al., 2010). Crull et al. described the dependence of *Salmonella* to express genes associated with biofilm production for survival in the tumour extracellularly, whereas Van Parys et al. showed that this process was not essential for *Salmonella* to survive in the extracellular space of tonsils. It remains to be seen whether this is strain (wild-type vs attenuated) or site-specific and so it may be of future interest to mutate biofilm-associated genes in *S*Tm$^{\Delta aroA\Delta sipB}$ to assess survival in polyps without this mechanism.

Following on from the generation and validation of *S*Tm$^{\Delta aroA\Delta sipB}$ double mutant, which is tolerated by the mice *in vivo* and cannot invade intracellularly, we next aimed to examine whether the double mutant bacteria could exert a functional anti-tumour effect. We initially tested this *in vitro* by utilising an MTT assay. This is a plate-based assay in which the rate of colour change is proportional to the rate of metabolic activity in the well and is used as an indirect measurement of cell viability. Briefly, the more metabolically active the cells, the more oxidoreductase enzymes they contain, and therefore the more MTT the cells are able to reduce to formazan. Confluent organoids were treated with PBS or equal CFUs of either *S*Tm$^{\Delta aroA}$ or *S*Tm$^{\Delta aroA\Delta sipB}$ and an MTT assay was used to measure cell viability on wells grown for 5 days from these treatment wells. We have shown previously that *in vitro* infection of *Apc*$^{Min/+}$ organoids stunts regrowth capacity via both MTT assays and stem forming assays (Mackie et al., 2021) and this work confirmed these findings **(Figure 5.2.4 A)**. Interestingly, the double mutant *S*Tm$^{\Delta aroA\Delta sipB}$ resulted in a reduction in viability at day 5 of growth that was between the reduction induced by *S*Tm$^{\Delta aroA}$ and the non-treated baseline **(Figure 5.2.4 A)**. These data suggested that there was some impact of the *S*Tm$^{\Delta aroA\Delta sipB}$ functionally on our tumour organoids despite being unable to invade intracellularly. We next aimed to translate

this *in vivo* in *Apc*$^{Min/+}$ mice as we knew that the double mutant could survive in this context. We hypothesised that we would again see this intermediate effect of slight reduction in polyp burden compared to that of *S*Tm$^{\Delta aroA}$. To measure this, we used a long-term treatment protocol where 8-week-old *Apc*$^{Min/+}$ mice were gavaged once a week for 8 weeks with either PBS or equal CFUs of *S*Tm$^{\Delta aroA}$ or *S*Tm$^{\Delta aroA\Delta sipB}$. This treatment begins after polyps begin to form in the mice, which has been published to occur from 4-6 weeks (Puppa et al., 2011; Yamada and Mori, 2007). As previously published, we observed a significant reduction in polyp burden (number of polyps per mouse) and polyp load (volume of polyps per mouse, mm^2) after oral gavage with *S*Tm$^{\Delta aroA}$ compared to PBS treated mice. Surprisingly we saw an even further reduction in both polyp burden and load after oral gavage with *S*Tm$^{\Delta aroA\Delta sipB}$ **(Figure 5.2.4 C)**. These data may suggest that *S*Tm$^{\Delta aroA\Delta sipB}$ represents a superior alternative to *S*Tm$^{\Delta aroA}$ as an agent for intestinal BCT. The differences in the mechanisms of action between these two strains is a remaining question. We hypothesise that increased clearance of polyps with extracellular-restricted bacteria is a result of the bacteria not triggering a host-defence process that is unique to detection of intracellular bacteria.

There were some areas of hyperplasia in the small intestines of *S*Tm$^{\Delta aroA\Delta sipB}$ treated mice which may represent polyps that have been cleared or new polyps forming due to the absence of *S*Tm$^{\Delta aroA\Delta sipB}$ at the end point. We had aimed to measure CFU at the end of the long-term treatment to compare the long-term survival of *S*Tm$^{\Delta aroA}$ to *S*Tm$^{\Delta aroA\Delta sipB}$, but there were too few polyps to dissect and lyse for this analysis. We currently do not know whether there is a need for continual lysis of the few infected cells in *S*Tm$^{\Delta aroA}$ treated mice to re-populate the extracellular tumour microenvironment, whereas in *S*Tm$^{\Delta aroA\Delta sipB}$ it may be the case that as there is no protective niche the bacteria are completely cleared during clearance of polyps.

Comparison of the long-term bacterial burden for the double mutant is an important future question, as if it is cleared better from the treated gut then *S*Tm$^{\Delta aroA\Delta sipB}$ would not only be a superior anti-tumour agent but may also represent a safer therapy for patients.

Further work is required to fully unpick the difference between the mechanisms of action of *S*Tm$^{\Delta aroA}$ and *S*Tm$^{\Delta aroA\Delta sipB}$ that underpin the increased protection seen with the double mutant. It should be noted that the *S*Tm$^{\Delta aroA}$ used in this work was UF20 and the double mutant was generated on SL3261 background and so these are not isogenic strains that are being compared. However, we see no functional difference in SL3261 and UF20 single deletion of *aroA* in terms of growth rates, CFU burden in organoids or mouse models the group has done previously. This suggests that the difference is likely due to the additional deletion of *sipB* but it should be confirmed by directly comparing SL3261 *ΔaroA* with *ΔaroAΔsipB*. Furthermore, the ability of cloned *sipB* in a plasmid added into *S*Tm$^{\Delta aroA\Delta sipB}$ to rescue the invasion defect and reduce tumour clearance should be tested to confirm that deletion of *sipB* is driving the phenotype.

It has been repeatedly shown in the literature that the adaptive immune system is largely dispensable for *Salmonella*-mediated BCT, and instead the myeloid compartment appears to drive the therapy. In 2014 it was shown that athymic mice were as protected against tumour development as wildtype mice when treated with attenuated *Salmonella,* whereas MyD88-/- mice were not protected (Kaimala et al., 2014). Recent work has shown that clearance of melanoma by *S*Tm$^{\Delta aroA}$ was largely dependent on monocytes. C57BL/6 mice with subcutaneous B16F10 melanoma tumours were given *S*Tm$^{\Delta aroA}$ intravenously. Significantly reduced tumour growth was observed, and this was associated with expansion of Ly6C+MHC-

II+ monocytes. These cells were actively proliferative and expressed a range of pro-inflammatory cytokines. Treatment of the mice with clodronate liposomes to deplete phagocyte populations led to a loss of the therapeutic effect of *S*Tm$^{\Delta aroA}$ (Johnson et al., 2021). Together this work demonstrates a key role for innate immune cells in the mechanism of action of BCT *in vivo*. This published data combined with the chemokine signature we saw upregulated in the Paneth cells following *S*Tm$^{\Delta aroA}$ treatment led us to hypothesise there would be increased recruitment of myeloid cells, specifically neutrophils and macrophages into colonised polyps *in vivo*. We hypothesised that there would be increases in these myeloid cells in mice treated with both bacterial strains as there were similar signatures in the sequencing for both intracellular and extracellular-restricted bacteria.

Neutrophils have been shown to restrict extracellular colonies of *Salmonella* typhimurium in the liver (Conlan, 1996). Therefore, the lack of early infiltration of neutrophils with either *S*Tm$^{\Delta aroA}$ or *S*Tm$^{\Delta aroA\Delta sipB}$ may aid the therapeutic response if in intestinal cancers BCT relies on extracellular colonisation of the tumour. Gut macrophages were observed at very low levels in the polyps, but there was a slight trend for an increase after *S*Tm$^{\Delta aroA}$ gavage. The trend for an increase in macrophage infiltration to polyps being *S*Tm$^{\Delta aroA}$ specific may be linked to the earlier observation that CCL20 was upregulated in mouse tumour organoids with intracellular permitted *S*Tm$^{\Delta aroA}$ but not extracellular-restricted **(Figure 4.2.6 A** and **B)**. CCL20 was however upregulated in both contexts in human tumour organoids **(Figure 4.2.6 C** and **D)** and so *S*Tm$^{\Delta aroA\Delta sipB}$ may also recruit macrophages in humans but not mice.

It has been shown that in addition to responding to parasitic infection, eosinophils also respond specifically to extracellular bacteria (Yousefi et al., 2008, 2012). Therefore, based on

our previous data that we see large intratumoural, but extracellular colonies with both *S*Tm$^{\Delta aroA}$ and *S*Tm$^{\Delta aroA\Delta sipB}$ we also included markers for eosinophils in this panel. The most striking difference in innate cell populations was the proportion of eosinophils infiltrating the polyps **(Figure 5.2.8 D)**. This increase compared to non-treated polyp infiltrate was similar between the bacterial strains, suggesting that the few intracellular *S*Tm$^{\Delta aroA}$ bacteria did not impact the recruitment of eosinophils. The question remains what the function of these infiltrating eosinophils is, which could be interrogated via visualisation using immunohistochemistry. It has been shown that one role of eosinophils in the control of bacteria is release of EETs (Yousefi et al., 2008) which are composed of mitochondrial DNA. It has been shown that EETs are only released in response to specific types of bacteria, and this includes *Salmonella* typhimurium, suggesting eosinophils may play a direct role in the early response in *Salmonella*-mediated BCT (Gurtner et al., 2021). These can be imaged *in vivo* and would possibly shed light on the interaction of these infiltrating eosinophils and the colonising bacteria. The necessity of the eosinophil infiltration for the therapeutic response could also be interrogated by generating ΔdblGATA *Apc*$^{Min/+}$ mice which would lack eosinophils and comparing polyp burden with *S*Tm$^{\Delta aroA}$ and *S*Tm$^{\Delta aroA\Delta sipB}$ treatment (Yu et al., 2002).

While this work was focussed on that very initial innate response to polyp colonisation, future work should aim to assess the recruitment of a wider range of immune cells over the duration of the long-term treatment. It has also been shown that CCL20 produced by colorectal cancer cells can drive Treg recruitment and that this was correlated with chemoresistance (Wang et al., 2019). Investigation of this during treatment with attenuated *Salmonella* will be critical to assessing whether it would be useful as an adjuvant therapy with existing chemotherapies. In addition, the chemokines shown to be upregulated also are known to recruit dendritic cells to

the site of infection, particularly CCL20. It has been shown in the human immortal colon carcinoma cell line CaCo-2 that detection of *Salmonella*-derived flagellin induced CCL20 release, which in turn recruited immature dendritic cells (Sierro et al., 2001). Flagellin is detected by epithelial cells by the PRR TLR5 at the cell membrane, and therefore could be triggered by the extracellular-restricted bacteria. It is of future interest to assess the recruitment and activity of dendritic cells to tumours colonised by *Salmonella*.

In summary, in this chapter I have generated and validated a double mutant strain of *Salmonella* typhimurium which is unable to intracellularly invade tumour organoids or polyps *in vivo*. This strain of bacteria induced superior clearance of intestinal polyps of $Apc^{Min/+}$ mice when compared to the widely researched vaccine strain, *S*Tm$^{\Delta aroA}$. Both these bacterial strains induce significant, rapid recruitment of eosinophils to the polyps *in vivo*, but the role of eosinophils in the clearance of these polyps remains to be investigated. This work demonstrates that intracellular invasion of intestinal tumours is dispensable for the protective effects of *Salmonella*-mediated BCT.

CHAPTER 6 – FINAL DISCUSSION

Bacterial cancer therapy using *Salmonella* typhimurium is a promising strategy for treating solid tumours in patients. It has been repeatedly demonstrated that safe, stable vaccine strains home to tumours *in vivo* and specifically colonise malignant tissue over surrounding normal tissues. Despite promising work in mouse models and cell lines *in vitro* there is a disappointing lack of translation into successful clinical trials in patients. We believe that this stems in part from a lack of understanding of the entire mechanisms of action of *Salmonella*-mediated BCT. In this work I aimed to unpick further which cells are most affected by the therapy to aid experimental design in the future, and directly compare the effects in a range of patient-derived organoids and mouse tumour organoids to investigate heterogenous therapy response.

The work presented in this thesis reveals novel mechanisms by which *Salmonella*-mediated therapy impacts the environment and cells of intestinal tumours. In chapter 3 I demonstrated that there is specific targeting of the proliferative cells within both mouse and human colorectal tumour organoids *in vitro*, the driving cells of tumour progression. This intracellular invasion requires the T3SS component sipB, revealing that bacteria-host cell cholesterol interactions are essential for optimal intracellular invasion within tumours. I then went on to investigate the necessity of this invasion to the therapeutic effect, using both chemical sequestering of cell cholesterol to inhibit invasion *in vitro* and a double mutant *S*Tm$^{\Delta aroA \Delta sipB}$ which could not invade intracellularly *in vivo*. Surprisingly we saw very similar transcriptional effects *in vitro* using bulk RNA-sequencing, primarily induction of several CXC family

chemokines. Largely, the *in vitro* work throughout chapters 3 and 4 that was carried out in mouse tumour organoids was faithfully recapitulated and in human tumour organoids. This suggests that the intrinsic effect of *S*Tm$^{\Delta aroA}$ appears to be similar within mouse and human colorectal tumour epithelial cells. This may indicate that the failure to translate *in vivo* mouse models of BCT to humans is due to inappropriate delivery, such as intravenous, leading to clearance of the bacteria by the more complex human complement system (Bergman et al., 2000). Finally, I demonstrated in chapter 5 that extracellular-restricted *Salmonella* typhimurium are sufficient to reduce polyp burden and load in *Apc*$^{Min/+}$ mice, in fact the *S*Tm$^{\Delta aroA\Delta sipB}$ strain reduced polyp burden to a greater degree than *S*Tm$^{\Delta aroA}$. It has been shown previously that extracellular bacteria can survive in tumours *in vivo* (Avogadri et al., 2005; Crull et al., 2011; Silva-Valenzuela et al., 2016), but this is the first work to my knowledge that demonstrates this population alone has a therapeutic effect using a classically intracellular pathogen such as *Salmonella* typhimurium. The generation of *S*Tm$^{\Delta aroA\Delta sipB}$ in this work represents the development of a useful tool for investigating the effects of an efficacious, extracellular-restricted bacterial strain in solid tumours.

Utilising several separate patient-derived organoid lines I identified that despite differences in the effect on stem transcripts following *S*Tm$^{\Delta aroA}$ treatment, there was a consistent functional impact on the growth of all treated patient lines. At present it was not possible to identify pre-existing characteristics that conferred either effect. In chapter 4, I demonstrated using single-cell RNA sequencing that there appear to be two distinct transcriptional responses in patient-derived organoids treated with *S*Tm$^{\Delta aroA}$. This difference correlates with the effects (or lack thereof) on stem transcripts by infection with *S*Tm$^{\Delta aroA}$, suggesting that there are multiple mechanisms by which *S*Tm$^{\Delta aroA}$ can impact tumour growth *in vitro*. One

response group (response A) appeared to upregulate genes that have been shown to be markers of response in bladder cancer patients treated with BCG, such as those associated with necrosis. This possibly has promising implications for success in patients of this response group based on the success of BCG vaccine. The other patient group (response B) resembled more closely genes we had previously seen altered in mouse models of colorectal cancer such as downregulation of stem cell transcripts and increased expression of mucosal markers (Mackie et al., 2021). It is possible that the more inflammatory markers upregulated in response group A (i.e., *HMGB1*) may induce a different immune response. Although the caveat for this work is that the number of patients in each group was low, and so future work may aim to screen more patient-derived organoids to identify if they are still consistently splitting into these two identified responses. Increasing the number of patients may aid identifying conserved features and what the functional difference, if any, are after *S*Tm$^{\Delta aroA}$ treatment. This information could then be used to stratify patients in terms of expected response and outcome in potential clinical trials.

One aspect of the therapy that was not investigated in this thesis is the effect on the tumour metabolome when colonised by *S*Tm$^{\Delta aroA\Delta sipB}$. We previously demonstrated that *S*Tm$^{\Delta aroA}$ rapidly and significantly alters the tumour metabolic environment *in vivo;* with decreased levels of sugars, TCA cycle intermediates and so-called oncometabolites such as 2-HG (Mackie et al., 2021). We hypothesised at the time that this competition for essential energy sources for the tumour by the colonising bacteria drove at least part of the metabolic response. It remains to be seen whether there is a difference in metabolite consumption between exclusively extracellular *S*Tm$^{\Delta aroA\Delta sipB}$ compared to *S*Tm$^{\Delta aroA}$, and what effect this had on the reduction of polyp burden. Research into initial colonisation of solid tumours by *Salmonella*

has previously demonstrated that survival within the tumour did not require intracellular invasion, but that further deletion of *eutC* impaired intratumoural survival (Silva-Valenzuela et al., 2016). *eutC* is an enzyme which breaks down ethanolamine, a product of respiration induced by anaerobic conditions in the inflamed gut. This work demonstrates that *S*Tm must be able to utilise available host metabolites to survive long term in the extracellular space. The use of carbon sources such as this which are produced in states of inflammation is a process which has evolved in several pathogens to confer a growth advantage over commensal bacteria, which cannot utilise such products (Thiennimitr et al., 2011). The extracellular space in tumours is a metabolite rich area which likely provides the majority of the energy sources to the bacteria compared to intracellular sources and so we expect *S*Tm$^{\Delta aroA\Delta sipB}$ to exert a similar effect on the metabolic environment of the tumours compared to *S*Tm$^{\Delta aroA}$.

Previous work has shown that BCG vaccine must come into prolonged and direct contact with the tumour epithelium to have a therapeutic response against superficial bladder cancer (Kavoussi et al., 1990; Zlotta et al., 1997). It is understood that while there are some similarities between BCG vaccine-mediated therapy in bladder cancer and *Salmonella*-mediated therapy in other cancers there are still significant gaps in the understanding of the latter, and so it remains to be seen whether direct contact is necessary in this context. While I have shown in chapters 4 and 5 that intracellular invasion is not necessary to exert anti-tumour effects in intestinal cancers, we do not know whether *S*Tm$^{\Delta aroA\Delta sipB}$ can still adhere to the outside of host cells and trigger a response in this way. As previously discussed, one study deleted expression of sipB in wild-type *Salmonella* and demonstrated reduced, but not abolished adherence to HeLa cells *in vitro*, which may suggest that this is impaired in our

double mutant. However, this study also showed reduced, but not abolished, invasion into HeLa cells *in vitro,* showing a less significantly impaired infection model compared with *S*Tm$^{\Delta aroA\Delta sipB}$ in tumour organoids (Chen et al., 2015). It is likely that the difference in results is due to a difference in invasion into a 3D organoid compared with a 2D monolayer culture rather than a stronger effect being conferred by double attenuation, as we demonstrated in chapter 3 abolished invasion into organoids with a single mutant of *sipB*. Therefore, we can hypothesise there may be an impact of *S*Tm$^{\Delta aroA\Delta sipB}$ adherence to the tumour epithelium which enables an effective anti-tumour response, but this should be investigated further. An experiment to dissect this would be to separate organoids from the bacteria through a transwell to assess whether the cells need to come into direct contact with the bacteria. If adherence is not necessary, it may be that the response is driven by secreted factors released by the bacteria, metabolic competition induced by bacteria in the extracellular space of the tumour or likely a combination of these effects.

Using bulk RNA-sequencing in chapter 4 we demonstrated that in PDO line 389 there was an increased number of genes associated with cell cycle enriched specifically in the context of intracellular-permitted *S*Tm$^{\Delta aroA}$, and we can see that this enrichment was representative of downregulated genes. This may be one explanation of why *in vitro S*Tm$^{\Delta aroA\Delta sipB}$ had less of an effect on tumour regrowth compared to *S*Tm$^{\Delta aroA}$. However, the observation in chapter 5 that there is a stronger reduction in polyp burden *in vivo* with *S*Tm$^{\Delta aroA\Delta sipB}$ implies that the bacteria still exert enough of an effect on cell cycle to inhibit tumour growth. An alternative explanation of this finding may be that the *in vitro* impact on tumour organoids measured by the stem forming assay and MTT assays is skewed toward a readout for intracellular invasion as the extracellular bacteria are removed after 2 hours in culture. While we know this is long enough

for *Salmonella* to have a dramatic effect on the tumour transcriptome, as shown by bulk RNA-sequencing, this may not yet translate to a functional impact. It is also possible that the extracellular-restricted bacteria exert a better anti-tumour response *in vivo* via non tumour cell intrinsic effects.

The observation in chapter 5 that the extracellular-restricted *S*Tm$^{\Delta aroA\Delta sipB}$ was superior at polyp clearance in *Apc*$^{Min/+}$ mice compared to *S*Tm$^{\Delta aroA}$ was a surprising one. These data raise the possibility that there is a process activated during intracellular invasion of tumour cells by *S*Tm$^{\Delta aroA}$ that limits the therapeutic benefit. It has been shown previously that during infection of intestinal epithelial cells, particularly during early infection, that intracellular *Salmonella* typhimurium can manipulate host cell signalling to maintain the viability of the host cell and thus maintain their intracellular niche (Steele-Mortimer et al., 2000; Lu et al., 2010). It is possible that bacterial effectors in tumour cells bearing intracellular *S*Tm$^{\Delta aroA}$ promote survival and thus restrict the clearance of some residual tumour cells. It is also worth noting that one of the DEGs uniquely expressed in both the mouse and human tumour organoids following intracellular-permitted *S*Tm$^{\Delta aroA}$ treatment was *Lcn2/LCN2.* In chapter 4 I discussed the role of lipocalin-2 in infection models. However, lipocalin-2 has also been implicated in the development of several types of cancer (Yang and Moses, 2009). Furthermore, recent work has posited a role for Lipocalin-2 specifically in colitis-associated tumourigenesis. Protein expression of LCN2 is upregulated in colonic tissue from AOM-DSS treated mice but not in normal colonic tissue. In three different human colorectal cancer cell lines treatment with IL-6 protein induced increased protein levels of LCN2, and this was inhibited with silencing RNA knockdown of STAT3 or NF-κB, or chemical inhibition of NF-κB. In addition, this group demonstrated upregulation of LCN2 by IL-6 was associated with induction of activation of

survival molecules via NF-κB/STAT3 signalling pathways (Kim et al., 2022). It is well known that IL-6/STAT-3 mediated inflammation has pro-tumorigenic roles (Corvinus et al., 2005; Hodge et al., 2005; Waldner et al., 2012). I showed that in the *Apc*$^{Min/+}$ colon tumour organoids, *Nfkb1* and *Lcn2* were upregulated specifically in intracellular infection, whereas the inhibitor of NF-κB signalling *Nfkbia* was upregulated in the context of extracellular-restricted bacteria. In summary, these data may suggest that intracellular bacteria activate NF-κB signalling which results in LCN2-mediated tumour promotion and that this is circumvented by the extracellular-restricted strain *S*Tm$^{\Delta aroA\Delta sipB}$. This mechanism could be interrogated in *Apc*$^{Min/+}$ mice via specific intracellular delivery of an NF-κB inhibitor by *S*Tm$^{\Delta aroA}$ to assess whether this confers a better polyp clearance. Additionally, it would be of interest to generate an *Lcn2* knockout in the gut epithelium of *Apc*$^{Min/+}$ or CAC mouse models and assess whether this confers an improvement in the therapeutic effect of *S*Tm$^{\Delta aroA}$.

Many chemotherapy drugs are alkylating agents which act to damage DNA and inhibit cell proliferation. We utilised one such drug, mitomycin C, in this work as an *in vitro* inhibitor of proliferation; MMC has historically been used as a treatment for solid tumours with some degree of efficacy as a monotherapy but dose-dependent systemic toxicity (Verweij and Pinedo, 1990; Bradner, 2001). We hypothesise that this may be a possible option for combination therapy with *S*Tm$^{\Delta aroA\Delta sipB}$. We demonstrate that this double mutant bacteria can significantly reduce the polyp burden in *Apc*$^{Min/+}$ mice *in vivo* without invading the tumour cells, and we hypothesise this is in part due to alterations to the metabolome of the polyp via competition imposed by the bacteria. As discussed above, there is some suggestion that the double mutant *Salmonella* has a weaker effect on the cell cycle associated genes possibly due to a lack of invasion into the proliferating cells. It may then aid the *S*Tm$^{\Delta aroA\Delta sipB}$ to target those

remaining cells via a proliferation inhibitor. In turn, *S*Tm$^{\Delta aroA\Delta sipB}$ may act to reduce the dosage needed of the chemotherapeutic agent or the length of time it needs to be administered for, and thus reduce side effects which are often associated with these therapies. One advantage of bacterial cancer therapy for primary tumours is the specific colonisation of the tumour and lack of systemic bacterial spread, however this combined with the lack of an adaptive immune response in *Salmonella*-mediated BCT means that there is a lack of efficacy for metastatic disease. Colorectal cancers are commonly metastatic at the point of diagnosis in patients, and so combination therapy with a "scavenger agent" to target secondary tumours may be a way to increase the population of patients this could treat.

It has been repeatedly observed that C57BL/6 mice have a mutation in *Nramp1* which results in increased susceptibility to *Salmonella*, via increased intracellular burdens (Govoni et al., 1996). It would therefore be of use to repeat the *in vivo* comparisons of *S*Tm$^{\Delta aroA}$ and *S*Tm$^{\Delta aroA\Delta sipB}$ in mice that are not deficient for *Nramp1*, for example Sv129S6 mice which express wild-type versions of the gene (Brown et al., 2013). The logical next step for this work would be to treat these mice with AOM-DSS to generate colitis-associated cancer and test the efficacy of both *S*Tm$^{\Delta aroA}$ and *S*Tm$^{\Delta aroA\Delta sipB}$. If the double mutant strain can colonise and clear the tumours in this model it would be interesting to analyse the immune cell infiltration into the tumours in this wild-type *Nramp*1 context. Nramp1 is a solute transporter which is expressed by macrophages, immature dendritic cells and neutrophils and acts to limit bacterial infection. Interestingly, in 2009 Valdez et al. demonstrated that *Nramp1-/-* mice had reduced numbers of neutrophils and macrophages recruited to the site of infection 1 day after gavage with *Salmonella* typhimurium (Valdez et al., 2009). As described in chapters 4 and 5, the observation of increased CXC family chemokines led us to anticipate significant infiltration

of macrophages and neutrophils into the colonised polyps *in vivo*. Furthermore, *Csf1* and *Csf2* were also upregulated in the bulk RNA-sequencing in mouse tumour derived organoids following *S*Tm$^{\Delta aroA}$ treatment, which also implicates macrophages in the response. Although there was a trend for an increase in these cell populations in treated mice compared to non-treated mice, this was not significant. It is possible that this upregulation of chemokines is restricted to the *in vitro* setting, and so this should be confirmed to occur *in vivo* However, the work in *Nramp* deficient mice suggests that the mice used in our study may limit the immune cell recruitment induced by chemokine expression following treatment with *S*Tm$^{\Delta aroA}$ and *S*Tm$^{\Delta aroA\Delta sipB}$. The implications of this are that we may not be seeing a representative picture of BCT-mediated immune responses in *Apc*$^{Min/+}$ mice, and this may vary in other mouse models and therefore patients.

To conclude, the data presented throughout this thesis demonstrate a novel mechanism by which the widely researched BCT strain *S*Tm$^{\Delta aroA}$ target the dividing cells within tumours intracellularly. It was then demonstrated that this despite this smoking gun of proliferating cells being actively infected, intracellular invasion is not necessary to exert dramatic effects on the tumour transcriptional landscape and most importantly tumour burden. Together, the work within this thesis presents a mechanism whereby a classically intracellular pathogen can exert effects on the gut epithelium from exclusively the extracellular space. These extracellular bacteria then exert a therapeutic response, by currently unknown mechanisms of detection by epithelial tumour cells and possible metabolic competition. These data highlight the importance of understanding where in the tumour BCT agents establish colonies and has implications for the design of therapies using engineered bacteria.

BIBLIOGRAPHY

Amarante-Mendes, G.P., Adjemian, S., Branco, L.M., et al. (2018) Pattern recognition receptors and the host cell death molecular machinery. *Frontiers in Immunology*, 9. doi:10.3389/fimmu.2018.02379.

Antonelli, A.C., Binyamin, A., Hohl, T.M., et al. (2020) Bacterial immunotherapy for cancer induces CD4-dependent tumor-specific immunity through tumor-intrinsic interferon-γ signaling. *PNAS*, 117 (31): 18627–18637. doi:10.1073/pnas.2004421117/-/DCSupplemental.

Avogadri, F., Martinoli, C., Petrovska, L., et al. (2005) Cancer Immunotherapy Based on Killing of Salmonella-Infected Tumor Cells. *Cancer Research*, 65 (9): 3920–3927. Available at: http://cancerres.aacrjournals.org/.

Baban, C.K., Cronin, M., O'Hanlon, D., et al. (2010) Bacteria as vectors for gene therapy of cancer. *Bioengineered Bugs*. 1 (6). doi:10.4161/bbug.1.6.13146.

Baker, A.M., Cross, W., Curtius, K., et al. (2019) Evolutionary history of human colitis-associated colorectal cancer. *Gut*, 68 (6): 985–995. doi:10.1136/gutjnl-2018-316191.

Barker, N., Van Es, J.H., Kuipers, J., et al. (2007) Identification of stem cells in small intestine and colon by marker gene Lgr5. *Nature*, 449 (7165): 1003–1007. doi:10.1038/nature06196.

Barker, N., Ridgway, R.A., Van Es, J.H., et al. (2009) Crypt stem cells as the cells-of-origin of intestinal cancer. *Nature*, 457 (7229): 608–611. doi:10.1038/nature07602.

Barron, M. and Li, J. (2016) Identifying and removing the cell-cycle effect from single-cell RNA-Sequencing data. *Scientific Reports*, 6 (September): 1–10. doi:10.1038/srep33892.

Bartfeld, S. and Clevers, H. (2015) Organoids as model for infectious diseases: Culture of human and murine stomach organoids and microinjection of helicobacter pylori. *Journal of Visualized Experiments*, 2015 (105). doi:10.3791/53359.

Bergman, I., Basse, P.H., Barmada, M.A., et al. (2000) Comparison of in vitro antibody-targeted cytotoxicity using mouse, rat and human effectors. *Cancer Immunology Immunotherapy*, 49 (4–5): 259–266. doi:10.1007/s002620000120.

Bertani, B. and Ruiz, N. (2018) Function and Biogenesis of Lipopolysaccharides. *EcoSal Plus*, 8 (1). doi:10.1128/ecosalplus.esp-0001-2018.

Bradner, W.T. (2001) Mitomycin C: A clinical update. *Cancer Treatment Reviews*, 27 (1): 35–50. doi:10.1053/ctrv.2000.0202.

Brady, G., Barbara, M. and Iscove, N.N. (1990) Representative in Vitro cDNA Amplification From Individual Hemopoietic Cells and Colonies. *METHODS IN MOLECULAR AND CELLULAR BIOLOGY*, 2: 17–25.

Broadway, K.M., Denson, E.A.P., Jensen, R. V., et al. (2015) Rescuing chemotaxis of the anticancer agent Salmonella enterica serovar Typhimurium VNP20009. *Journal of Biotechnology*, 211: 117–120. doi:10.1016/j.jbiotec.2015.07.010.

Broemer, M., Krappmann, D. and Scheidereit, C. (2004) Requirement of Hsp90 activity for IκB kinase (IKK) biosynthesis and for constitutive and inducible IKK and NF-κB activation. *Oncogene*, 23 (31): 5378–5386. doi:10.1038/sj.onc.1207705.

Brosens, L.A.A., Offerhaus, G.J.A. and Giardiello, F.M. (2015) Hereditary Colorectal Cancer: Genetics and Screening. *Surgical Clinics of North America*. 95 (5) pp. 1067–1080. doi:10.1016/j.suc.2015.05.004.

Brown, D.E., Libby, S.J., Moreland, S.M., et al. (2013) Salmonella enterica Causes More Severe Inflammatory Disease in C57/BL6 Nramp1G169 Mice Than Sv129S6 Mice. *Veterinary Pathology*, 50 (5): 867–876. doi:10.1177/0300985813478213.

Broz, P., Ohlson, M.B. and Monack, D.M. (2012) Innate immune response to Salmonella typhimurium, a model enteric pathogen. *Gut Microbes*, 3 (2): 62–70. doi:10.4161/gmic.19141.

Bürtin, F., Mullins, C.S. and Linnebacher, M. (2020) Mouse models of colorectal cancer: Past, present and future perspectives. *World Journal of Gastroenterology*, 26 (13): 1394–1426. doi:10.3748/WJG.V26.I13.1394.

Castellarin, M., Warren, R.L., Freeman, J.D., et al. (2012) Fusobacterium nucleatum infection is prevalent in human colorectal carcinoma. *Genome Research*, 22 (2): 299–306. doi:10.1101/gr.126516.111.

Chalabi, M., Fanchi, L.F., Dijkstra, K.K., et al. (2020) Neoadjuvant immunotherapy leads to pathological responses in MMR-proficient and MMR-deficient early-stage colon cancers. *Nature Medicine*, 26 (4): 566–576. doi:10.1038/s41591-020-0805-8.

Chaudhuri, D., Chowdhury, A.R., Biswas, B., et al. (2018) Salmonella Typhimurium infection leads to colonization of the mouse brain and is not completely cured with antibiotics. *Frontiers in Microbiology*, 9 (JUL): 1–12. doi:10.3389/fmicb.2018.01632.

Chen, R., Kang, R. and Tang, D. (2022) The mechanism of HMGB1 secretion and release. *Experimental and Molecular Medicine*. 54 (2) pp. 91–102. doi:10.1038/s12276-022-00736-w.

Chen, S., Zhang, C., Liao, C., et al. (2015) Deletion of Invasion Protein B in Salmonella enterica Serovar Typhimurium Influences Bacterial Invasion and Virulence. *Current Microbiology*, 71 (6): 687–692. doi:10.1007/s00284-015-0903-x.

Chen, W., Liu, F., Ling, Z., et al. (2012) Human intestinal lumen and mucosa-associated microbiota in patients with colorectal cancer. *PLoS ONE*, 7 (6). doi:10.1371/journal.pone.0039743.

Christgen, S., Zheng, M., Kesavardhana, S., et al. (2020) Identification of the PANoptosome: A Molecular Platform Triggering Pyroptosis, Apoptosis, and Necroptosis (PANoptosis). *Frontiers in Cellular and Infection Microbiology*, 10. doi:10.3389/fcimb.2020.00237.

Clairmont, C., Lee, K.C., Pike, J., et al. (2000) Biodistribution and genetic stability of the novel antitumor agent VNP20009, a genetically modified strain of Salmonella typhimurium. *Journal of Infectious Diseases*, 181 (6): 1996–2002. doi:10.1086/315497.

Co, J.Y., Margalef-Català, M., Li, X., et al. (2019) Controlling Epithelial Polarity: A Human Enteroid Model for Host-Pathogen Interactions. *Cell Reports*, 26 (9): 2509-2520.e4. doi:10.1016/j.celrep.2019.01.108.

Co, J.Y., Margalef-Català, M., Monack, D.M., et al. (2021) Controlling the polarity of human gastrointestinal organoids to investigate epithelial biology and infectious diseases. *Nature Protocols*. 16 (11) pp. 5171–5192. doi:10.1038/s41596-021-00607-0.

Conlan, J.W. (1996) Neutrophils Prevent Extracellular Colonization of the Liver Microvasculature by Salmonella typhimurium. *INFECTION AND IMMUNITY*, 64 (3): 1043–1047.

Copland, A., Mackie, G.M., Scarfe, L., et al. (2023) Salmonella cancer therapy metabolically disrupts tumours at the collateral cost of T cell immunity. *BioRxiv*. doi:10.1101/2023.01.12.523780.

Corvinus, F.M., Orth, C., Moriggl, R., et al. (2005) Persistent STAT3 activation in colon cancer is associated with enhanced cell proliferation and tumor growth. *Neoplasia*, 7 (6): 545–555. doi:10.1593/neo.04571.

Crull, K., Rohde, M., Westphal, K., et al. (2011) Biofilm formation by salmonella enterica serovar typhimurium colonizing solid tumours. *Cellular Microbiology*, 13 (8): 1223–1233. doi:10.1111/j.1462-5822.2011.01612.x.

Dai, W., Zhou, F., Tang, D., et al. (2019) Single-cell transcriptional profiling reveals the heterogenicity in colorectal cancer. *Medicine (United States)*, 98 (34): 0–7. doi:10.1097/MD.0000000000016916.

Daniel Saltzman, B.A., Katsanis, E., Heise, C.P., et al. (1996) Antitumor Mechanisms of Attenuated Salmonella typhimurium Containing the Gene for Human Interleukin-2: A Novel Antitumor Agent? *Cancer Biotherapy and Radiopharmaceuticals*, 11: 145–153.

Datsenko, K.A. and Wanner, B.L. (2000) One-step inactivation of chromosomal genes in Escherichia coli K-12 using PCR products. *PNAS*, (12): 6640–6645. Available at: www.pnas.orgcgidoi10.1073pnas.120163297.

Davis, H., Irshad, S., Bansal, M., et al. (2015) Aberrant epithelial GREM1 expression initiates colonic tumorigenesis from cells outside the stem cell niche. *Nature Medicine*, 21 (1): 62–70. doi:10.1038/nm.3750.

Deguine, J. and Barton, G.M. (2014) MyD88: A central player in innate immune signaling. *F1000Prime Reports*, 6. doi:10.12703/P6-97.

Deng, K., Lin, S., Zhou, L., et al. (2012) High Levels of Aromatic Amino Acids in Gastric Juice during the Early Stages of Gastric Cancer Progression. *PLoS ONE*, 7 (11). doi:10.1371/journal.pone.0049434.

Dunlap, N.E., Benjamin, W.H., Mccall, R.D., et al. (1991) A “safe-site” for Salmonella typhimurium is within splenic cells during the early phase of infection in mice. *Microbial Pathogenesis*, 10: 297–310.

Eaden, J.A., Abrams, K.R. and Mayberry, J.F. (2001) The risk of colorectal cancer in ulcerative colitis: a meta-analysis. *Gut*, 48: 526–535. Available at: www.gutjnl.com.

Eberwine, J., Yeh, H., Miyashiro, K., et al. (1992) Analysis of gene expression in single live neurons. *PNAS*, 89: 3010–3014.

Eller, K., Schroll, A., Banas, M., et al. (2013) Lipocalin-2 Expressed in Innate Immune Cells Is an Endogenous Inhibitor of Inflammation in Murine Nephrotoxic Serum Nephritis. *PLoS ONE*, 8 (7). doi:10.1371/journal.pone.0067693.

Fàbrega, A. and Vila, J. (2013) Salmonella enterica serovar Typhimurium skills to succeed in the host: Virulence and regulation. *Clinical Microbiology Reviews*, 26 (2): 308–341. doi:10.1128/CMR.00066-12.

Fattinger, S.A., Geiser, P., Samperio Ventayol, P., et al. (2021a) Epithelium-autonomous NAIP/NLRC4 prevents TNF-driven inflammatory destruction of the gut epithelial barrier in Salmonella-infected mice. *Mucosal Immunology*, 14 (3): 615–629. doi:10.1038/s41385-021-00381-y.

Fattinger, S.A., Sellin, M.E. and Hardt, W.D. (2021b) Epithelial inflammasomes in the defense against Salmonella gut infection. *Current Opinion in Microbiology*. 59 pp. 86–94. doi:10.1016/j.mib.2020.09.014.

Felgner, S., Frahm, M., Kocijancic, D., et al. (2016) Aroa-deficient Salmonella enterica serovar Typhimurium is more than a metabolically attenuated mutant. *mBio*, 7 (5): 1–12. doi:10.1128/mBio.01220-16.

Fishel, R., Kay Lescoe, M., Ft Rao, M.S., et al. (1993) The Human Mutator Gene Homolog MSHP and Its Association with Hereditary Nonpolyposis Colon Cancer. *Cell*, 75: 1027–1038.

Fleming, M., Ravula, S., Tatishchev, S.F., et al. (2012) Colorectal carcinoma: Pathologic aspects. *Journal of Gastrointestinal Oncology*, 3 (3): 153–173. doi:10.3978/j.issn.2078-6891.2012.030.

Forbes, N.S. (2010) Engineering the perfect (bacterial) cancer therapy. *Nature Reviews Cancer*. 10 (11) pp. 785–794. doi:10.1038/nrc2934.

Franzén, O., Gan, L.M. and Björkegren, J.L.M. (2019) PanglaoDB: A web server for exploration of mouse and human single-cell RNA sequencing data. *Database*, 2019 (1): 1–9. doi:10.1093/database/baz046.

Fredrick S. Leach, Nicholas C. Nicolaides, Nickolas Papadopoulos, et al. (1993) Mutations of mutS Homolog in Hereditary Nonpolyposis Colorectal Cancer. *Cell*, 75: 1215–1225.

Fridlender, Z.G., Sun, J., Kim, S., et al. (2009) Polarization of Tumor-Associated Neutrophil Phenotype by TGF-β: “N1” versus “N2” TAN. *Cancer Cell*, 16 (3): 183–194. doi:10.1016/j.ccr.2009.06.017.

Fuge, O., Vasdev, N., Allchorne, P., et al. (2015) Immunotherapy for bladder cancer. *Research and Reports in Urology*, 7: 65–79. doi:10.2147/RRU.S63447.

Fushimi, T., Kojima, A., Moore, M.A.S., et al. (2000) Macrophage inflammatory protein 3α transgene attracts dendritic cells to established murine tumors and suppresses tumor growth. *Journal of Clinical Investigation*, 105 (10): 1383–1393.

Galán, J.E. (2021) Salmonella Typhimurium and inflammation: a pathogen-centric affair. *Nature Reviews Microbiology*. 19 (11) pp. 716–725. doi:10.1038/s41579-021-00561-4.

Galan, J.E. and Curtiss III, R. (1989) Cloning and molecular characterization of genes whose products allow Salmonella typhimurium to penetrate tissue culture cells. *Proc. Nati. Acad. Sci. USA*, 86: 6383–6387. Available at: https://www.pnas.org.

Gal-Mor, O., Boyle, E.C. and Grassl, G.A. (2014) Same species, different diseases: How and why typhoidal and non-typhoidal Salmonella enterica serovars differ. *Frontiers in Microbiology*, 5 (AUG). doi:10.3389/fmicb.2014.00391.

Galon, J., Costes, A., Sanchez-Cabo, F., et al. (2006) Type, Density, and Location of Immune Cells Within Human Colorectal Tumours Predict Clinical Outcome. *Science*, 313 (5795): 1960–1964. doi:10.1029/2004GL021533.

Garner, M.J., Hayward, R.D. and Koronakis, V. (2002) The Salmonella pathogenicity island 1 secretion system directs cellular cholesterol redistribution during mammalian cell entry and intracellular trafficking. *Cellular Microbiology*, 4 (3): 153–165. doi:10.1046/j.1462-5822.2002.00181.x.

Ghosh, P. (2004) Process of Protein Transport by the Type III Secretion System. *Microbiology and Molecular Biology Reviews*, 68 (4): 771–795. doi:10.1128/mmbr.68.4.771-795.2004.

Gillis, C.C., Hughes, E.R., Spiga, L., et al. (2018) Dysbiosis-Associated Change in Host Metabolism Generates Lactate to Support Salmonella Growth. *Cell Host and Microbe*, 23 (1): 54-64.e6. doi:10.1016/j.chom.2017.11.006.

Gniadek, T.J., Augustin, L., Schottel, J., et al. (2020) A Phase I, Dose Escalation, Single Dose Trial of Oral Attenuated Salmonella typhimurium Containing Human IL-2 in Patients With Metastatic Gastrointestinal Cancers. *Journal of Immunotherapy*, 43 (7): 217–221. Available at: www.immunotherapy-journal.com.

Govoni, G., Vidal, S., Gauthier, S., et al. (1996) The Bcg/Ity/Lsh Locus: Genetic Transfer of Resistance to Infections in C57BL/6J Mice Transgenic for the Nramp1 Gly169 Allele. *INFECTION AND IMMUNITY*, 64 (8): 2923–2929.

Grivennikov, S., Karin, E., Terzic, J., et al. (2009) IL-6 and Stat3 Are Required for Survival of Intestinal Epithelial Cells and Development of Colitis-Associated Cancer. *Cancer Cell*, 15 (2): 103–113. doi:10.1016/j.ccr.2009.01.001.

Guesdon, W., Auray, G., Pezier, T., et al. (2015) CCL20 displays antimicrobial activity against cryptosporidium parvum, but its expression is reduced during infection in the intestine of neonatal mice. *Journal of Infectious Diseases*, 212 (8): 1332–1340. doi:10.1093/infdis/jiv206.

Guinney, J., Dienstmann, R., Wang, X., et al. (2015) The Consensus Molecular Subtypes of Colorectal Cancer. *Nature Medicine*, 21 (11): 1350–1356. doi:10.7303/syn2623706.

Gurtner, A., Gonzalez-Perez, I. and Arnold, I.C. (2021) Intestinal eosinophils, homeostasis and response to bacterial intrusion. *Seminars in Immunopathology*, 43: 295–306. doi:10.1007/s00281-021-00856-x/Published.

Han, J., Gu, X., Li, Y., et al. (2020) Mechanisms of BCG in the treatment of bladder cancer-current understanding and the prospect. *Biomedicine and Pharmacotherapy*, 129 (June): 110393. doi:10.1016/j.biopha.2020.110393.

Han, S.H., Shim, S., Kim, M.J., et al. (2017) Long-term culture-induced phenotypic difference and efficient cryopreservation of small intestinal organoids by treatment timing of Rho kinase inhibitor. *World Journal of Gastroenterology*, 23 (6): 964–975. doi:10.3748/wjg.v23.i6.964.

Hankey, W., Frankel, W.L. and Groden, J. (2018) Functions of the APC tumor suppressor protein dependent and independent of canonical WNT signaling: implications for therapeutic targeting. *Cancer and Metastasis Reviews*, 37 (1): 159–172. doi:10.1007/s10555-017-9725-6.

Hao, Y., Hao, S., Andersen-nissen, E., et al. (2020) Integrated analysis of multimodal single-cell data. *bioRxiv preprint*. doi:: https://doi.org/10.1101/2020.10.12.335331.

Haraga, A., Ohlson, M.B. and Miller, S.I. (2008) Salmonellae interplay with host cells. *Nature Reviews Microbiology*. 6 (1) pp. 53–66. doi:10.1038/nrmicro1788.

Hayward, R.D., Cain, R.J., McGhie, E.J., et al. (2005) Cholesterol binding by the bacterial type III translocon is essential for virulence effector delivery into mammalian cells. *Molecular Microbiology*, 56 (3): 590–603. doi:10.1111/j.1365-2958.2005.04568.x.

Heimann, D.M. and Rosenberg, S.A. (2003) Continuous Intravenous Administration of Live Genetically Modified Salmonella Typhimurium in Patients With Metastatic Melanoma. *Journal of Clinical Oncology*, 26 (2): 179–180.

Hodge, D.R., Hurt, E.M. and Farrar, W.L. (2005) The role of IL-6 and STAT3 in inflammation and cancer. *European Journal of Cancer*, 41 (16): 2502–2512. doi:10.1016/j.ejca.2005.08.016.

Hoiseth, S.K. and Stocker, B.A.D. (1981) Aromatic-dependent Salmonella typhimurium are non-virulent and effective as live vaccines. *Nature*, 291: 238–239.

Hoover, D.M., Boulègue, C., De Yang, et al. (2002) The structure of human macrophage inflammatory protein-3α/CCL20. Linking antimicrobial and CC chemokine receptor-6-binding activities with human β-defensins. *Journal of Biological Chemistry*, 277 (40): 37647–37654. doi:10.1074/jbc.M203907200.

Hoption Cann, S.A., van Netten, J.P. and van Netten, C. (2003) Dr William Coley and tumour regression: a place in history or in the future. *Postgraduate Medical Journal*, 79: 672–680.

Hu, Z., Ding, J., Ma, Z., et al. (2019) Quantitative evidence for early metastatic seeding in colorectal cancer. *Nature Genetics*, 51 (7): 1113–1122. doi:10.1038/s41588-019-0423-x.

Huyghe, N., Baldin, P. and Van den Eynde, M. (2019) Immunotherapy with immune checkpoint inhibitors in colorectal cancer: what is the future beyond deficient mismatch-repair tumours? *Gastroenterology Report*, 8 (October 2019): 11–24. doi:10.1093/gastro/goz061.

Hwang, B., Lee, J.H. and Bang, D. (2018) Single-cell RNA sequencing technologies and bioinformatics pipelines. *Experimental and Molecular Medicine*. 50 (8). doi:10.1038/s12276-018-0071-8.

Jasperson, K.W., Tuohy, T.M., Neklason, D.W., et al. (2010) Hereditary and Familial Colon Cancer. *Gastroenterology*, 138 (6): 2044–2058. doi:10.1053/j.gastro.2010.01.054.

Johnson, S.A., Ormsby, M.J., Wessel, H.M., et al. (2021) Monocytes mediate Salmonella Typhimurium-induced tumor growth inhibition in a mouse melanoma model. *European Journal of Immunology*, 51 (12): 3228–3238. doi:10.1002/eji.202048913.

Jones, B.D., Ghori, N. and Falkow, S. (1994) Salmonella typhlrnurium Initiates Murine Infection by Penetrating and Destroying the Specialized Epithelial M Cells of the Peyer's Patches. *The Journal of Experimental Medicine*, pp. 15–23.

Kaimala, S., Mohamed, Y.A., Nader, N., et al. (2014) Salmonella-mediated tumor regression involves targeting of tumor myeloid suppressor cells causing a shift to M1-like phenotype and reduction in suppressive capacity. *Cancer Immunology, Immunotherapy*, 63 (6): 587–599. doi:10.1007/s00262-014-1543-x.

Kasinskas, R.W. and Forbes, N.S. (2006) Salmonella typhimurium specifically chemotax and proliferate in heterogeneous tumor tissue in vitro. *Biotechnology and Bioengineering*, 94 (4): 710–721. doi:10.1002/bit.20883.

Kasper, C.A., Sorg, I., Schmutz, C., et al. (2010) Cell-cell propagation of NF-κB transcription factor and MAP kinase activation amplifies innate immunity against bacterial infection. *Immunity*, 33 (5): 804–816. doi:10.1016/j.immuni.2010.10.015.

Katsiampoura, A., Raghav, K., Jiang, Z., et al. (2018) Modeling of patient derived xenografts in colorectal cancer. *Molecular Cancer Therapeutics*, 16 (7): 1435–1442. doi:10.1158/1535-7163.MCT-16-0721.Modeling.

Kavoussi, L.R., Brown, E.J., Ritchey, J.K., et al. (1990) Fibronectin-mediated Calmette-Guerin bacillus attachment to murine bladder mucosa. Requirement for the expression of an antitumor response. *Journal of Clinical Investigation*, 85 (1): 62–67. doi:10.1172/JCI114434.

Kim, J. and Lee, H.K. (2022) Potential Role of the Gut Microbiome In Colorectal Cancer Progression. *Frontiers in Immunology*, 12. doi:10.3389/fimmu.2021.807648.

Kim, K., Jeong, J.H., Lim, D., et al. (2015) L-Asparaginase delivered by Salmonella typhimurium suppresses solid tumors. *Molecular Therapy - Oncolytics*, 2 (March): 15007. doi:10.1038/mto.2015.7.

Kim, S.L., Shin, M.W., Seo, S.Y., et al. (2022) Lipocalin 2 potentially contributes to tumorigenesis from colitis via IL-6/STAT3/NF-κB signaling pathway. *Bioscience Reports*, 42 (5). doi:10.1042/BSR20212418.

Kitsou, M., Ayiomamitis, G.D. and Zaravinos, A. (2020) High expression of immune checkpoints is associated with the TIL load, mutation rate and patient survival in colorectal cancer. *International Journal of Oncology*, 57 (1): 237–248. doi:10.3892/ijo.2020.5062.

Knodler, L.A., Crowley, S.M., Sham, H.P., et al. (2014) Noncanonical inflammasome activation of caspase-4/caspase-11 mediates epithelial defenses against enteric bacterial pathogens. *Cell Host and Microbe*, 16 (2): 249–256. doi:10.1016/j.chom.2014.07.002.

Kolb-Mäurer, A., Wilhelm, M., Weissinger, F., et al. (2002) Interaction of human hematopoietic stem cells with bacterial pathogens. *Blood*, 100 (10): 3703–3709. doi:10.1182/blood-2002-03-0898.

Kolligs, F.T. (2016) Diagnostics and epidemiology of colorectal cancer. *Visceral Medicine*, 32 (3): 158–164. doi:10.1159/000446488.

Kong, Q., Six, D.A., Liu, Q., et al. (2012) Phosphate groups of lipid a are essential for Salmonella enterica serovar typhimurium virulence and affect innate and adaptive immunity. *Infection and Immunity*, 80 (9): 3215–3224. doi:10.1128/IAI.00123-12.

Kowalczyk, M.S., Tirosh, I., Heckl, D., et al. (2015) Single-cell RNA-seq reveals changes in cell cycle and differentiation programs upon aging of hematopoietic stem cells. *Genome Research*, 25 (12): 1860–1872. doi:10.1101/gr.192237.115.

Kraiczy, J., Nayak, K.M., Howell, K.J., et al. (2019) DNA methylation defines regional identity of human intestinal epithelial organoids and undergoes dynamic changes during development. *Gut*, 68 (1): 49–61. doi:10.1136/gutjnl-2017-314817.

Kröger, C., Dillon, S.C., Cameron, A.D.S., et al. (2012) The transcriptional landscape and small RNAs of Salmonella enterica serovar Typhimurium. *Proceedings of the National Academy of Sciences of the United States of America*, 109 (20). doi:10.1073/pnas.1201061109.

Kumar, A., Gautam, V., Sandhu, A., et al. (2023) Current and emerging therapeutic approaches for colorectal cancer: A comprehensive review. *World Journal of Gastrointestinal Surgery*, 15 (4): 495–519. doi:10.4240/wjgs.v15.i4.495.

de Lau, W., Kujala, P., Schneeberger, K., et al. (2012) Peyer's Patch M Cells Derived from Lgr5 + Stem Cells Require SpiB and Are Induced by RankL in Cultured "Miniguts" . *Molecular and Cellular Biology*, 32 (18): 3639–3647. doi:10.1128/mcb.00434-12.

Lechuga, S. and Ivanov, A.I. (2017) Disruption of the epithelial barrier during intestinal inflammation: Quest for new molecules and mechanisms. *Biochimica et Biophysica Acta - Molecular Cell Research*. 1864 (7) pp. 1183–1194. doi:10.1016/j.bbamcr.2017.03.007.

Lewin, K. (1969) The Paneth cell in disease. *Gut*, 10: 804–811.

Li, Q.H., Wang, Y.Z., Tu, J., et al. (2020) Anti-EGFR therapy in metastatic colorectal cancer: Mechanisms and potential regimens of drug resistance. *Gastroenterology Report*. 8 (3) pp. 179–191. doi:10.1093/gastro/goaa026.

Li, X. and Wang, C.Y. (2021) From bulk, single-cell to spatial RNA sequencing. *International Journal of Oral Science*. 13 (1). doi:10.1038/s41368-021-00146-0.

Liang, S., Wang, C., Shao, Y., et al. (2022) Recent advances in bacteria-mediated cancer therapy. *Frontiers in Bioengineering and Biotechnology*. 10. doi:10.3389/fbioe.2022.1026248.

Lièvre, A., Bachet, J.B., Le Corre, D., et al. (2006) KRAS mutation status is predictive of response to cetuximab therapy in colorectal cancer. *Cancer Research*, 66 (8): 3992–3995. doi:10.1158/0008-5472.CAN-06-0191.

Liu, Q., Liu, Q., Zhao, X., et al. (2016a) Immunogenicity and cross-protective efficacy induced by outer membrane proteins from salmonella typhimurium mutants with truncated LPS in mice. *International Journal of Molecular Sciences*, 17 (3). doi:10.3390/ijms17030416.

Liu, Q., Ran, D., Wang, L., et al. (2023) Association between Ki67 expression and therapeutic outcome in colon cancer. *Oncology Letters*, 25 (6). doi:10.3892/ol.2023.13858.

Liu, X., Jiang, S., Piao, L., et al. (2016b) Radiotherapy combined with an engineered Salmonella typhimurium inhibits tumor growth in a mouse model of colon cancer. *Experimental Animals*, 65 (4): 413–418.

Liu, Y., Xu, B., Liu, M., et al. (2021) Long non-coding RNA SNHG25 promotes epithelial ovarian cancer progression by up-regulating COMP. *Journal of Cancer*, 12 (6): 1660–1668. doi:10.7150/jca.47344.

Liu, Y.W., Denkmann, K., Kosciow, K., et al. (2013) Tetrathionate stimulated growth of Campylobacter jejuni identifies a new type of bi-functional tetrathionate reductase (TsdA) that is widely distributed in bacteria. *Molecular Microbiology*, 88 (1): 173–188. doi:10.1111/mmi.12176.

Liu, Z., Gu, Y., Shin, A., et al. (2020) Analysis of Myeloid Cells in Mouse Tissues with Flow Cytometry. *STAR Protocols*, 1 (1). doi:10.1016/j.xpro.2020.100029.

Lkhagva, E., Chung, H.J., Hong, J., et al. (2021) The regional diversity of gut microbiome along the GI tract of male C57BL/6 mice. *BMC Microbiology*, 21 (1). doi:10.1186/s12866-021-02099-0.

López-Arribillaga, E., Yan, B., Lobo-Jarne, T., et al. (2021) Accumulation of paneth cells in early colorectal adenomas is associated with beta-catenin signaling and poor patient prognosis. *Cells*, 10 (11). doi:10.3390/cells10112928.

Lotze, M.T. and Tracey, K.J. (2005) High-mobility group box 1 protein (HMGB1): Nuclear weapon in the immune arsenal. *Nature Reviews Immunology*. 5 (4) pp. 331–342. doi:10.1038/nri1594.

Lou, L., Zhang, P., Piao, R., et al. (2019) Salmonella Pathogenicity Island 1 (SPI-1) and Its Complex Regulatory Network. *Frontiers in Cellular and Infection Microbiology*. 9. doi:10.3389/fcimb.2019.00270.

Love, M.I., Huber, W. and Anders, S. (2014) Moderated estimation of fold change and dispersion for RNA-seq data with DESeq2. *Genome Biology*, 15 (12). doi:10.1186/s13059-014-0550-8.

Lu, R., Wu, S., Liu, X., et al. (2010) Chronic effects of a salmonella type III secretion effector protein AvrA in vivo. *PLoS ONE*, 5 (5). doi:10.1371/journal.pone.0010505.

Ludwig, A.T., Moore, J.M., Luo, Y., et al. (2004) Tumor Necrosis Factor-Related Apoptosis-Inducing Ligand: A Novel Mechanism for Bacillus Calmette-Guérin-Induced Antitumor Activity. *CANCER RESEARCH*, 64: 3386–3390. Available at: http://aacrjournals.org/cancerres/article-pdf/64/10/3386/2514392/zch01004003386.pdf.

Luo, X., Ittensohn, M., Low, B., et al. (1999) Genetically modified Salmonella typhimurium inhibited growth of primary tumors and metastase. *Proc Annu Meet Am Assoc Cancer Res*, 40: 3146.

Luo, X., Li, Z., Lin, S., et al. (2001) Antitumor Effect of VNP20009, an Attenuated Salmonella, in Murine Tumor Models. *Oncology Research*, 12: 501–508. Available at: www.cognizlmtrommunication.com.

Mackie, G.M., Copland, A., Takahashi, M., et al. (2021) Bacterial cancer therapy in autochthonous colorectal cancer affects tumor growth and metabolic landscape. *JCI Insight*, 6 (23). doi:10.1172/jci.insight.139900.

Magré, L., Verstegen, M.M.A., Buschow, S., et al. (2023) Emerging organoid-immune co-culture models for cancer research: From oncoimmunology to personalized immunotherapies. *Journal for ImmunoTherapy of Cancer*, 11 (5): 1–10. doi:10.1136/jitc-2022-006290.

Martin, M.L., Zeng, Z., Adileh, M., et al. (2018) Logarithmic expansion of LGR5+ cells in human colorectal cancer. *Cellular Signalling*, 42: 97–105. doi:10.1016/j.cellsig.2017.09.018.

Maxfield, F.R. and Wüstner, D. (2012) “Analysis of Cholesterol Trafficking with Fluorescent Probes.” In *Methods in Cell Biology*. Academic Press Inc. pp. 367–393. doi:10.1016/B978-0-12-386487-1.00017-1.

McCarthy, E.F. (2006) The toxins of William B. Coley and the treatment of bone and soft-tissue sarcomas. *The Iowa orthopaedic journal*, 26: 154–158.

Ménard, S., Lacroix-Lamandé, S., Ehrhardt, K., et al. (2022) Cross-Talk Between the Intestinal Epithelium and Salmonella Typhimurium. *Frontiers in Microbiology*. 13. doi:10.3389/fmicb.2022.906238.

Mikuda, N., Schmidt-Ullrich, R., Kärgel, E., et al. (2020) Deficiency in IκBα in the intestinal epithelium leads to spontaneous inflammation and mediates apoptosis in the gut. *Journal of Pathology*, 251 (2): 160–174. doi:10.1002/path.5437.

Miller, R.G. (1984) THE USE AND ABUSE OF FILIPIN TO LOCALIZE CHOLESTEROL IN MEMBRANES. *Cell Biology International Reports*, 8 (7): 519.

Mlecnik, B., Bindea, G., Angell, H.K., et al. (2016) Integrative Analyses of Colorectal Cancer Show Immunoscore Is a Stronger Predictor of Patient Survival Than Microsatellite Instability. *Immunity*, 44 (3): 698–711. doi:10.1016/j.immuni.2016.02.025.

Moser, A.R., Pitot, H.C. and Dove, W.F. (1990) A dominant mutation that predisposes to multiple intestinal neoplasia in the mouse. *Science*, 247 (4940): 322–324. doi:10.1126/science.2296722.

Myeni, S.K. and Zhou, D. (2010) The C terminus of SipC binds and bundles F-actin to promote Salmonella invasion. *Journal of Biological Chemistry*, 285 (18): 13357–13363. doi:10.1074/jbc.M109.094045.

Nandi, B., Shapiro, M., Samur, M.K., et al. (2016) Stromal CCR6 drives tumor growth in a murine transplantable colon cancer through recruitment of tumor-promoting macrophages. *OncoImmunology*, 5 (8). doi:10.1080/2162402X.2016.1189052.

Nemunaitis, J., Cunningham, C., Senzer, N., et al. (2003) Pilot trial of genetically modified, attenuated Salmonella expressing the E. coli cytosine deaminase gene in refractory cancer patients. *Cancer Gene Therapy*, 10 (10): 737–744. doi:10.1038/sj.cgt.7700634.

Nguyen, V.H., Kim, H.S., Ha, J.M., et al. (2010) Genetically engineered Salmonella typhimurium as an imageable therapeutic probe for cancer. *Cancer Research*, 70 (1): 18–23. doi:10.1158/0008-5472.CAN-09-3453.

Nicoletti, C. (2000) Unsolved mysteries of intestinal M cells. *Gut*. 47 (5) pp. 735–739. doi:10.1136/gut.47.5.735.

Nighot, M., Rawat, M., Al-Sadi, R., et al. (2019) Lipopolysaccharide-Induced Increase in Intestinal Permeability Is Mediated by TAK-1 Activation of IKK and MLCK/MYLK Gene. *American Journal of Pathology*, 189 (4): 797–812. doi:10.1016/j.ajpath.2018.12.016.

Nishihara, R., Wu, K., Lochhead, P., et al. (2013) Long-Term Colorectal-Cancer Incidence and Mortality after Lower Endoscopy. *New England Journal of Medicine*, 369 (12): 1095–1105. doi:10.1056/nejmoa1301969.

Olson, T.S. and Ley, K. (2002) Chemokines and chemokine receptors in leukocyte trafficking. *Am J Physiol Regul Integr Comp Physiol .*, 283 (1). doi:10.1152/ajpregu.00738.2001.-Che.

Overman, M.J., Lonardi, S., Yeung, K., et al. (2018) Durable Clinical Benefit With Nivolumab Plus Ipilimumab in DNA Mismatch Repair-Deficient/Microsatellite Instability-High Metastatic Colorectal Cancer. *J Clin Oncol*, 36: 773–779. doi:10.1200/JCO.

Overman, M.J., McDermott, R., Leach, J.L., et al. (2017) Nivolumab in patients with metastatic DNA mismatch repair-deficient or microsatellite instability-high colorectal cancer (CheckMate 142): an open-label, multicentre, phase 2 study. *The Lancet Oncology*, 18 (9): 1182–1191. doi:10.1016/S1470-2045(17)30422-9.

Pan, Y., Huang, J., Xing, R., et al. (2013) Metallothionein 2A inhibits NF-κB pathway activation and predicts clinical outcome segregated with TNM stage in gastric cancer patients following radical resection. *Journal of Translational Medicine*, 11 (1). doi:10.1186/1479-5876-11-173.

Parys, A. Van, Boyen, F., Verbrugghe, E., et al. (2012) Salmonella Typhimurium induces SPI-1 and SPI-2 regulated and strain dependent downregulation of MHC II expression on porcine alveolar macrophages. *Veterinary Research*, 43. Available at: http://www.veterinaryresearch.org/content/43/1/52.

Van Parys, A., Boyen, F., Volf, J., et al. (2010) Salmonella Typhimurium resides largely as an extracellular pathogen in porcine tonsils, independently of biofilm-associated genes csgA, csgD and adrA. *Veterinary Microbiology*, 144 (1–2): 93–99. doi:10.1016/j.vetmic.2009.12.021.

Pavlova, B., Volf, J., Ondrackova, P., et al. (2011) SPI-1-encoded type III secretion system of Salmonella enterica is required for the suppression of porcine alveolar macrophage cytokine expression. *Veterinary Research*, 42 (1). doi:10.1186/1297-9716-42-16.

Pawelek, J.M., Low, K.B. and Bermudes, D. (1997) Tumor-targeted Salmonella as a novel anticancer vector. *Cancer Research*, 57 (20): 4537–4544.

Peng, Z., Wang, C.X., Fang, E.H., et al. (2014) Role of epithelial-mesenchymal transition in gastric cancer initiation and progression. *World Journal of Gastroenterology*, 20 (18): 5403–5410. doi:10.3748/wjg.v20.i18.5403.

Porter, R.J., Murray, G.I. and McLean, M.H. (2020) Current concepts in tumour-derived organoids. *British Journal of Cancer*, 123 (8): 1209–1218. doi:10.1038/s41416-020-0993-5.

Porwollik, S., Santiviago, C.A., Cheng, P., et al. (2014) Defined single-gene and multi-gene deletion mutant collections in salmonella enterica sv typhimurium. *PLoS ONE*, 9 (7). doi:10.1371/journal.pone.0099820.

Poynter, J.N., Siegmund, K.D., Weisenberger, D.J., et al. (2008) Molecular characterization of MSI-H colorectal cancer by MLHI promoter methylation, immunohistochemistry, and mismatch repair germline mutation screening. *Cancer Epidemiology Biomarkers and Prevention*, 17 (11): 3208–3215. doi:10.1158/1055-9965.EPI-08-0512.

Puppa, M.J., White, J.P., Sato, S., et al. (2011) Gut barrier dysfunction in the Apc Min/+ mouse model of colon cancer cachexia. *Biochimica et Biophysica Acta - Molecular Basis of Disease*, 1812 (12): 1601–1606. doi:10.1016/j.bbadis.2011.08.010.

Que, F., Wu, S. and Huang, R. (2013) Salmonella pathogenicity Island 1(SPI-1) at work. *Current Microbiology*, 66 (6): 582–587. doi:10.1007/s00284-013-0307-8.

de Queiroz, N.M.G.P., Marinho, F. V., de Araujo, A.C.V.S.C., et al. (2021) MyD88-dependent BCG immunotherapy reduces tumor and regulates tumor microenvironment in bladder cancer murine model. *Scientific Reports*, 11 (1). doi:10.1038/s41598-021-95157-6.

Raffatellu, M., George, M.D., Akiyama, Y., et al. (2009) Lipocalin-2 Resistance Confers an Advantage to Salmonella enterica Serotype Typhimurium for Growth and Survival in the Inflamed Intestine. *Cell Host and Microbe*, 5 (5): 476–486. doi:10.1016/j.chom.2009.03.011.

Rauch, I., Deets, K.A., Ji, D.X., et al. (2017) NAIP-NLRC4 Inflammasomes Coordinate Intestinal Epithelial Cell Expulsion with Eicosanoid and IL-18 Release via Activation of Caspase-1 and -8. *Immunity*, 46 (4): 649–659. doi:10.1016/j.immuni.2017.03.016.

Reichman, H., Itan, M., Rozenberg, P., et al. (2019) Activated eosinophils exert antitumorigenic activities in colorectal cancer. *Cancer Immunology Research*, 7 (3): 388–400. doi:10.1158/2326-6066.CIR-18-0494.

Rodriguez, N.R.M., Eloi, M.D., Huynh, A., et al. (2012) Expansion of paneth cell population in response to enteric salmonella enterica serovar typhimurium infection. *Infection and Immunity*, 80 (1): 266–275. doi:10.1128/IAI.05638-11.

Rubinstein, M.R., Wang, X., Liu, W., et al. (2013) Fusobacterium nucleatum Promotes Colorectal Carcinogenesis by Modulating E-Cadherin/β-Catenin Signaling via its FadA Adhesin. *Cell Host and Microbe*, 14 (2): 195–206. doi:10.1016/j.chom.2013.07.012.

Sadeghipour, E., Garcia, M.A., Nelson, W.J., et al. (2018) Shear-induced damped oscillations in an epithelium depend on actomyosin contraction and E-cadherin cell adhesion. *eLife*. doi:10.7554/eLife.39640.001.

Saltzman, D., Augustin, L., Leonard, A., et al. (2018) Low dose chemotherapy combined with attenuated Salmonella decreases tumor burden and is less toxic than high dose chemotherapy in an autochthonous murine model of breast cancer. *Surgery (United States)*, 163 (3): 509–514. doi:10.1016/j.surg.2017.09.036.

Saltzman, D.A., Heise, C.P., Hasz, D.E., et al. (1996) Attenuated Salmonella typhimurium containing interleukin-2 decreases MC-38 hepatic metastases: A novel anti-tumor agent. *Cancer Biotherapy and Radiopharmaceuticals*, 11 (2): 145–153. doi:10.1089/cbr.1996.11.145.

Samperio Ventayol, P., Geiser, P., Letizia, M., et al. (2021) Bacterial detection by NAIP/NLRC4 elicits prompt contractions of intestinal epithelial cell layers. *PNAS*, 118 (16). doi:10.1073/pnas.2013963118/-/DCSupplemental.

Santos, A.J.M., Meinecke, M., Fessler, M.B., et al. (2013) Preferential invasion of mitotic cells by Salmonella reveals that cell surface cholesterol is maximal during metaphase. *Journal of Cell Science*, 126 (14): 2990–2996.

dos Santos, A.M.P., Ferrari, R.G. and Conte-Junior, C.A. (2019) Virulence Factors in Salmonella Typhimurium: The Sagacity of a Bacterium. *Current Microbiology*. 76 (6) pp. 762–773. doi:10.1007/s00284-018-1510-4.

Sato, T., Stange, D.E., Ferrante, M., et al. (2011) Long-term expansion of epithelial organoids from human colon, adenoma, adenocarcinoma, and Barrett's epithelium. *Gastroenterology*, 141 (5): 1762–1772. doi:10.1053/j.gastro.2011.07.050.

Sato, T., Vries, R.G., Snippert, H.J., et al. (2009) Single Lgr5 stem cells build crypt-villus structures in vitro without a mesenchymal niche. *Nature*, 459 (7244): 262–265. doi:10.1038/nature07935.

Sawant, K. V., Poluri, K.M., Dutta, A.K., et al. (2016) Chemokine CXCL1 mediated neutrophil recruitment: Role of glycosaminoglycan interactions. *Scientific Reports*, 6. doi:10.1038/srep33123.

Schutyser, E., Struyf, S. and Van Damme, J. (2003) The CC chemokine CCL20 and its receptor CCR6. *Cytokine and Growth Factor Reviews*. 14 (5) pp. 409–426. doi:10.1016/S1359-6101(03)00049-2.

See, W.A., Zhang, G., Chen, F., et al. (2009) Bacille-Calmette Guèrin induces caspase-independent cell death in urothelial carcinoma cells together with release of the necrosis-associated chemokine high molecular group box protein 1. *BJU International*, 103 (12): 1714–1720. doi:10.1111/j.1464-410X.2008.08274.x.

Sellin, M.E., Müller, A.A., Felmy, B., et al. (2014) Epithelium-intrinsic NAIP/NLRC4 inflammasome drives infected enterocyte expulsion to restrict salmonella replication in the intestinal mucosa. *Cell Host and Microbe*, 16 (2): 237–248. doi:10.1016/j.chom.2014.07.001.

Shao, X., Liao, J., Lu, X., et al. (2020) scCATCH: Automatic Annotation on Cell Types of Clusters from Single-Cell RNA Sequencing Data. *iScience*, 23 (3). doi:10.1016/j.isci.2020.100882.

Siegel, R.L., Miller, K.D., Goding Sauer, A., et al. (2020) Colorectal cancer statistics, 2020. *CA: A Cancer Journal for Clinicians*, 70 (3): 145–164. doi:10.3322/caac.21601.

Sierro, F., Dubois, B., Coste, A., et al. (2001) Flagellin stimulation of intestinal epithelial cells triggers CCL20-mediated migration of dendritic cells. *Proceedings of the National Academy of Sciences of the United States of America*, 98 (24): 13722–13727. doi:10.1073/pnas.241308598.

Silhavy, T.J., Kahne, D. and Walker, S. (2010) The bacterial cell envelope. *Cold Spring Harbor perspectives in biology*, 2 (5). doi:10.1101/cshperspect.a000414.

Silva-Valenzuela, C.A., Desai, P.T., Molina-Quiroz, R.C., et al. (2016) Solid tumors provide niche-specific conditions that lead to preferential growth of Salmonella. *Oncotarget*, 7 (23): 35169–35180. doi:10.18632/oncotarget.9071.

Simons, M.P., O'donnell, M.A. and Griffith, T.S. (2008) Role of Neutrophils in BCG Immunotherapy for Bladder Cancer. *Urol Oncol*, 26 (4): 341–345.

Singh, V., Yeoh, B.S., Chassaing, B., et al. (2016) Microbiota-Inducible Innate Immune Siderophore Binding Protein Lipocalin 2 Is Critical for Intestinal Homeostasis. *Cmgh*, 2 (4): 482-498.e6. doi:10.1016/j.jcmgh.2016.03.007.

Spiga, L., Winter, M.G., Furtado de Carvalho, T., et al. (2017) An Oxidative Central Metabolism Enables Salmonella to Utilize Microbiota-Derived Succinate. *Cell Host and Microbe*, 22 (3): 291-301.e6. doi:10.1016/j.chom.2017.07.018.

Stecher, B., Robbiani, R., Walker, A.W., et al. (2007) Salmonella enterica serovar typhimurium exploits inflammation to compete with the intestinal microbiota. *PLoS Biology*, 5 (10): 2177–2189. doi:10.1371/journal.pbio.0050244.

Steele-Mortimer, O., Knodler, L.A., Marcus, S.L., et al. (2000) Activation of Akt/protein kinase B in epithelial cells by the Salmonella typhimurium effector SigD. *Journal of Biological Chemistry*, 275 (48): 37718–37724. doi:10.1074/jbc.M008187200.

Stritzker, J., Weibel, S., Seubert, C., et al. (2010) Enterobacterial tumor colonization in mice depends on bacterial metabolism and macrophages but is independent of chemotaxis and motility. *International Journal of Medical Microbiology*, 300 (7): 449–456. doi:10.1016/j.ijmm.2010.02.004.

Tang, D., Kang, R., Coyne, C.B., et al. (2012) PAMPs and DAMPs: Signal 0s that spur autophagy and immunity. *Immunological Reviews*, 249 (1): 158–175. doi:10.1111/j.1600-065X.2012.01146.x.

Tang, F., Barbacioru, C., Wang, Y., et al. (2009) mRNA-Seq whole-transcriptome analysis of a single cell. *Nature Methods*, 6 (5): 377–382. doi:10.1038/nmeth.1315.

Terzić, J., Grivennikov, S., Karin, E., et al. (2010) Inflammation and Colon Cancer. *Gastroenterology*, 138 (6). doi:10.1053/j.gastro.2010.01.058.

Thiennimitr, P., Winter, S.E., Winter, M.G., et al. (2011) Intestinal inflammation allows Salmonella to use ethanolamine to compete with the microbiota. *Proceedings of the National Academy of Sciences of the United States of America*, 108 (42): 17480–17485. doi:10.1073/pnas.1107857108.

Toso, J.F., Gill, V.J., Hwu, P., et al. (2002) Phase I study of the intravenous administration of attenuated Salmonella typhimurium to patients with metastatic melanoma. *Journal of Clinical Oncology*, 20 (1): 142–152. doi:10.1200/JCO.20.1.142.

Tsuchiya, K. (2020) Inflammasome-associated cell death: Pyroptosis, apoptosis, and physiological implications. *Microbiology and Immunology*. 64 (4) pp. 252–269. doi:10.1111/1348-0421.12771.

Ulgen, E., Ozisik, O. and Sezerman, O.U. (2019) PathfindR: An R package for comprehensive identification of enriched pathways in omics data through active subnetworks. *Frontiers in Genetics*, 10 (SEP). doi:10.3389/fgene.2019.00858.

Umeda, K., Tanaka, S., Ihara, F., et al. (2017) Transcriptional profiling of Toll-like receptor 2-deficient primary murine brain cells during Toxoplasma gondii infection. *PLoS ONE*, 12 (11): 1–26. doi:10.1371/journal.pone.0187703.

Valdez, Y., Grassl, G.A., Guttman, J.A., et al. (2009) Nramp1 drives an accelerated inflammatory response during Salmonella -induced colitis in mice. *Cellular Microbiology*, 11 (2): 351–362. doi:10.1111/j.1462-5822.2008.01258.x.

Varricchi, G., Galdiero, M.R., Loffredo, S., et al. (2018) Eosinophils: The unsung heroes in cancer? *OncoImmunology*. 7 (2). doi:10.1080/2162402X.2017.1393134.

Vatandoust, S., Price, T.J. and Karapetis, C.S. (2015) Colorectal cancer: Metastases to a single organ. *World Journal of Gastroenterology*, 21 (41): 11767–11776. doi:10.3748/wjg.v21.i41.11767.

Veglia, F., Hashimoto, A., Dweep, H., et al. (2021) Analysis of classical neutrophils and polymorphonuclear myeloid-derived suppressor cells in cancer patients and tumor-bearing mice. *Journal of Experimental Medicine*, 218 (4). doi:10.1084/JEM.20201803.

Verweij, J. and Pinedo, H.M. (1990) Mitomycin C: Mechanism of action, usefulness and limitations. *AntiCancer Drugs*, 1 (1): 5–13.

Vu, T. and Datta, P.K. (2017) Regulation of EMT in colorectal cancer: A culprit in metastasis. *Cancers*. 9 (12). doi:10.3390/cancers9120171.

Waldner, M.J., Foersch, S. and Neurath, M.F. (2012) Interleukin-6 - A key regulator of colorectal cancer development. *International Journal of Biological Sciences*. 8 (9) pp. 1248–1253. doi:10.7150/ijbs.4614.

Walsh, D., McCarthy, J., O'Driscoll, C., et al. (2013) Pattern recognition receptors-Molecular orchestrators of inflammation in inflammatory bowel disease. *Cytokine and Growth Factor Reviews*. 24 (2) pp. 91–104. doi:10.1016/j.cytogfr.2012.09.003.

Wang, D., Yang, L., Yu, W., et al. (2019) Colorectal cancer cell-derived CCL20 recruits regulatory T cells to promote chemoresistance via FOXO1/CEBPB/NF-κB signaling. *Journal for ImmunoTherapy of Cancer*, 7 (1). doi:10.1186/s40425-019-0701-2.

Wang, X., Qiu, L., Li, Z., et al. (2018) Understanding the multifaceted role of neutrophils in cancer and autoimmune diseases. *Frontiers in Immunology*, 9 (NOV). doi:10.3389/fimmu.2018.02456.

W.B. Coley (1912) Disappearance of a recurrent carcinoma after injections of mixed toxins. *Annals of Surgery*, 55: 897–898.

Van De Wetering, M., Francies, H.E., Francis, J.M., et al. (2015) Prospective derivation of a living organoid biobank of colorectal cancer patients. *Cell*, 161 (4): 933–945. doi:10.1016/j.cell.2015.03.053.

Williamson, I.A., Arnold, J.W., Samsa, L.A., et al. (2018) A High-Throughput Organoid Microinjection Platform to Study Gastrointestinal Microbiota and Luminal Physiology. *Cellular and Molecular Gastroenterology and Hepatology*, 63: 301–319.

Winter, S.E., Thiennimitr, P., Winter, M.G., et al. (2010) Gut inflammation provides a respiratory electron acceptor for Salmonella. *Nature*, 467 (7314): 426–429. doi:10.1038/nature09415.

Wlodarska, M., Kostic, A.D. and Xavier, R.J. (2015) An integrative view of microbiome-host interactions in inflammatory bowel diseases. *Cell Host and Microbe*. 17 (5) pp. 577–591. doi:10.1016/j.chom.2015.04.008.

World Health Organisation (2023) *Colorectal cancer*. [Internet] Available at https://www.who.int/news-room/fact-sheets/detail/colorectal-cancer. Accessed on: 05/01/2024.

Xing, J., Yin, T., Li, S., et al. (2021) Sequential Magneto-Actuated and Optics-Triggered Biomicrorobots for Targeted Cancer Therapy. *Advanced Functional Materials*, 31 (11). doi:10.1002/adfm.202008262.

Yamada, Y. and Mori, H. (2007) Multistep carcinogenesis of the colon in ApcMin/+ mouse. *Cancer Science*. 98 (1) pp. 6–10. doi:10.1111/j.1349-7006.2006.00348.x.

Yang, J. and Moses, M.A. (2009) Lipocalin 2: A Multifaceted Modulator of Human Cancer. *Cell Cycle*, 8 (15): 2347–2352.

Yang, N., Zhu, X., Chen, L., et al. (2008) Oral administration of attenuated S. typhimurium carrying shRNA-expressing vectors as a cancer therapeutic. *Cancer Biology and Therapy*, 7 (1): 147–153. doi:10.4161/cbt.7.1.5195.

Yin, T., Diao, Z., Blum, N.T., et al. (2022) Engineering Bacteria and Bionic Bacterial Derivatives with Nanoparticles for Cancer Therapy. *Small*. 18 (12). doi:10.1002/smll.202104643.

Yoon, W., Park, Y.C., Kim, J., et al. (2017) Application of genetically engineered Salmonella typhimurium for interferon-gamma–induced therapy against melanoma. *European Journal of Cancer*, 70: 48–61. doi:10.1016/j.ejca.2016.10.010.

Yousefi, S., Gold, J.A., Andina, N., et al. (2008) Catapult-like release of mitochondrial DNA by eosinophils contributes to antibacterial defense. *Nature Medicine*, 14 (9): 949–953. doi:10.1038/nm.1855.

Yousefi, S., Simon, D. and Simon, H.U. (2012) Eosinophil extracellular DNA traps: Molecular mechanisms and potential roles in disease. *Current Opinion in Immunology*. 24 (6) pp. 736–739. doi:10.1016/j.coi.2012.08.010.

Yu, C., Cantor, A.B., Yang, H., et al. (2002) Targeted deletion of a high-affinity GATA-binding site in the GATA-1 promoter leads to selective loss of the eosinophil lineage in vivo. *Journal of Experimental Medicine*, 195 (11): 1387–1395. doi:10.1084/jem.20020656.

Yu, J., Rossi, R., Hale, C., et al. (2009) Interaction of enteric bacterial pathogens with murine embryonic stem cells. *Infection and Immunity*, 77 (2): 585–597. doi:10.1128/IAI.01003-08.

Yu, Y.A., Shabahang, S., Timiryasova, T.M., et al. (2004) Visualization of tumors and metastases in live animals with bacteria and vaccinia virus encoding light-emitting proteins. *Nature Biotechnology*, 22 (3): 313–320. doi:10.1038/nbt937.

Zhang, L. and Shay, J.W. (2017) Multiple Roles of APC and its Therapeutic Implications in Colorectal Cancer. *Journal of the National Cancer Institute*, 109 (8): 1–10. doi:10.1093/jnci/djw332.

Zhang, S., Adams, L.G., Nunes, J., et al. (2003) Secreted effector proteins of Salmonella enterica serotype typhimurium elicit host-specific chemokine profiles in animal models of typhoid fever and enterocolitis. *Infection and Immunity*, 71 (8): 4795–4803. doi:10.1128/IAI.71.8.4795-4803.2003.

Zhang, Y.G., Zhu, X., Lu, R., et al. (2019) Intestinal epithelial HMGB1 inhibits bacterial infection via STAT3 regulation of autophagy. *Autophagy*, 15 (11): 1935–1953. doi:10.1080/15548627.2019.1596485.

Zhao, H., Ming, T., Tang, S., et al. (2022) Wnt signaling in colorectal cancer: pathogenic role and therapeutic target. *Molecular Cancer*. 21 (1). doi:10.1186/s12943-022-01616-7.

Zhao, M., Yang, M., Li, X.-M., et al. (2005) Tumor-targeting bacterial therapy with amino acid auxotrophs of GFP-expressing Salmonella typhimurium. *PNAS*, 102 (3): 755–760. Available at: www.pnas.orgcgidoi10.1073pnas.0408422102.

Zheng, J.H. and Min, J.-J. (2016) Targeted Cancer Therapy Using Engineered Salmonella typhimurium . *Chonnam Medical Journal*, 52 (3): 173. doi:10.4068/cmj.2016.52.3.173.

Zheng, J.H., Nguyen, V.H., Jiang, S.N., et al. (2017) Two-step enhanced cancer immunotherapy with engineered Salmonella typhimurium secreting heterologous flagellin. *Science Translational Medicine*. doi:10.1126/scitranslmed.aak9537.

Zhou, D., Mooseker, M.S. and Galán, J.E. (1999) *Role of the S. typhimurium Actin-Binding Protein SipA in Bacterial Internalization*. Available at: https://www.science.org.

Zlotta, A.R., Drowart, A., Van Vooren, J.-P., et al. (1997) EVOLUTION AND CLINICAL SIGNIFICANCE OF THE T CELL PROLIFERATIVE AND CYTOKINE RESPONSE DIRECTED AGAINST THE FIBRONECTIN BINDING ANTIGEN 85 COMPLEX OF BACILLUS CALMETTE-GUERIN DURING INTRAVESICAL TREATMENT OF SUPERFICIAL BLADDER CANCER. *J Urol.*, 157: 492–498.

Zu, C. and Wang, J. (2014) Tumor-colonizing bacteria: A potential tumor targeting therapy. *Critical Reviews in Microbiology*. 40 (3) pp. 225–235. doi:10.3109/1040841X.2013.776511.

APPENDIX 1: SINGLE-CELL RNA-SEQUENCING SCRIPTS

Cells were sequenced by the Genomics Birmingham centre and I converted base call files from the Illumina sequencer to FASTQ files using the cellranger 'mkfastq' pipeline remotely using Python version 2.7.14. These files were then read into R studio version 4.1.1 and analysed using primarily the Seurat pipeline, detailed in the following R scripts.

```
###Open libraries needed and set working directory to single cell folder

library(dplyr)
library(Seurat)
library(patchwork)
library(gplots)
library(cowplot)
library(ggplot2)
setwd("/rds/projects/m/mackiegm-human-sc-rna-seq/")

###Load dataset in and add in characteristics
dirname = ("/rds/projects/m/mackiegm-human-sc-rna-seq /both_runs_count/")
samples = c("064_nt","064_stm","389_nt","389_stm","411_nt","411_stm","964_nt","964_stm")
treatment = c("nt", "stm","nt", "stm","nt", "stm","nt", "stm")
patient = c("064", "064", "389", "389", "411", "411", "964", "964")
responsive = c("RA", "RA", "RA", "RA", "RB", "RB", "RB", "RB")
input_dirs = paste0(dirname,samples,"/outs/raw_feature_bc_matrix/")
outdir = ("/rds/projects/m/mackiegm-human-sc-rna-seq/QC_plots/")

###Make Seurat object with all patient info added
alldata = list()
for (i in 1:8) {
  message(samples[i])
  scrna_data <- Read10X(data.dir = input_dirs[i])
  alldata[[i]] <- CreateSeuratObject(counts = scrna_data, project = samples[i], min.cells = 3,
min.features = 200)
  alldata[[i]]$treatment = treatment[i]
  alldata[[i]]$patient = patient[i]
  alldata[[i]]$samples = samples[i]
  alldata[[i]]$responsive = responsive[i]
}

###Calculate mitochondrial reads percent
for (i in 1:8) {
  alldata[[i]][["percent.mito"]] <- PercentageFeatureSet(object = alldata[[i]], pattern = "^MT-")
  }

###Plot unfiltered data in violin plot
for (I in 1:8) {
```

```
VlnPlot(alldata[[i]], features = c(("nFeature_RNA", "nCount_RNA", "percent.mito"), ncol = 3)
}

###Filter data based on low and too high reads and high mito – removes dead cells/debris and also clumps not single cells
for (i in 1:8){
  alldata[[i]] <-subset(alldata[[i]], subset= nFeature_RNA > 200 & nFeature_RNA <2500 & percent.mito <15)
}

ncells_filtered = data.frame(sample=samples, ncells=NA)
for(i in 1:8){
  ncells_filtered$ncells[i] = length(alldata[[i]]$patient)
}

write.table(ncells_filtered, file = paste0(outdir,"ncells_filtered.tsv"),row.names = FALSE, col.names = TRUE, quote = FALSE)

###389_stm extra filtering as many debris/dead cell data points
alldata[[4]] <- subset(alldata[[4]], subset = nCount_RNA > 1000)
ncells_filtered389 = data.frame(sample=samples, ncells=NA)
for(i in 1:8){
  ncells_filtered389$ncells[i] = length(alldata[[i]]$patient)
}
write.table(ncells_filtered389, file = paste0(outdir,"ncells_filtered389stm.tsv"),row.names = FALSE, col.names = TRUE, quote = FALSE)

saveRDS(alldata, "389stm_filtered_alldata.rds")

###Violin plots of filtered data to visualise spread
for (I in 1:8) {
VlnPlot(alldata[[i]], features = c(("nFeature_RNA", "nCount_RNA", "percent.mito"), ncol = 3)
}

###Log normalise data and identify highly variable features
for (i in 1:8){
  message(samples[i])
  alldata[[i]] <- NormalizeData(alldata[[i]], normalization.method = "LogNormalize", scale.factor = 10000)
  alldata[[i]] <- FindVariableFeatures(alldata[[i]], selection.method = "vst", nfeatures = 2000)
}

### Select features that are repeatedly variable across datasets for integration
features <- SelectIntegrationFeatures(object = alldata)
anchors <- FindIntegrationAnchors(object = alldata, anchor.features = features)

saveRDS(alldata, "389stm_filtered_alldata.rds")
saveRDS(anchors, "389stm_filtered_anchors.rds")
saveRDS(features, "389stm_filtered_integrationfeatures.rds")
```

```
### This command creates an 'integrated' data assay – allows comparison of cell types and markers CONSERVED or CHANGED across datasets
data.combined <- IntegrateData(anchorset = anchors)
### Specify that we will perform downstream analysis on the corrected data. Note that the original unmodified data still resides in the 'RNA' assay – can use this later for plotting features
DefaultAssay(data.combined) <- "integrated"

saveRDS(data.combined, "389stm_filtered_integrateddata.rds")
saveRDS(`389stm_filtered_integrateddata`, "data.combined_389F.rds")

### Run the standard workflow for visualization and clustering
data.combined_389F <- ScaleData(data.combined_389F, verbose = FALSE)
data.combined_389F <- RunPCA(data.combined_389F, npcs = 100, verbose = FALSE)

###Determine dimensionality. NOTE: This process can take a long time for big datasets – elbow plot quicker but less reliable – combine both
data.combined_389F <- JackStraw(data.combined_389F, dims = 100)
data.combined_389F <- ScoreJackStraw(data.combined_389F, dims = 1:100)
JackStrawPlot(data.combined_389F, dims = 1:100)
ElbowPlot(data.combined_389F, ndims = 100)

saveRDS(data.combined_389F, "data.combined_389F.rds")

### Based on JackStraw-use 40Pcs for clustering
data.combined_389F <- RunUMAP(data.combined_389F, reduction = "pca", dims = 1:40)
data.combined_389F <- FindNeighbors(data.combined_389F, reduction = "pca", dims = 1:40)
data.combined_389F <- FindClusters(data.combined_389F, resolution = 0.5)

### Visualise PCs – can see point at which the PCs become too similar to be significant
DimHeatmap(data.combined_389F, dims = 1:20, cells = 500, balanced = TRUE)
DimHeatmap(data.combined_389F, dims = 21:40, cells = 500, balanced = TRUE)

### Visualization by treatment
p1 <- DimPlot(data.combined_389F, reduction = "umap", split.by = "treatment")
p2 <- DimPlot(data.combined_389F, reduction = "umap", label = TRUE, repel = TRUE)
p1 + p2

### A list of cell cycle markers, from Tirosh et al, 2015, (ref in methods) is loaded with Seurat.  We can segregate this list into markers of G2/M phase and markers of S phase
s.genes <- cc.genes$s.genes
g2m.genes <- cc.genes$g2m.genes

data.combined_389F_ccscore <- CellCycleScoring(data.combined_389F, s.features = s.genes, g2m.features = g2m.genes, set.ident = TRUE)

### view cell cycle scores and phase assignments
head(data.combined_389F_ccscore[[]])
write.table(data.combined_389F_ccscore@meta.data, file = paste0(outdir, "data.combined_389F_cellcycle.tsv"), row.names = FALSE, col.names = TRUE, quote = FALSE)
```

```
data.combined_389F_ccscore <- RunPCA(data.combined_389F_ccscore, features = c(s.genes,
g2m.genes))
DimPlot(data.combined_389F_ccscore)
data.combined_389F_ccscore$CC.Difference <- data.combined_389F_ccscore$S.Score -
data.combined_389F_ccscore$G2M.Score
data.combined_389F_ccscore <- ScaleData(data.combined_389F_ccscore, vars.to.regress =
"CC.Difference", features = rownames(data.combined_389F_ccscore))
DimPlot(data.combined_389F_ccscore)
saveRDS(data.combined_389F_ccscore, "ccscoring_389F.rds")

### Find markers for every cluster compared to all remaining cells, report only the positive ones
cell.markers <- FindAllMarkers(data.combined_389F, only.pos = TRUE, min.pct = 0.25, logfc.threshold
= 0.25)
write.table(cell.markers, file = paste0(outdir,"389stm_filtered_clustermarkers.tsv"),row.names =
FALSE, col.names = TRUE, quote = FALSE)
cell.markers %>% group_by(cluster) %>% top_n(n = 2, wt = avg_logFC)
top10 <- cell.markers %>% group_by(cluster) %>% top_n(n = 10, wt = avg_logFC)
write.table(top10, file = paste0(outdir,"top10genesUPpercluster_389F.tsv"),row.names = FALSE,
col.names = TRUE, quote = FALSE)
DoHeatmap(data.combined_389F, features = top10$gene)

saveRDS(cell.markers, "clustermarkers_389F.rds")
saveRDS(top10, "top10genes_percluster_389F.rds")
saveRDS(data.combined_389F, "data.combined_389F.rds")

### This script reads in the upregulated cluster markers and the PanglaoDB database, and finds
putative celltypes based on all upregulated genes for each cluster.

### 1. read data
### cluster markers (only upregulated genes)
cluster_markers <- read.table("389stm_filtered_plots/all_clustermarkers.txt", header = TRUE)
table(cluster_markers$cluster)
clusterIDs = 0:15
n_clusters = length(clusterIDs)

### PanglaoDB gut cell specific database read in from downloaded file
panglaodb <- as.data.frame(read.csv("PanglaoDB_markers_27_Mar_2020_text.txt", sep = "\t"))

### 2. identify clusters' cell types
### matrix listing the number of genes in each cell type for each cluster
cell_type_table <- matrix(NA, nrow = n_clusters, ncol = n_celltypes)
colnames(cell_type_table) = celltype_IDs
rownames(cell_type_table) = paste0("c-",clusterIDs)
for (c in 0:15) {
  ### extract this cluster's markers
  upreg_genes = cluster_markers$gene[ cluster_markers$cluster == c ]
  ### find these gene entries in panglaoDB
  panglaodb_upreg_genes <- panglaodb %>% subset(official.gene.symbol %in% upreg_genes)
  ### count how many genes are listed for each cell type
  ### use c+1, to start the rows from 1 rather than 0
```

```
  cell_type_table[c+1,] = summary(panglaodb_upreg_genes$cell.type)
}
### check that the first column (empty cell type) is indeed empty
celltype_IDs[1]
cell_type_table[,1]
### delete the 1st column with empty cell type name, as all values are 0.
cell_type_table <- cell_type_table[,3:n_celltypes]

### plot matrix listing the number of genes in each cell type for each cluster
pdf(file="PanglaoDB_cluster_id.pdf", width=12, height=12, paper="special", onefile=T,title="")
par(mar=c(6,7,1.5,2),mgp=c(4,1.5,0))
heatmap.2(cell_type_table,
        main = '',
        Rowv = TRUE, Colv = TRUE, dendrogram = "both", scale = "none",
        col = colorRampPalette(c("white","red"),space="rgb")(5),
        symkey = FALSE,
        breaks = c(0:5), cellnote = cell_type_table, notecol="black", notecex = 2,
        trace = "none" , #cex.main = 3, cex.axis = 5, cex.lab = 5, #mar=c(14,14),
        #RowSideColours = cols_XX,
        ylab = "cluster ID", xlab = "cell type", cexRow = 1.5, cexCol = 1.5,
        margins = c(15,8),
        #labRow = chromo_size_table$chromo, labCol = chromo_size_table$chromo,
        key.title = "upregulated genes", key.xlab = "number of genes")#, keysize = 0.5)
dev.off()

###scCATCH script
### install devtools and install scCATCH
install.packages(pkgs = 'devtools')
devtools::install_github('ZJUFanLab/scCATCH')
library(scCATCH)

###load data in
data.combined_389F <- readRDS("Y:/Csilla/data.combined_389F.rds")

clu_markers <- findmarkergenes(data.combined_389F, species = 'Human', cluster = 'All',
match_CellMatch = FALSE, cancer = NULL, tissue = NULL, cell_min_pct = 0.25, logfc = 0.25, pvalue =
0.05)
saveRDS(clu_markers, "scCATCH_Clu_markers.rds")

clu_markers <- readRDS("Y:/Csilla/scCATCH_Clu_markers.rds")

clu_ann_cancer <- scCATCH(clu_markers, species = 'Human', cancer = c("Colon Cancer", "Colorectal
Cancer"), tissue = c("Colon", "Colorectum", "Gastrointestinal tract", "Intestine"))
saveRDS(clu_ann_cancer, "scCATCH_clu_annotations_cancer.rds")

clu_ann_normal <- scCATCH(clu_markers, species = 'Human', cancer = NULL, tissue = c("Colon",
"Colorectum", "Gastrointestinal tract", "Gut", "Intestinal crypt", "Intestine", "Jejunum", "Large
intestine", "Small intestinal crypt", "Small intestine"))
saveRDS(clu_ann_normal, "scCATCH_clu_annotations_normal.rds")
```

```
###Assigning cell identities into Seurat file
new.cluster.ids <- c("Paneth cell 1", "Tumour 1", "Progenitor 1", "Dying Tumour", "Tumour 2",
"Goblet cell", "Tumour 3", "Tumour 4", "Progenitor 2", "Enterocyte 1", "Tumour 5", "Enterocyte 2",
"Stem cell", "Paneth cell 2", "Progenitor 3", "Tumour 6")

names(new.cluster.ids) <- levels(data.combined_389F)

data.combined.cluster_ids <- RenameIdents(data.combined_389F, new.cluster.ids)
saveRDS(data.combined.cluster_ids, "data.combined_389F_clusterids.rds")

DimPlot(data.combined.cluster_ids, reduction = "umap", label = TRUE, pt.size = 0.5, label.size = 10)
DimPlot(data.combined.cluster_ids, reduction = "umap", label = TRUE, pt.size = 0.5, label.size = 10,
split.by = "treatment")
DimPlot(data.combined.cluster_ids, reduction = "umap", label = TRUE, pt.size = 0.5, label.size = 10,
split.by = "responsive")
DimPlot(data.combined.cluster_ids, reduction = "umap", label = TRUE, pt.size = 1.5, label.size = 10,
split.by = "responsive", shape.by = "treatment")

markers.to.plot <- c("TFF3", "MUC2", "KRT19", "PROM1", "CXCL3", "ATOH1", "LYZ", "LGR5",
"SMOC2", "OLFM4", "CDX1", "CEACAM1", "NEAT1")
DotPlot(data.combined.cluster_ids, features = markers.to.plot, cols = c("blue", "red"), dot.scale = 8) +
RotatedAxis()

###Cell population shifts with treatments
data.combined <- data.combined.cluster_ids

### Store cluster identities in object@meta.data$my.clusters
data.combined <- Seurat::StashIdent(object = data.combined, save.name = "my.clusters")

###Find degs based on treatment - positive logfc = upregulated in ident.1 vs ident.2
Idents(data.combined) <- data.combined@meta.data$my.clusters
DefaultAssay(data.combined) <- "RNA"
treatment.degs <- FindMarkers(data.combined, ident.1 = "stm", ident.2 = "nt", verbose = TRUE,
group.by="treatment", logfc.threshold = log(1.3))
patient.degs <- FindMarkers(data.combined, ident.1 = "064", ident.2 = "389", ident.3 = "411",
ident.4= "964", verbose = TRUE, group.by="patient", logfc.threshold = log(2))
response.degs <- FindMarkers(data.combined, ident.1 = “RB”, ident.2 = "RA", verbose = TRUE,
group.by="responsive", logfc.threshold = log(2))
responseB.treatment.degs <- FindMarkers(data.combined, ident.1 = "964_stm", ident.2 = "964_nt",
verbose = TRUE, group.by="samples", logfc.threshold = log(1.3))
responseB2.treatment.degs <- FindMarkers(data.combined, ident.1 = "411_stm", ident.2 = "411_nt",
verbose = TRUE, group.by="samples", logfc.threshold = log(1.3))
responseA.treatment.degs <- FindMarkers(data.combined, ident.1 = "064_stm", ident.2 = "064_nt",
verbose = TRUE, group.by="samples", logfc.threshold = log(1.3))
responseA2.treatment.degs <- FindMarkers(data.combined, ident.1 = "389_stm", ident.2 = "389_nt",
verbose = TRUE, group.by="samples", logfc.threshold = log(1.3))
response.BASELINE.degs <- FindMarkers(data.combined, ident.1 = c("411_nt", "964_nt"), ident.2 =
c("389_nt", "064_nt"), verbose = TRUE, group.by="samples", logfc.threshold = log(2))

write.table(treatment.degs, file= "Y:/Csilla/treatment.degs.tsv")
```

```
write.table(patient.degs, file = "Y:/Csilla/patient.degs.tsv")
write.table(response.degs, file = "Y:/Csilla/response.degs.tsv")
write.table(responseB.treatment.degs, file = "Y:/Csilla/responseB964.treatment.degs.tsv")
write.table(responseB2.treatment.degs, file = "Y:/Csilla/responseB411.treatment.degs.tsv")
write.table(responseA.treatment.degs, file = "Y:/Csilla/responseA064.treatment.degs.tsv")
write.table(responseA2.treatment.degs, file = "Y:/Csilla/responseA389.treatment.degs.tsv")
write.table(response.BASELINE.degs, file = "Y/Csilla/response.BASELINE.degs.tsv")

####Use values in csvs to calculate percentage cell types and plot in prism

######
#COMBINE RESPONSE BS
responseBs.degs <-read.delim("Y:/Csilla/responseBs.degs.tsv")

###The basic scatter plot: x is "log2FoldChange", y is "pvalue"
ggplot(responseBs.degs, aes(x=avg_log2FC, y=p_val_adj)) + geom_point()
### Convert directly in the aes()
plot <- ggplot(responseBs.degs, aes(x=avg_log2FC, y=-log10(p_val_adj))) + geom_point()
### Add more simple "theme"
plot <- ggplot(responseBs.degs, aes(x=avg_log2FC, y=-log10(p_val_adj))) + geom_point() +
theme_minimal()
### Add vertical lines for log2FoldChange thresholds, and one horizontal line for the p-value
threshold
plot2 <- plot + geom_vline(xintercept=c(-0.3, 0.3), col="red") +
  geom_hline(yintercept=-log10(0.05), col="red")

###The significantly differentially expressed genes are the ones found in the upper-left and upper-
right corners. Add a column to the data frame to specify if they are UP- or DOWN- regulated
(log2FoldChange respectively positive or negative)

### add a column of Nas for genes that do not sig change
responseBs.degs$diffexpressed <- "NO"
### if log2Foldchange > 0.3 and pvalue < 0.05, set as "UP"
responseBs.degs$diffexpressed[responseBs.degs$avg_log2FC > 0.3 & responseBs.degs$p_val_adj <
0.05] <- "UP"
### if log2Foldchange < -0.3 and pvalue < 0.05, set as "DOWN"
responseBs.degs$diffexpressed[responseBs.degs$avg_log2FC < -0.3 & responseBs.degs$p_val_adj <
0.05] <- "DOWN"

### Re-plot but this time colour the points with "diffexpressed"
plot <- ggplot(responseBs.degs, aes(x=avg_log2FC, y=-log10(p_val_adj), col=diffexpressed)) +
geom_point() + theme_minimal()

### Add lines as before...
plot2 <- plot + geom_vline(xintercept=c(-0.3, 0.3), col="red") +
  geom_hline(yintercept=-log10(0.05), col="red")

### Change point colour

### 1. by default, it is assigned to the categories in an alphabetical order):
```

```
plot3 <- plot2 + scale_colours_manual(values=c("blue", "black", "red"))

### 2. to automate a bit: create a named vector: the values are the colours to be used, the names are the categories they will be assigned to:
mycolours <- c("blue", "red", "black")
names(mycolours) <- c("DOWN", "UP", "NO")
plot3 <- plot2 + scale_colour_manual(values = mycolours)

### Now write down the name of genes beside the points. Create a new column "degslabel" to degs, that will contain the name of genes differentially expressed (NA in case they are not)
responseBs.degs$degslabel <- NA
responseBs.degs$degslabel[responseBs.degs$diffexpressed != "NO"] <-
responseBs.degs$gene_names[responseBs.degs$diffexpressed != "NO"]

ggplot(responseBs.degs, aes(x=avg_log2FC, y=-log10(p_val_adj), col=diffexpressed, label =
degslabel)) +
  geom_point() +
  theme_minimal()+
  geom_text() +
  labs(title= "STm vs NT differentially expressed genes in responseBs")+
  coord_cartesian(clip = "off")

### Finally, we can organize the labels nicely using the "ggrepel" package and the geom_text_repel() function
### load library
library(ggrepel)
### plot adding up all layers we have seen so far
ggplot(responseBs.degs, aes(x=avg_log2FC, y=-log10(p_val_adj), col=diffexpressed, label=degslabel))
+
  geom_point() +
  theme_minimal() +
  geom_text_repel() +
  scale_color_manual(values=c("blue", "black", "red")) +
  geom_vline(xintercept=c(-0.3, 0.3), col="red") +
  geom_hline(yintercept=-log10(0.05), col="red") +
  labs(title= "STm vs NT differentially expressed genes in responseBs")+
  coord_cartesian(clip = "off")

##### COMBINE RESPONSE AS
######

responseAs.degs <-read.delim("Y:/Csilla/responseAs.degs.tsv")

### The basic scatter plot: x is "log2FoldChange", y is "pvalue"
ggplot(responseAs.degs, aes(x=avg_log2FC, y=p_val_adj)) + geom_point()
### Convert directly in the aes()
plot <- ggplot(responseAs.degs, aes(x=avg_log2FC, y=-log10(p_val_adj))) + geom_point()
### Add more simple "theme"
plot <- ggplot(responseAs.degs, aes(x=avg_log2FC, y=-log10(p_val_adj))) + geom_point() +
theme_minimal()
```

```
### Add vertical lines for log2FoldChange thresholds, and one horizontal line for the p-value
threshold
plot2 <- plot + geom_vline(xintercept=c(-0.3, 0.3), col="red") +
  geom_hline(yintercept=-log10(0.05), col="red")

###The significantly differentially expressed genes are the ones found in the upper-left and upper-
right corners. Add a column to the data frame to specify if they are UP- or DOWN- regulated
(log2FoldChange respectively positive or negative)

### add a column of Nas for genes that do not sig change
responseAs.degs$diffexpressed <- "NO"
### if log2Foldchange > 0.3 and pvalue < 0.05, set as "UP"
responseAs.degs$diffexpressed[responseAs.degs$avg_log2FC > 0.3 & responseAs.degs$p_val_adj <
0.05] <- "UP"
### if log2Foldchange < -0.3 and pvalue < 0.05, set as "DOWN"
responseAs.degs$diffexpressed[responseAs.degs$avg_log2FC < -0.3 & responseAs.degs$p_val_adj <
0.05] <- "DOWN"

### Re-plot but this time colours the points with "diffexpressed"
plot <- ggplot(responseAs.degs, aes(x=avg_log2FC, y=-log10(p_val_adj), col=diffexpressed)) +
geom_point() + theme_minimal()

###Add lines as before...
plot2 <- plot + geom_vline(xintercept=c(-0.3, 0.3), col="red") +
  geom_hline(yintercept=-log10(0.05), col="red")

## Change point colours

### 1. by default, it is assigned to the categories in an alphabetical order):
plot3 <- plot2 + scale_color_manual(values=c("blue", "black", "red"))

### 2. to automate a bit: ceate a named vector: the values are the colours to be used, the names are
the categories they will be assigned to:
mycolours <- c("blue", "red", "black")
names(mycolours) <- c("DOWN", "UP", "NO")
plot3 <- plot2 + scale_colour_manual(values = mycolours)

### Now write down the name of genes beside the points...
### Create a new column "delabel" to de, that will contain the name of genes differentially
expressed (NA in case they are not)
responseAs.degs$degslabel <- NA
responseAs.degs$degslabel[responseAs.degs$diffexpressed != "NO"] <-
responseAs.degs$gene_names[responseAs.degs$diffexpressed != "NO"]

ggplot(responseAs.degs, aes(x=avg_log2FC, y=-log10(p_val_adj), col=diffexpressed, label =
degslabel)) +
  geom_point() +
  theme_minimal()+
  geom_text() +
  labs(title= "STm vs NT differentially expressed genes in non-responseBs")+
```

```
  coord_cartesian(clip = "off")

### Finally, we can organize the labels nicely using the "ggrepel" package and the geom_text_repel() function
### load library
library(ggrepel)
### plot adding up all layers we have seen so far
ggplot(responseAs.degs, aes(x=avg_log2FC, y=-log10(p_val_adj), col=diffexpressed, label=degslabel)) +
  geom_point() +
  theme_minimal() +
  geom_text_repel() +
  scale_color_manual(values=c("blue", "black", "red")) +
  geom_vline(xintercept=c(-0.5, 0.5), col="red") +
  geom_hline(yintercept=-log10(0.05), col="red") +
  labs(title= "STm vs NT differentially expressed genes in non-responseBs")+
  coord_cartesian(clip = "off")


###PLOT VIOLIN PLOTS FOR GENES OF INTEREST – LCN2 plus chemokines from bulk data

DefaultAssay(data.combined_389F) <- "RNA"


###LCN2

FeaturePlot(data.combined_389F, features = "LCN2”, cols = c("grey", "red"), split.by = c(“patient”, "treatment"), order = TRUE , pt.size = 1)

FeaturePlot(data.combined_389F, features = "LCN2", cols = c("grey", "red"), split.by = "treatment", order = TRUE , pt.size = 1)

###No difference between patients – export plots (‘split.by = treatment’ only) with pooled to streamline


### CHEMOKINE PLOTS

FeaturePlot(data.combined_389F, features = c("CXCL1", “CXCL2”, “CXCL3”, “CCL20”), cols = c("grey", "red"), split.by = c(“patient”, "treatment"), order = TRUE , pt.size = 1)

FeaturePlot(data.combined_389F, features = c("CXCL1", “CXCL2”, “CXCL3”, “CCL20”), cols = c("grey", "red"), split.by = "treatment", order = TRUE , pt.size = 1)

###No difference between patients – export plots with pooled (‘split.by = treatment’ only) to streamline again
```

APPENDIX 2: BULK RNA SEQUENCING SCRIPTS

The following scripts were written and used in R Studio version 4.1.1 to analyse bulk RNA sequencing data provided as aligned read counts by Lexogen GmbH.

```
###Install DESeq2 and open packages for visualising PCA plots
BiocManager::install("DESeq2")
library(DESeq2)
library(PCAtools)
library(ggplot2)

###Read in the count data for human and mouse separately
countdata_hu=read.csv("coldata_hu.csv", row.names=1)
metadata_hu <- read.csv("metadata_hu.csv", row.names=1)

countdata_ms=read.csv(“coldata_ms.csv”, row.names=1)
metadata_ms <- read.csv(“metadata_ms.csv”, row.names=1)

###Create human dds with count data and metadata
dds_hu <- DESeqDataSetFromMatrix(countData=countdata_hu,
                      colData=metadata_hu,
                      design=~condition)
dds_hu <- DESeq(dds_hu)

###rlog function normalisation of library and plotting of PCA
rld_hu=rlog(dds_hu,blind=F)
write.csv(assay(rld_hu),file="norm_hu.csv")
pdf("PCA_hu.pdf")
plotPCA(rld_hu, intgroup="condition", ntop=500)
dev.off()

###Repeat with mbcd only and no mbcd
countdata_hu_mbcd=read.csv("coldata_hu_mbcd.csv", row.names=1)
metadata_hu_mbcd <- read.csv("metadata_hu_mbcd.csv", row.names=1)
dds_hu_mbcd <- DESeqDataSetFromMatrix(countData=countdata_hu_mbcd,
                      colData=metadata_hu_mbcd,
                      design=~condition)

dds_hu_mbcd <- DESeq(dds_hu_mbcd)

#rlog function normalisation of library and plotting of PCA with mbcd only
rld_hu_mbcd=rlog(dds_hu_mbcd,blind=F)

write.csv(assay(rld_hu_mbcd),file="norm_hu_mbcd.csv")
pdf("PCA_hu_mbcd.pdf")
```

```
plotPCA(rld_hu_mbcd, intgroup="condition", ntop=500)
dev.off()

countdata_hu_nombcd=read.csv(“coldata_hu_nombcd.csv”, row.names=1)
metadata_hu_nombcd <- read.csv(“metadata_hu_nombcd.csv”, row.names=1)

dds_hu_nombcd <- DESeqDataSetFromMatrix(countData=countdata_hu_nombcd,
                    colData=metadata_hu_nombcd,
                    design=~condition)

dds_hu_nombcd <- DESeq(dds_hu_nombcd)

#rlog function normalisation of library and plotting of PCA with no mbcd
rld_hu_nombcd=rlog(dds_hu_nombcd,blind=F)

write.csv(assay(rld_hu_nombcd),file="norm_hu_nombcd.csv")
pdf("PCA_hu_nombcd.pdf")
plotPCA(rld_hu_nombcd, intgroup="condition", ntop=500)
dev.off()



###Create mouse dds with count data and metadata
dds_ms <- DESeqDataSetFromMatrix(countData=countdata_ms,
                    colData=metadata_ms,
                    design=~condition)
dds_ms <- DESeq(dds_ms)

###rlog function normalisation of library and plotting of PCA
rld_ms=rlog(dds_ms,blind=F)
write.csv(assay(rld_ms),file="norm_ms.csv")
pdf("PCA_ms.pdf")
plotPCA(rld_ms, intgroup="condition", ntop=500)
dev.off()

###Repeat with mbcd only and no mbcd
countdata_ms_mbcd=read.csv("coldata_ms_mbcd.csv", row.names=1)
metadata_ms_mbcd <- read.csv("metadata_ms_mbcd.csv", row.names=1)
dds_ms_mbcd <- DESeqDataSetFromMatrix(countData=countdata_ms_mbcd,
                    colData=metadata_ms_mbcd,
                    design=~condition)

dds_ms_mbcd <- DESeq(dds_ms_mbcd)

#rlog function normalisation of library and plotting of PCA with mbcd only
rld_ms_mbcd=rlog(dds_ms_mbcd,blind=F)

write.csv(assay(rld_ms_mbcd),file="norm_ms_mbcd.csv")
pdf("PCA_ms_mbcd.pdf")
plotPCA(rld_ms_mbcd, intgroup="condition", ntop=500)
```

```
dev.off()

countdata_ms_nombcd=read.csv(“coldata_ms_nombcd.csv”, row.names=1)
metadata_ms_nombcd <- read.csv(“metadata_ms_nombcd.csv”, row.names=1)

dds_ms_nombcd <- DESeqDataSetFromMatrix(countData=countdata_ms_nombcd,
                    colData=metadata_ms_nombcd,
                    design=~condition)

dds_ms_nombcd <- DESeq(dds_ms_nombcd)

#rlog function normalisation of library and plotting of PCA with no mbcd
rld_ms_nombcd=rlog(dds_ms_nombcd,blind=F)

write.csv(assay(rld_ms_nombcd),file="norm_ms_nombcd.csv")
pdf("PCA_ms_nombcd.pdf")
plotPCA(rld_ms_nombcd, intgroup="condition", ntop=500)
dev.off()


###Make gene names row names for human
countdata_hu_genenames=read.csv("coldata_hu_genenames.csv")
rownames(countdata_hu_genenames) <- make.names(countdata_hu_genenames$gene, unique =
TRUE)
countdata_hu_genenames <- countdata_hu_genenames[, -1]

dds_hu <- DESeqDataSetFromMatrix(countData=countdata_hu_genenames,
                    colData=metadata,
                    design=~condition)
dds_hu <-DESeq(dds_hu)

countdata_hu_genenames <- as.matrix(countdata_hu_genenames)


### Make gene names row names for mouse
countdata_ms_genenames=read.csv("coldata_ms_genenames.csv")
rownames(countdata_ms_genenames) <- make.names(countdata_ms_genenames$gene, unique =
TRUE)
countdata_ms_genenames <- countdata_ms_genenames[, -1]

dds_ms <- DESeqDataSetFromMatrix(countData=countdata_ms_genenames,
                    colData=metadata,
                    design=~condition)
dds_ms <-DESeq(dds_ms)

countdata_ms_genenames <- as.matrix(countdata_ms_genenames)


####HUMAN WORKFLOW FOR VOLCANO PLOTS
```

```
##Pre-filter rows with at least 10 reads total to remove data for debris
keep <- rowSums(counts(dds_hu)) >= 10
dds_hu <- dds_hu[keep,]

##Instruct to compare NT v STm - i.e log2(stm/nt)
dds_hu$condition <- relevel(dds_hu$condition, ref = "NT")
dds_hu <- DESeq(dds_hu)
res <- results(dds_hu)
res_hu
res_hu <- results(dds_hu, contrast=c("condition","STm","NT"))
dds_hu <- DESeq(dds_hu)
res_hu_nt_stm <- results(dds_hu)
res_hu
resultsNames(dds_hu)

### Use apeglm for Bayesian shrinkage of lfc – helps visualisation
library(apeglm)
res_huLFC_nt_stm <- lfcShrink(dds_hu, coef="condition_STm_vs_NT", type="apeglm")
res_huLFC_nt_stm

library("BiocParallel")
register(SnowParam(4))

resOrdered_hu <- res_hu[order(res_hu$pvalue),]
summary(res_hu)
res_hu05 <- results(dds_hu, alpha=0.05)
summary(res_hu05)
resorderedsig_hu <- subset(resOrdered_hu, padj < 0.05)
resorderedsig_hu
orderbylogfc_hu <- resorderedsig_hu[order(resorderedsig_hu$log2FoldChange),]

write.csv(as.data.frame(orderbylogfc_hu),
      file="stmvnt_results_hu_orderbylogfc.csv")
write.csv(as.data.frame(resorderedsig_hu),
      file="condition_stmvnt_results_hu.csv")

#Make volcano plot from DEGs for hu stm v nt
Orderedresults_hu <- read.csv("stmvnt_results_hu_orderbylogfc.csv", row.names = 1)
mat <- as.matrix(orderedresults_hu)
library(EnhancedVolcano)
resvp <- as.data.frame(res_huLFC_nt_stm)

pdf("volcano_hu_stmvnt.pdf")
EnhancedVolcano(resvp,
          lab = rownames(resvp),
          x = 'log2FoldChange',
          y = 'pvalue',
          title = 'STm v NT in human PDOs',
          pCutoff = 10e-3,
          FCcutoff = 1.5,)
```

```
dev.off()


###Reapeat with instruction to compare MBCD v STm.MBCD - i.e log2(stm.mbcd/mbcd)
dds_hu$condition <- relevel(dds_hu$condition, ref = "MBCD")
dds_hu <- DESeq(dds_hu)
res <- results(dds_hu)
res
res <- results(dds_hu, contrast=c("condition","STm.MBCD","MBCD"))
dds_hu <- DESeq(dds_hu)
res_mbcd_stm.mbcd <- results(dds_hu)
res
resultsNames(dds_hu)

#shrinking lfc is good for visualisation:
library(apeglm)
res_huLFC_mbcd_stm.mbcd <- lfcShrink(dds_hu, coef="condition_STm.MBCD_vs_MBCD",
type="apeglm")

res_huLFC_mbcd_stm.mbcd

library("BiocParallel")
register(SnowParam(4))

resOrdered <- res[order(res$pvalue),]
summary(res)

res05 <- results(dds_hu, alpha=0.05)
summary(res05)

resorderedsig <- subset(resOrdered, padj < 0.05)
resorderedsig

orderbylogfc <- resorderedsig[order(resorderedsig$log2FoldChange),]

write.csv(as.data.frame(orderbylogfc),
      file="stm.mbcdvmbcd_results_hu_orderbylogfc.csv")

write.csv(as.data.frame(resorderedsig),
      file="condition_stm.mbcdvmbcd_results_hu.csv")


#Make volcano plot from DEGs
Orderedresults_hu <- read.csv("stm.mbcdvmbcd_results_hu_orderbylogfc.csv", row.names = 1)

mat <- as.matrix(orderedresults_hu)

library(EnhancedVolcano)
resvp <- as.data.frame(res_huLFC_mbcd_stm.mbcd)
```

```
pdf("volcano_hu_stm.mbcdvmbcd.pdf")
EnhancedVolcano(resvp,
        lab = rownames(resvp),
        x = 'log2FoldChange',
        y = 'pvalue',
        title = 'STm + MBCD vs MBCD in human PDOs',
        pCutoff = 10e-3,
        FCcutoff = 1.5,)
dev.off()


###MOUSE WORKFLOW FOR VOLCANO PLOTS


##Pre-filter rows with at least 10 reads total to remove data for debris
keep <- rowSums(counts(dds_ms)) >= 10
dds_ms <- dds_ms[keep,]

##Instruct to compare NT v STm - i.e log2(stm/nt)
dds_ms$condition <- relevel(dds_ms$condition, ref = "NT")
dds_ms <- DESeq(dds_ms)
res <- results(dds_ms)
res_ms
res_ms <- results(dds_ms, contrast=c("condition","STm","NT"))
dds_ms <- DESeq(dds_ms)
res_ms_nt_stm <- results(dds_ms)
res_ms
resultsNames(dds_ms)

### Use apeglm for Bayesian shrinkage of lfc – helps visualisation
library(apeglm)
res_msLFC_nt_stm <- lfcShrink(dds_ms, coef="condition_STm_vs_NT", type="apeglm")
res_msLFC_nt_stm

library("BiocParallel")
register(SnowParam(4))

resOrdered_ms <- res_ms[order(res_ms$pvalue),]
summary(res_ms)
res_ms05 <- results(dds_ms, alpha=0.05)
summary(res_ms05)
resorderedsig_ms <- subset(resOrdered_ms, padj < 0.05)
resorderedsig_ms
orderbylogfc_ms <- resorderedsig_ms[order(resorderedsig_ms$log2FoldChange),]

write.csv(as.data.frame(orderbylogfc_ms),
      file="stmvnt_results_ms_orderbylogfc.csv")
write.csv(as.data.frame(resorderedsig_ms),
      file="condition_stmvnt_results_ms.csv")
```

```
#Make volcano plot from DEGs for ms stm v nt
Orderedresults_ms <- read.csv("stmvnt_results_ms_orderbylogfc.csv", row.names = 1)
mat <- as.matrix(orderedresults_ms)
library(EnhancedVolcano)
resvp <- as.data.frame(res_msLFC_nt_stm)

pdf("volcano_ms_stmvnt.pdf")
EnhancedVolcano(resvp,
        lab = rownames(resvp),
        x = 'log2FoldChange',
        y = 'pvalue',
        title = 'STm v NT in mouse tumour organoids',
        pCutoff = 10e-3,
        FCcutoff = 1.5,)
dev.off()


###Reapeat with instruction to compare MBCD v STm.MBCD - i.e log2(stm.mbcd/mbcd)
dds_ms$condition <- relevel(dds_ms$condition, ref = "MBCD")
dds_ms <- DESeq(dds_ms)
res <- results(dds_ms)
res
res <- results(dds_ms, contrast=c("condition","STm.MBCD","MBCD"))
dds_ms <- DESeq(dds_ms)
res_mbcd_stm.mbcd <- results(dds_ms)
res
resultsNames(dds_ms)

#shrinking lfc is good for visualisation:
library(apeglm)
res_msLFC_mbcd_stm.mbcd <- lfcShrink(dds_ms, coef="condition_STm.MBCD_vs_MBCD",
type="apeglm")
res_msLFC_mbcd_stm.mbcd

library("BiocParallel")
register(SnowParam(4))
resOrdered <- res[order(res$pvalue),]
summary(res)
res05 <- results(dds_ms, alpha=0.05)
summary(res05)
resorderedsig <- subset(resOrdered, padj < 0.05)
resorderedsig
orderbylogfc <- resorderedsig[order(resorderedsig$log2FoldChange),]

write.csv(as.data.frame(orderbylogfc),
      file="stm.mbcdvmbcd_results_ms_orderbylogfc.csv")
write.csv(as.data.frame(resorderedsig),
      file="condition_stm.mbcdvmbcd_results_ms.csv")

#Make volcano plot from DEGs
```

```
Orderedresults_ms <- read.csv("stm.mbcdvmbcd_results_ms_orderbylogfc.csv", row.names = 1)

mat <- as.matrix(orderedresults_ms)

library(EnhancedVolcano)
resvp <- as.data.frame(res_msLFC_mbcd_stm.mbcd)

pdf("volcano_ms_stm.mbcdvmbcd.pdf")
EnhancedVolcano(resvp,
        lab = rownames(resvp),
        x = 'log2FoldChange',
        y = 'pvalue',
        title = 'STm + MBCD vs MBCD in mouse tumour organoids',
        pCutoff = 10e-3,
        FCcutoff = 1.5,)
dev.off()


####VENN DIAGRAM WORKFLOW HUMAN

 library(VennDiagram)

###UP regulated human
 ### Prior to this make excel file of the DEGs for each of the conditions. Then I define which column is which (giving the vectors below, and indicating number of rows as these will differ depending on DEG number)

x=read.csv("up_389.csv",header=T)
A=x[1:649,1]
B=x[1:1408,2]
C=x[1:145,3]
venn.diagram(x=list("STm vs NT"=A,"STm+MBCD vs STm"=B,"STm+MBCD vs MBCD"=C),
filename="Venn_389_up.png", fill=c("red","blue","darkgreen"), hei=5500, width=5500, res=300,
cex=2, cat.cex=2)
x=calculate.overlap(x=list("STm vs NT"=A,"STm+MBCD vs STm"=B,"STm+MBCD vs MBCD"=C))

overlap_up_389_all3 <- as.data.frame(x[["a5"]])
overlap_up_389_all3 <- write.csv(x[["a5"]], "all3_up_389.csv")
overlap_up_389_extracell <- as.dataframe(x[["a2"]])
overlap_up_389_extracell <- write.csv(x[["a2"]], "extracell_389.csv")
overlap_up_389_extracell2 <- as.data.frame(x[["a4"]])
overlap_up_389_extracell2 <- write.csv(x[["a4"]], "extracell2_389.csv")
overlap_up_389_mbcd <- as.data.frame(x[["a6"]])
overlap_up_389_mbcd <- write.csv(x[["a6"]], "mbcd_389.csv")
unique_up_389_stmvnt <- as.data.frame(x[["a1"]])
unique_up_389_stmvnt <- write.csv(x[["a1"]], "unique_stmvnt_389.csv")
unique_up_389_extracell_only <- as.data.frame(x[["a7"]])
unique_up_389_extracell_only <- write.csv(x[["a7"]], "unique_up_389_extracellstm.csv")

###DOWN regulated human
```

```
x=read.csv("down_389.csv",header=T)
A=x[1:368,1]
B=x[1:1157,2]
C=x[1:67,3]
venn.diagram(x=list("STm vs NT"=A,"STm+MBCD vs STm"=B,"STm+MBCD vs MBCD"=C),
filename="Venn_389_down.png", fill=c("red","blue","darkgreen"), hei=5500, width=5500, res=300,
cex=2, cat.cex=2)
x=calculate.overlap(x=list("STm vs NT"=A,"STm+MBCD vs STm"=B,"STm+MBCD vs MBCD"=C))


overlap_down_389_all3 <- as.data.frame(x[["a5"]])
overlap_down_389_extracell <- as.data.frame(x[["a2"]])
overlap_down_389_extracell2 <-as.data.frame(x[["a4"]])
overlap_down_389_mbcd <- as.data.frame(x[["a6"]])
unique_down_389_stmvnt <- as.data.frame(x[["a1"]])
unique_down_389_extracell_only <- as.data.frame(x[["a7"]])
unique_down_389_extracell_only <- write.csv(x[["a7"]], "unique_down_389_extracellstm.csv")
unique_down_389_stmvnt <- write.csv(x[["a1"]], "unique_down_389_stmvnt.csv")
all3_up <- read.csv("all3_up_389.csv")
all3_up <- as.data.frame(all3_up)
all3 <- rbind(all3_up, overlap_down_389_all3)
expression <- read.csv("norm_hu_389_gene.csv")

all3_nt <- read.csv("all3_389_nt.csv")
all3_stm <- read.csv("all3_389_stm.csv")
all3_mbcd <- read.csv("all3_389_mbcd.csv")
all3_stm.mbcd <- read.csv("all3_389_stm.mbcd.csv")
all3 <- rbind(all3_nt, all3_mbcd, all3_stm, all3_stm.mbcd)

#####MOUSE REPEAT VENN WORKFLOW

###UP regulated mouse

x=read.csv("up_ms.csv",header=T)
A=x[1:440,1]
B=x[1:1567,2]
C=x[1:36,3]
venn.diagram(x=list("STm vs NT"=A,"STm+MBCD vs STm"=B,"STm+MBCD vs MBCD"=C),
filename="Venn_ms_up.png", fill=c("red","blue","darkgreen"), hei=5500, width=5500, res=300,
cex=2, cat.cex=2)
x=calculate.overlap(x=list("STm vs NT"=A,"STm+MBCD vs STm"=B,"STm+MBCD vs MBCD"=C))


overlap_up_ms_all3 <- as.data.frame(x[["a5"]])
overlap_up_ms_extracell <- as.data.frame(x[["a2"]])
overlap_up_ms_extracell2 <-as.data.frame(x[["a4"]])
overlap_up_ms_mbcd <- as.data.frame(x[["a6"]])
unique_up_ms_stmvnt <- as.data.frame(x[["a1"]])
overlap_up_ms_all3 <- write.csv(x[["a5"]], "all3_up_ms.csv")
```

```
overlap_up_ms_extracell <- write.csv(x[["a2"]], "overlap_extracell_ms.csv")
overlap_up_ms_extracell2 <- write.csv(x[["a4"]], "overlap_extracell2_ms.csv")
overlap_up_ms_mbcd <- write.csv(x[["a6"]], "overlap_mbcd_ms.csv")
unique_up_ms_stmvnt <- write.csv(x[["a1"]], "unique_up_ms_stmvnt.csv")

###DOWN regulated mouse

x=read.csv("down_ms.csv",header=T)#basically i make an excel file of the DEGs for the four conditions. Then I define which column is which (giving the vectors below, and indicating number of rows as these will differ depending on DEG number)
A=x[1:246,1]
B=x[1:1343,2]
C=x[1:23,3]
venn.diagram(x=list("STm vs NT"=A,"STm+MBCD vs STm"=B,"STm+MBCD vs MBCD"=C), filename="Venn_ms_down.png", fill=c("red","blue","darkgreen"), hei=5500, width=5500, res=300, cex=2, cat.cex=2)
x=calculate.overlap(x=list("STm vs NT"=A,"STm+MBCD vs STm"=B,"STm+MBCD vs MBCD"=C))


overlap_down_ms_all3 <- as.data.frame(x[["a5"]])
overlap_down_ms_extracell <- as.data.frame(x[["a2"]])
overlap_down_ms_extracell2 <-as.data.frame(x[["a4"]])
overlap_down_ms_mbcd <- as.data.frame(x[["a6"]])
unique_down_ms_stmvnt <- as.data.frame(x[["a1"]])
unique_down_ms_extracell_only <- as.data.frame(x[["a7"]])
overlap_down_ms_all3 <- write.csv(x[["a5"]], "all3_down_ms.csv")
overlap_down_ms_extracell <- write.csv(x[["a2"]], "overlap_extracell_ms_down.csv")
overlap_down_ms_extracell2 <- write.csv(x[["a4"]], "overlap_extracell2_ms_down.csv")
overlap_down_ms_mbcd <- write.csv(x[["a6"]], "overlap_mbcd_ms_down.csv")
unique_down_ms_stmvnt <- write.csv(x[["a1"]], "unique_down_ms_stmvnt.csv")
unique_down_ms_extracell_only <- write.csv(x[["a7"]], "unique_down_ms_extracellstm.csv")


###Pathway analysis using pathfinder HUMAN

install.packages("pathfindR")
library(pathfindR)

###Read in csv of DEGs between stm v nt
stmvnt389 <- read.csv("stmvnt_389_DEGs.csv")
stmvnt389 <- as.data.frame(stmvnt389)
output_df <- run_pathfindR(stmvnt389)

pdf("stmvnt_389_pathfindR.pdf")
enrichment_chart(result_df = output_df,
                 top_terms = 15)
dev.off()

write.csv(output_df, "stmvnt_389_pathfindR.csv")
```

```
###Read in csv of stm+mbcd v mbcd
stm.mbcdvmbcd <- read.csv("stm.mbcdvmbcd_389_DEGs.csv")
stm.mbcdvmbcd <-as.data.frame(stm.mbcdvmbcd)
output_df_mbcd <- run_pathfindR(stm.mbcdvmbcd)

pdf("stm.mbcdvmbcd_389_pathfindR.pdf")
enrichment_chart(result_df = output_df_mbcd,
        top_terms = 15)
dev.off()

write.csv(output_df_mbcd, "stm.mbcdvmbcd_389_pathfindR.csv")


###Repeat pathway analysis for MOUSE

stmvntms <- read.csv("stmvnt_ms_DEGs.csv")
stmvntms <- as.data.frame(stmvntms)
output_df <- run_pathfindR(stmvntms)
output_df <- read.csv("stmvnt_ms_pathfindR.csv")

emf("stmvnt_ms_pathfindR.emf")
enrichment_chart(result_df = output_df,
        top_terms = 10)
dev.off()

write.csv(output_df, "stmvnt_ms_pathfindR.csv")

stm.mbcdvstm <- read.csv("stm.mbcdvstm_ms_DEGs.csv")
stm.mbcdvstm <-as.data.frame(stm.mbcdvstm)
output_df_stm.mbcd <- run_pathfindR(stm.mbcdvstm)

pdf("stm.mbcdvstm_ms_pathfindR.pdf")
enrichment_chart(result_df = output_df_stm.mbcd,
        top_terms = 10)
dev.off()

write.csv(output_df_stm.mbcd, "stm.mbcdvstm_ms_pathfindR.csv")

stm.mbcdvmbcd <- read.csv("stm.mbcdvmbcd_ms_DEGs.csv")
stm.mbcdvmbcd <-as.data.frame(stm.mbcdvmbcd)
output_df_mbcd <- run_pathfindR(stm.mbcdvmbcd)
output_df_mbcd <- read.csv("stm.mbcdvmbcd_ms_pathfindR.csv")

emf("stm.mbcdvmbcd_ms_pathfindR.emf")
enrichment_chart(result_df = output_df_mbcd,
        top_terms = 10)
dev.off()

write.csv(output_df_mbcd, "stm.mbcdvmbcd_ms_pathfindR.csv")
```